

# Surface and Interface Characterization of Lithium Metal Anodes for the Application in Solid-State Batteries

Dem Fachbereich Biologie und Chemie  
der Justus-Liebig-Universität Gießen  
vorgelegte Dissertation zur Erlangung  
des akademischen Grades  
Doktor der Naturwissenschaften  
– Dr. rer. nat. –

**Svenja-Katharina Otto**

———— Juni 2022 ————



Dekan / Dean	Prof. Dr. Thomas Wilke
1. Gutachter / 1 <sup>st</sup> Reviewer	Prof. Dr. Jürgen Janek (Justus-Liebig-Universität Gießen)
2. Gutachter / 2 <sup>nd</sup> Reviewer	Prof. Dr. Herbert Over (Justus-Liebig-Universität Gießen)
Eingereicht / Submitted	23.06.2022
Disputation / Disputation	



## **Eidesstattliche Erklärung**

Die vorliegende Arbeit wurde im Zeitraum vom 01.04.2019 bis 23.06.2022 am Physikalisch-Chemischen Institut der Justus-Liebig-Universität Gießen unter Betreuung von Prof. Dr. Jürgen Janek angefertigt.

Ich erkläre: Ich habe die vorgelegte Dissertation selbstständig und ohne unerlaubte fremde Hilfe und nur mit den Hilfen angefertigt, die ich in der Dissertation angegeben habe. Alle Textstellen, die wörtlich oder sinngemäß aus veröffentlichten Schriften entnommen sind, und alle Angaben, die auf mündlichen Auskünften beruhen, sind als solche kenntlich gemacht. Ich stimme einer evtl. Überprüfung meiner Dissertation durch eine Antiplagiat-Software zu. Bei den von mir durchgeführten und in der Dissertation erwähnten Untersuchungen habe ich die Grundsätze guter wissenschaftlicher Praxis, wie sie in der „Satzung der Justus-Liebig-Universität Gießen zur Sicherung guter wissenschaftlicher Praxis“ niedergelegt sind, eingehalten.

Gießen, 23.06.2022

---

Svenja-Katharina Otto



## Abstract

The use of lithium metal anodes (LMAs) in solid state batteries (SSBs) is a promising approach to develop secondary batteries with high energy and power densities. These are needed to meet the demand of rapidly developing markets like the one for electric vehicles. Since LMAs provide an about ten times higher theoretical capacity than common graphite intercalation anodes, they are regarded as ideal future anode material. However, in combination with liquid electrolytes, severe safety issues arise for secondary batteries with LMAs due to dendrite formation and resulting short circuits. In contrast, solid electrolytes (SEs) are expected to be a safe solution, as they are more stable at high temperatures and in the case of inorganic SE not flammable. Still, also for SEs, the implementation of LMAs is challenging. Especially the lithium|SE (Li|SE) interface properties are regarded as a key challenge for the successful use of LMAs in secondary batteries. One well-described problem in this context is the reactivity of lithium towards most SEs, which can lead to interphase formation and consequently to high interfacial resistance, as well as lithium loss. Another central factor is mostly unknown or neglected: Due to the high reactivity of lithium, lithium foil and other exposed lithium surfaces are always covered with some kind of reaction layer, which can have a detrimental effect on the interfacial properties in the battery. For LIBs with liquid electrolyte the effect of this surface passivation layer has already been evaluated and proven to be highly important. In case of SSBs, the effects are probably even more severe, as the lithium surface film cannot dissolve into the electrolyte. Consequently, a detailed investigation is needed.

Therefore, this doctoral thesis focuses on the characterization of lithium surfaces, their changes under handling and storage conditions which are typical for battery research, and how these changes affect the anode interface resistance in SSBs. First, a reliable characterization strategy with X-ray photoelectron spectroscopy and time-of-flight secondary ion mass spectrometry (ToF-SIMS) was developed. The characterization described in literature so far has often been insufficient in terms of experimental design and data interpretation due to several pitfalls. In the present work, these pitfalls were identified, explained and detailed guidelines for reliable lithium surface characterization are given. Based on this, lithium foil was characterized after glovebox storage under various conditions. The steady growth of the lithium surface passivation layer could be attributed to water contaminations in the glovebox atmosphere. Next, the impact of the layer thickness was investigated with a model SSB, finding that the anode interface resistance increases significantly with the presence of an only nanometer-thick passivation layer. The SE roughness and the cell preparation pressure were found to have a strong effect on the resulting interface resistance.

In addition, the Li|SE interphase formation was investigated with ToF-SIMS. It is shown that ToF-SIMS can reliably indicate the stability of Li|SE interfaces and can provide information on the microstructure of the interphases. The combination with atomic force microscopy allowed to determine the thickness of forming interlayers, which were thicker than previously reported.

Overall, the results of this doctoral thesis expand the knowledge about lithium surfaces, as well as interfaces in SSBs and are one step towards the implementation of LMAs in secondary batteries. The results are a good base for reliable LMA characterization in general and give an improved understanding of the reactivity of lithium surfaces towards atmospheric gases as residues in gloveboxes. Notably, the importance of lithium surface passivation layers was demonstrated for SSBs, what was not considered in literature before. Furthermore, ToF-SIMS was established as a complementary technique for Li|SE interface characterization, expanding the possibilities to obtain a complete picture of the interfaces in SSBs and helping to design tailored modifications.



## Zusammenfassung

Die Implementierung von Lithiummetallanoden (LMA) in Festkörperbatterien (FKB) ist ein vielversprechender Ansatz, um Sekundärbatterien mit hohen Energie- und Leistungsdichten zu verwirklichen und damit zum Beispiel die zukünftige Elektrifizierung des Verkehrs zu ermöglichen. FKB mit LMA weisen eine etwa zehnmal höhere theoretische Kapazität im Vergleich zu herkömmlichen Lithiumionen-Batterien (LIB) mit Graphit-Interkalationsanode auf und gelten damit als ideales Anodenmaterial der Zukunft. Während bei der Verwendung von Lithiummetall als Anodenmaterial in Kombination mit Flüssigelektrolyten Sicherheitsprobleme auftreten, stellt die Kombination aus LMA und Festelektrolyt (FE) eine deutlich sichere Lösung dar. Der FE weist eine größere thermische Stabilität auf und ist im Fall von anorganischen FE nicht entflammbar. Trotzdem stellt die Verwendung der LMA in FKB eine Herausforderung dar. Aufgrund der hohen Reaktivität von Lithium kommt es oftmals zu chemischen Reaktionen an der Grenzfläche zwischen LMA und FE. Die entstehenden Reaktionsschichten können den Zellwiderstand erhöhen und so die Eigenschaften und Leistungsfähigkeit der FKB verschlechtern. Während diese Problematik weithin bekannt ist, wird eine andere Eigenschaft des für den Zellbau verwendeten Lithiums zumeist vernachlässigt: Lithiumfolien und andere Lithiumoberflächen sind immer mit einer Reaktions- bzw. Passivierungsschicht bedeckt, die ebenfalls die Grenzflächeneigenschaften in der Batterie beeinflusst. Während für LIB mit flüssigem Elektrolyten der Einfluss der Passivierungsschicht auf die Eigenschaften der Batteriezelle bereits nachgewiesen wurde, ist der Effekt für FKB noch nicht untersucht, obwohl stärkere Effekte zu erwarten sind, da sich die Passivierungsschicht nicht im FE lösen kann. Daher ist eine detaillierte Untersuchung des Einflusses erforderlich.

Im Rahmen der hier vorliegenden Dissertation wurde zunächst eine verlässliche Charakterisierungsstrategie für Lithiumoberflächen mittels Röntgen-Photoelektronenspektroskopie und Flugzeit-Sekundärionen-Massenspektrometrie (ToF-SIMS) entwickelt. Dabei wurden auch Fehler, die in der bisherigen Literatur häufig zu falschen Ergebnissen führten, identifiziert, erläutert und Richtlinien für das experimentelle Vorgehen sowie die gesicherte Dateninterpretation erstellt. Auf dieser Grundlage wurden anschließend Lithiummetallfolien nach der Lagerung in Gloveboxen unter verschiedenen Bedingungen charakterisiert. Des Weiteren wurde der Einfluss der Dicke der Passivierungsschicht auf den Anodengrenzflächenwiderstand in FKB untersucht. Dabei wurde festgestellt, dass der Widerstand bereits durch eine wenige Nanometer dünne Passivierungsschicht erheblich zunimmt. Zudem konnte gezeigt werden, dass die Rauigkeit des FE und der angelegte Druck bei der Zellpräparation einen wichtigen Einfluss auf den Grenzflächenwiderstand haben.

In einer weiteren experimentellen Studie wurde ToF-SIMS als Methode zur Charakterisierung von Li|FE-Grenzflächen etabliert. Dabei wurde die Stabilität der Grenzflächen mittels Tiefenprofilierung ermittelt und die 3D-Struktur von sich bildenden Reaktionsschichten visualisiert. Durch Kombination mit Rasterkraftmikroskopie konnte zudem die Dicke der sich bildenden Reaktionsschichten bestimmt werden.

Die Ergebnisse dieser Dissertation erweitern das Verständnis für Lithiumoberflächen sowie für Li|FE-Grenzflächen in FKB und sind somit ein wichtiger Schritt hin zum erfolgreichen Einsatz von LMA in Sekundärbatterien. Die Arbeit erweitert zudem das Verständnis für die Reaktivität von Lithiumoberflächen gegenüber Atmosphärgasen und zeigt die Bedeutung der sich bildenden Passivierungsschichten für FKB auf, was bisher in der Literatur nicht ausreichend berücksichtigt wurde. Darüber hinaus bietet diese Arbeit die Grundlage für eine verlässliche Charakterisierung von Lithiummetalloberflächen und etabliert ToF-SIMS als Methode für die Charakterisierung von Li|FE-Grenzflächen.



## List of Abbreviations

AES	Auger electron spectroscopy
AFM	atomic force microscopy
ALD	atomic layer deposition
CAM	cathode active material
DFT	density function theory
DSC	differential scanning calorimetry
EELS	electron energy loss spectroscopy
EDX	energy dispersive X-ray analysis
ESW	electrochemical stability window
FIB	focused ion beam
FTIR	Fourier transform infrared spectroscopy
IR	infrared spectroscopy
KE	kinetic energy
L	Langmuir
LATP	$\text{Li}_{1.5}\text{Al}_{0.5}\text{Ti}_{1.5}(\text{PO}_4)_3$
LGPS	$\text{Li}_{10}\text{GeP}_2\text{S}_{12}$
LIB	lithium ion battery
LiPON	$\text{Li}_{3.6}\text{PO}_{3.4}\text{N}_{0.6}$
LiSiPS	$\text{Li}_7\text{SiPS}_8$
LLZO	$\text{Li}_{6.25}\text{Al}_{0.25}\text{La}_3\text{Zr}_2\text{O}_{12}$
LMA	lithium metal anode
LPSCI	$\text{Li}_6\text{PS}_5\text{Cl}$
LUMO	lowest unoccupied molecular orbital
MCI	mixed ionic-electronic conducting interphase
MD	molecular dynamics
NMR	nuclear magnetic resonance
PBR	Pilling-Bedworth ratio
SE	solid electrolyte
SEI	solid electrolyte interphase
SEM	scanning electron microscopy
SSB	solid-state battery
TEM	transmission electron microscopy
TGA	thermal gravimetric analysis
ToF-SIMS	time-of-flight secondary ion mass spectrometry
UHV	ultra-high vacuum
UPS	ultraviolet photoelectron spectroscopy
UV	ultraviolet
XPS	X-ray photoelectron spectroscopy
XRD	X-ray diffraction analysis



## Table of Contents

<b>1</b>	<b>Introduction .....</b>	<b>1</b>
<b>2</b>	<b>Fundamentals .....</b>	<b>5</b>
<b>2.1</b>	<b>Lithium metal and its reactivity .....</b>	<b>5</b>
2.1.1	Properties of lithium metal .....	5
2.1.2	Reactivity of lithium toward the atmospheric gases.....	6
<b>2.2</b>	<b>Surface passivation layers on lithium metal .....</b>	<b>16</b>
2.2.1	Relevance of the lithium surface passivation layers for battery research .....	16
2.2.2	Characterization of the lithium surface passivation layer.....	18
<b>2.3</b>	<b>Lithium metal   solid electrolyte interfaces.....</b>	<b>21</b>
2.3.1	Types of lithium metal   solid electrolyte interfaces .....	21
2.3.2	Characterization of lithium metal   solid electrolyte interfaces .....	22
<b>3</b>	<b>Results .....</b>	<b>25</b>
<b>3.1</b>	<b>Publication 1: “In-Depth Characterization of Lithium-Metal Surfaces with XPS and ToF-SIMS: Toward Better Understanding of the Passivation Layer” .....</b>	<b>25</b>
<b>3.2</b>	<b>Publication 2: “Storage of Lithium Metal: The Role of the Native Passivation Layer for the Anode Interface Resistance in Solid State Batteries” .....</b>	<b>37</b>
<b>3.3</b>	<b>Publication 3: “In situ Investigation of Lithium Metal - Solid Electrolyte Anode Interfaces with ToF-SIMS” .....</b>	<b>49</b>
<b>4</b>	<b>Conclusions.....</b>	<b>61</b>
<b>5</b>	<b>Outlook.....</b>	<b>63</b>
<b>6</b>	<b>References .....</b>	<b>65</b>
<b>7</b>	<b>Appendix.....</b>	<b>75</b>
<b>7.1</b>	<b>Supporting Information.....</b>	<b>75</b>
7.1.1	Publication 1 .....	75
7.1.2	Publication 2.....	88
7.1.3	Publication 3.....	98
<b>7.2</b>	<b>Scientific Contributions .....</b>	<b>102</b>
7.2.1	List of Publications.....	102
7.2.2	List of Conference Contributions.....	103
<b>8</b>	<b>Acknowledgement.....</b>	<b>105</b>



## 1 Introduction

The history of lithium metal anodes (LMAs) is not limited to research during the last years or decade. Already in the 1970s, the first primary batteries with LMAs were developed by Exxon.<sup>1</sup> Until today, these non-rechargeable batteries are widely applied. One well-known example are Li-I<sub>2</sub> primary batteries employed for instance in cardiac pacemakers. Also in the 1970s, Stanley Whittingham at Exxon used LMAs in the first viable lithium secondary batteries and Moli Energy even commercialized secondary lithium metal batteries in the late 1980s. The cells could be cycled hundreds of times and millions of them were sold. However, the safety of these secondary batteries was problematic and accidents occurred frequently.<sup>1</sup> Mostly lithium dendrite formation led to short circuiting of the batteries causing thermal runaway with the risk of explosion and fires. Consequently, the secondary cells with LMAs lost their position on the commercial market.<sup>2</sup> NEC and Mitsui tried to solve the safety issues in the following years, but failed despite of over 500,000 tested lithium metal cells. Instead, Sony succeeded to commercialize reliable secondary lithium ion batteries (LIBs) with a carbonaceous intercalation anode instead of a LMA in 1991 and thus the efforts to commercialize LMAs in secondary batteries were stopped.<sup>1</sup> Since then, the LIBs with intercalation anode became the predominant energy storage system in many application fields, were successfully optimized during the decades and revolutionized areas of modern life such as communication by enabling high performance mobile phones and laptops.<sup>2</sup> In 2019, the success story of LIB development was even honored with the Nobel Prize in Chemistry.<sup>3</sup>

However, the energy density of conventional LIBs nowadays reaches its theoretical limit, while the demand for batteries with higher energy and power densities increases.<sup>4,5</sup> State-of-the-art LIBs can reach a gravimetric energy density of about 250 Wh kg<sup>-1</sup> and a volumetric energy density of about 700 Wh l<sup>-1</sup>, what is not sufficient for the demands of e.g. the transportation sector with a growing market for electric vehicles.<sup>1</sup> Theoretically, the comeback of LMAs could serve this demand, as pure lithium provides the highest theoretical specific capacity of all metals.<sup>6</sup> For practical lithium metal-air batteries, a specific energy of about 950 Wh kg<sup>-1</sup> and a volumetric energy density of about 1,100 Wh l<sup>-1</sup> are predicted.<sup>1</sup> Accordingly, there is on-going research aiming to allow the application of LMAs for instance through artificial solid electrolyte interphases.<sup>7</sup> Still, dendrite formation, as well as uneven stripping and plating leading to safety issues and lithium loss are unsolved problems inhibiting the commercialization in secondary batteries.<sup>8-10</sup>

Another and potentially more promising approach to allow the safe use of LMAs in secondary batteries is the replacement of the common liquid electrolytes by solid ones. Solid electrolytes (SEs) can provide higher stability at elevated temperatures, are in case of inorganic SEs even not flammable and therefore improve battery safety compared to combustible liquid electrolytes. In addition, SEs may improve other critical features in comparison to liquid electrolytes, e.g. stopping unwanted chemical cross-talk between the electrodes and preventing dendrite formation due to higher mechanical rigidity. In combination with LMAs, batteries with SEs can also reach higher energy or power density than conventional LIBs.<sup>5</sup> A first practical example on the way to applicable systems are the LMA polymer batteries by Bolloré.<sup>11</sup> However, for SEs the implementation of LMAs is also not straight forward. Challenges for solid-state batteries (SSBs) are volume changes of the electrodes, inhomogeneous electrodeposition, dendrite formation, interface delamination and pore formation.<sup>12,13</sup> Furthermore, most SEs are reduced at low potential and therefore interphases form in contact with lithium metal.<sup>5</sup>

The overall properties in SSBs mainly rely on the conductivity of the SE on the one hand and the characteristics and stability of the solid-solid interfaces on the other hand. While noticeable results

are achieved for the synthesis of SEs with ionic conductivities in the range of liquid ones, interfaces and interphases still limit the performance of SSBs.<sup>14</sup> Importantly, the problem of interface stability is also not limited to the anode side. The interfaces on the cathode side of SSBs are critical, too. Consequently, literature often highlights that interfacial issues are the key points for SSBs and interphase formation is commonly discussed.<sup>15-17</sup> For the LMA|SE interface on the anode side, modification of the lithium anode surface, either chemically or mechanically, is regarded as one of the key approaches to improve the battery performance.<sup>18,19</sup> Besides, it is commonly agreed that detailed characterization is needed to understand and subsequently improve the interface stability.<sup>14-16</sup>

Another challenge related to LMA|SE interfaces is not that much in focus. If the lithium anode is prepared from lithium foil, what is a common strategy in research, the resulting interface is not a direct Li|SE contact, as lithium metal is covered with a surface passivation layer.<sup>20</sup> This surface film is directly formed on fresh lithium surfaces even with traces of reactive gases or is tailored for surface stabilization on commercial lithium foil.<sup>11</sup> For liquid electrolytes, the important impact of the lithium surface passivation layer on the overall battery performance was already demonstrated.<sup>21</sup> For SEs, the effects are potentially even more severe, as the film cannot dissolve as in liquid electrolytes. The surface modification of LMAs is altered by the surface passivation layer, too.<sup>21</sup> Consequently, a critical evaluation of the lithium surface status, the origin of the status and the impact in the battery is very important for a successful implementation of LMA in SSBs.

In this doctoral thesis, the surface passivation layer on lithium metal and its impact on the anode interface in SSBs are investigated. The overall aim is to understand the role of the lithium surface film for the development of SSBs to allow the successful implementation of LMA in general. In addition, time-of-flight secondary ion mass spectrometry (ToF-SIMS) is explored as characterization method for Li|SE interfaces and interphases to gain new insights for SSB development.

In the first publication of this thesis, entitled: “*In-Depth Characterization of Lithium-Metal Surfaces with XPS and ToF-SIMS: Toward Better Understanding of the Passivation Layer*”, reliable characterization strategies for the investigation of lithium surfaces are explored and expanded (see chapter 3.1).<sup>22</sup> X-ray photoelectron spectroscopy (XPS) and ToF-SIMS are presented as suitable complementary methods for lithium surface characterization, which can provide a complete 3D-picture of the surface passivation layer. The chemical nature of the lithium surface passivation layer is described in detail as nanometer-thick film with an upper hydroxide- and carbonate-rich region on top of an inner oxide-rich one. Importantly, several pitfalls for the characterization of lithium surfaces like lithium plating through electron beam exposure, reactivity under ultra-high vacuum (UHV) conditions and decomposition of lithium compounds through argon sputtering are described and used to explain previous mistakes in literature. Besides, guidelines for experimental design and data interpretation of lithium surface characterization are summarized to help others avoiding these mistakes in the future.

In the second publication, entitled: “*Storage of Lithium Metal: The Role of the Native Passivation Layer for the Anode Interface Resistance in Solid State Batteries*”, the characterization strategies and knowledge from publication 1 are used to investigate the effect of glovebox storage on the lithium surface passivation layer and the resulting impact on SSBs (see chapter 3.2).<sup>23</sup> As a basis, it is important to understand the reactivity of lithium metal towards the atmospheric gases which are the main contaminants in common gloveboxes. With the help of reactivity experiments and corresponding XPS and ToF-SIMS analytics, water traces are identified to cause the steady growth

of the lithium surface passivation film during storage. Against the other atmospheric components, lithium metal is protected by a covering passivation layer. In case the layer is damaged, complete conversion of lithium metal to  $\text{Li}_3\text{N}$  through reaction with nitrogen is identified. A growing passivation layer thickness is found to have an importantly detrimental effect on SSBs by increasing the anode interface resistance significantly. The preparation pressure of the cell and the roughness of the used  $\text{Li}_{6.25}\text{Al}_{0.25}\text{La}_3\text{Zr}_2\text{O}_{12}$  (LLZO) garnet SE also influence the determined interface resistances. Overall, the results let arise the question whether lithium metal foil can be used successfully in SSBs at all. Considering the potentially occurring surface changes and the detrimental effect of the surface film on the interface resistance, so-called “anode-free” concepts or vapor deposition of lithium on the SE appear to be more promising.

In the third publication, entitled: “*In situ Investigation of Lithium Metal - Solid Electrolyte Anode Interfaces with ToF-SIMS*”, the focus of the thesis is shifted from the lithium surface passivation layer and its impact on the SSB to the reactivity of lithium towards SEs (see chapter 3.3).<sup>24</sup> Learning from publication 2 that the passivation film on lithium foil may hinder the application in SSBs, it seems even more important to investigate the anode interphase formation through plating in anode-free cells or vapor deposition of lithium on the SE. Both concepts are mimicked in the work through *in situ* lithium plating or vapor deposition with an effusion cell on SE pellets, respectively. To complement XPS and transmission electron microscopy (TEM) analyses that are commonly reported in literature for Li|SE interphase investigation, ToF-SIMS was explored. The method is capable to provide information on the sub- $\mu\text{m}$  scale what is between the ones of XPS and TEM. In the publication, ToF-SIMS depth profiling through the described lithium layers on SE pellets is successfully used to classify the stability of Li|SE interfaces and to investigate the microstructure of forming interphases. Through combination with atomic force microscopy (AFM), additional roughness and thickness information are obtained. The experimental values reveal that previous estimations based on impedance spectroscopy underestimate the thickness of interphases between lithium and argyrodite-type SE. The more accurate values are vital to understand the interface behavior and tailor future battery concepts.

Overall, the results expand the understanding of lithium surfaces, as well as Li|SE interfaces and can help to develop SSBs with a LMA. Especially, the work highlights the importance of the lithium surface passivation layer on lithium foil, which is commonly neglected in battery research, but may be a key factor hindering the development of competitive SSBs with LMA. Additionally, the results are expected to greatly improve the understanding for lithium metal reactivity and lithium surface characterization in the battery community and in general. With the given guidelines and explanations, other researchers have a reliable basis to set out on. Furthermore, this work highlights that ToF-SIMS is a valuable technique for the characterization of Li|SE interfaces and interphases. The information which are obtained with the developed method are complementary to the prior knowledge and can help to develop new strategies for stable Li|SE interfaces.



## 2 Fundamentals

In the following, a summary of the fundamental knowledge which is important to understand this doctoral thesis is given. This includes a detailed description of the scientific context of the thesis. A special focus is set on the topic of lithium reactivity toward the atmospheric gases, which is only summarized and not elaborated in detail in the publications. However, the subject is vital to understand the formation of lithium surface reaction and passivation layers. The impact of those on SSB research is a core result of the thesis.

### 2.1 Lithium metal and its reactivity

#### 2.1.1 Properties of lithium metal

Lithium was discovered and classified as alkali metal in 1817 by the Swedish scientist August Arfvedson when analyzing the mineral petalite which is today known to be an aluminum-lithium silicate with the formula  $\text{LiAl}(\text{Si}_2\text{O}_5)_2$ . The name lithium was derived from the Greek word *lithos*, meaning stone, as the element was found in minerals and not only in plants what was thought to be the case for other alkali elements at that time. In the following decades, lithium remained only a laboratory curiosity without any industrial application, mainly because it was very difficult to prepare in pure form. It took until 1893 to develop a method for lithium preparation in practical amounts, when Guntz discovered that electrolysis of molten lithium chloride worked much better when adding potassium chloride to lower the melting point. Being available in larger amounts, lithium became also more interesting for application and its properties were studied in detail.<sup>25</sup>

Lithium is at room temperature a soft, ductile and malleable silver-white metal. Usual metallic properties of lithium are the high electronic and heat conductivities.<sup>26</sup> The atomic number of lithium is 3 and its atomic weight is 6.941 u. Naturally, two lithium isotopes occur, namely  $^6\text{Li}$  with an abundance of 7.52 at% and  $^7\text{Li}$  with an abundance of 92.48 at%.<sup>27</sup> At room temperature, lithium crystallizes in a body-centered cubic phase.<sup>28</sup>

Beside these general properties, it became soon clear that lithium is in many ways a special and extraordinary metal. Importantly, lithium is the lightest and most electropositive metal. With a density of  $0.59 \text{ g/cm}^3$ , the resulting theoretical specific coulometric capacity of lithium is 3860 mAh/g. The reduction potential versus the standard hydrogen electrode is -3.04 V. These properties make lithium attractive for the use as anode material in batteries to reach high energy density.<sup>29</sup> Disadvantageously, only 18 ppm of lithium have been detected in the earth's crust, what is a very low abundance compared to other metals.<sup>30</sup> Consequently, the amount of accessible lithium may not be sufficient to satisfy the demand. Furthermore, the production costs are relatively high in comparison to other potential anode metals like aluminum, zinc or magnesium.<sup>30</sup>

Compared to the other alkali metals, lithium is regarded as anomalous. The main reason for the unexpected properties is the relatively small size of the lithium atom. With 1.50-1.56 Å lithium has the smallest atomic radius of all metals.<sup>27</sup> Consequently also the  $\text{Li}^+$  ion, owning only 2 core electrons, exhibits an exceptionally high charge/radius ratio explaining anomalous properties of the lithium salts like stable nitride formation.<sup>31</sup> In general, lithium forms highly stable binary compounds as the single "s" electron in the outer shell is easily removed to form a positive ion. The first ionization energy of lithium is only 5.39 eV. However, lithium is exclusively monovalent, as the remaining 1s core electrons are difficult to remove. The second ionization energy of lithium is 75.64 eV.<sup>27</sup>

Even though lithium is least reactive toward the atmospheric gases in comparison to the other alkali metals, it is still highly flammable and reactive. Consequently, it does not occur as a metal in nature, instead usually only in ionic compounds such as lithium carbonate.<sup>26</sup> For the application of lithium, the high reactivity poses the problem of potentially undesired reactions and the resulting products. Thus, the reactivity of lithium toward its surrounding needs to be carefully investigated.

### 2.1.2 Reactivity of lithium toward the atmospheric gases

The atmospheric gases are very likely to come in contact with the lithium surface as they are the main contaminations during processing, transport and handling.<sup>32</sup> Therefore detailed knowledge about the interaction of lithium with the atmospheric gases is vital to understand the surface properties of lithium and accordingly the interface properties in later batteries. The first knowledge about lithium reactivity toward atmospheric gases was gained around 1900, however at this time, pure lithium was virtually unknown as working under inert atmosphere was not yet established. Starting in the 1950s, it became general knowledge that lithium needs to be handled and studied while paying attention to reactions in air and dry-box handling became common.<sup>33</sup> Therefore, the following discussion will mainly focus on work done from 1950 on. Earlier works are only mentioned as the previous interpretation the discussed studies set out on.

In general, the literature about the reactivity of lithium with the atmospheric components is inconsistent and was published from scientists working in various fields, not only on lithium for battery research. For example, lithium was regarded as potential primary coolant for nuclear fusion reactors or plasma facing surface for gettering in fusion devices.<sup>27</sup> In other studies, lithium is investigated regarding its combustion properties for potential chemical energy storage.<sup>34</sup> Accordingly, the studies to investigate the interaction of lithium with the atmospheric gases are quite differently designed and put the focus on different kinds of samples and reaction parameters. For example, while the research based on combustion puts the focus on large scale samples and quickly occurring macroscopic sample changes, the research aiming to use lithium for gettering, investigates lithium thin films and their initial reactions under UHV conditions. Consequently, the applied characterization methods are also different and able to characterize the reactions on a different scale. For instance, a slow or surface passivating reaction which is not detectable in a thermal gravimetric analysis (TGA) study where the mass gain of a big lithium chunk is followed, may be easily followed with surface sensitive techniques probing only the upmost nanometers of a sample. For battery research both kinds of experiments are interesting. However, when discussing the different studies and drawing conclusions from them, it is important to take the perspective of the authors into account. In the following this perspective will be given by writing about studies focusing on the “macroscopic scale” and those dealing with the “surface scale”.

In the next chapters, first, the reactivity of lithium toward the pure atmospheric gases is discussed, mentioning also potential effects of contaminations and mixtures with other gases. Afterwards, the reactivity in air is reviewed and finally conclusions for battery research are drawn considering the results from publication 2.

Before, the concept of Pilling-Bedworth ratios (PBRs) is introduced as it will appear in the following sections. Pilling and Bedworth described that the relative molar volume of a metal and the corresponding metal oxide indicates, whether the metal oxide forms a covering and therefore potentially protective layer on the metal.<sup>35</sup> The PBR is calculated as given in Equation 1 to classify the metal oxides regarding their protectivity.

If the calculated ratio is smaller than 1, the oxide film is porous and therefore unprotective. Consequently, the oxidation reaction is on-going. A covering and potentially protective film forms for ratios between 1 and 2, whereas a ratio larger than 2 will lead to cracking and an unprotective film. The ratio can also serve to estimate whether other compounds than oxides form covering films on a metal.<sup>36</sup> However, it should be noted that the ratios are no irrevocable proof, but a valid basis to explain the nature of a reaction layer. Besides, a covering reaction layer does not definitely protect from high reaction rates as reactive species may diffuse through quickly.

**Equation 1**

$$\text{PBR} = \frac{V_{\text{Oxide}}}{n \cdot V_{\text{Metal}}} = \frac{M_{\text{Oxide}} \cdot \rho_{\text{Metal}}}{n \cdot M_{\text{Metal}} \cdot \rho_{\text{Oxide}}}$$

$V_x$  : Molar volume of phase x

$n$  : Number of metal atoms in the formula of the oxide

$M_x$  : Molar mass of x

$\rho_x$  : Density of x

#### i. Water vapor

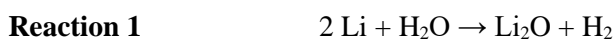
Already in 1953, Deal and Svec published their work about the kinetics of the reaction between lithium and water vapor on a macroscopic scale assuming that lithium and water react to LiOH and H<sub>2</sub>.<sup>37</sup> The authors monitored the rate of hydrogen evolution as only parameter and observed for a water vapor pressure of 29.3 to 73.3 mbar a logarithmic rate which was independent of the water vapor pressure. The authors conclude from their experiment that diffusion through the forming LiOH reaction layer is the rate determining reaction step.<sup>37</sup>

These results were complemented by Irvine et al. about 10 years later, who reported three different stages for the reaction of lithium with water vapor on the macroscopic scale.<sup>38</sup> They measured the weight gain of lithium during reaction with water using a microbalance and studied the forming reaction products with X-ray diffraction analysis (XRD). First a LiOH film is formed showing a constant growth rate. After some reaction time, LiOH·H<sub>2</sub>O starts to nucleate locally on the LiOH and grows by spreading over the outer surface. In the third stage, LiOH formation and conversion to its monohydrate take place simultaneously until full conversion of the lithium metal. As the forming LiOH·H<sub>2</sub>O is found to be porous, transport of water molecules to the inner LiOH film is possible without lattice diffusion through the reaction product layer. The LiOH film is reported to be covering without any pores or cracks, accordingly the reacting species need to diffuse through the hydroxide film. The observed rate law depends on the water partial pressure as the rate determining step changes accordingly. For pressures below 6.1 mbar, the reaction rate was pressure dependent indicating that either the transport of water through the porous LiOH·H<sub>2</sub>O or the adsorption at the LiOH interface are rate-controlling. In the pressure range from 6.1 to 16.8 mbar, a linear growth rate which is pressure independent was observed. The authors explain the observation of a linear rate with the fact that the thickness of the hydroxide film remains constant through simultaneous reaction of lithium to LiOH and sequentially LiOH to LiOH·H<sub>2</sub>O. Consequently, the diffusion distance remains constant and no logarithmic rate is observed. At high pressures (>29.3 mbar), the conversion is pressure independent and diffusion controlled as found by Deal and Svec.<sup>38</sup>

On the surface scale, the primary changes of lithium in contact with water were studied with XPS by Hoenigman et al. finding the initial formation of mostly Li<sub>2</sub>O and only little LiOH. Between 100 and 200 Langmuir (L) exposure, the LiOH signal became more prominent and indicated a second

reaction stage with increasing LiOH formation.<sup>39</sup> Full oxidation of one monolayer lithium was found for the exposure to 11-12 L water vapor.<sup>40</sup> Also in other reports about the surface changes of clean lithium surfaces in contact with water vapor, the initial formation of oxide, followed by multilayers of hydroxide and oxide mixtures, is described.<sup>41,42</sup>

In 2005, Phillips et al. summarized the previous studies about the reaction of lithium with water vapor on macroscopic and surface scale.<sup>43</sup> The authors suggested a multi-layer corrosion structure and an extended reaction sequence to explain the previous studies. First, lithium reacts with water and forms Li<sub>2</sub>O and hydrogen (Reaction 1). The oxide reacts further with water to form hydroxide (Reaction 2) which subsequently forms LiOH·H<sub>2</sub>O with additional water in case the water vapor pressure is higher than the decomposition pressure of LiOH·H<sub>2</sub>O (Reaction 3). Accordingly, they propose a third layer of Li<sub>2</sub>O under the LiOH and LiOH·H<sub>2</sub>O reaction layers described by Irvine et al.<sup>38</sup> The different rate laws which were observed experimentally are explained by the combined occurrence of the described reactions. For details the reader is referred to the described review.<sup>43</sup> In addition, Phillips et al. hypothesize based on calorimetric and spectroscopic studies that there may be additional LiH forming between Li<sub>2</sub>O and lithium (Reaction 4), as hydrogen evolution is found to be delayed at low water vapor pressure. They propose a metastable steady state situation for the growth of the reaction layer with the Li<sub>2</sub>O and LiH layers reaching constant thickness and the LiOH (as well as LiOH·H<sub>2</sub>O at higher vapor pressure) layer growing with reaction time. Even though this model incorporates all previous experimental results, the authors themselves conclude that more studies are needed to illustrate e.g. the nature of the Li<sub>2</sub>O layer. Besides, knowledge about the diffusing species is still missing.<sup>43</sup>



Later studies do not give definite answers either. Skinner et al. described in 2013 that the utmost monolayer of lithium is oxidized by 1-2 L of water vapor, what is an about 10 times higher rate than found before on the surfaces scale.<sup>44</sup> Wulfsberg et al. reported that H<sub>2</sub>O initially forms LiH and LiOH when reacting with lithium thin films, before H<sub>2</sub>O starts to physisorb. This may provide evidence that LiH is indeed part of the reaction layer as suggested by Phillips et al.<sup>43</sup> Still, the detection of LiOH instead of Li<sub>2</sub>O does not fit with the proposed reaction sequence.<sup>45</sup>

In general, all studies agree that lithium and water react on-going. The literature usually describes a covering LiOH reaction layer through which water diffuses for further reaction and indeed LiOH may form a covering layer on lithium according to its PBR of 1.26. However, some reports point out that LiOH may become brittle and develop cracks when getting thicker, leading not to diffusion but to reaction limitation and therefore a constant reaction rate.<sup>42</sup> Still, the mechanism, the kinetics and even the chemical nature of the forming reaction products are a matter of debate. This highlights the complexity for lithium-gas reactions and constitutes the uncertainty about this topic. For the reaction with water the presence of contaminations and other gases seems to be of minor importance as the point is not highlighted in literature. The other way around, water is an important catalyst and influences the reactivity toward other gases as detailed in the following sections.

## ii. Carbon dioxide

In a TGA study on lithium combustion, Markowitz et al. summarized in 1962 that no detectable reaction between lithium and carbon dioxide occurs on the macroscopic scale up to temperatures of 250 °C.<sup>33</sup> However, on the surface scale, investigating the initial interaction of lithium surfaces with carbon dioxide, a reaction was observed. For example, David et al. found a reaction in an Auger electron spectroscopy (AES) study<sup>46</sup> and Etxebarria et al. reported an oxidation of lithium metal by CO<sub>2</sub>. Still, the reaction is described as slow and even after exposure of a fresh metal surface to 1000 L of CO<sub>2</sub>, metallic lithium is detected by ultraviolet photoelectron spectroscopy (UPS).<sup>32</sup> The slow kinetics explain why the reaction cannot be followed on the macroscopic scale.

A possible explanation for the slow kinetics is the nature of the Li<sub>2</sub>CO<sub>3</sub> reaction layer. The PBR of Li<sub>2</sub>CO<sub>3</sub> on lithium is 1.34, what indicates a covering and potentially protective layer. Therefore, Li<sub>2</sub>CO<sub>3</sub> is expected to reduce further corrosion. Besides, Li<sub>2</sub>CO<sub>3</sub> is reported to be the most stable of the various reaction products between lithium and the atmospheric gases, forming a dense film protecting against further corrosion.<sup>47</sup> Also, for the reaction of lithium with CO<sub>2</sub> and O<sub>2</sub>, a thin and homogeneous coating layer is described due to the good passivation effect of Li<sub>2</sub>CO<sub>3</sub>.<sup>48</sup>

A lithium carbonate coating on lithium metal can even significantly slow down the reaction with water vapor, as Li<sub>2</sub>CO<sub>3</sub> shows low solubility in water also compared to other alkali salts.<sup>27</sup> Accordingly, Yang et al. described air-stable lithium after plating in a CO<sub>2</sub>-atmosphere. As reason for the air stability, a Li<sub>2</sub>CO<sub>3</sub> surface layer which does not react with oxygen or nitrogen and is barely soluble in water is given. Corrosion at room temperature is only reported for relative humidity levels of 70% and more. Furthermore, the carbonate surface layer does not influence the electrochemical properties significantly in comparison to pure lithium metal as Li<sub>2</sub>CO<sub>3</sub> is a decent lithium ion conductor.<sup>49</sup> With about 6 · 10<sup>-2</sup> mS · cm<sup>-1</sup> at 300 K the lithium ion conductivity of Li<sub>2</sub>CO<sub>3</sub> is in the same order as the one of some SE.<sup>50</sup> In other reports, a lithium surface with passivating Li<sub>2</sub>CO<sub>3</sub> layer after CO<sub>2</sub> exposure even showed superior cycling performance compared to lithium treated in Ar<sup>47</sup> and a Li<sub>2</sub>CO<sub>3</sub> film was reported to help maintaining a low ionic resistance of lithium anodes in liquid cells.<sup>51</sup>

In order to find out the reaction mechanism of the initial interaction between CO<sub>2</sub> and lithium, Zhuang et al. conducted an XPS study.<sup>52</sup> They suggest based on the species observed by XPS that CO<sub>2</sub> first adsorbs on the lithium surface and reacts to Li<sub>2</sub>O with lithium leaving adsorbed CO on the surface. The adsorbed CO reacts with more lithium to elemental carbon and Li<sub>2</sub>O. The Li<sub>2</sub>O is subsequently converted to Li<sub>2</sub>CO<sub>3</sub> through reaction with CO<sub>2</sub>. This reaction mechanism is shown as pathway A in Figure 1. Furthermore, the authors discuss that if carbonate is obtained without the formation of elemental carbon, the reaction requires another oxygen source like water.<sup>52</sup> Based on these results, Etxebarria et al. investigated the reaction mechanism between lithium and CO<sub>2</sub> in an ambient pressure XPS study.<sup>53</sup> They discuss the reaction sequence proposed by Zhuang et al. as one possible option, but give another mechanism as favored sequence since the determined amount of elemental carbon was too small to explain pathway A. The alternative reaction mechanism is shown as pathway B in Figure 1. After initial formation of Li<sub>2</sub>O and adsorbed CO, the two species form an oxalate intermediate with additional CO<sub>2</sub>. The intermediate then reacts to Li<sub>2</sub>CO<sub>3</sub> and CO. Continuous CO evolution is given as reason for the absence of elemental carbon formation in this pathway.<sup>53</sup> An oxalate intermediate was also proposed earlier for the reaction between alkali metals and CO<sub>2</sub> by Axelsson et al.<sup>54</sup>

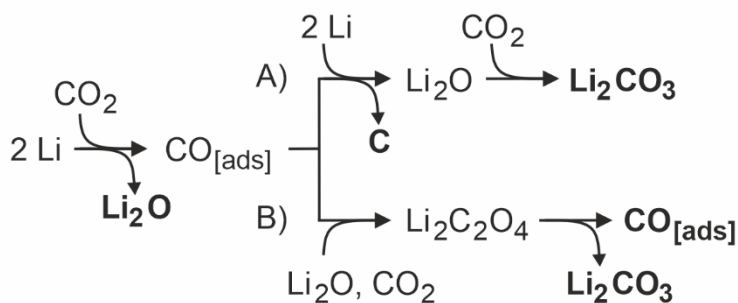


**Figure 1:** Proposed pathways for the reaction mechanism between lithium and CO<sub>2</sub>, modified according to Etxebarria et al.<sup>53</sup> who favor pathway B.

In general, Jeppson et al. noted in a report from 1978 that the purity of lithium and the materials with which it interacts play a significant role for the nature of most lithium reactions.<sup>27</sup> While the interaction with water vapor is an exception from this, the reaction of lithium with CO<sub>2</sub> is significantly influenced by other gases. For example, the presence of water may catalyze the reaction, even though the kinetics are slow compared to other wet gases.<sup>33</sup> This makes it very difficult to study the intrinsic reactivity of the pure gas toward lithium since even under UHV conditions residual gas and contaminations are present. In publication 1 of this thesis, the UHV atmosphere in the used XPS chamber was found to be responsible for pronounced changes of lithium samples within standard measurement periods.<sup>22</sup> Besides, the authors of several studies found considerable amounts of other gases in their reaction atmospheres, which will influence the results.<sup>47</sup> Also the studied lithium surfaces themselves may cause problems as they are quite differently prepared. Described preparation methods are for example scraping, lithium plating or vapor deposition where film thickness and substrate may also influence the reactivity.<sup>44,45</sup> Furthermore, impurities such as sodium segregate to the surface of lithium metal and can influence the reactivity as found by AES.<sup>55</sup>

At this point, theoretical calculations may help to answer the questions regarding reactivity and reaction products more reliably. A density function theory (DFT) study including molecular dynamics (MD) simulations indicates an interaction of lithium surfaces and CO<sub>2</sub> as well as the formation of C<sub>2</sub>O<sub>2</sub> and subsurface oxide products.<sup>56</sup> Other DFT studies also support a chemical interaction between CO<sub>2</sub> and lithium.<sup>32</sup> However, molecular simulations and computed activation barriers indicate that the reaction of pure CO<sub>2</sub> and lithium is not feasible at room temperature. Water or its reaction products with lithium are needed for the reaction.<sup>57</sup>

Overall this gives an inconclusive picture for the reactivity of lithium toward CO<sub>2</sub>. Experimental studies suggest that a thin reaction layer forms which may be beneficial in terms of corrosion prevention and electrochemical performance. Still, theoretical studies about the reaction are not conclusive whether an initial reaction between lithium metal and carbon dioxide is even possible. The experimental studies seem to have low relevance in answering this question, as contaminations and traces of other gases which may act as catalyst, cannot be avoided completely.

### iii. Oxygen

Similarly as for CO<sub>2</sub>, no detectable reaction between lithium and dry oxygen was reported on the macroscopic scale in a TGA study at temperatures up to 250 °C.<sup>33</sup> In some reports, oxygen is even regarded as an inert carrier gas for reactions with lithium.<sup>38</sup> Also, Jeppson et al. summarized the reactivity of lithium toward oxygen stating that lithium is highly resistant to oxidation and no

reaction occurs for solid lithium in dry oxygen at room temperature.<sup>27</sup> Other older, as well as recent reports which investigate the interaction of lithium and oxygen on a macroscopic scale agree that solid lithium does not react in dry oxygen at room temperature.<sup>42</sup> Some of the reports base their conclusions on irreproducible methods such as the visual impression of the lithium after air exposure.<sup>58</sup> However, taking all reports into account, the overall conclusion seems to be valid for the macroscopic scale.

As reason for the on macroscopic scale negligible reaction between lithium and oxygen, the formation of a passivating oxide film is given.<sup>59,60</sup> Still, the PBR of  $\text{Li}_2\text{O}$  on lithium is with only 0.56 importantly smaller than one and therefore indicates a porous and non-protective reaction layer. Very slow reaction kinetics may be an alternative, but unproven explanation.

For the reaction of lithium and oxygen, water may act as a catalyst and lead to reaction rates which are detectable at macroscopic scale. Schiemann et al. stated that small amounts of water vapor may catalyze the interaction and lead to an ongoing reaction.<sup>60</sup> Equally, Jeppson et al. described that as soon as moist oxygen is brought in contact with lithium, the formation of  $\text{Li}_2\text{O}$  takes place.<sup>27</sup> Even though the explanation that the presence of water breaks the oxide film<sup>59</sup> is questionable regarding the PBR of  $\text{Li}_2\text{O}$ , the overall statement that water increases the reaction rate seems accurate.

Focusing on studies investigating the reaction between lithium and oxygen with surface sensitive techniques, gives a completely different impression, as all studies describe an ongoing reaction of lithium and dry  $\text{O}_2$  to  $\text{Li}_2\text{O}$ .<sup>45,55</sup> Furthermore, the reactivity is usually defined as high and in many cases described as comparable to the one of water, even though the given rates differ.<sup>44,46</sup>

For example, Wang et al. determined a sticking coefficient of one for the reaction of a clean lithium surface and oxygen using AES and ellipsometry under UHV conditions. A 75 Å thick lithium film prepared by vapor deposition completely reacted to  $\text{Li}_2\text{O}$  with continuous reaction probability of approximately unity.<sup>61</sup> Etxebarria et al. reported complete oxidation of a lithium surface after exposure to 9 L of  $\text{O}_2$  as observed by UPS.<sup>32</sup> In an XPS study by Hoenigman et al., the authors reported a faster initial reaction for oxygen with deposited lithium metal films than for water and concluded that molecular oxygen is more reactive to lithium than water vapor.<sup>39</sup> Similarly, Zavadil and Armstrong found in an XPS, electron energy loss spectroscopy (EELS) and microgravimetry study that the reaction with  $\text{O}_2$  does not passivate a lithium surface and the reaction goes on forming a surface film of several hundreds of nanometers thickness. They found the reactivity of oxygen toward a clean lithium surface to be similar or initially even higher than for water.<sup>41</sup>

In contrast, Li et al. studied the reaction of oxygen and freshly plated lithium inside a TEM instrument, finding for dry oxygen a diffusion limitation after an initial  $\text{Li}_2\text{O}$  reaction layer had formed. If 1 mol% of  $\text{H}_2\text{O}$  is added to the reaction gas, the thickness of the reaction layer grows linearly until all lithium is consumed and the main reaction product is  $\text{LiOH}$  instead of  $\text{Li}_2\text{O}$ .<sup>62</sup> As Zavadil and Armstrong report the presence of water traces (< 1 ppm) in their  $\text{O}_2$  dosing gas what leads to additional hydroxide formation at atmospheric pressure<sup>41</sup>, the presence of contaminations and especially  $\text{H}_2\text{O}$  could be the reason for contradicting rates and the observed high reactivities. Still, for examples, Etxebarria et al. identified with XPS  $\text{Li}_2\text{O}$  as only product even after exposure of up to 1000 L  $\text{O}_2$ , what does not indicate water contamination.<sup>32</sup>

However, same as for  $\text{CO}_2$ , it seems questionable whether the described experimental studies can really answer questions about the initial reactivity between lithium and  $\text{O}_2$ . Theoretical calculations may help, yet still the available studies do not even agree if an interaction is possible. A DFT study shows that a metallic ad-layer is formed upon interaction of lithium and oxygen.<sup>56</sup> Also other DFT

simulations support an interaction of lithium and oxygen.<sup>32</sup> In contrast, based on Monte Carlo-simulations and computed activation free energies at the DFT level of theory, Shang et al. conclude that the reaction of oxygen and lithium cannot take place at room temperature, but the presence of water may catalyze the reaction.<sup>57</sup>

In summary, the studies which focus on the reaction of lithium and oxygen on a macroscopic scale all agree that the formation of reaction products is negligible. The formation of a protective oxide film is reported as reason, even though this is not in accordance with the PBR of  $\text{Li}_2\text{O}$  on lithium. In contrast, reports investigating the reaction with surface sensitive methods mostly agree that the reactivity of oxygen toward lithium is initially high. The TEM study by Li et al. may give a hint that water is responsible for the observed ongoing reactivity and the reaction between lithium and oxygen is intrinsically slow after initial oxide formation. This would also explain the results on the macroscopic scale. However, reliable theoretical calculations are needed to answer this question. So far, the available theoretical studies do not agree whether a reaction between pure lithium and oxygen is possible.

#### iv. Nitrogen

Unlike the other alkali metals, lithium forms a stable nitride, namely  $\text{Li}_3\text{N}$ . In early macroscopic studies about the reactivity of lithium and nitrogen, a reaction of lithium with dry nitrogen is only reported at elevated temperatures. This was confirmed in TGA experiments by Markowitz et al. who did not find any detectable reaction between nitrogen and lithium up to 160 °C.<sup>33</sup> Conversion to lithium nitride was only reported for wet nitrogen. The authors interpret that the nucleation of lithium nitride is quite slow, however as soon as some lithium nitride or another contamination is present, e.g.  $\text{LiOH}$  after reaction with water, further nitridation can follow even at room temperature. At low water content, the main product is  $\text{Li}_3\text{N}$ , with increasing water contamination more  $\text{LiOH}$  is detected.<sup>33</sup> Also other authors agree that lithium does not react with dry nitrogen below 160 °C<sup>27,42</sup> and that water can catalyze the reaction at room temperature. The presence of a lithium hydroxide film or water as a catalyst is regarded as necessary for the reaction with nitrogen.<sup>42</sup> Also other impurities like potassium or magnesium lead to a lithium-nitrogen reaction whereas oxygen and hydrogen in the nitrogen gas inhibit or even prevent the formation of nitride completely due to formation of protective reaction layers.<sup>42,59</sup>

These macroscopic studies may fit with some more recent studies conducted with surface sensitive methods and describing a slow reaction between lithium and nitrogen that would not be detectable on a macroscopic scale. For example, David et al. conducted an AES study, finding that  $\text{N}_2$  only slowly reacts with lithium metal surfaces, especially compared to oxygen and water.<sup>46</sup> The investigation of nitrogen interaction with freshly plated lithium inside a TEM instrument showed similar results as for oxygen. For dry nitrogen the reaction is diffusion limited after an initial and covering  $\text{Li}_3\text{N}$  reaction layer formed. If 1 mol% of  $\text{H}_2\text{O}$  is added to the reaction gas, the thickness of the reaction layer grows linearly until all lithium is consumed and the main reaction product is  $\text{LiOH}$ .<sup>62</sup>

In contrast, Jain et al. studied the reaction of lithium and nitrogen at room temperature and found that the nitridation is importantly affected by the surface properties of the metal.<sup>63</sup> They question the interpretations made previously based on weight gain studies. In their own studies using differential scanning calorimetry (DSC) they observe a reaction of dry nitrogen and lithium at room temperature and identify complete nitride formation by XRD. In addition, the authors report that a surficial oxide/hydroxide layer on the lithium passivates against further reaction with nitrogen at

room temperature. The passivated lithium starts to react with nitride at about 180 °C, what may be the reaction observed in previous reports targeting the macroscopic scale.<sup>63</sup>

Also, the PBR of 0.64 indicates a non-protective reaction layer of lithium nitride on lithium metal and contradicts the reports about a covering reaction layer leading to diffusion limitation. Accordingly,  $\text{Li}_3\text{N}$  which forms through reaction of lithium and nitrogen at room temperature was reported to be porous.<sup>64</sup>

There are also several studies which investigate  $\text{Li}_3\text{N}$  on lithium as anode coating layer in battery research to improve the electrochemical behavior of LMAs. In these cases, the  $\text{Li}_3\text{N}$  is usually formed at room temperature, for example through conversion of lithium to  $\text{Li}_3\text{N}$  in a nitrogen filled glovebox<sup>65</sup> or through other  $\text{N}_2$  gas treatment of lithium.<sup>48</sup> Even though the direct reaction of fresh lithium foil and dry  $\text{N}_2$  at room temperature is claimed, these studies cannot be used to draw reliable conclusions as contaminations are very likely and partly even reported.<sup>66</sup>

One recent study by Etxebarria et al. using UPS as surface sensitive method states that clean lithium metal cannot react with  $\text{N}_2$  at all.<sup>32</sup> Lithium metal was exposed to 1000 L of  $\text{N}_2$  and no observable changes occurred. These results are supported by DFT calculations.<sup>32</sup> Complementary, theoretical studies may be especially helpful to understand the reaction between lithium and nitrogen, as it seems to be dominated even more than for oxygen and carbon dioxide by contaminations and traces of impurities. Shang et al. also conclude based on their MD-simulations and computed DFT-activation free energies that the reaction between lithium and nitrogen cannot occur at ambient conditions. But as for the other atmospheric gases, the presence of water and its reactions products can enable the reaction.<sup>57</sup> In contrast, another density function theory study indicates initial reactivity for the interaction of lithium surfaces and nitrogen.<sup>56</sup>

Overall, the reactivity between lithium and nitrogen is the most unclear case of the atmospheric gases. Neither investigations on the macroscopic scale, nor studies using surface sensitive techniques or theoretical calculations even agree within the research field and scale whether a reaction is possible or not. The reason for the contradicting experimental reports is probably that the reaction is strongly affected by other gases, as well as contaminations. Those may on the one hand catalyze the reaction, as described for water or on the other hand, prevent it through passivating surface layers.

#### v. Air

In early reports, the reactivity of lithium in air was summarized as formation of a black nitride tarnish. However, already in 1962, Markowitz et al. started to question this interpretation.<sup>33</sup> Their findings indicate that water vapor must be crucial for the reactivity of lithium in air and that the primary reaction of lithium in the presence of wet gases is the formation of  $\text{LiOH}$  with water. Even though the authors also identify lithium nitride as reaction product in air, they suggest that the black color is caused by amorphous lithium metal viewed through a thin, transparent  $\text{LiOH}$  coating as wet Argon leads to a black coating on lithium metal, too.<sup>33</sup> In a later review from 1990, Rhein et al. reported that when lithium reacts with water in air or nitrogen atmosphere, no nitride is formed and only products of the lithium-water reaction are identified.<sup>42</sup> Additionally, lithium did not gain any weight in a TGA study during exposure to dry air. When traces of water were present, various reactions were reported to occur leading to the formation of  $\text{LiOH}$ ,  $\text{LiOH}\cdot\text{H}_2\text{O}$ ,  $\text{Li}_2\text{CO}_3$  and  $\text{Li}_3\text{N}$ .<sup>42</sup>

Also, in more recent studies, it remains a matter of debate whether  $\text{Li}_3\text{N}$  is formed upon exposure to air or not. Momma et al. deposited lithium under dry air or argon.<sup>67</sup> Under argon a surface film

composed of LiOH, Li<sub>2</sub>CO<sub>3</sub> and Li<sub>2</sub>O formed according to XPS analysis. In dry air a reaction layer consisting in addition of Li<sub>3</sub>N is formed and this treatment showed superior cycle life when the lithium was used as anode in batteries with liquid electrolyte. The authors conclude that the atmosphere for initial preparation of lithium anodes should be tuned to improve the battery performance.<sup>67</sup> Hart et al. studied in 2016 the exposure of lithium to ambient and dry air.<sup>36</sup> The authors themselves suggested that the surface of their samples is probably already covered with a surface film before they started the experiment. The mass gain of the lithium was tracked with a microbalance and showed the initial formation of LiOH and following conversion to Li<sub>2</sub>CO<sub>3</sub>. The results were also in accordance with the observed volume expansion of the lithium sample. The reaction slowed down with time and partly showed a square root behavior. If the water content of initially 44-51% relative humidity at room temperature was reduced, the reaction rate slowed down significantly.<sup>36</sup> Otero et al. studied the interaction of metallic lithium with ambient air at 50% relative humidity at room temperature and found during the first 300 s of reaction only LiOH as a reaction product using XPS and energy dispersive X-ray analysis (EDX) characterisation.<sup>68</sup> For the growth of the film they found a diffusion limitation which is attributed to the diffusion of water through the growing LiOH film.<sup>68</sup>

In summary, it is possible to conclude from these studies that water is the major factor for the reactivity of lithium in air and that the main initial product is LiOH. With longer reaction, subsequent conversion to Li<sub>2</sub>CO<sub>3</sub> was observed, what is reasonable in view of the Gibbs free energy of formation for the lithium compounds. Whether other products such as Li<sub>3</sub>N form in minor amounts remains unclear from the available literature. The previous chapters about the reactivity toward the pure gases showed that water can catalyze the reactions with O<sub>2</sub>, N<sub>2</sub> and CO<sub>2</sub>. Therefore, it seems likely that the reactions occur to a certain extent that may depend on various factors such as the relative humidity. As these factors are different for the available studies, the products are detected in only some of the experiments.

#### vi. Conclusions for battery research

Looking at all the discussed reports about the reactivity of the atmospheric gases toward lithium and their contradicting conclusions, it seems hard to understand the interactions in detail. Nevertheless, important and valuable conclusions can be drawn for battery research and the handling of lithium in general.

Firstly, the high and on-going reactivity of water toward lithium is a general agreement.<sup>43</sup> In publication 2 of this thesis it was shown that lithium covered with a thin passivation layer composed of LiOH, Li<sub>2</sub>CO<sub>3</sub> and Li<sub>2</sub>O, as well as freshly scraped lithium surfaces show high reactivity toward water.<sup>23</sup> Therefore minimizing the interaction with water is important to avoid degradation of the lithium surface, what is generally done by working in gloveboxes or dry rooms.<sup>69</sup> In gloveboxes water levels down to 0.1 ppm are achievable, what corresponds to a dewpoint of -90 °C at atmosphere pressure. For dry rooms a typical dewpoint is -60 °C, what equals 10.5 ppm of water at atmosphere pressure.

Secondly, the actual reactivity toward the other atmospheric components (oxygen, carbon dioxide and nitrogen) may be a matter of debate, still it is mostly agreed that contaminations and water residuals influence the reactions quite significantly. Even ppm traces of moisture can catalyze the reaction of lithium with all gases.<sup>70</sup> As this level of contamination cannot be avoided in gloveboxes or dry rooms, the reactivity under these conditions is more interesting for battery research than the question of initial reactivity. Experiments presented in publication 2 showed that the reactivity of

oxygen and carbon dioxide is negligible under typical glove box atmosphere.<sup>23</sup> However, nitrogen may react on-going with fresh lithium surfaces under the same conditions. Consequently, the use of nitrogen filters to control the nitrogen content in gloveboxes is important for battery research.

Last, some compounds on the lithium surface exhibit a protective effect against further corrosion. This was especially found for  $\text{Li}_2\text{CO}_3$  which is reported to even slow down the reaction with water.<sup>27</sup> In publication 2, a thin passivation layer composed of  $\text{LiOH}$ ,  $\text{Li}_2\text{CO}_3$  and  $\text{Li}_2\text{O}$  was shown to prevent the reaction with nitrogen under glovebox atmosphere.<sup>23</sup> The reactivity of lithium foil with a surface passivation layer and fresh lithium surfaces toward the atmospheric gases under glovebox conditions is schematically summarized in Figure 2. Overall, surface reaction layers can be an effective way to protect the lithium from undefined changes and are important for lithium storage and handling. However, the effect of the protective layer on the battery performance needs to be carefully considered. Accordingly, the impact and characterization of surface passivation layers on lithium metal anodes is discussed in the next chapter.

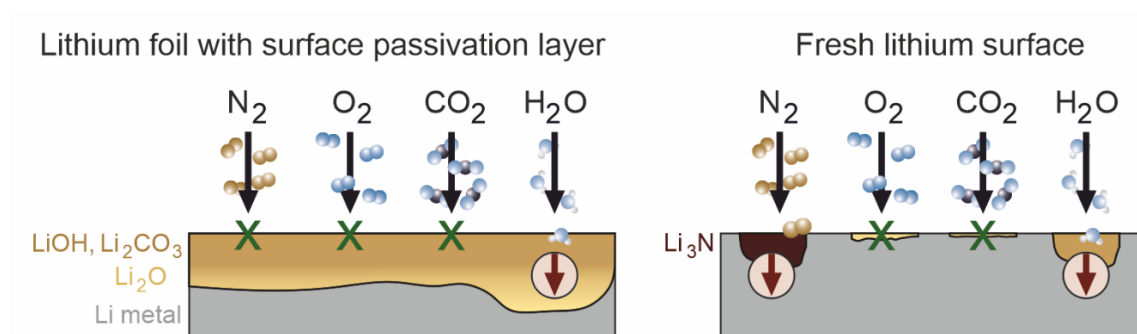


**Figure 2:** Schematic representation of the reactivity of different lithium samples under glovebox conditions.<sup>23</sup>

## 2.2 Surface passivation layers on lithium metal

### 2.2.1 Relevance of the lithium surface passivation layers for battery research

From the previous chapter it follows that a lithium metal surface will always react with residual gases and contaminations during transport, storage and handling, resulting in reaction and/or passivation layers on the surface.<sup>71</sup> To avoid undefined and uncontrolled reactions, the manufactures of lithium products apply special treatments leading to protective surface passivation layers. Schmuch et al. summarized the production of lithium metal starting with concentration of the Li-containing raw materials, which are usually brines, through evaporation and conversion to LiCl.<sup>11</sup> The next step is the electrolysis of molten LiCl to metal, followed by distillation for purification. Afterwards the final lithium product is formed, e.g. into foils by extrusion and/or rolling.<sup>11</sup> Lithium strips as thin as 250  $\mu\text{m}$  may be produced by extrusion. For lower thicknesses, which are usually required for batteries, extruded lithium cannot be produced with uniform thickness. Therefore, it is necessary to roll the lithium. As lithium sticks to metal rolls which are used for conventional rolling methods, the rolls are covered with a solid polymer such as polyethylene or polypropylene.<sup>72</sup> As a last production step, stabilization of the lithium surface through passivation by gas treatment or coating layers is applied.<sup>11</sup> Patents reveal that liquid lamination additives which ease the rolling process and passivate the lithium surface at the same time are used. Described are additives consisting of hydrocarbon segments and ester or ether links.<sup>73</sup> In other patents, P- and F-containing passivating agents<sup>74</sup>, as well as polymers<sup>75</sup> are mentioned to produce surface passivated lithium. As discussed in the previous chapter, gas treatment with  $\text{CO}_2$  leading to a  $\text{Li}_2\text{CO}_3$  passivation layer is another option to passivate the lithium metal surface.<sup>49</sup> In case lithium is produced in form of chunks, it is usually covered with heavier paraffin oils and mixtures of light hydrocarbons like benzene. In case these compounds are absolutely water-free, they can be used in contact with lithium without any corrosion.<sup>76</sup> However, in battery research lithium foils with the described surface passivation layers are mostly used.<sup>11</sup>

These surface passivation layers on commercial lithium foils are known for decades to significantly affect the battery performance.<sup>46</sup> Importantly, dendrite formation, which is one of the main problems for the use of LMAs in secondary batteries, was linked with the lithium surface chemistry in many studies. For example, Schily et al. showed that lithium deposition leading to dendrite formation is related to the nature of the surface layer.<sup>55</sup> Harry et al. found that crystalline impurities in the uncycled lithium anodes are a cause for dendrite formation.<sup>77</sup> Similarly, Maslyn et al. described that impurity particles near the lithium anode surface are nucleation points for dendrite formation and reduction of these impurities increases the cycle life importantly.<sup>78</sup> Meyerson et al. agreed that the initial surface chemistry dominates dendrite nucleation. In their study, inhomogeneously distributed organics lead to an inhomogeneous SEI which then favors dendrite formation.<sup>79</sup> Also in general, defects such as secondary phases affect the uniformity of stripping and plating during cycling of secondary batteries.<sup>80</sup> Consequently, also the surface morphology, which is additionally important for dendrite formation, is affected.<sup>81,82</sup>

Beside dendrite formation, Becking et al. demonstrated in 2017 that the lithium surface passivation layer has an important impact on the overall cell resistance of batteries with liquid electrolyte.<sup>21</sup> Through roll-pressing of the as-received lithium foil, the authors prepared a lithium foil with thinner and flatter passivation layer. The modified foil showed lower resistance in a symmetric lithium cell during the first cycles and the lithium deposition was more homogeneous than without treatment. With increasing cycle number the effect decreased.<sup>21</sup> Similarly, Wang et al. described that a freshly sliced lithium anode exhibits lower interfacial impedance and electrode overpotential in a battery

with liquid electrolyte compared to an anode with a native passivation film.<sup>83</sup> Furthermore, the results of the electrochemical measurements are more consistent when using the sliced lithium as anode.<sup>83</sup> In publication 2 of the presented work, the impact of the lithium surface passivation layer on the interfacial resistance in batteries with solid electrolyte is evaluated.<sup>23</sup> For a LLZO garnet SE with an intrinsically negligible small charge transfer resistance towards lithium<sup>84,85</sup>, a huge impact of the lithium passivation layer thickness was demonstrated and an important effect of preparation pressure and SE roughness is described as shown in Figure 3.<sup>23</sup>

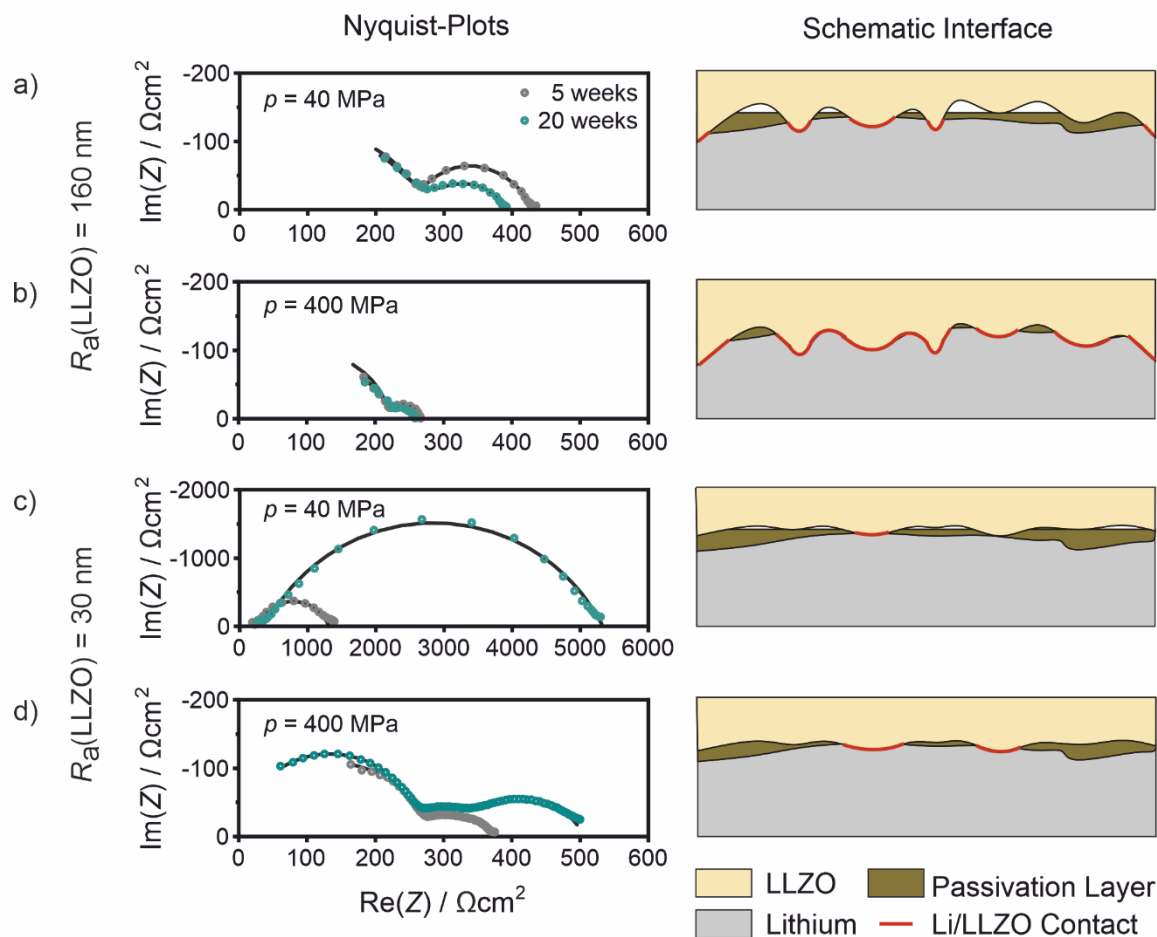


**Figure 3:** Influence of LLZO SE roughness and cell preparation pressure ( $p$ ) on the obtained Nyquist-Plots of lithium foil with different passivation layer thicknesses.<sup>23</sup> The tested lithium foils were stored for 5 or 20 weeks in closed plastic boxes in a glovebox resulting in overall passivation layer thicknesses of about 130 and 35 nm, respectively. (a) LLZO SE with an average roughness of 160 nm and cell preparation pressure of 40 MPa: No significant difference is observed for the tested lithium foil, as the SE may penetrate through both passivation layers. (b) LLZO SE with an average roughness of 160 nm and cell preparation pressure of 400 MPa: The interface contribution becomes negligible small as mostly direct Li|LLZO contact is present. (c) LLZO SE with an average roughness of 30 nm and cell preparation pressure of 40 MPa: The interface contribution is high for both lithium foils as the SE can rarely penetrate through the passivation layers. The thicker passivation layer shows an importantly higher interface contribution. (d) LLZO SE with an average roughness of 30 nm and cell preparation pressure of 400 MPa: The interface contributions become smaller for both tested lithium foils as the higher pressure leads to flattening and penetration through the passivation layers. However, for the SE with low roughness, there is still a difference present between thinner and thicker passivation layer.<sup>23</sup>

## 2.2.2 Characterization of the lithium surface passivation layer

### 2.2.2.1 Short introduction into XPS and ToF-SIMS

At this point the methods XPS and ToF-SIMS are shortly introduced to provide the reader an overview about the measurement principles and the information that are accessible with the techniques. Those readers who are familiar with the methods may skip the chapter.

#### i. XPS <sup>86</sup>

For XPS analysis, the sample is irradiated with monochromatic soft X-rays. Common X-rays sources are Mg K<sub>α</sub> (1253.6 eV) and Al K<sub>α</sub> (1486.6 eV). These photons interact with the sample atoms and cause electron emission by the photoelectric effect. Even though the X-rays penetrate μm-deep into the sample, only electrons emitted in the surface near nanometers leave the sample, as the electrons undergo inelastic energy loss processes on their way to the surface. Electrons which are emitted from deeper sample regions lose all their kinetic energy before reaching the surface. For the electrons which are emitted without loss processes, the kinetic energy (KE) is given by Equation 2.

#### Equation 2

$$KE = h\nu - BE - \Phi_s$$

$h\nu$  : Energy of the photon

BE : Binding energy of the atomic orbital from which the electron originates

$\Phi_s$  : Spectrometer work function

The KE of the electrons is measured in XPS analysis, usually by a scanning analyzer that only allows electrons within the specified energy range to pass through to the detector. To minimize the collision of the electrons with gas molecules, the samples are characterized under UHV conditions. Knowing the photon energy, as well as the spectrometer work function, the kinetic energy is used to determine the corresponding binding energy. As each element has a unique set of binding energies, XPS is capable to identify the elements in the surface region of the sample. In addition, the number of emitted electrons for an element is proportional to its concentration in the analyzed sample volume. Therefore, XPS can be used for quantification within the detection limit of about 0.1 at% and an error range of about  $\pm 5$  at%. As the binding energy of the electrons in an element is influenced by its chemical state, variations in the elemental binding energy can be used to identify the compound the electron is bound in. Combination of XPS analysis with sputtering also allows to characterize sub-surface regions and to determine the qualitative depth distribution of elements and compounds.

#### ii. ToF-SIMS <sup>87</sup>

For ToF-SIMS analysis, primary ions are accelerated to the sample surface. The bombardment induces a collision cascade leading to the emission of secondary species from the uppermost surface layers. Most of these ejected particles are neutral, but about 1% are charged secondary ions. These are not necessarily species which are present in this form in the sample. They can also result from impact-induced fragmentation and/or reaction in the gas phase. Consequently, ToF-SIMS is not inherently compound-specific. However, the characteristic fragmentation of compounds can be determined by measuring reference samples and compound-specific methods such as XPS provide additional prior knowledge for the interpretation of ToF-SIMS data.

The secondary ions are extracted by an electric field and analyzed with a ToF mass analyzer. Same as for XPS, the samples are characterized under UHV conditions, to avoid collision with gas molecules and resulting energy loss of the detected species. Other than for XPS, the signal intensity of secondary ions in ToF-SIMS analysis is not directly dependent on the concentration in the analyzed sample surface. Importantly, the signal intensity depends also on the ionization probability which is affected by the chemical matrix surrounding the corresponding element or compound. The correlation is given in Equation 3.

**Equation 3** 
$$I_s^x = I_p \cdot y_x \cdot a^\pm \cdot \Theta_x \cdot \eta$$

$I_s^x$  : Secondary ion current

$I_p$  : Primary ion current

$y_x$  : Sputter yield

$a^\pm$  : Ionization probability

$\Theta_x$  : Fractional concentration of species x

$\eta$  : Transmission of the used SIMS instrument

What is on the one hand a disadvantage, since quantification with ToF-SIMS requires time-consuming calibration and is for complex systems nearly impossible, enables on the other hand detection of trace amounts. With ToF-SIMS, detection in the ppm to ppb range is possible under favorable conditions. Other advantages of ToF-SIMS are the high lateral resolution in the sub- $\mu\text{m}$  range, as well as the high depth resolution of below 1 nm which can be achieved for depth profiles.

#### 2.2.2.2 Methods for the characterization of lithium surfaces

Considering the important influence of the lithium surface passivation layer, detailed characterization is necessary to gain knowledge about its properties and subsequently understand the performance of lithium metal anodes. However, most literature neglects the initial lithium surface status leading to the conclusion by Etxebarria et al. that the lack of knowledge about the pristine lithium anode hinders strategies for effective stabilization in secondary batteries.<sup>32</sup> In this context, the target of publication 1 of this thesis was to develop reliable surface characterization strategies for lithium metal surfaces.

In the literature, several techniques were applied to study the surface of lithium, with XPS being the most common one. On as-received lithium all authors observed only carbon, oxygen and lithium as elements with XPS. Kanamura et al. identified signals for LiOH and  $\text{Li}_2\text{CO}_3$ , as well as for hydrocarbons before argon sputtering.<sup>20</sup> After sputtering additional signals for  $\text{Li}_2\text{O}$  and  $\text{Li}_2\text{C}_2$  appeared. The authors interpret that  $\text{Li}_2\text{O}$  is present in a second layer under an upper one consisting of hydroxide and carbonate. Carbide is attributed to sputter damage.<sup>20</sup> After even longer sputter time, an additional peak was observed in the Li 1s spectrum which is attributed to lithium metal.<sup>88</sup> In general, these observations are in agreement with most other studies, only the thickness of the passivation layer is found to differ in a range of 10-100 nm.<sup>89-91</sup> Yen et al. show similar XPS spectra as the other authors, but interpret that a  $\text{Li}_2\text{O}/\text{CO}_2$  adduct is present on a  $\text{Li}_2\text{O}$  layer.<sup>92</sup> However, as shown in publication 1, comparison with XPS spectra of reference samples indicates that the presence of  $\text{Li}_2\text{CO}_3$  is more likely.<sup>22</sup> Also from a chemical point of view the presence of  $\text{Li}_2\text{CO}_3$  is expected, as it is the most stable lithium compound composed of carbon, oxygen and lithium.<sup>36</sup>

In addition to XPS, infrared spectroscopy (IR) and Raman spectroscopy are used in several studies to investigate the passivation layer on pristine lithium. Using Fourier transform infrared spectroscopy (FTIR) for untreated lithium foil, Aurbach et al. identified peaks which are typical for  $\text{Li}_2\text{CO}_3$  and a broad band which indicates the presence of  $\text{Li}_2\text{O}$  and Li-N compounds.<sup>59</sup> In other FTIR studies additional organic compounds and hydroxides were observed.<sup>93,94</sup> Using Raman spectroscopy, Schmitz et al. observed carbide and highlighted it as important contaminant on the surface of battery grade material.<sup>95</sup> To support their findings, the authors hydrolyzed lithium in water and analyzed the evolving gases by mass spectrometry. The presence of  $m/z$  26 attributed to  $\text{H}_2\text{C}_2$  is given as indicator for the presence of carbide in lithium. As origin, carbon or mild steel electrodes used during fused salt electrolysis are suggested.<sup>95</sup> However, it remains a matter of debate whether carbide is initially present on the lithium surface or only produced during the Raman spectroscopy measurement through carbonate decomposition resulting from local heating as stated by Naudin et al.<sup>94</sup>

Other techniques which are less commonly used to characterize lithium surfaces include EDX<sup>95</sup>, which can be used to study the elemental contaminations, Scanning AES<sup>93</sup> and ToF-SIMS<sup>79</sup>, which are capable to localize the surface chemistry in the sub- $\mu\text{m}$  range, as well as X-ray tomography<sup>78</sup> to visualize impurity particles near the surface and throughout the lithium metal. To study the morphology of lithium surfaces, scanning electron microscopy (SEM) and AFM are commonly used.<sup>93</sup> Surface defects and pinholes on the lithium metal surface can be visualized with SEM.<sup>92</sup> Beside the general structure and topography with grain-boundaries, ridge-lines and flat areas, the overall roughness is accessible with AFM.<sup>21,96</sup>

In conclusion, most of the available studies on lithium surface passivation layers agree on an outer carbonate and hydroxide layer of 1-20 nm thickness on top of a 10-100 nm thick  $\text{Li}_2\text{O}$  layer, as well as additional local contaminations.<sup>94</sup> This picture fits well with the reaction layer described after exposure of lithium to  $\text{CO}_2$  atmosphere.<sup>53</sup> Consequently, the lithium surface passivation through  $\text{CO}_2$  gas treatment is probably a common method in industry. Based on all these information, the combination of XPS and ToF-SIMS was chosen to develop a reliable characterization strategy for the native passivation layer on lithium surfaces.<sup>22</sup> The two methods provide complementary information and in combination all features of the lithium surface passivation layer can be characterized as shown in Figure 4.<sup>22</sup>

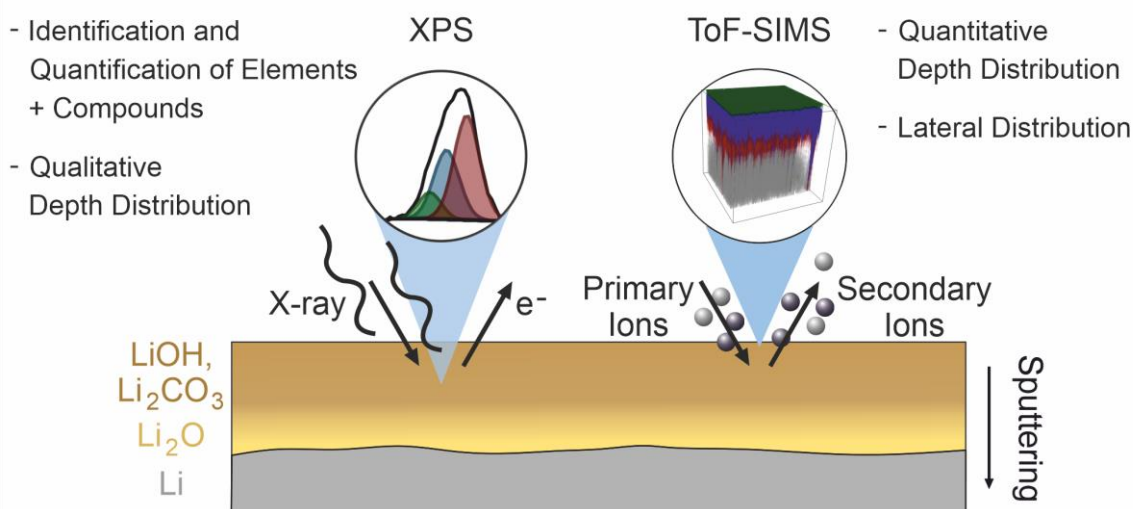


**Figure 4:** XPS and ToF-SIMS analysis of lithium metal surfaces: the provided complementary information are listed for both techniques.<sup>22</sup>

### 2.3 Lithium metal | solid electrolyte interfaces

In the previous chapters it became clear that a surface passivation layer cannot be avoided for lithium foil or exposed lithium surfaces. At the same time, the passivation film can be highly detrimental for the performance of SSBs. Accordingly, cell preparation methods which avoid lithium foil or exposed lithium surfaces may be favorable. Possible alternatives are lithium vapor deposition directly on the SE or anode-free concepts, for which lithium is chemically stored in the cathode active material (CAM) and plated during the first battery charging.<sup>97</sup> These concepts may also help to reduce costs for excess lithium, as well as cell manufacturing since the preparation of thin lithium foils is a complex and expensive process.<sup>11,98</sup> On the other hand, the problem of interphase formation may be especially critical and needs thoughtful investigation as freshly vapor deposited or plated lithium is more reactive than lithium foil with a surface passivation layer. Therefore, the following chapter deals with Li|SE interfaces and interphases, discussing their properties and characterization.

#### 2.3.1 Types of lithium metal | solid electrolyte interfaces

In order to find out whether a SE is stable in contact with lithium, the corresponding electrochemical stability window (ESW) needs to be evaluated. The ESW takes the two driving forces for a reaction between SE and lithium into account, which are the chemical and the electrochemical potential of the contacted materials.<sup>12</sup> The relationship of the two variables for lithium is given in Equation 4. Up-to-date quantum mechanical calculations can predict the position of the ESW reliably. For a rough approximation of the Li|SE stability, the electronic band gap estimation can be used. In this approach, the (electro-)chemical potential of the lithium is evaluated. In case it is higher than the lowest unoccupied molecular orbital (LUMO) of the SE, a reduction of the SE takes place.<sup>99</sup> However, the band gap approach only considers an upper limit of the ESW and may therefore be misleading in some cases.<sup>12</sup>

#### Equation 4

$$\mu_{\text{Li}} = \mu_{\text{Li}}^{\circ} - eV$$

$\mu_{\text{Li}}$  : Electrochemical potential of lithium metal

$\mu_{\text{Li}}^{\circ}$  : Chemical potential of lithium metal

$e$  : Elementary charge

$V$  : Applied voltage

In general, there are three different possibilities what may happen at the Li|SE interface as visualized in Figure 5.<sup>100</sup> The first option is a stable interface for which no reaction takes place. This is the ideal, but quite rare, case. Only few SEs are chemically and additionally in application electrochemically stable in contact with lithium.<sup>99</sup> The reason is the very low reduction potential of lithium versus the standard hydrogen electrode of  $-3.04$  V. Consequently, the SEs are mostly reduced and interphases form. If the interphase consists of ionically and electronically conductive reaction products, it is called mixed ionic-electronic conducting interphase (MCI). In this case, the reaction between lithium and SE is on-going which leads to self-discharge of the battery.<sup>101</sup> If the reaction products are ionically conductive, but electronically insulating, a kinetically stable interphase forms upon reaction. The corresponding third interface type was named kinetically stabilized solid electrolyte interphase (SEI) by Wenzel et al.<sup>101</sup> It is important to note that the electronic conductivity of materials is never zero, but may be very small. Usually interphases are named SEI if the interphase growth is regarded as negligible, which naturally depends on the

considered application and time scale. For SSBs, either a stable Li|SE interface or an interphase with low resistance is required. If this is not the case, protective films may help to stabilize the interface.<sup>5</sup>

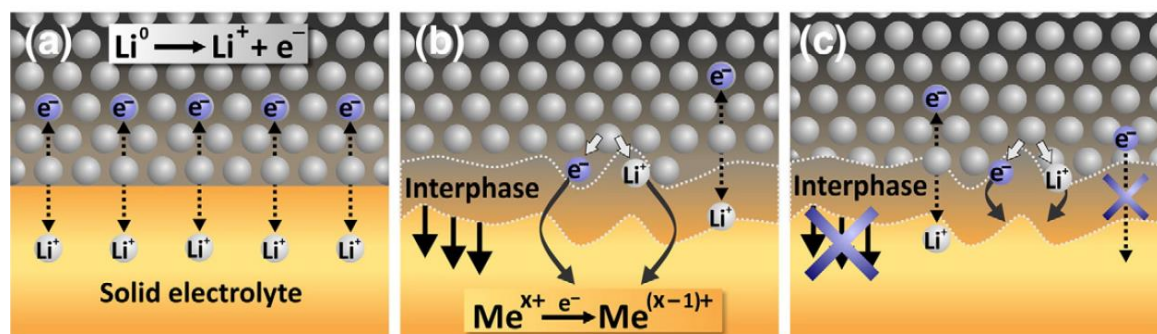


**Figure 5:** Interface types between SEs and lithium: (a) thermodynamically stable interface, (b) ionically and electronically conductive interphase (MCI) and (c) ionically conductive but electronically isolating interphase (SEI).<sup>100</sup> Reprinted with permission. Copyright © Elsevier

### 2.3.2 Characterization of lithium metal | solid electrolyte interfaces

#### i. Challenges

The biggest challenge for the characterization of Li|SE interfaces is that they are inherently buried and therefore difficult to access.<sup>14</sup> There are several strategies to make the interfaces analytically available, for example mechanical disassembling or sample preparation through various etching and sputtering techniques. However, rigid Li|SE interfaces are difficult to penetrate with most tools. Furthermore, the interfaces can be damaged during disassembly or other preparation.<sup>102</sup> Model systems can help to avoid these difficult preparation steps and lead to samples which are more appropriate for characterization. However, it is important to consider in which parts the model systems differ from the real sample. For example, Li|SE interfaces are often mimicked by depositing small amounts of lithium on SE surfaces and analyzing the resulting reaction products. For this kind of strategy, Connell and Fuchs et al. highlighted that the result critically depends on the energy impact upon characterization and interface preparation. They described this challenge for Li|LLZO interfaces.<sup>103</sup> Accordingly, the lithium deposition in model systems should imitate the deposition for real SSBs to allow meaningful conclusions. In this context, Gibson et al. emphasized that more energetic lithium deposition, such as sputter deposition, can induce interfacial mixing and surface damage which is not present for vapor deposition and plating.<sup>104</sup> As lithium vapor deposition and plating resemble actual preparation methods for SSBs, they may be more suitable to study the actual interface properties.

Another challenge is to find the analytical methods that can detect and characterize the whole interphase including the smallest concentration and dimensions of the reaction products at the interface.<sup>14</sup> A proper detection limit is required as well as sufficient spatial and depth resolution. When interpreting the results of a method, it should be kept in mind that only a certain detection range is covered and reaction products may occur outside this range.<sup>102</sup> Similarly to the challenge that one method cannot cover the entire detection range, a single analytical method can hardly provide all necessary information about a Li|SE interface.<sup>102</sup> Commonly, information about elemental concentration, chemical composition, as well as compound distribution are needed to fully understand an interface. Thus, a combination of complementary techniques is usually needed. A particular challenge for the Li|SE interface characterization is the high reactivity of the

compounds as detailed in chapter 2.1 for lithium itself.<sup>105</sup> Accordingly, samples need to be handled, transferred and analyzed under inert conditions. *In situ* and *operando* approaches can help to avoid this difficulty as the chances for contaminations are reduced. Furthermore, sample changes through the analysis itself need to be considered as many materials are sensitive to high energetic ion or electron beams.<sup>106</sup>

## ii. Methods

The most common method for investigating Li|SE interfaces is XPS.<sup>102,107–109</sup> In 2015, Wenzel et al. presented an *in situ* XPS method using the internal argon sputter gun to deposit lithium from a target on the investigated SE.<sup>100</sup> XPS analysis was performed between the deposition steps to follow the interphase growth. This strategy was used to investigate various SEs and combined with time resolved electrochemical impedance spectroscopy to follow the interphase formation in a battery.<sup>101,108,110</sup> Liu et al. investigated the stability of  $\text{Li}_2\text{S}$ ,  $\text{P}_2\text{S}_5$ ,  $\text{Li}_7\text{P}_3\text{S}_{11}$  and  $\text{Li}_2\text{P}_4\text{S}_6$  against lithium through stepwise lithium evaporation and subsequent XPS analysis to identify the decomposition products.<sup>109</sup> In another study, synchrotron-based high energy XPS was used to study the stability of  $\text{Li}_{1.5}\text{Al}_{0.5}\text{Ti}_{1.5}(\text{PO}_4)_3$  (LATP) protected against lithium with a  $\text{Li}_3\text{PO}_4$  film prepared by atomic layer deposition (ALD).<sup>111</sup> Compared to the laboratory-scale XPS analyses, synchrotron radiation allows faster measurements at higher resolution and a tunable depth sensitivity leading to the option of static depth profiling to avoid sputtering and thus potential damage.<sup>111</sup>

Still, XPS analysis alone usually does not provide sufficient information on the lateral scale, as the analytical spot size cannot be smaller than 3–5  $\mu\text{m}$  for conventional instruments. In some cases, the combination with AES, providing a lateral resolution down to tenths of nanometers, is used to overcome this limitation. For example, Wood et al. used *operando* XPS and *in situ* AES to characterize the Li| $\text{Li}_2\text{S}$ - $\text{P}_2\text{S}_5$  interphase during simulated cycling through virtual electrodes under UHV conditions.<sup>112</sup> Lithium plating/charging was mimicked with the electron gun and discharging with an ultraviolet (UV) light source.<sup>112</sup> Davis et al. studied the impact of an  $\text{Al}_2\text{O}_3$  interlayer on the degradation of  $\text{Li}_{10}\text{GeP}_2\text{S}_{12}$  (LGPS) through lithium, applying *operando* XPS, AES and *operando* optical microscopy.<sup>113</sup>

Another, by now established, technique for Li|SE interface investigations is TEM. Usually, battery materials are hard to investigate with TEM due to chemical reactivity and beam-sensitivity, but cryogenic conditions can allow the investigation of sensitive materials.<sup>106</sup> Ma et al. applied TEM to investigate the stability of cubic LLZO towards lithium metal finding a tetragonal-like LLZO interphase that prevents further interface reactions at a thickness of only about 5 unit cells.<sup>114</sup> Hood et al. used *in situ* electron microscopy to study the interaction of  $\text{Li}_{3.6}\text{PO}_{3.4}\text{N}_{0.6}$  (LiPON) with lithium metal.<sup>115</sup> The authors could show that a stable and approximately 60 nm thick interlayer forms consisting of a P-rich region towards the LiPON and a P-deficient region towards the lithium. The findings explain the extended cyclability which is achieved in SSBs with LiPON SE indicating high stability, as well as theoretical calculations indicating that LiPON reacts with lithium.<sup>115</sup>

Other applied techniques for Li|SE interface characterization are X-ray tomography, solid-state nuclear magnetic resonance (NMR) and neutron scattering techniques,<sup>116</sup> as well as theoretical methods such as computational predictions.<sup>117</sup> For more details about these methods and additional ones, the reader is referred to current reviews which provide an excellent overview.<sup>102,118,119</sup>

So far, ToF-SIMS has not been established for the characterization of Li|SE interfaces. However, the method is well suited to characterize samples on the length scale between those accessible with XPS and TEM. Also, the information provided by ToF-SIMS analysis is complementary to that

obtained by the common methods. In publication 3, ToF-SIMS is introduced as valuable technique for Li|SE interface investigation, providing information about interface stability and interphase microstructure as visualized in Figure 6.<sup>24</sup>

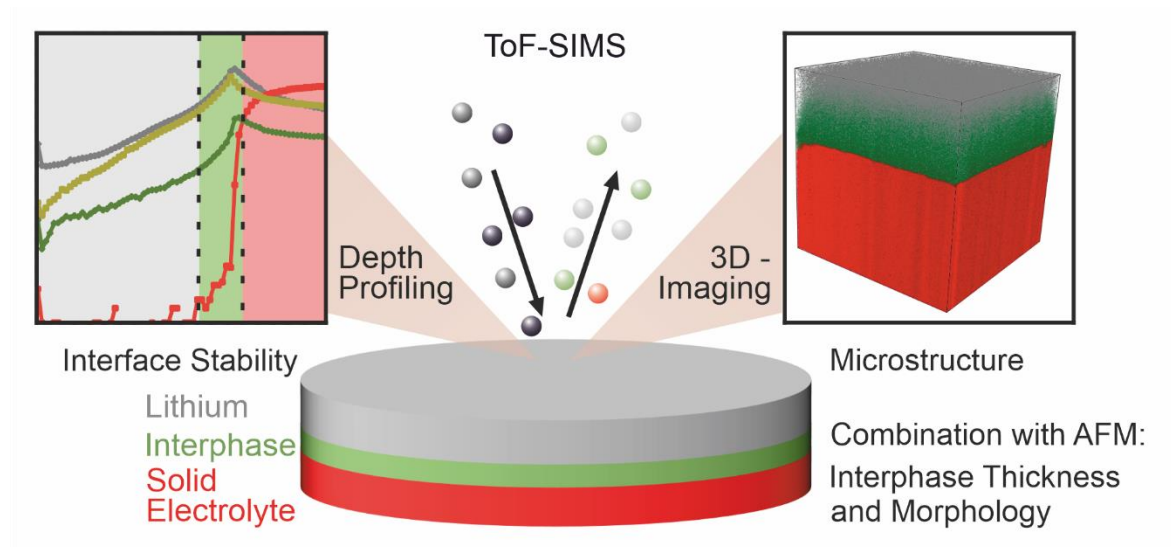


**Figure 6:** Information obtained by ToF-SIMS measurements for the characterization of Li|SE interfaces. The combination of ToF-SIMS with AFM gives additional information about the thickness and morphology of forming interphases.<sup>24</sup>

### 3 Results

When starting the work for this doctoral thesis in 2019, the presence of surface passivation layers on LMAs was widely ignored in battery research. Although a number of reports on the influence of these surface layers in batteries with liquid electrolyte demonstrated its importance, the variety of literature about LMAs and their proposed use in SSB probably detracted from the topic. In addition, there was no awareness of the protective layer on industrial produced lithium foil or the rapid formation of lithium surface reaction layers under supposedly inert conditions such as glovebox atmosphere. Falsely, commercial lithium foils, as well as polished or freshly cut surfaces were often regarded as bare lithium. This misinterpretation is favored by the very inconsistent literature about lithium reactivity towards residual gases in inert atmospheres. Therefore, the objectives of this work were to understand the formation of lithium surface passivation layers under conditions that are typical for battery research, to reliably characterize these layers and to subsequently investigate their impact on SSBs. Consequently, the characterization of the Li|SE interface was also an important part of this thesis.

In the first publication of this doctoral thesis, reliable strategies for lithium surface characterization with XPS and ToF-SIMS are presented. This includes guidelines for the characterization, as well as an explanation of pitfalls and common failures in literature. At the same time, a 3D structure of the lithium surface passivation film on commercially available lithium foils is derived from the measurements. The second publication addresses the effects of glovebox storage on the surface properties of lithium and explains the observed changes by the reactivity of lithium to atmospheric contaminants that are commonly found in gloveboxes. In addition, the impact of the lithium passivation layer growth on the anode interface resistance in SSBs is described. In the third publication, ToF-SIMS is used for systematic characterization of Li|SE interfaces. The method provides complementary information to data obtained with other established techniques, and the combination with AFM allows experimental determination of Li|SE interphase thicknesses.

#### 3.1 Publication 1: “In-Depth Characterization of Lithium-Metal Surfaces with XPS and ToF-SIMS: Toward Better Understanding of the Passivation Layer”

In publication 1 of this doctoral thesis, the characterization of lithium surfaces with XPS, ToF-SIMS and EDX was explored. Lithium foil and freshly cut lithium samples, which are often used as anodes, were studied to gain insights for battery research.

The combination of XPS and ToF-SIMS characterization revealed a complete 3D picture of the lithium surfaces with their passivation layers. For all investigated lithium samples, mostly lithium carbonate and hydroxide were identified on top of a lithium oxide rich region, which is in contact with lithium metal. Using ToF-SIMS depth profiling, the thickness of the passivation layer was found to be in the range of several nanometers for all samples, although the exact composition and thickness depend on the storage and handling conditions. Unlike previous reports on the characterization of lithium surfaces, not only experimental data were given, but also the interpretation was explained in detail to provide guidance to other researchers. In addition, pitfalls for lithium surface characterization, which led to misinterpretation in previous studies, were identified and explained. For the first time, the effect of lithium plating through electron beam exposure of electrically contacted lithium samples was described and explained. Furthermore, it was pointed out that due to the decomposition of lithium compounds by argon sputtering and the

reactivity of lithium under UHV conditions, results can only be compared for lithium samples which were analyzed under exactly the same conditions.

Overall, the results of the first publication provide a profound basis for the characterization of lithium surfaces with XPS and ToF-SIMS. Consequently, they can help to improve the quality of characterization done for these and similar kinds of samples. Furthermore, the work highlights that a surface reaction layer is present on all types of lithium used as anodes in battery research, which needs to be considered when interpreting electrochemical experiments.

The experiments for this work were designed and planned by the first author under the supervision of A. Henss and J. Janek. Y. Moryson performed the XPS measurements and analyzed the corresponding data. J. Sann supported the analyses of the XPS data. The first author performed the EDX and ToF-SIMS measurements and analyzed the data. K. Pepler and A. Henss assisted the scientific discussion of the EDX and ToF-SIMS data, respectively. The manuscript was written by the first author and edited by six co-authors.

Reprinted with permission from Otto, S.-K.; Moryson, Y.; Krauskopf, T.; Pepler, K.; Sann, J.; Janek, J.; Henss, A. In-Depth Characterization of Lithium-Metal Surfaces with XPS and ToF-SIMS: Toward Better Understanding of the Passivation Layer. *Chemistry of Materials* **2021**, *33* (3), 859–867. DOI: 10.1021/acs.chemmater.0c03518. Copyright © 2021 American Chemical Society.

# In-Depth Characterization of Lithium-Metal Surfaces with XPS and ToF-SIMS: Toward Better Understanding of the Passivation Layer

Svenja-K. Otto, Yannik Moryson, Thorben Krauskopf, Klaus Peppler, Joachim Sann, Jürgen Janek, and Anja Henss\*



Cite This: *Chem. Mater.* 2021, 33, 859–867



Read Online

ACCESS |

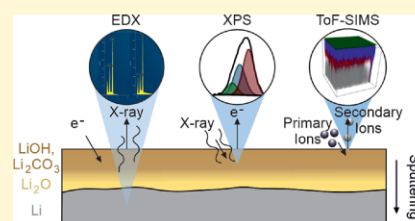
 Metrics & More

 Article Recommendations

 Supporting Information

**ABSTRACT:** To significantly increase the energy density of lithium-based batteries, the use of lithium metal as an anode is an option despite all of the associated challenges. Due to its high reactivity, lithium is covered with a passivation layer that may affect cell performance and reproducibility of electrochemical characterization. In most studies, this is ignored and lithium metal is used without considering the passivation layer and carrying out a proper characterization of the surface. Against this background, we systematically characterized various lithium samples with X-ray photoelectron spectroscopy (XPS), time-of-flight secondary-ion mass spectrometry (ToF-SIMS), and complementary energy-dispersive X-ray spectroscopy (EDX), resulting in a

complete three-dimensional chemical picture of the surface passivation layer. On all analyzed lithium samples, our measurements indicate a nanometer-thick inorganic passivation layer consisting of an outer lithium hydroxide and carbonate layer and an inner lithium oxide-rich region. The specific thickness and composition of the passivation layer depend on the treatment before use and the storage and transport conditions. Besides, we offer guidelines for experimental design and data interpretation to ensure reliable and comparable experimental conditions and results. Lithium plating through electron beam exposure on electrically contacted samples, the reactivity of freshly formed lithium metal even under ultrahigh-vacuum (UHV) conditions, and the decomposition of lithium compounds by argon sputtering are identified as serious pitfalls for reliable lithium surface characterization.



## INTRODUCTION

The challenges of electrical energy storage and electrification of transportation are the driving force behind intensive effort in the development of improved lithium-ion batteries (LIB). Widely, lithium metal is considered as a promising next-generation anode material that could meet the demand for batteries with higher energy and power density than commonly used LIBs.<sup>1</sup> Therefore, lithium-metal anodes (LMAs) have attracted extensive research interest due to its kinetics and morphology.<sup>2–4</sup> Still, the application of lithium anodes faces serious challenges and problems, such as low coulombic efficiency, morphological instability, poor cycle life, and safety issues, that have not been solved yet.<sup>5–7</sup>

In this context, a number of previous reports as well as recent papers emphasize the importance of precise knowledge on the properties of the lithium surface and its passivation layer for battery applications.<sup>8–10</sup> These reports mostly agree that the passivation layer is crucial for the cell performance, as it influences the reactivity toward the electrolyte.<sup>11–15</sup> In 2003, Naudin et al. summarized the known information in a surface passivation model, assuming an outer layer of thickness 1–20 nm composed of Li<sub>2</sub>CO<sub>3</sub> and LiOH, as well as an inner Li<sub>2</sub>O layer of thickness 10–100 nm.<sup>16</sup> Mainly, X-ray photoelectron spectroscopy (XPS), infrared (IR) spectroscopy, and Raman spectroscopy were used as analytical methods.<sup>16,17</sup> More recent

reports aim to understand the effects of the lithium passivation layer and any surface contamination in more detail. For example, Kamphaus et al. investigated the influence of Li<sub>2</sub>O, LiOH, and Li<sub>2</sub>CO<sub>3</sub> surface passivation layers on the interfacial reactivity of the LMA with XPS and ab initio molecular dynamics calculations.<sup>18</sup> Other authors studied the contamination of LMA as a possible cause of dendrite formation.<sup>19–21</sup> Becking et al. modified the surface film on lithium foils with a roll-press technique producing a foil with a thinner and flatter passivation layer, which showed superior cycling behavior.<sup>22</sup> Interesting results on the reactivity and passivation layer of lithium were also obtained in nonbattery applications, e.g., in magnetic fusion energy reactors as a blanket material or as a nuclear reactor coolant.<sup>23–26</sup> Additionally, patent specifications reveal that the surface of commercial lithium metal is commonly prepassivated to reduce corrosion during storage and to increase safety. The described methods include CO<sub>2</sub> gas treatments, wax or polymer coatings, as well as treatments with phosphorous or fluorinating

Received: September 1, 2020

Revised: January 4, 2021

Published: January 19, 2021



agents.<sup>3</sup> All of these reports complement the older model of a LiOH and Li<sub>2</sub>CO<sub>3</sub> passivation layer on top of an oxide-rich layer in contact with lithium metal, and they highlight that the chemical nature, morphology, and thickness of the LMA passivation layer influence the reactivity of lithium and the later battery cell performance. Notably, these effects are often not considered in publications targeting battery cell performance, where the LMA surface is usually not analyzed. In case the pristine lithium metal surface is characterized, design and interpretation of the analyses are often poor.

To advance the knowledge on lithium-metal surfaces, to highlight serious pitfalls of analyzing lithium-metal samples and to attract more attention to the surface state of LMAs, we present here results from systematic XPS and time-of-flight secondary-ion mass spectrometry (ToF-SIMS) analyses of various lithium samples, which are commonly used for battery applications. We reveal detailed information on the chemical nature, composition, and spatial and depth distribution of the passivation compounds. Energy-dispersive X-ray spectroscopy (EDX) is considered as an additional nondestructive method to gain more information about thicker passivation layers and bulk regions. Along with the conclusions on the composition and three-dimensional (3D) distribution of compounds in the passivation layer, this multianalytical approach reveals information about factors influencing the passivation layer and demonstrates the potential and limitations of the different techniques. We propose how the analytical techniques should be combined to achieve maximum benefit from their complementary information content. Optimized experimental design, including sample preparation, measurement options, and reference analyses, as well as data interpretation as guidelines for lithium metal surface characterization are suggested. We believe that these factors are important for the understanding of the underlying surface and degradation reactions, which is essential for the characterization, handling, and successful application of LMAs.

## EXPERIMENTAL SECTION

For highly reactive, air-sensitive samples such as lithium, reliable and reproducible characterization is specifically challenging and requires special precaution. Most importantly, samples have to be protected from undefined changes through reaction with the gas phase on the way to the analysis chamber. Therefore, sample transfer has to be performed without contact with air atmosphere, but unwanted reactions are not limited to the sample transfer and also occur inside the analysis instruments. Therefore, we prepared, transferred, and analyzed all samples which are directly compared under exactly the same conditions. All preparation and sample handling were done in a glovebox under argon atmosphere ( $p(\text{H}_2\text{O})/p < 0.1$  ppm,  $p(\text{O}_2)/p < 0.1$  ppm). As reference samples, LiOH (98 wt %), Li<sub>2</sub>O<sub>2</sub> (90 wt %), Li<sub>2</sub>CO<sub>3</sub> (99.997 wt %), Li<sub>2</sub>O (97 wt %), and LiH (95 wt %) powders (all Sigma-Aldrich) were characterized. Before analysis, the powders were either compacted in a handpress or pressed to pellets (3t, 1.5 min). Lithium foil 1 (>99.8 wt %, Albemarle Germany GmbH, former Rockwood Lithium GmbH), lithium foil 2 (>99.9 wt % Li, Honjo Metal), and slices cut from a lithium rod (99.8%, abcr GmbH) were investigated as lithium samples. They were analyzed as received (directly out of the transport packages received from the supplier) or stored in closed plastic boxes under a glovebox atmosphere before analysis.

XPS measurements were carried out with a PHI VersaProbe II instrument (ULVAC-PHI, Inc.). All samples were transferred to the instrument in an argon-filled transfer vessel. Monochromatic Al K<sub>α</sub> radiation (1486.6 eV) was used; the power of the X-ray source was 50 or 100 W, and the beam voltage was 15 or 20 kV. The examined areas were

0.03 mm<sup>2</sup> or 1 mm<sup>2</sup>. For depth profiling, Ar<sup>+</sup> ions with accelerating voltages between 1 and 4 kV were applied, using the following sputter steps: (1) surface, (2) 3 min 1 kV, (3) 8 min 2 kV, (4) 12 min 4 kV, (5) 30 min 4 kV. For the survey spectra, a pass energy of 93.9 eV, and for the detail spectra, a pass energy of 23.5 eV were used. Data evaluation was carried out with the software CasaXPS (version 2.3.18, Casa Software Ltd). All data were calibrated in relation to the signal of adventitious carbon at 284.8 eV or to the O 1s lithium oxide signal at 528.5 eV if no carbon was present. A Shirley background was used, and all spectra were fitted with a GL line shape, except the asymmetric Li metal signal, where an LF line shape was used. Lithium samples were electrically isolated with nonconductive double-sided tape (tesa) for the measurements if not stated differently.

ToF-SIMS measurements were conducted using a ToF-SIMS 5 instrument (IONTOF GmbH), which is equipped with a 25 kV Bi cluster primary-ion gun for analysis and a 20 kV gas cluster ion beam (GCIB), as well as a dual-source column with Ar<sup>+</sup> and Cs<sup>+</sup> low-energy guns for depth profiling. All samples were transferred from the glovebox to the instrument with an argon-filled Leica EM VCT500 shuttle (Leica Microsystems). Depth profiles on lithium foils were measured in spectrometry mode (bunched) and fast imaging mode (unbunched). The spectrometry mode provides a high signal intensity and a high mass resolution (40 000 cts/s, full width at half maximum, FWHM  $m/\Delta m = 5000$  @  $m/z = 17.00$  (OH<sup>-</sup>)), while the imaging mode allows better lateral resolution (<500 nm, 20/80% definition). Count rates and mass resolution are lower in imaging mode (20 000 cts/s, FWHM  $m/\Delta m = 100$  @  $m/z = 17$  (OH<sup>-</sup>)). Depth profiles in spectrometry mode were acquired with Ar<sub>1500</sub><sup>+</sup> cluster ions (10 keV, 10 nA, 300 × 300 μm<sup>2</sup>) as sputter species and Bi<sup>+</sup> (1.2 pA, 100 × 100 μm<sup>2</sup>) as primary ions. Between two sputter frames, analysis was performed after 2 s of pause time, in random raster mode, measuring two frames with 128 × 128 pixels and 1 shot/pixel. For depth profiling of the very surface, less energetic Ar<sub>1500</sub><sup>+</sup> (5 keV, 0.5 nA, 300 × 300 μm<sup>2</sup>) sputter ions and sputter steps of 5 s were used. The analysis parameters remained the same. For the depth profiles combined with analysis in imaging mode, Ar<sub>1500</sub><sup>+</sup> (10 keV, 10 nA, 500 × 500 μm<sup>2</sup>) sputter ions and Bi<sup>+</sup> (0.2 pA, 200 × 200 μm<sup>2</sup>) primary ions were used. After every sputter frame, analysis was performed with 2 s pause time, in sawtooth raster mode, measuring five frames with 1024 × 1024 pixels and 1 shot/pixel. The cycle time for all measurements was 100 μs. All measurements were carried out in positive- and negative-ion modes to compare the result. Data evaluation was carried out with the software SurfaceLab 7.0 (IONTOF GmbH). For the ToF-SIMS analyses, grounded samples without electron neutralization were measured if not stated differently.

EDX was done using a windowless XMAX EXTREME EDX detector (Oxford Instruments), which is attached to a Merlin high-resolution scanning electron microscope (SEM, Carl Zeiss AG). For sample transfer, an argon-filled Leica EM VCT500 shuttle (Leica Microsystems) was used. The electron acceleration voltage was varied between 1 and 5 kV, while the probing current was kept constant at 1 nA. EDX spectra were measured with a view field of 125 × 100 μm<sup>2</sup>, using a resolution of 1024 pixels to scan three frames (pixel dwell time, 100 μs). For each sample and electron beam energy, three measurements at different areas were taken. The software AZtec 4.3 (Oxford Instruments) was used for automatic quantification of the elements Li, C, and O in all spectra. X-ray emission depths were calculated from simulations done with the software casino.<sup>27</sup> The samples were attached to the sample holder using nonconductive double-sided tape if not stated differently.

## RESULTS AND DISCUSSION

**EDX Analysis of Lithium Foil.** To quickly obtain initial information on contaminations as well as on the element composition of the passivation layer, the lithium samples were examined nondestructively with EDX. The method was also applied to get qualitative information on the depth distribution of the different elements by varying the SEM electron acceleration voltage. A higher acceleration voltage causes deeper penetration, and X-rays are emitted out of deeper sample

regions. In Figure 1, the development of the elemental composition as a function of the acceleration voltage is shown

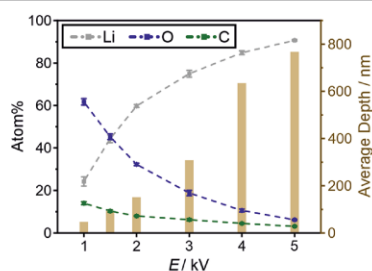


**Figure 1.** EDX static depth profile: determined atomic fractions of Li, O, and C as a function of the electron acceleration voltage for a sample of lithium foil 2 and calculated (casino) average generation depth of detected Li  $K_{\alpha}$  emission in lithium for the applied voltages.

for lithium foil 2. Since the atomic fraction of Li increases while the O and C fractions decrease with increasing acceleration voltage, the oxygen and carbon content of the lithium foil is higher in the upper region. To get an idea about the probed depths, the average emission depth of the detected Li  $K_{\alpha}$  X-rays was calculated for pure lithium metal (Figure 1) using the freeware casino.<sup>27</sup> As expected, the probed depth is much higher than with surface-sensitive techniques such as XPS and ToF-SIMS.

**XPS Depth Profiling of Lithium Foil.** With XPS, quantitative element- and compound-specific information is obtained within the detection limit of about 1 atom %. To enable the identification of different compounds with their specific binding energies, it is necessary to measure reference samples. Even though many authors have reported the binding energies for common lithium compounds, it is essential to determine the binding energies for the specific XPS instrument as the values vary due to charging.<sup>28</sup> Figure S1 shows the binding energies of the reference compounds LiOH,  $\text{Li}_2\text{CO}_3$ ,  $\text{Li}_2\text{O}$ , and  $\text{Li}_2\text{O}_2$ , as well as of that of lithium metal for our XPS measurements.

Depth profiling of the reference compounds was performed to remove the possibly contaminated surface and to evaluate the stability of the compounds against  $\text{Ar}^+$  sputtering (S1, S3). Importantly, LiOH and  $\text{Li}_2\text{CO}_3$  partly decomposed to  $\text{Li}_2\text{O}$ , which needs to be considered for the following interpretation.<sup>29,30</sup>

To complement the EDX results for the lithium samples, we performed XPS depth profiles that provide information about the probed lithium species and their qualitative depth distribution. The XPS spectra obtained for the depth profile of lithium foil 1 are shown in Figure 2a. All observed signals are in accordance with previous reports showing hydroxide and carbonate on an oxide-rich region, which is in contact with lithium metal.<sup>31–33</sup> This observation indicates a passivation bilayer on the lithium foil. A more detailed discussion is given in S2. We emphasize that the composition of the sample is changed to some extent by sputtering (see S3) and that this change must be considered when interpreting the measurement results. As a consequence, conclusions can only be drawn based on a semiquantitative comparison of different samples, as discussed for an example later in this paper. Besides, it is important to note for the interpretation of all lithium spectra that one can exclude a major fraction of lithium metal, if plasmon-loss features are not observed. This is not always taken into account in the literature and will then lead to incorrect conclusions.<sup>34</sup>

The XPS signals for the different species were fitted using area constraints, which were calculated from the relative sensitivity factors (RSF) of the elements and the stoichiometry of the compounds. Binding energy constraints were set with respect to the relative positions of the reference spectra. The profile of the calculated fractions of elements and compounds for lithium foil 1 with increasing depth is shown in Figure 2b,c. It is important to note that the shown sputter steps do not scale linearly with sputter time or even sputter depth, but were chosen to show the qualitative depth distribution of all compounds. Initially, low energy and short time were used to detect changes within the passivation layer, followed by higher energy and longer time to evaluate deeper regions of the sample.

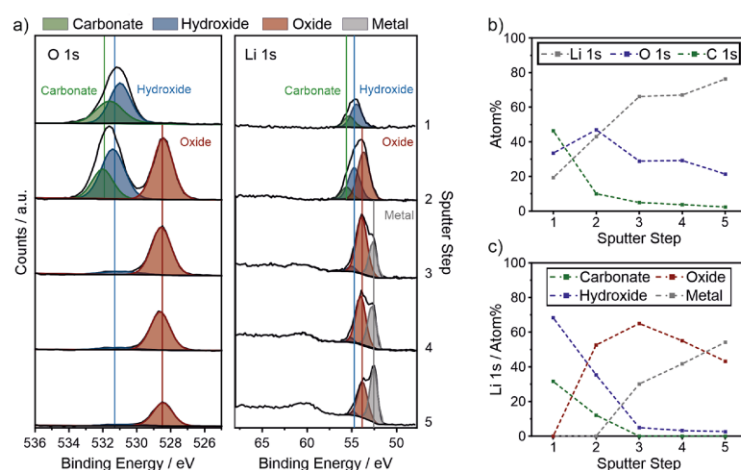


**Figure 2.** (a) O 1s and Li 1s detail spectra for the XPS depth profile of lithium foil 1 and evolution of atom fractions for (b) elements and (c) lithium compounds calculated from the depth profile. The following parameters were used as sputter steps: (1) surface, (2) 3 min 1 kV, (3) 8 min 2 kV, (4) 12 min 4 kV, (5) 30 min 4 kV.

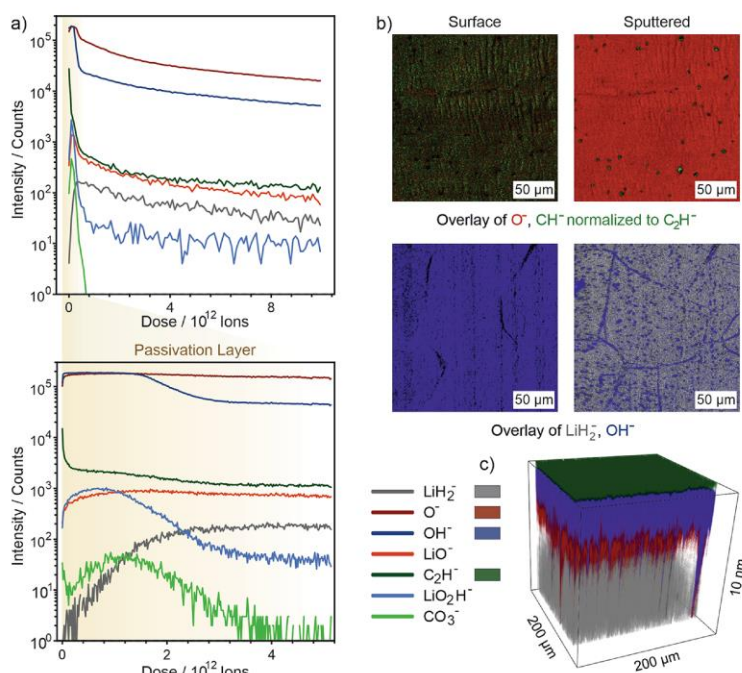


**Figure 3.** (a) ToF-SIMS depth profiles of as-received lithium foil 1 measured in spectrometry negative-ion mode. As sputter species, argon cluster ions with a size of 1500 atoms and energies of 10 or 5 kV were used to sputter deeper into the sample or to study the passivation layer in detail, respectively. (b) ToF-SIMS overlay images of lithium foil surfaces and the corresponding images after depth profiling, which show contaminations in addition to the passivation layer. (c) 3D reconstruction of a depth profile of lithium foil 1. The depth was calculated assuming a constant sputter rate of 0.50 nm/s.

**ToF-SIMS Depth Profiling of Lithium Foil.** Although the main elements, compounds, and qualitative depth distribution of the passivation layer on the lithium samples could be identified by XPS depth profiling, the lateral and depth resolutions of XPS analyses are rather low. In addition, the sensitivity toward lithium is low and hydrogen cannot be detected at all. Therefore, we applied ToF-SIMS to take advantage of its higher sensitivity, as well as of its superior lateral and depth resolution to get more information about the three-dimensional distribution of the different compounds. Due to matrix effects, the ToF-SIMS results are only semiquantitative and not inherently compound-specific. Therefore, we also investigated reference samples to identify specific secondary ions (SIs) for the different lithium compounds. The selection of the specific SIs is discussed in S4. Even by using reference spectra, the assignment of the chosen SIs for the interpretation of the depth profiles of lithium foil is not straightforward. An SI may be specific for the compound within the set of reference samples, but not in another chemical environment. Possible sources of error—besides the mentioned matrix effect—are decomposition processes, undefined contaminations, and mass interference. Therefore, all our interpretations are based on combining XPS results with signal developments in the ToF-SIMS depth profiles. In addition, we always considered groups of different SI signals rather than single SIs.

Figure 3a presents the ToF-SIMS depth profiles of a sample of lithium foil 1. The profiles match with the XPS results, showing that the passivation by oxide formation (typical SIs:  $\text{O}^-$ ,  $\text{LiO}^-$ ; Li without further note is  $^7\text{Li}$ ) reaches deeper than passivation by carbonate (typical SI:  $\text{CO}_3^-$ ) or hydroxide formation (typical SIs:  $\text{OH}^-$ ,  $\text{LiO}_2\text{H}^-$ ). This supports the picture of a bilayered

passivation structure. LiH was not identified as a component of the passivation film with XPS, but the ToF-SIMS depth profiles show an increased intensity of typical hydride SIs ( $\text{LiH}_2^-$ ) after the first sputter cycles. As discussed above, this is no unequivocal proof for the presence of LiH, but we take it as an indication of its presence. Further evaluation of typical ToF-SIMS signals of lithium compounds will be necessary to answer if LiH is a compound of the passivation layer. This will be part of future work. Interestingly, all signal intensities in the ToF-SIMS depth profiles decrease at high sputter doses. As XPS depth profiling shows increasing amounts of lithium metal with a higher sputter dose, this observation indicates that there are no SIs that are typical for lithium metal (i.e., the ionization probabilities of all SIs are lower in lithium metal than in lithium compounds). This is also the case for lithium cluster ions such as  $\text{Li}_2^-$  and  $^6\text{LiLi}^-$  or element ions like  $^6\text{Li}^-$  and  $\text{Li}^-$ . Generally, the same information as in the negative-ion mode can be extracted from depth profiles measured for positive polarity (shown in S5). However, the negative-ion mode provides more chemical information as there are less specific and meaningful signals in the positive ToF-SIMS spectra.

From the depth profile shown in Figure 3a, the thickness of the passivation layer was calculated using a sputter rate of 0.50 nm/s (see S6 for discussion of the sputter rates determined from profilometry results). The inflection points of the  $\text{OH}^-$  and  $\text{O}^-$  signals were used as indicators for the end of the upper carbonate/hydroxide and oxide passivation layers, respectively. Based on these assumptions, the upper carbonate/hydroxide passivation film is only 2 nm thick. Including the oxide-rich region, the thickness of the complete passivation layer sums up to about 3 nm. In the literature, thicknesses between tens and

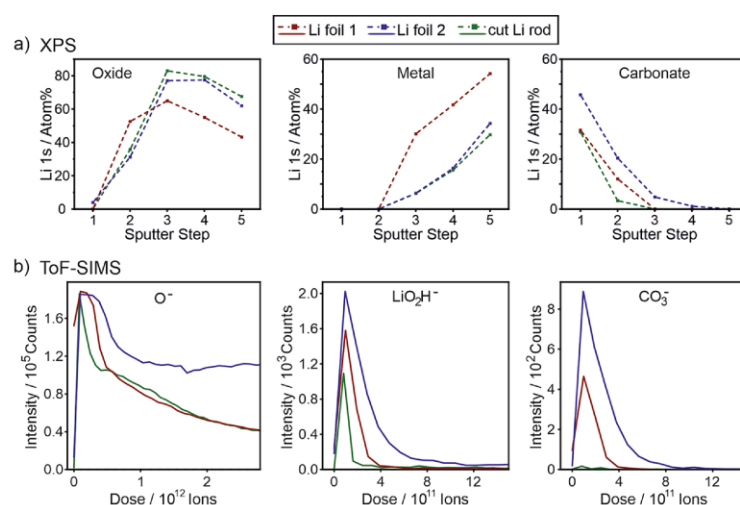


**Figure 4.** (a) Comparison of the calculated fractions of compounds for the XPS depth profiles of lithium foil 1, lithium foil 2, and sliced lithium rod. (b) ToF-SIMS depth profiles for the same lithium samples measured in spectrometry negative-ion mode. Evolution of the  $\text{O}^-$ ,  $\text{LiO}_2\text{H}^-$ , and  $\text{CO}_3^-$  signals is presented to compare the thicknesses of the oxide, hydroxide, and carbonate passivation film, respectively.

hundreds of nanometers are reported.<sup>15,16,35</sup> This wide range is surely caused by the different pretreatment and history of the analyzed lithium foils, as well as by the used methods, the experimental design, and the assumptions made for depth calibration. In comparison to the literature, especially the thickness we determined for the oxide-rich region is quite low. Also, regarding the XPS measurements that show no oxide signal before sputtering, common estimations would result at least in a thickness of 6 nm for the upper hydroxide and carbonate passivation layer. This calculation is based on an inelastic mean free path for electrons ( $\lambda$ ) of 2 nm<sup>36</sup> and 95% of the detected XPS signal coming from the depth up to  $3\lambda$ . However, several factors like surface contamination, decreasing signal intensity from growing depth, low XPS sensitivity toward lithium, and the error range of the values taken for the interpretation of XPS and ToF-SIMS measurements influence the results. Therefore, we believe that our ToF-SIMS results give a good representation of the investigated samples and show the passivation film thickness with an error range of few nanometers.

**ToF-SIMS Imaging of Lithium Foil.** To access lateral information on the passivation layer, we measured depth profiles of the lithium foils in the imaging mode. Figure 3b,c shows the overlay images and a 3D reconstruction, respectively. The raw images are presented in S7. The images show that most areas of the lithium foils were homogeneously covered by a passivation layer with the sequence indicated by the XPS and ToF-SIMS spectrometry depth profiles. In some regions, additional contaminations were detected. The contaminations were enriched in spots or lines, with the latter being most likely grain boundaries. These observations add local contaminants to the simple layered passivation model. We note that the outer sample surface is homogeneously covered with adsorbed hydrocarbons, which have to be removed by sputtering before the contaminations can be detected.

**Combined Analyses of Lithium Samples.** To find the factors influencing the lithium surface passivation film and how the effects can be investigated best with the used characterization methods, two further samples were investigated. First, a

second commercial lithium foil, which was stored longer in a closed plastic box under a glovebox atmosphere ( $p(\text{H}_2\text{O})/p < 0.1$  ppm,  $p(\text{O}_2)/p < 0.1$  ppm) before analysis (lithium foil 2), was analyzed to find the potential differences between different commercial lithium surfaces and to investigate the influence of storage. Second, a piece of a freshly sliced lithium rod was prepared to analyze a lithium surface without any commercial prepassivation. All of these samples are representatives for lithium anodes, as storage under a glovebox atmosphere and preparation of fresh lithium surfaces are common procedures in battery research. The analyses of the three samples were performed under the exact same experimental conditions to account for sample changes through the analyses themselves. Figure 4a shows the evolution of the atom fractions calculated from XPS depth profiling for all three samples. Qualitatively, the same elements (only Li, C, and O) and compounds were present on all samples. Comparing the two lithium metal foils, the calculated lithium metal fraction was always lower for lithium foil 2. Furthermore, the calculated carbonate fraction was considerably higher for foil 2 and it took more sputter time to remove all carbonate. In addition, the calculated oxide fraction increased more slowly than for lithium foil 1. As lithium foil 2 was kept longer in the glovebox before measurement than lithium foil 1, this observation could either result from different commercial prepassivation of the lithium foils or from storage. To differentiate the two factors, a piece of lithium foil 1 was measured after 2 weeks of storage in a glovebox. As lower lithium metal and higher carbonate fractions were observed, we assume that a longer storage time correlates with a thicker passivation layer, which is formed through reaction with residual gases in the glovebox. Consequently, a lower lithium metal fraction and a higher carbonate fraction may be good indicators for a thicker passivation layer, which develops in the glovebox.

The intention of analyzing a freshly sliced lithium sample was to characterize a very thin, initial passivation layer. However, the calculated lithium metal fractions were not higher for the sliced sample. Considering literature reports about freshly prepared lithium surfaces, this observation is not surprising. Lithium

metal is reported to react quickly with traces of contaminations in the glovebox, shuttle modules, and ultrahigh-vacuum (UHV) chambers.<sup>12,18,37</sup> Interestingly, the calculated carbonate fraction for the sliced sample was lower than that for lithium foil 2, while the fraction of lithium metal was similar. This observation indicates that the rapidly formed passivation layer on the freshly sliced sample had a different composition from the passivation layer on the commercial lithium foils. As lithium carbonate is reported to form relatively slowly and out of intermediates, a reduced amount on freshly sliced lithium is reasonable.<sup>24,36</sup>

Exemplary ToF-SIMS depth profiles for the three samples are shown in Figure 4b. All profiles are broadest for lithium foil 2, which indicates that the passivation layer of this sample was thickest. From the shown O<sup>-</sup> profile, a passivation layer thickness of 5 nm is estimated. The results are in accordance with the XPS analyses, which also show a qualitatively similar, but thicker passivation layer for lithium foil 2. All ToF-SIMS profiles of the sliced sample are narrower than those of the lithium foils or completely vanished as in the case of CO<sub>3</sub><sup>2-</sup>. Even though a reduced carbonate contamination fits with the XPS results, a thinner oxide and hydroxide passivation layer is not in accordance. Probably, the differences are attributed to the transport and the atmospheres in the used instruments, since sample preparation and storage were the same. As discussed above, the sliced sample was affected because the freshly prepared surface was highly reactive. The commercially prepassivated lithium foils are not as prone for reaction, which allowed a correlation of the different analyses. In addition, it is important to note that there can always be a small variance in the ToF-SIMS profiles. This is especially true for the lithium samples with a thicker passivation layer as shown in S8 for two different profiles of lithium foil 2 in comparison to one of lithium foil 1. For a quantitative evaluation, these variances need to be considered, but the qualitative conclusions discussed above are not influenced. Investigation of these samples with EDX could not add any information as much more sample volume than the several nanometer thin upper passivation was probed even at low beam energies (Figure 1). EDX may be used for the characterization of thicker passivation layers as discussed in S9.

**Lithium Plating through Electron Beam Exposure.** XPS depth profiling through Ar<sup>+</sup>-sputtering did not end at pure lithium metal for all investigated samples, but always led to a mixture of oxide and metal. Interestingly, electron beam cleaning is reported as a strategy to obtain pure lithium metal.<sup>18</sup> A closer look at the report shows that the term “electron beam cleaning” is misleading. Actually, we assume that the reported treatment rather induces an electrochemically driven mass flow of lithium toward the surface of the sample and does not lead to surface cleaning in the conventional sense. If a lithium sample with an electronically insulating passivation layer is electronically connected to the sample holder, electron beam irradiation causes a potential difference between the sample surface and the grounded sample holder. To compensate the negative charge on the surface, lithium ions migrate through the passivation layer to the surface and recombine with the excess electrons to form lithium metal. The electronically insulating passivation layer plays the same role as the separator electrolyte in a battery, and the effect is comparable to lithium plating. The difference between sputter cleaning and lithium plating is schematically shown in Figure 5. While the passivation layer is removed through sputter cleaning and a deeper region of the lithium sample is then analyzed, fresh lithium metal is plated on top of the passivation film through the electron beam exposure

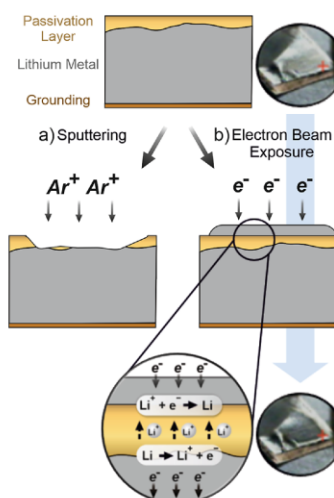


**Figure 5.** Scheme showing the difference between (a) sputter cleaning and (b) lithium plating through electron beam exposure of electrically contacted samples. XPS camera images show the sample change through lithium plating. The pictures were taken before and after 5 min of lithium plating.

and mimics a cleaned lithium foil. We induced lithium plating in the XPS instrument with the electron neutralizer on lithium foil prepared on copper tape and observed the plated lithium metal in the camera images as darker regions on the sample.

Obviously, the investigation of lithium samples in electrical contact with the grounded holder is not recommended if the electron neutralizer is used during the measurement, as lithium plating will unavoidably take place. The two potentially valid options in the case of XPS are, first, to prepare the lithium foil in electrical contact with the holder and to measure without neutralizer or, second, to isolate the sample from the holder and to use neutralization to create a floating potential. We chose the second option, because the first one bears the risk of undefined sample charging for insulating parts, as described in the literature.<sup>12</sup> Importantly, enforced lithium plating for grounded lithium samples with a passivation layer is a general problem for all measurement techniques with negatively charged probes. The effect is shown for ToF-SIMS measurements with flood gun in S10 and is discussed for EDX in S11. Still, the effect can of course be used for reactivity studies or other targeted studies, as already described in the literature.<sup>38,39</sup> For instance, Wood et al. used lithium plating enforced by the electron gun bias to investigate the SEI formation of a Li/LPS interface with XPS.<sup>39</sup>

**Sample Changes under UHV Conditions.** Even though lithium plating is unwanted during the investigation of the lithium passivation layer, it can be used to generate clean lithium metal in the XPS chamber. After a few minutes of lithium plating, fractions of about 80% lithium metal were determined, which is far more than after hours of sputter cleaning. Therefore, we used a surface prepared in situ by lithium plating to test the stability of lithium metal in the XPS instrument. Even under UHV conditions of 10<sup>-9</sup> mbar, full coverage of a sample surface with a monolayer of adsorbate is reached within approximately 1000 s (assuming an adhesion coefficient of 1). Consequently, sample changes in the analysis instruments play an important role for the interpretation of the results and must be considered. The surface changes of lithium samples in the used XPS instrument

are presented in Figure 6. Within 2 h, the calculated fraction of metal in the Li 1s region drops from 81 to 57%. At the same time,

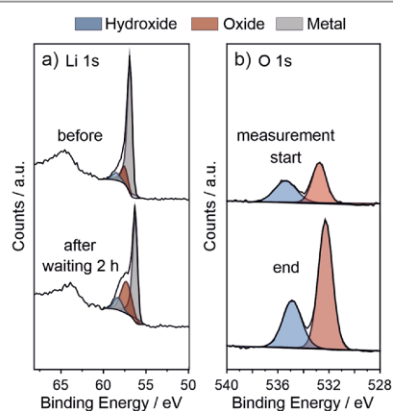


**Figure 6.** (a) Li 1s spectrum of plated lithium before and after 2 h of waiting time in the XPS instrument. (b) O 1s detail spectra taken at the start and end of one measurement cycle (XPS depth profile, sliced lithium rod). The intensity of the hydroxide and oxide peaks increases and the ratio shifts toward a higher lithium oxide fraction.

the calculated oxide fraction increases from 13 to 33% and the hydroxide fraction increases from 6 to 10%. Consequently, lithium metal reacted to oxide and hydroxide in the XPS chamber. Having in mind that measuring survey and detail spectra for the Li, C, and O 1s regions in the presented quality takes about 1 h, significant changes during measurement are expected, as also shown in Figure 6b. This demonstrates that a reliable comparison between analyses of different samples is only possible if the analyses are run under precisely the same experimental conditions regarding chamber atmosphere and measurement sequence. Even though unwanted reactions of the samples with the chamber atmosphere influence the quantitative results, qualitative relations and comparisons are valid in this case. This issue plays a non-negligible role for all (U)HV characterization techniques and was considered for all analyses discussed in this study.

## CONCLUSIONS

In this study, we use EDX, XPS, and TOF-SIMS to characterize the passivation layer on various lithium samples. We show that the passivation film of lithium samples is mainly homogeneous with additional local organic and inorganic contaminants. Our measurements indicate a bilayered structure, which is composed of a layer of hydroxide and carbonate on top of an oxide-rich region, which is in contact with lithium metal. The layers are only a few nanometers thick in the case of the investigated lithium foils. Through analysis of lithium samples with different preparation and storage histories, we found that the thickness and composition of the surface passivation layer depend on preparation, storage, and transport of the samples. It is shown that storage in a glovebox cannot fully prevent sample changes through reaction and already 2 weeks of storage may cause a thicker layer and sample inhomogeneity. Besides, even transport from the glovebox to the analysis instruments under glovebox atmosphere can lead to rapid passivation of highly reactive samples like freshly sliced lithium, while commercially repassivated lithium foils are less affected.

In addition to these results, we demonstrate the potentials and limits of EDX, XPS, and ToF-SIMS as analytical techniques for the characterization of the passivation layer on lithium samples. It is shown that a multianalytical approach is required for a comprehensive and reliable characterization of the passivation film. While XPS depth profiling provides important information about the quantitative composition and sequence of the passivation compounds, ToF-SIMS analyses add information about the passivation thickness, the sample homogeneity, and the lateral distribution of the compounds. The combined analysis gives a complete three-dimensional chemical picture of the lithium metal surfaces. Complementary, EDX measurements may provide information about thicker passivated layers and bulk contaminations.

Also, we show that the design of the measurements has a strong impact on the obtained results and can lead to unreliable data and serious misinterpretations. Importantly, we show that lithium plating occurs upon electron beam exposure of electrically contacted lithium samples, with the native passivation layer acting as a solid electrolyte. We demonstrated that surface reactions of lithium with the residual gas need to be considered even under UHV conditions, as significant changes occur within standard measurement periods. Together with the discussed decomposition of lithium compounds by argon sputtering, this observation shows that only measurements performed under exactly the same conditions are comparable. Concerning data evaluation, it is proposed that a reliable XPS fit model for compound quantification should include relative position constraints that are determined from reference samples and area constraints based on a valid physicochemical model. For the interpretation of ToF-SIMS data, it is most important to critically evaluate secondary ions that are considered as specific fragments of compounds with regard to matrix effects. Complementary XPS analyses are needed for a reliable interpretation. Overall, our work provides a guideline for robust characterization procedures that can be used to obtain reliable information on the surface composition and chemistry of lithium samples.

## ASSOCIATED CONTENT

### Supporting Information

The Supporting Information is available free of charge at <https://pubs.acs.org/doi/10.1021/acs.chemmater.0c03518>.

Characterization of reference samples with XPS, XPS depth profiles, decomposition by argon sputtering, characterization of reference samples with ToF-SIMS, ToF-SIMS depth profiling, determination of sputter rates with ToF-SIMS, ToF-SIMS imaging, variation in ToF-SIMS depth profiles, EDX analysis of lithium samples with thicker passivation layers, lithium plating through ToF-SIMS measurements, and lithium plating through EDX measurements (PDF)

## AUTHOR INFORMATION

### Corresponding Author

Anja Henss – Institute of Physical Chemistry, Justus Liebig University Giessen, D-35392 Giessen, Germany; Center for Materials Research (LaMa), Justus Liebig University Giessen, D-35392 Giessen, Germany; [orcid.org/0000-0001-5009-6512](https://orcid.org/0000-0001-5009-6512); Email: [anja.henss@phys.chemie.uni-giessen.de](mailto:anja.henss@phys.chemie.uni-giessen.de)

## Authors

Svenja-K. Otto – Institute of Physical Chemistry, Justus Liebig University Giessen, D-35392 Giessen, Germany

Yannik Moryson – Institute of Physical Chemistry, Justus Liebig University Giessen, D-35392 Giessen, Germany

Thorben Krauskopf – Institute of Physical Chemistry, Justus Liebig University Giessen, D-35392 Giessen, Germany

Klaus Pepler – Institute of Physical Chemistry, Justus Liebig University Giessen, D-35392 Giessen, Germany

Joachim Sann – Institute of Physical Chemistry, Justus Liebig University Giessen, D-35392 Giessen, Germany

Jürgen Janek – Institute of Physical Chemistry, Justus Liebig University Giessen, D-35392 Giessen, Germany; Center for Materials Research (LaMa), Justus Liebig University Giessen, D-35392 Giessen, Germany; [orcid.org/0000-0002-9221-4756](https://orcid.org/0000-0002-9221-4756)

Complete contact information is available at:

<https://pubs.acs.org/10.1021/acs.chemmater.0c03518>

## Notes

The authors declare no competing financial interest.

## ACKNOWLEDGMENTS

The authors acknowledge the financial support by the BMBF (Bundesministerium für Bildung und Forschung) within the FestBatt–Cluster of Competence for Solid-state Batteries (03XP0176D), the MaLiBa (03XP0185D), and the ProLiFest (03XP0253B) projects. T.K. and S.-K.O. acknowledge the financial support (Kékulé scholarship) by the Funds of the Chemical Industry (FCI). The authors thank Felix Walther and Sven Kayser for the very helpful discussions about data interpretation.

## REFERENCES

- (1) Janek, J.; Zeier, W. G. A solid future for battery development. *Nat. Energy* **2016**, *1*, No. 1167.
- (2) Zheng, J.; Kim, M. S.; Tu, Z.; Choudhury, S.; Tang, T.; Archer, L. A. Regulating electrodeposition morphology of lithium: towards commercially relevant secondary Li metal batteries. *Chem. Soc. Rev.* **2020**, *49*, 2701–2750.
- (3) Schmich, R.; Wagner, R.; Höppl, G.; Placke, T.; Winter, M. Performance and cost of materials for lithium-based rechargeable automotive batteries. *Nat. Energy* **2018**, *3*, 267–278.
- (4) Liand, X.; Pang, Q.; Kochetkov, I. R.; Sampere, M. S.; Huang, H.; Sun, X.; Nazar, L. F. A facile surface chemistry route to a stabilized lithium metal anode. *Nat. Energy* **2017**, *2*, 1–7.
- (5) Ahn, J.; Park, J.; Kim, J. Y.; Yoon, S.; Lee, Y. M.; Hong, S.; Lee, Y.-G.; Phatak, C.; Cho, K. Y. Insights into Lithium surface: Stable Cycling by Controlled 10- $\mu\text{m}$ -deep Surface Relief, Reinterpreting the Natural Surface Defect on Lithium Metal Anode. *ACS Appl. Energy Mater.* **2019**, *2*, S656–S664.
- (6) Cheng, X.-B.; Zhang, R.; Zhao, C.-Z.; Zhang, Q. Toward Safe Lithium Metal Anode in Rechargeable Batteries: A Review. *Chem. Rev.* **2017**, *117*, 10403–10473.
- (7) Lin, D.; Liu, Y.; Cui, Y. Reviving the lithium metal anode for high-energy batteries. *Nat. Nanotechnol.* **2017**, *12*, 194–206.
- (8) Zheng, H.; Wu, S.; Tian, R.; Xu, Z.; Zhu, H.; Duan, H.; Liu, H. Intrinsic Lithiophilicity of Li–Garnet Electrolytes Enabling High-Rate Lithium Cycling. *Adv. Funct. Mater.* **2020**, *30*, No. 1906189.
- (9) Zhou, H.; Yu, S.; Liu, H.; Liu, P. Protective coatings for lithium metal anodes: Recent progress and future perspectives. *J. Power Sources* **2020**, *450*, No. 227632.
- (10) Ryou, M.-H.; Lee, Y. M.; Lee, Y.; Winter, M.; Bieker, P. Mechanical Surface Modification of Lithium Metal: Towards Improved Li Metal Anode Performance by Directed Li Plating. *Adv. Funct. Mater.* **2015**, *25*, 834–841.
- (11) David, D. J.; Froning, M. H.; Wittberg, T. N.; Moddemann, W. E. Surface reactions of lithium with the environment. *Appl. Surf. Sci.* **1981**, *7*, 185–195.
- (12) Fujieda, T. Surface of lithium electrodes prepared in Ar + CO<sub>2</sub> gas. *J. Power Sources* **1994**, *52*, 197–200.
- (13) Schily, U.; Heitbaum, J. Surface analysis of freshly cut Li samples: Na-segregation and film forming reaction by O<sub>2</sub>, SO<sub>2</sub>, and liquid LiAlCl<sub>4</sub> · 3(SO<sub>2</sub>). *Electrochim. Acta* **1992**, *37*, 731–738.
- (14) Kanamura, K.; Tamura, H.; Shiraishi, S.; Takehara, Z.-i. Morphology and chemical compositions of surface films of lithium deposited on a Ni substrate in nonaqueous electrolytes. *J. Electroanal. Chem.* **1995**, *394*, 49–62.
- (15) Kanamura, K. XPS Analysis of Lithium Surfaces Following Immersion in Various Solvents Containing LiBF<sub>4</sub>. *J. Electrochem. Soc.* **1995**, *142*, No. 340.
- (16) Naudin, C.; Bruneel, J. L.; Chami, M.; Desbat, B.; Grondin, J.; Lassègues, J. C.; Servant, L. Characterization of the lithium surface by infrared and Raman spectroscopies. *J. Power Sources* **2003**, *124*, 518–525.
- (17) Ismail, I.; Noda, A.; Nishimoto, A.; Watanabe, M. XPS study of lithium surface after contact with lithium-salt doped polymer electrolytes. *Electrochim. Acta* **2001**, *46*, 1595–1603.
- (18) Kamphaus, E. P.; Angarita-Gomez, S.; Qin, X.; Shao, M.; Engelhard, M. H.; Mueller, K. T.; Murugesan, V.; Balbuena, P. B. Role of inorganic surface layer on solid electrolyte interphase evolution at Li-metal anodes. *ACS Appl. Mater. Interfaces* **2019**, *11*, 31467–31476.
- (19) Harry, K. J.; Hallinan, D. T.; Parkinson, D. Y.; MacDowell, A. A.; Balsara, N. P. Detection of subsurface structures underneath dendrites formed on cycled lithium metal electrodes. *Nat. Mater.* **2014**, *13*, 69.
- (20) Maslyn, J. A.; Frenck, L.; Loo, W. S.; Parkinson, D. Y.; Balsara, N. P. Extended Cycling through Rigid Block Copolymer Electrolytes Enabled by Reducing Impurities in Lithium Metal Electrodes. *ACS Appl. Energy Mater.* **2019**, *2*, 8197–8206.
- (21) Meyerson, M. L.; Sheavly, J. K.; Dolocan, A.; Griffin, M. P.; Pandit, A. H.; Rodriguez, R.; Stephens, R. M.; Vanden Bout, D. A.; Heller, A.; Mullins, C. B. The effect of local lithium surface chemistry and topography on solid electrolyte interphase composition and dendrite nucleation. *J. Mater. Chem. A* **2019**, *7*, No. 513.
- (22) Becking, J.; Gröbmeyer, A.; Kolek, M.; Rodehorst, U.; Schulze, S.; Winter, M.; Bieker, P.; Stan, M. C. Lithium-Metal Foil Surface Modification: An Effective Method to Improve the Cycling Performance of Lithium-Metal Batteries. *Adv. Mater. Interfaces* **2017**, *4*, No. 1700166.
- (23) Harilal, S. S.; Allain, J. P.; Hassanein, A.; Hendricks, M. R.; Nieto-Perez, M. Reactivity of lithium exposed graphite surface. *Appl. Surf. Sci.* **2009**, *255*, 8539–8543.
- (24) Hart, C. A.; Skinner, C. H.; Capece, A. M.; Koel, B. E. Sorption of atmospheric gases by bulk lithium metal. *J. Nucl. Mater.* **2016**, *468*, 71–77.
- (25) Jeppson, D. W. *Lithium Literature Review: Lithium's Properties and Interactions*; Hanford Engineering Development Laboratory, 1978; pp 1–80.
- (26) Rhein, R. A. *Lithium Combustion: A Review*; Ordnance Systems Department, Naval Weapons Center, 1990; pp 1–60.
- (27) Drouin, D.; Couture, A. R.; Joly, D.; Tastet, X.; Aimez, V.; Gauvin, R. CASINO V2.42: a fast and easy-to-use modeling tool for scanning electron microscopy and microanalysis users. *Scanning* **2007**, *29*, 92–101.
- (28) Wood, K. N.; Teeter, G. XPS on Li-Battery-Related Compounds: Analysis of Inorganic SEI Phases and a Methodology for Charge Correction. *ACS Appl. Energy Mater.* **2018**, *1*, 4493–4504.
- (29) Edström, K.; Herstedt, M.; Abraham, D. P. A new look at the solid electrolyte interphase on graphite anodes in Li-ion batteries. *J. Power Sources* **2006**, *153*, 380–384.
- (30) Dedryvère, R.; Laruelle, S.; Grubeon, S.; Poizot, P.; Gonbeau, D.; Tarascon, J.-M. Contribution of X-ray Photoelectron Spectroscopy to

the Study of the Electrochemical Reactivity of CoO toward Lithium. *Chem. Mater.* **2004**, *16*, 1056–1061.

(31) Kanamura, K.; Tamura, H.; Takehara, Z.-i. XPS analysis of a lithium surface immersed in propylene carbonate solution containing various salts. *J. Electroanal. Chem.* **1992**, *333*, 127–142.

(32) Kanamura, K.; Tamura, H.; Shiraiishi, S.; Takehara, Z.-i. XPS Analysis for Lithium Surface Immersed in Tetrahydrofuran Containing Various Salts. *Denki Kagaku oyobi Kogyo Butsuri Kagaku* **1993**, *61*, 1377–1382.

(33) Kanamura, K. X-Ray Photoelectron Spectroscopic Analysis and Scanning Electron Microscopic Observation of the Lithium Surface Immersed in Nonaqueous Solvents. *J. Electrochem. Soc.* **1994**, *141*, No. 2379.

(34) Tang, W.; Yin, X.; Chen, Z.; Fu, W.; Loh, K. P.; Zheng, G. W. Chemically polished lithium metal anode for high energy lithium metal batteries. *Energy Storage Mater.* **2018**, *14*, 289–296.

(35) Yen, S. P. S. Chemical and Morphological Characteristics of Lithium Electrode Surfaces. *J. Electrochem. Soc.* **1981**, *128*, No. 1434.

(36) Etxebarria, A.; Yun, D.-J.; Blum, M.; Ye, Y.; Sun, M.; Lee, K.-J.; Su, H.; Muñoz-Márquez, M. A.; Ross, P. N.; Crumlin, E. J. Revealing in situ Li metal anode surface evolution upon exposure to CO<sub>2</sub> using Ambient Pressure X-ray Photoelectron Spectroscopy. *ACS Appl. Mater. Interfaces* **2020**, *12*, 26607–26613.

(37) Li, Y.; Li, Y.; Sun, Y.; Butz, B.; Yan, K.; Koh, A. L.; Zhao, J.; Pei, A.; Cui, Y. Revealing Nanoscale Passivation and Corrosion Mechanisms of Reactive Battery Materials in Gas Environments. *Nano Lett.* **2017**, *17*, 5171–5178.

(38) He, Y.; Ren, X.; Xu, Y.; Engelhard, M. H.; Li, X.; Xiao, J.; Liu, J.; Zhang, J.-G.; Xu, W.; Wang, C. Origin of lithium whisker formation and growth under stress. *Nat. Nanotechnol.* **2019**, *14*, 1042–1047.

(39) Wood, K. N.; Steirer, K. X.; Hafner, S. E.; Ban, C.; Santhanagopalan, S.; Lee, S.-H.; Teeter, G. Operando X-ray photoelectron spectroscopy of solid electrolyte interphase formation and evolution in Li<sub>2</sub>S-P<sub>2</sub>S<sub>5</sub> solid-state electrolytes. *Nat. Commun.* **2018**, *9*, No. 2490.



### 3.2 Publication 2: “Storage of Lithium Metal: The Role of the Native Passivation Layer for the Anode Interface Resistance in Solid State Batteries”

In publication 2 of this doctoral thesis, the XPS and ToF-SIMS characterization elaborated in publication 1 was used to study lithium foil after storage in gloveboxes. The observed effects were explained by the reactivity of lithium under glovebox conditions and their impact on the anode interface resistance in SSBs was described.

It was found that storage of commercial lithium foil under glovebox conditions did neither change the compounds of the surface passivation layer nor their qualitative depth distribution. However, the thickness of the surface film increased with storage time. The storage conditions and the contamination level in the glovebox influenced the extent of the layer growth. Only sealing the lithium foil in a pouch bag was found to be effective for minimizing the changes of the foil. Since mainly the hydroxide rich region of the surface passivation film grew, it was suspected that water dominated the sample changes. Reactivity experiments with model samples, namely commercial lithium foil and freshly cut lithium surfaces, showed that water exhibited high reactivity towards both types of samples. As expected, the commercial lithium foil with its covering passivation layer was protected against reaction with all other pure atmospheric gases including  $N_2$ , what supports the assumption that residual moisture is the main factor for changes of lithium foil surfaces in gloveboxes. In contrast, the freshly cut lithium surfaces, as well as lithium foil with damaged passivation layer reacted with  $N_2$  until full conversion to  $Li_3N$ . Accordingly, the nitrogen concentration in gloveboxes is highly important when working with unprotected lithium surfaces. Oxygen and carbon dioxide only lead to very thin reaction layers.

To explore the effect of the lithium foil passivation layer for SSBs, foil with different passivation layer thickness was investigated in a model setup with LLZO SE and an ideal lithium counter electrode. It was found that the surface passivation layer can lead to extremely high interface resistances, which grow with the thickness of the layer. Importantly, the determined interface resistance mainly depends on the surface roughness of the LLZO pellet and the cell preparation pressure. A high roughness of the SE and a high preparation pressure allow the SE to penetrate through the passivation layer and thus reduce the interfacial resistance. However, a high SE roughness is detrimental in terms of homogeneous charge distribution and high preparation pressures in the range of 400 MPa are not realistic for application. Consequently, the surface passivation layer on lithium foil is an important obstacle for SSBs and alternative methods for lithium anode preparation or anode-free concepts may be favorable.

Overall, the second publication expands the knowledge on the aging of commercial lithium foil during common glovebox storage and explains the changes with the reactivity of lithium towards the atmospheric gases as residuals in the glovebox atmosphere. Furthermore, the results demonstrate that the surface passivation layer on lithium foil needs to be considered for SSBs and may even hinder the successful use of the foil.

The first author designed and planned the experiments for this work under the supervision of A. Henss and J. Janek. Y. Moryson performed the XPS measurements and analyzed the corresponding data. J. Sann supported the analyses of the XPS data. The first author performed the ToF-SIMS measurements and analyzed the data. A. Henss assisted the scientific discussion of the ToF-SIMS data. T. Fuchs and C. Lerch built the SSBs and conducted the electrochemical testing. T. Fuchs analyzed the data from electrochemical testing. The focused ion beam (FIB)-SEM measurements were performed by B. Mogwitz and the corresponding data analysis was done by the first author. The manuscript was written by the first author and edited by seven co-authors.

Reprinted with permission from Otto, S.-K.; Fuchs, T.; Moryson, Y.; Lerch, C.; Mogwitz, B.; Sann, J.; Janek, J.; Henss, A. Storage of Lithium Metal: The Role of the Native Passivation Layer for the Anode Interface Resistance in Solid State Batteries. *ACS Applied Energy Materials* **2021**, *4* (11), 12798–12807. DOI: 10.1021/acsaem.1c02481. Copyright © 2021 American Chemical Society.

# Storage of Lithium Metal: The Role of the Native Passivation Layer for the Anode Interface Resistance in Solid State Batteries

Svenja-K. Otto, Till Fuchs, Yannik Moryson, Christian Lerch, Boris Mogwitz, Joachim Sann, Jürgen Janek,\* and Anja Henss\*



Cite This: *ACS Appl. Energy Mater.* 2021, 4, 12798–12807



Read Online

ACCESS |

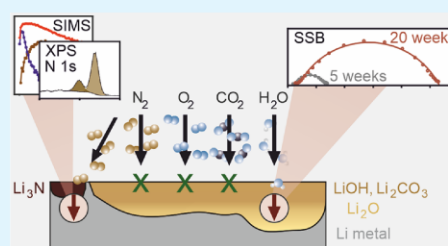
Metrics & More

Article Recommendations

Supporting Information

**ABSTRACT:** To overcome current challenges of lithium metal anodes (LMAs), which hinder their wide industrial application, the chemical composition of the lithium metal surface is an important factor. Due to its high reactivity and depending on the pre-treatment during processing, lithium is covered with a passivation layer composed of mainly  $\text{Li}_2\text{CO}_3$ ,  $\text{LiOH}$ , and  $\text{Li}_2\text{O}$ , what is mostly neglected in later electrochemical studies. Here, we investigate the effect of storage time and conditions on the surface passivation layer of commercial lithium foils, based on lithium surface characterization with X-ray photoelectron spectroscopy and time-of-flight secondary ion mass spectrometry, finding that only sealed pouch bags can prevent lithium surface changes effectively. Otherwise, the passivation layer thickness increases steadily, even in gloveboxes with a low degree of contaminations. Testing the stored lithium foils in solid-state batteries with LLZO as model solid electrolyte, it is demonstrated that the solid electrolyte roughness and the applied pressure have a huge impact on the obtained impedance. While the passivation layer has no major effect on the interface resistance with a rough LLZO pellet and at high pressure, it clearly affects the interface resistance with smoother LLZO surfaces and at lower pressure. Consequently, the lithium passivation layer may hinder the application of the LMA in a solid-state battery what we discuss in depth. By reactivity experiments with model lithium surfaces, we show that water residuals are the main reason for the aging of lithium foil in gloveboxes. Additionally, nitrogen reacts with fresh lithium surfaces and lithium foils with an incomplete or damaged passivation layer. The results demonstrate that storage conditions are important factors for the surface state of lithium metal and consequently for the application as an anode material.

**KEYWORDS:** lithium metal anode, native passivation layer, interface resistance, solid state batteries, lithium metal reactivity, glovebox storage



## INTRODUCTION

To meet the demand for batteries with higher energy density, systems with a lithium metal anode (LMA) are promising, as they can potentially provide a more than 10 times higher specific capacity than the graphite anodes used in most of the current commercial systems.<sup>1,2</sup> Yet, the wide industrial application of lithium metal in batteries is still hindered by severe problems such as lithium loss, dendrite formation and the need for a high stack pressure.<sup>3</sup> One important factor to better understand and overcome these issues is the precise knowledge of the chemical state and morphology of the lithium metal surface.<sup>4</sup> Therefore, recent research often focuses on the modification of the LMA surface to improve their reversibility, morphological stability and rate performance.<sup>5–7</sup> Interestingly, most studies neglect that lithium metal is inherently covered by a passivation layer, whose composition, thickness, morphology, and homogeneity are crucial for the resulting performance.<sup>8–12</sup> For example, Becking et al. showed that mechanical flattening and thinning of the native passivation layer on a lithium metal foil leads to improved

cycling behaviour.<sup>8</sup> Etzbarria et al. reported that lithium with similar purity purchased from different suppliers shows limited reproducibility with up to 7% variation in the measured capacity.<sup>13</sup> Accordingly, the authors emphasize the need for controlled pre-passivation and functionalization of lithium anode surfaces.<sup>13</sup>

On the route to a proper chemical characterization of the lithium passivation layer, we recently demonstrated how to reliably apply and combine X-ray photoelectron spectroscopy (XPS) and time-of-flight secondary ion mass spectrometry (ToF-SIMS) as surface sensitive methods.<sup>14</sup> The results indicate in general agreement with older reports an inorganic passivation layer composed of  $\text{LiOH}$  and  $\text{Li}_2\text{CO}_3$  on top of

Received: August 16, 2021

Accepted: October 28, 2021

Published: November 10, 2021



Li<sub>2</sub>O as main components with a thickness of several nanometers for all analyzed lithium samples.<sup>15–17</sup> The composition of the passivation layer depends on the sample treatment, as well as the storage and transport conditions. Only two weeks of storage in a glovebox leads to a more inhomogeneous and almost doubled passivation film thickness on commercial lithium metal foil.<sup>14</sup> As storage is unavoidable for the work with a lithium foil, at least in the academic domain, we aim to explore and understand the effects of storage and especially its impact on the electrochemical performance in more detail.

In general, atmospheric gases such as nitrogen, oxygen, water, and carbon dioxide are residues in the usual argon atmosphere in gloveboxes and are the main components that come into contact with the lithium metal surfaces during storage or during processing. Therefore, the reactivity toward these components will be mainly responsible for aging during storage and reactions during processing. There are reports about the reactivity of lithium toward atmospheric gases dating back beyond the 1960s.<sup>18–24</sup> While all these reports agree on a high reactivity of lithium toward water, the results presented so far on the reactivity toward other atmospheric gases are quite contradicting—probably due to different levels of humidity in the individual studies. For example, some authors report a high reaction rate for clean lithium surfaces with oxygen,<sup>25,26</sup> while others describe the reactivity of lithium toward oxygen as negligible and even consider oxygen as an inert gas.<sup>18,19</sup> Some recent publications discuss and try to overcome these contradictions; however, without entirely answering all open questions such as the inherent reactivity of nitrogen toward lithium conclusively.<sup>13,27</sup>

In view of the incomplete and partly contradictory picture of the lithium metal surface, it is an important question of practical relevance, how typical storage and processing steps influence the lithium metal passivation layer and the resulting anode and cell properties. To answer this question, this study describes the influence of different storage conditions on the lithium passivation layer on commercial lithium foils and quantifies the influence of storage by XPS and ToF-SIMS characterization. The interface resistance of the lithium foils is tested in a model solid-state battery (SSB) and the results are interpreted in terms of the state of the lithium metal surface. The observed sample changes are explained with the reactivity of lithium model samples. Overall, the results are valuable for the general understanding, control, and reduction of lithium metal reactivity with the processing environment and the impact for the use as anode in solid state cells.

## ■ EXPERIMENTAL SECTION

Commercial lithium foil (>99.9 wt % Li, Honjo Metal) was stored in three different gloveboxes under an argon atmosphere: glovebox 1— $p(\text{H}_2\text{O}$  and  $\text{O}_2)/p$  of about 1 ppm and variations up to 10 ppm, glovebox 2— $p(\text{H}_2\text{O}$  and  $\text{O}_2)/p < 0.1$  ppm and variations of up to 1 ppm, and glovebox 3— $p(\text{H}_2\text{O}$  and  $\text{O}_2)/p < 0.1$  ppm and variations of up to 3 ppm,  $p(\text{N}_2)/p$  about 1 ppm. The storage time was 2, 5, 10, or 20 weeks. As storage conditions, storage in open boxes (direct exposure to the glovebox atmosphere and its variations), storage in closed plastic boxes, in closed plastic boxes with additional sealing in a pouch bag, and storage in the original transport package (metal box and sealed pouch bag) were tested. Fresh lithium surfaces for exposure to pure atmospheric gases or glovebox atmosphere were prepared by slicing a lithium rod (99.8%, abcr GmbH). Please find an overview of all lithium samples in Supporting Information 1. All

samples which are directly compared were prepared, transferred, and analyzed under exactly the same conditions.

XPS measurements were conducted with a PHI VersaProbe II instrument (ULVAC-PHI, Inc.). All samples were transferred to the instrument in an argon-filled transfer vessel. Monochromatic Al K<sub>α</sub> radiation (1486.6 eV) was used; the power of the X-ray source was 100 W and the beam voltage was 20 kV (high power mode). The examined areas had a size of 0.13 mm<sup>2</sup>. Charge neutralization was carried out with the electron and ion guns. For depth profiling, Ar<sup>+</sup> ions with accelerating voltages between 1 kV and 4 kV were applied as sputter species, using the following analysis steps: (1) before sputtering, (2) 3 min 1 kV, (3) 8 min 2 kV, (4) 5 min 4 kV, (5) 10 min 4 kV, (6) 15 min 4 kV, (7) 20 min 4 kV, (8) 25 min 4 kV, and (9) 30 min 4 kV. For the survey spectra, a pass energy of 93.9 eV and for the detail spectra a pass energy of 23.5 eV was used. Data were analyzed with the software CasaXPS (version 2.3.18, Casa Software Ltd). All data were calibrated relative to the signal of adventitious carbon at 284.8 eV or to the O 1s lithium oxide signal at 531.46 eV, if no carbon was present. A Shirley background was used and all spectra were fitted with a GL line shape, except for the asymmetric Li metal signal, where a LF line shape was used. Lithium samples were electrically isolated with non-conductive double-sided tape (tesa) for the measurements.

ToF-SIMS measurements were carried out using a ToF-SIMS 5 instrument (IONTOF GmbH), which is equipped with a 20 kV gas cluster ion beam (GCIB) for depth profiling and a 25 kV Bi cluster primary-ion gun for analysis. All samples were transferred from the gloveboxes to the instrument with an argon-filled Leica EMVCT500 shuttle (Leica Microsystems). Depth profiles of the lithium samples were measured in spectrometry mode [bunched, 40 000 cts/s, full width at half maximum, FWHM  $m/\Delta m = 5000@m/z = 17.00$  (OH<sup>-</sup>)] and were acquired with Ar<sub>1500</sub><sup>+</sup> cluster ions (10 keV, 10 nA,  $300 \times 300 \mu\text{m}^2$ ) as sputter species and Bi<sup>+</sup> ( $1.2 \text{ pA}$ ,  $100 \times 100 \mu\text{m}^2$ ) as primary ions. Between two sputter frames, analysis was performed after 2 s of pause time, in random raster mode, measuring two frames with  $128 \times 128$  pixels and 1 shot/pixel. The cycle time for all measurements was 100 μs. All measurements were carried out in negative-ion mode. Data evaluation was carried out with the software SurfaceLab 7.2 (IONTOF GmbH). For the ToF-SIMS analyses, the lithium samples were electrically isolated with a non-conductive double-sided tape (tesa). For charge neutralization, a flood gun with an energy of 21 eV and a current of 10 μA was used. To estimate the thickness of the passivation layer from the ToF-SIMS depth profiles, the turning points of the LiO<sub>2</sub>H<sub>2</sub><sup>-</sup> and LiO<sup>-</sup> signals were used to define the end of the hydroxide and oxide rich regions, respectively. Carbonate signals were most intense on the very surface of the samples, but the intensity dropped quickly and remained approximately stable within the region of high LiO<sub>2</sub>H<sub>2</sub><sup>-</sup> signal intensity. For the estimation, we neglected these changes and used an average sputter yield of lithium hydroxide and carbonate for thickness calculation (32.4 atoms/ions) for the hydroxide rich region. From the fluence until the turning point of the LiO<sup>-</sup> signal, the one for the LiO<sub>2</sub>H<sub>2</sub><sup>-</sup> signal was subtracted. The remaining fluence was converted into a layer thickness of the oxide rich region using the sputter yield of lithium oxide (13.7 atoms/ions). The overall thickness of the passivation layer is calculated as the sum of the two regions.

The nominal composition of the herein prepared garnet solid electrolyte (SE), based on the used precursors, was Li<sub>6.25</sub>Al<sub>0.25</sub>La<sub>3</sub>Zr<sub>7</sub>O<sub>12</sub> (LLZO). First, ZrO<sub>2</sub> (99.9%, Sigma-Aldrich), La(OH)<sub>3</sub> (99.9%, Sigma-Aldrich), Li<sub>2</sub>CO<sub>3</sub> (>99.0%, Sigma-Aldrich), and Al<sub>2</sub>O<sub>3</sub> (99.8%, abcr) were homogenized in a planetary ball mill. Subsequent calcination was carried out in MgO crucibles under an oxygen flow (150 sccm) at 1000 °C for 4 h. The following steps were exclusively performed in an argon environment (MBraun, glovebox 2). Sintering of pellets was carried out at 1230 °C for 4 h under 150 sccm of oxygen flow. For a detailed description, the reader is referred to previous literature on LLZO.<sup>28</sup>

Cells were assembled by polishing the garnet pellets with SiC paper and subsequent lithium attachment. Lithium foils were attached to the SE by a small hand-pressing tool under an applied uniaxial pressure of

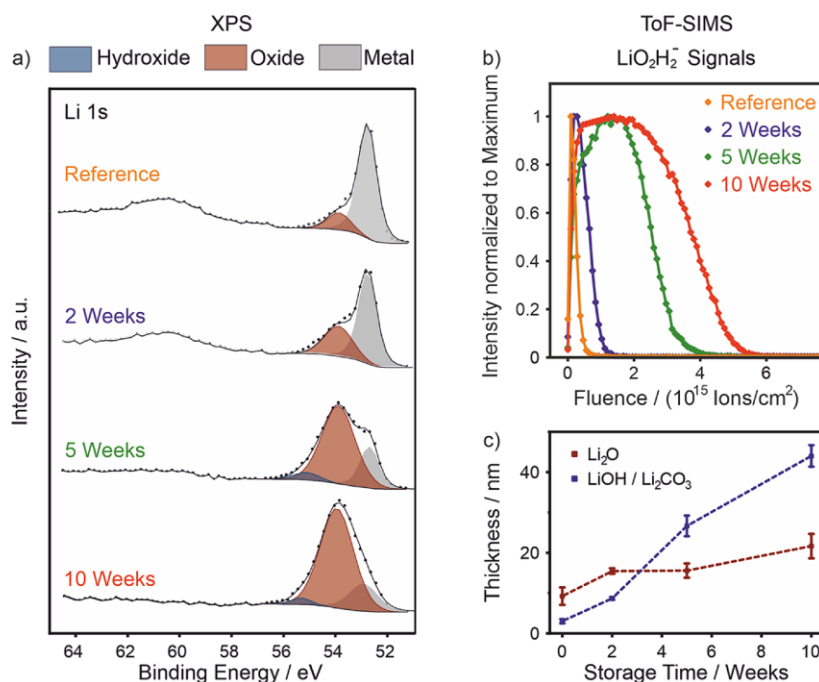


**Figure 1.** Surface-analytical results for lithium metal foil stored in closed plastic boxes in glovebox 1 for up to 10 weeks with (a) XPS after sputter step 6 (sputtering with 1 kV for 3 min, 2 kV for 8 min and 4 kV for 30 min) and (b) results from ToF-SIMS depth profiling. The  $\text{LiO}_2\text{H}_2^-$  signal is shown as representative for LiOH. (c) Passivation layer thickness as a function of storage time from the ToF-SIMS depth profiles. The reference sample was stored in the original transport package and is given as zero weeks in (c).

around 40 MPa. As a counter electrode, a resistance-free ideal electrode  $\text{Li}_d$  was prepared according to previous publications utilizing high isostatic pressure (380 MPa for 30 min).<sup>28,29</sup> Electrochemical characterization was carried out using a SP300 potentiostat by BioLogic in combination with the software EC-Lab (V.11). Cells were contacted with Ni current collector tabs and sealed in a pouch foil. Potentiostatic electrochemical impedance spectroscopy (PEIS) measurements were carried out in the frequency range between 7 MHz and 100 mHz. Fitting of impedance data was carried out using RelaxIS 3 by RhD Instruments. The impedance data were normalized to the geometrical electrode area based on the bulk impedance contribution, which is constant throughout the experiment.

The roughness of the LLZO pellets was measured with a profilometer (Alpha-Step IQ Surface Profiler, KLA Tencor) under an argon atmosphere. For both polishes (P1000 and P4000), three measurements were conducted with a scan length of 500  $\mu\text{m}$  each. The profiles were levelled by setting two zones to the same average height. The  $R_a$  value was calculated from the levelled profiles as roughness parameter. In the following, the average of the three determined  $R_a$  values is given as roughness.

For testing the reactivity of lithium foil or fresh lithium surfaces toward atmospheric gases, the samples were placed in a gas stream of 100 sccm. The gases  $\text{N}_2$ ,  $\text{O}_2$ , and  $\text{CO}_2$  were dried by streaming through Sicapent (Sigma-Aldrich) before reaction. The relative humidity of the resulting gas flow was measured as < 0.05% at 22 °C and  $101.33 \times 10^3$  Pa. For exposure to  $\text{H}_2\text{O}$ , a 100 sccm Ar stream was moistened with water to a relative humidity of 20% ( $\pm 1\%$ ) at 22 °C and  $101.33 \times 10^3$  Pa. The fresh lithium surfaces were directly cut in the stationary gas stream. The lithium foil was exposed to dry argon before it was placed in the stream of reaction gas what did not lead to any impact on the sample status. Samples were exposed to the gases for 22 h. Afterward, the line was flushed with dry Ar for 30 min, before the samples were transferred back to a glovebox.

## RESULTS AND DISCUSSION

**Influence of Storage Conditions on the Passivation Layer of Lithium Foil.** In Figure 1, XPS and ToF-SIMS characterization of lithium foil that was stored in closed plastic boxes for up to 10 weeks is shown. The samples were stored in a glovebox with relatively high degree of contamination (box 1), explicitly with  $p(\text{H}_2\text{O}$  and  $\text{O}_2)/p$  of about 1 ppm and variations up to 10 ppm.

First, the XPS analyses show that the lithium compounds on the lithium foils and their qualitative depth distribution do not change with storage time. As described previously, lithium hydroxide and carbonate are detected in the near-surface regions. In the deeper regions of the samples, which are accessible after sputtering, lithium oxide is detected and after even longer sputtering, the lithium metal is observed. For further details, we refer to our previous publication with thorough information on experimental design, data evaluation, and interpretation.<sup>14</sup>

While the compounds on the lithium foils remain the same through storage, composition and depth distribution change significantly. First, the carbonate fraction on the surface of the foils increases with storage time and reaches 100% after five weeks, while the hydroxide fraction decreases accordingly. The quantification of the fractions as a function of storage time is shown in Supporting Information 2. In addition, the oxide fraction, which is determined after a defined sputter time, is higher and the metal fraction is therefore lower, which indicates a thicker passivation layer. This trend is shown qualitatively in Figure 1a and is quantified in Supporting Information 2. For example, after only two weeks of storage,

changes of almost 20% compared to the reference (storage in transport package, 0 weeks) are observed.

The ToF-SIMS depth profiles can be used to quantitatively compare the thickness of the passivation layers. The profiles clearly show that after longer storage time, a higher fluence is needed until the intensities of passivation-related signals drop, which proves the presence of a thicker passivation layer. Figure 1b shows this behavior for the  $\text{LiO}_2\text{H}_2^-$  signal which is specific for LiOH within the compounds found by XPS analyses. The thicknesses of the lithium hydroxide and carbonate, as well as of the lithium oxide-rich regions were estimated as described in the experimental section. Interestingly, the main increase is observed for the hydroxide-rich region, whose thickness of about 44 nm after 10 weeks of storage is almost 15 times higher than for the reference with 3 nm. The thickness of the oxide-rich region is roughly doubled from 9 to 21 nm within the same period of time. Also, a higher variation in the evaluated thicknesses is observed for longer storage time, what indicates more inhomogeneous samples. The growth of the passivation layer does not seem to slow down within the investigated time period and appears approximately linear which indicates interface controlled kinetics. Please note that it is not possible to gain more direct kinetic insights for the growth of the passivation layer and calculate a rate constant from the shown data, as the conditions (the partial pressures of reactive gases) were not stable over time. However, the results can be well used to estimate the typical sample changes under comparable storage conditions and times.

**Comparison of Different Storage Conditions.** In order to find out, how the degree of contamination in a glovebox and storage conditions other than in closed plastic boxes influence the passivation layer, several additional tests were performed. First, lithium foils were stored in closed plastic boxes in a glovebox with  $p(\text{H}_2\text{O}$  and  $\text{O}_2)/p < 0.1$  ppm and variations of only up to 1 ppm. The results are presented in Supporting Information 3 and show qualitatively the same trends as described for a higher fraction of  $\text{O}_2$  and  $\text{H}_2\text{O}$  contamination. However, the changes are less pronounced which is reasonable for the reduced degree of contamination.

Furthermore, open storage and additional protection through a sealed pouch bag were tested. Open storage leads to more pronounced growth of the passivation layer as shown in Supporting Information 4. In contrast, an additional pouch bag can prevent sample changes almost completely. Also, no differences in passivation layer thickness were observed for the lithium foil which remained in the unopened transport packages for six months. Accordingly, storing lithium foil in pouch bags is recommended also for gloveboxes with low degree of contamination. Storage in plastic boxes should only be considered for short periods of time and open storage in gloveboxes should be avoided completely.

**Influence of Lithium Foil Surface Changes due to Storage on Interface Resistance.** For electrochemical cells with a liquid electrolyte, the impact of different lithium passivation layers was already described by Becking et al.<sup>8</sup> A major result was that mechanically differently treated lithium surfaces show initially different electrochemical behavior, an effect that disappears during longer stripping/plating periods. The influence on SSB performance has not been reported so far. As the components of the passivation layer can hardly dissolve in the SE and will therefore remain immobile at the lithium/SE interface, the influence of the passivation layer may be more severe than in liquid electrolytes. Therefore, we chose

to test the differently stored lithium foils in a solid-state cell with LLZO as model SE to evaluate the influence of the changing surface properties. LLZO is virtually stable against lithium and therefore no additional reactivity issues need to be considered. Even though some authors report a reaction at the Li/LLZO interface, the effect is in any case very small and does not influence the interface resistance significantly.<sup>30–32</sup>

All lithium foils stored in the gloveboxes 1 and 2 were tested in symmetrical cells with an ideal lithium electrode as a counter electrode. The ideal lithium electrodes are prepared by pressing sliced and pressed pieces of a lithium rod without surface passivation layer against the SE. Please find further explanation for the concept of ideal lithium electrodes in Supporting Information 5. For this kind of setup, there are three different contributions to the overall impedance visible in a Nyquist plot, which are the LLZO bulk contribution at high frequencies of about 4 MHz, the LLZO grain boundary contribution at about 50 kHz and the contribution of the Li/LLZO interface at low frequencies as shown in Figure 2a. As the ideal lithium counter electrode does not add any impedance,<sup>28</sup> the observed interface contribution can be attributed exclusively to the interface of the working electrode, that is, the lithium foil.

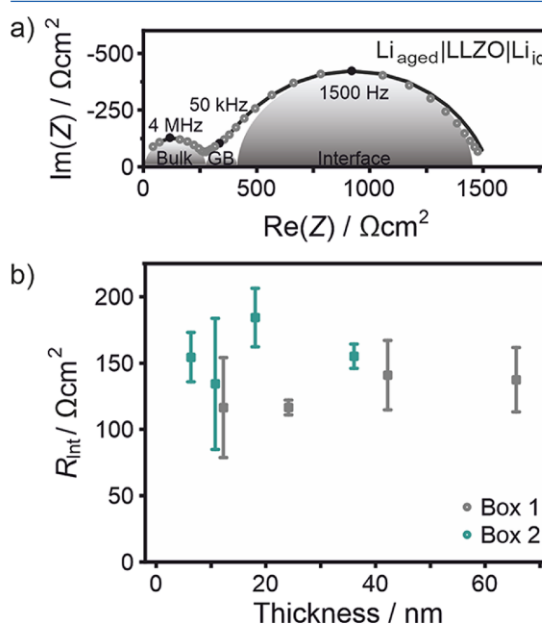


**Figure 2.** Results from impedance spectroscopy of stored lithium metal foil used as electrode within a symmetric transference cell with LLZO as SE (and an ideal lithium metal counter electrode). (a) Example of a Nyquist plot showing the contributions of LLZO bulk, grain boundaries (GB) and Li/LLZO interface. For the used setup the ideal lithium counter electrode does not add any interface contribution. Accordingly, the low-frequency part of the spectrum is attributed to the Li/LLZO foil interface. (b) Interface resistances for lithium foil stored for up to 10 weeks in closed plastic boxes in glovebox 1 ( $p(\text{H}_2\text{O}$  and  $\text{O}_2)/p$  of about 1 ppm and variations up to 10 ppm) or glovebox 2 ( $p(\text{H}_2\text{O}$  and  $\text{O}_2)/p < 0.1$  ppm and variations of only up to 1 ppm). The maximum variance of the measured values for each sample is given as error. The reference samples were stored in the original transport packages.

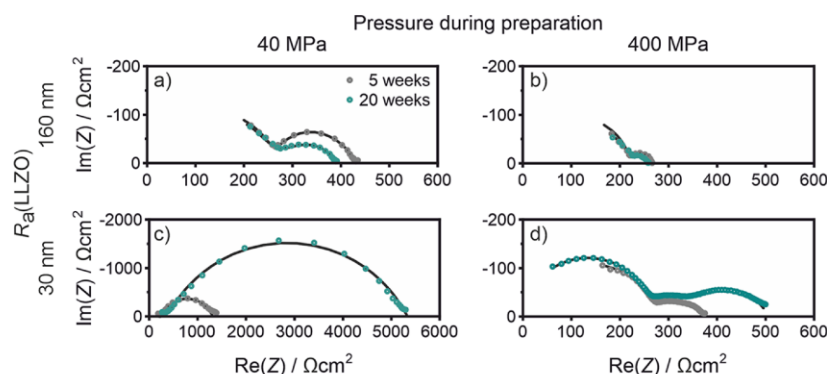


**Figure 3.** Nyquist-Plots for different LLZO roughness and pressure during preparation. (a) LLZO pellet polished with P1000 to an average roughness of about 160 nm including a maximal variation of 1.9  $\mu\text{m}$  in height and use of a preparation pressure of about 40 MPa. (b) LLZO polished with P1000 and preparation pressure of 400 MPa. (c) LLZO pellet polished with P4000 to an average roughness of about 30 nm with a maximal variation in height of 0.35  $\mu\text{m}$  and use of a preparation pressure of about 40 MPa. (d) LLZO polished with P4000 and preparation pressure of 400 MPa. The tested lithium foils were stored for 5 or 20 weeks in closed plastic boxes in glovebox 1 what led to overall passivation layer thicknesses of about 130 and 35 nm, respectively.

The interface resistances determined from impedance measurements of the differently stored lithium foils are shown in Figure 2b. The representative Nyquist Plots for selected lithium foil samples are shown in Supporting Information 6. Even though the overall passivation layer thicknesses of the tested lithium foils vary between only 6 nm for the reference samples and more than 65 nm for 10 weeks of storage in box 1, no trends or significant differences were determined for the interface resistances. All measured values are in the range of 115–185  $\Omega\text{cm}^2$ , which is comparable, considering the maximum variance of the measured values for each sample.

What seems to be counter-intuitive at first glance may be explained with the roughness of the used LLZO pellet. After polishing with P1000 abrasive paper, an average roughness of about 160 nm including a maximum variation of 1.9  $\mu\text{m}$  in height was determined. Through pressing the soft lithium foil with its surface passivation layer onto the LLZO SE with high roughness, the morphology of the foils will be changed severely. The SE may penetrate through the passivation layer in some areas, the passivation layer may be flattened in other areas and pores may form where the lithium cannot fully fill “valleys” in the LLZO surface. The result is a highly heterogeneous pattern of direct Li/LLZO contacts, areas with a passivation-layer derived interphase and areas with pores. All these local contributions sum up to the measured impedance as constriction resistances, to which the original passivation layer thickness in the measured range does not show any distinct impact.

**Influence of Roughness and Pressure on Interface Resistance.** In order to explore the effect of roughness and mechanical pressure in more detail, an additional set of measurements with varying pressure and differently polished LLZO pellets was conducted. In Figure 3, impedance measurements for lithium foils with a very thick passivation layer (about 130 nm overall, 20 weeks) and with medium thickness (about 35 nm overall, 5 weeks) are shown. In Figure 4, schematic representations for the Li/LLZO interfaces of the different measurements are shown to visualize the discussed interface status.

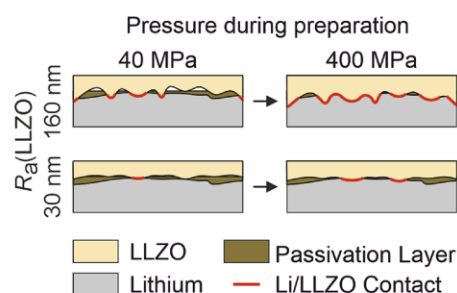


**Figure 4.** Schematic representations for the Li/LLZO interfaces measured with different LLZO pellet roughness and preparation pressure. LLZO pellets were polished with P1000 to an average roughness of about 160 nm including a maximal variation of 1.9  $\mu\text{m}$  in height and with P4000 to an average roughness of about 30 nm with a maximal variation in height of 0.35  $\mu\text{m}$ . For a LLZO pellet with high roughness, the SE penetrates through the lithium passivation what leads to the formation of almost ideal Li/LLZO interfaces for all investigated lithium foils at high preparation pressure of 400 MPa. For a LLZO pellet with lower roughness, the penetration of the passivation layer is less pronounced and it depends on the thickness of the passivation layer whether an almost ideal Li/LLZO interfaces can form at high preparation pressure.

First, a representative Nyquist plot under the measurement conditions which were used before is shown in Figure 3a. As found previously, no significant differences are observed. Increasing the pressure to 400 MPa during preparation for the tested cells (Figure 3b) even eliminates the small differences present before, what demonstrates that the applied (stack) pressure has strong impact. As the interface contribution vanishes almost completely for both samples, penetration through the passivation layer seems to be dominating in both cases and almost ideal interfaces with mostly direct Li/LLZO contact form.

To confirm this assumption the Li/LLZO interface contact for the tested preparation pressures was investigated by focused ion beam scanning electron microscopy (FIB-SEM) under cryo conditions. The results are presented in Supporting Information 7. While pores could be identified at the Li/LLZO

interface for a preparation pressure of 40 MPa, close contact without any pores was observed for a preparation pressure of 400 MPa. Even though the lithium passivation layer and accordingly, the penetration through the layer could not be resolved, previous works by Krauskopf et al. suggest that a direct LiLLZO contact and therefore penetration through the passivation layer have to be present, as this leads to the absence of an interface resistance.<sup>28,33</sup>

To test the effect of lower roughness, LLZO pellets were polished with P4000 to an average roughness of about 30 nm with a maximal variation in height of only 0.35  $\mu\text{m}$ . For this roughness, impedance measurements of the same lithium foils with passivation layer thicknesses of 130 and 35 nm showed a much higher interface resistance for the thicker passivation layer at a preparation pressure of 40 MPa. As the roughness and accordingly, also the surface area of the used LLZO pellets were lower, the above described changes of the lithium foils through penetration, flattening of the passivation layer, and pore formation are probably less pronounced, which makes the influence of the passivation layer thickness more severe. The differences also remained noticeable at higher preparation pressure. For the LLZO pellet polished to an average roughness of 30 nm and a preparation pressure of 400 MPa, the lithium foil with thinner passivation layer forms an almost ideal interface as the interface contribution is very small. In contrast, a significant interface contribution remains for the lithium foil with thicker passivation layer. For the latter, the lower roughness of the LLZO pellet prevents the formation of a mostly ideal LiLLZO interface and the effect of the passivation layer thickness remains measurable.

This leads to the conclusion that a rough SE pellet has overall better interfacial properties for the application of lithium metal foils, in the sense of a lower polarization resistance. Taking this thought to the extreme, a most applicable, very rough SE would lead to porous LLZO infiltrated with lithium as described in literature.<sup>34–36</sup> However, a rough surface significantly increases the risk of dendrite formation, which should actually be minimized by using smooth SE surfaces.<sup>37</sup> Thus, the presence of the resistive passivation layer would require an optimized SE surface morphology that may be difficult to achieve. From our perspective, the issues related to the resistive passivation layer of lithium metal and its negative influence on the solid-state cell impedance can probably only be overcome completely by employing “anode-free” concepts and avoiding lithium metal passivation at all.<sup>38</sup>

In any case, our experiments show that the roughness of the SE and the pressure applied during the measurements play an important role for the interface resistance of the lithium metal foil in contact with LLZO. This is not only caused by the mere interface contact as such, but also strongly influenced by the presence of the native passivation layer. At this point, we like to note that the total impedance of an SSB cell should not exceed a value in the order of a few  $10 \Omega\text{cm}^2$ , to allow sufficiently high charge rates. As shown by our data, the impedance of LiLLZO interfaces with an intact passivation interlayer will be too high for practical applications.

**Causes for Lithium Foil Aging during Storage.** As already mentioned, residuals of atmospheric gases are the main contaminations in gloveboxes and responsible for undesired reactions and aging processes of lithium foil during storage. Therefore, the reactivity of lithium toward these atmospheric gases plays a key role for the growth of the passivation layer. In

Supporting Information 8, some selected studies on the reactivity of lithium toward atmospheric gases are summarized. All authors agree that the reactivity of lithium toward water is high. Nevertheless, the various reports contain partly contradicting results for the inherent reactivity of  $\text{N}_2$ ,  $\text{O}_2$ , and  $\text{CO}_2$  with clean lithium surfaces. However, all authors stress that impurities such as traces of water have a huge impact on the observed reactivity. Because a complete absence of water is nearly impossible and a lithium surface without any impurities can hardly be prepared, these factors are probably the reason for the contradicting reports.<sup>39,40</sup> Furthermore, commercial lithium foils are usually pre-treated to prevent undefined samples changes which additionally influences the reactivity.<sup>3</sup>

To explain the increase of the passivation layer thickness for the stored lithium foil, we exposed pieces of lithium foil to the dried gases  $\text{N}_2$ ,  $\text{O}_2$ , and  $\text{CO}_2$ , as well as to  $\text{H}_2\text{O}$  with Ar as carrier gas. Within 22 h of exposure, only  $\text{H}_2\text{O}$  induced detectable sample changes as shown in Figure 5. XRD

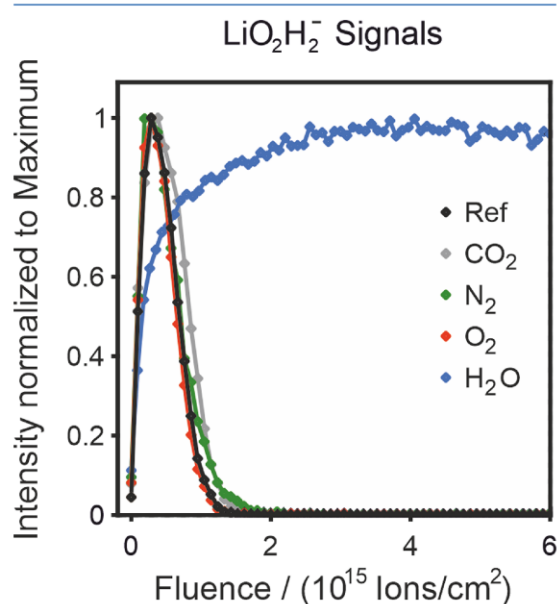


**Figure 5.** ToF-SIMS depth profiles of lithium foil exposed for 22 h to dried  $\text{N}_2$ ,  $\text{O}_2$ , and  $\text{CO}_2$ , as well as to  $\text{H}_2\text{O}$  with Ar as carrier gas. The  $\text{LiO}_2\text{H}_2^-$  signal is shown as representative for LiOH. Only the sample exposed to  $\text{H}_2\text{O}$  shows significant changes compared to the reference. The same accounts for other signals and XPS depth profiles.

characterization indicated full conversion to LiOH for the sample exposed to  $\text{H}_2\text{O}$ . Consequently, water residuals are probably the main reason for aging of lithium foil during storage in gloveboxes. This is in accordance with the observation that the main increase in thickness is related to the growth of the lithium hydroxide rich region of the passivation layer. Increasing carbonate formation on the surface may be attributed to a follow up reaction of LiOH with  $\text{CO}_2$  as described in the literature.<sup>41</sup> However,  $\text{CO}_2$  itself does not provide sufficient driving force for further surface reactions and layer growth, as  $\text{Li}_2\text{CO}_3$  forms a covering layer on lithium according to its Pilling–Bedworth ratio (PBR) of 1.35. Please find the PBRs of selected lithium compounds and an explanation of the respective calculations in Supporting

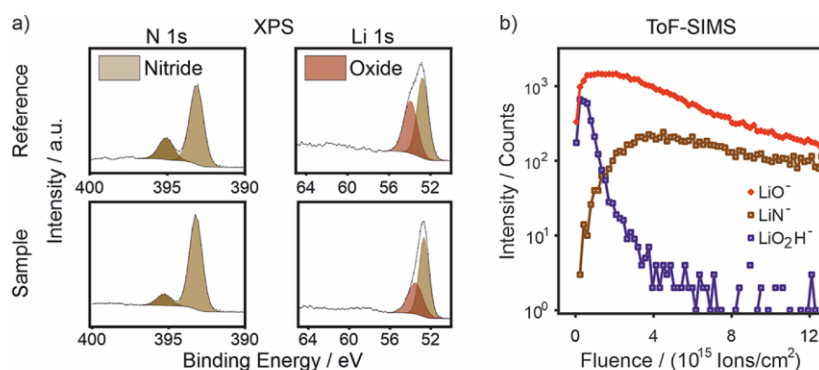


**Figure 6.** XPS and ToF-SIMS results for a lithium foil which reacted to  $\text{Li}_3\text{N}$ . (a) XP spectra of the N 1s and Li 1s regions of a reference  $\text{Li}_3\text{N}$  powder sample and a tarnished lithium foil after sputter step 6 (sputtering with 1 kV for 3 min, 2 kV for 8 min and 4 kV for 30 min). As the same signals are present, the analyses confirm the formation of  $\text{Li}_3\text{N}$  for the tarnished foil. (b) ToF-SIMS depth profile of a tarnished lithium foil. In the beginning of the profile the intensity of oxide and hydroxide signals is dominating. After longer sputter time, the  $\text{LiN}^-$  signal intensity increases what indicates that the  $\text{Li}_3\text{N}$  is not present on the very surface but in the bulk of the sample.

**Information 9.** Only judging from the PBRs,  $\text{LiOH}$  may also form covering and therefore potentially protecting layers on lithium metal, while  $\text{Li}_2\text{O}$  forms no covering layer. This may be the reason why  $\text{LiOH}$  and  $\text{Li}_2\text{CO}_3$  are found on the very surface of the analyzed lithium foil and  $\text{Li}_2\text{O}$  is only present below.

**Impact of Nitrogen Gas.** Some pieces of the stored lithium foil tarnished and became brittle. This was mostly the case for pieces which were punched out before storage for later use in electrochemical cells. A photograph of the tarnished foils compared to aged lithium foil is given in [Supporting Information 10](#). These tarnished samples could no longer be used as anodes because they did not provide sufficient electronic conductivity. Accordingly, it is important to evaluate these sample changes in more detail.

Characterization of the tarnished and brittle samples with XRD indicate full conversion to  $\text{Li}_3\text{N}$ , which agrees with the electrochemical testing, as  $\text{Li}_3\text{N}$  is a poor electronic conductor.<sup>42</sup> In [Figure 6a](#), XPS spectra after sputtering of a  $\text{Li}_3\text{N}$  reference and a tarnished lithium foil are presented. The spectra show the same signals what confirms the presence of  $\text{Li}_3\text{N}$ . Sputtering was necessary, as no nitrogen could be detected on the sample surfaces. Therefore, it cannot be ruled out that sputter damage changed the samples before analysis, what may be the reason for the observation of two signals in the nitrogen 1s region. In literature, the signal at about 393.1 eV is referred to  $\text{Li}_3\text{N}$ , while the signal at higher binding energy (about 395.1 eV) is just attributed to an unspecified impurity.<sup>39</sup> Possibly, a lithium–nitrogen compound with lower lithium content formed through sputtering or decomposition. This would fit with the higher, but compared to other nitrides still low binding energy as other metal nitrides appear in the N 1s region at binding energies higher than 395 eV.<sup>43</sup> In the Li 1s region, the  $\text{Li}_3\text{N}$  signal is present at around 52.6 eV, which is within the range of error identical to the position for lithium metal. However, the absence of plasmon-loss features for  $\text{Li}_3\text{N}$  allows the differentiation.

The ToF-SIMS depth profile of the tarnished sample is shown in [Figure 6b](#) and also indicates that the near-surface region does not contain  $\text{Li}_3\text{N}$ , as the  $\text{LiN}^-$  signal intensity at the beginning of the profile is very low, while the intensity of oxide and hydroxide related signals dominates. Still, with

longer sputtering, the intensity increases and becomes virtually constant, which supports full conversion of the sample into  $\text{Li}_3\text{N}$ . The complete conversion indicates that the reaction of lithium and nitrogen is not self-limiting under a glovebox atmosphere. This agrees with the fact that the PBR = 0.69 of  $\text{Li}_3\text{N}$  on lithium metal is significantly smaller than 1. Consequently,  $\text{Li}_3\text{N}$  most probably does not form a covering layer which could prevent further reaction. The formation of porous  $\text{Li}_3\text{N}$  on commercial lithium foil after reaction with  $\text{N}_2$  was also reported by Li et al.<sup>44</sup> Reaction of liquid lithium may allow for the formation of pinhole-free  $\text{Li}_3\text{N}$ ; however, for lithium foil, this is definitely not an option.<sup>44</sup>

As lithium hydroxide and carbonate form a stable and well-covering passivation layer according to their PBRs, lithium foils covered with these compounds appear to be protected against reaction with nitrogen. It is also reported that  $\text{Li}_2\text{CO}_3$  protects lithium from reaction with all atmospheric gases except  $\text{H}_2\text{O}$ .<sup>45</sup> Consequently, this passivation layer must have been at least partly destroyed for the samples which tarnished and reacted with nitrogen forming  $\text{Li}_3\text{N}$ . To verify this, we prepared a bunch of samples through tearing and ripping instead of controlled slicing to destroy the passivation layer on purpose. In most cases, the samples prepared in this way reacted to  $\text{Li}_3\text{N}$ .

**Protecting Effect of Passivation Layer.** In order to understand the influence of the passivation layer on top of commercial lithium foils on the reaction behavior against atmospheric gases, we exposed sliced lithium without an inherent passivation layer to the pure atmospheric gases. While only thin reaction layers formed within 22 h of exposure to  $\text{CO}_2$  and  $\text{O}_2$ , a thick reaction layer formed in contact with  $\text{N}_2$ . Similar observations were found for sliced lithium which was stored in gloveboxes without a  $\text{N}_2$  filter. For a glovebox equipped with a nitrogen filter (glovebox 3), no  $\text{Li}_3\text{N}$  formed on a sliced sample. In [Supporting Information 11 and 12](#), these results are shown in more detail.

These observations indicate that a native and well covering passivation layer, composed of lithium carbonate and hydroxide as found on commercial lithium foils, is needed to prevent the reaction of lithium metal with nitrogen gas. Consequently, special attention should be paid to  $\text{Li}_3\text{N}$  contamination, in particular for the processing of fresh lithium

samples in gloveboxes without nitrogen filter. Additionally, it should be avoided to prepare small pieces or punch out lithium foil before storage, as this increases the risk of damaging the native protecting passivation layer. We like to note that our experiments do not answer the question of the intrinsic reactivity between lithium and nitrogen, as trace contaminations may influence the results in the gloveboxes and the gas reaction chamber. However, the described experiments explain the observed sample changes due to  $\text{Li}_3\text{N}$  formation in gloveboxes.

## CONCLUSIONS

In this study, we investigate the effect of glovebox storage on the passivation layer on commercial lithium foils and the impact of this passivation layer on the interface resistance when the foils are used as anodes in SSBs. To better understand the formation and influence of the passivation layer, the reactivity of lithium metal toward the atmospheric gases  $\text{N}_2$ ,  $\text{O}_2$ ,  $\text{H}_2\text{O}$ , and  $\text{CO}_2$ , which are the main impurities present in gloveboxes, is investigated.

XPS characterization of stored lithium foil shows that the compounds within the passivation layer and their qualitative depth distribution do not change with storage time. However, the composition changes toward a higher carbonate fraction on the surface and a thicker passivation layer, as the sputtering time required to reach the metal-rich region increases. ToF-SIMS depth profiles show a dominating increase of thickness for the hydroxide-rich region and a more inhomogeneous passivation layer. The thickness of the passivation layer depends on the storage conditions. Storage in closed plastic boxes can reduce the growth compared to open storage, but only an additional pouch bag can almost completely prevent sample changes. Therefore, pouching of a lithium foil is always recommended for storage time longer than one day.

Characterization of the stored lithium foils with impedance spectroscopy in a transference cell with LLZO as SE showed that the interface resistance largely depends on the preparation conditions, rather than on the passivation layer. For LLZO with high roughness compared to the passivation layer thickness, no differences in resistance between various lithium samples were observed. In addition, a pressure of 400 MPa leads to an almost ideal interface, as the LLZO penetrates through the passivation layer and forms direct LiLLZO contacts. For LLZO with lower roughness compared to the passivation layer thickness, this is not possible and interface resistances are observed for lithium foil with thicker passivation layer even at a pressure of 400 MPa. Our results show that an intact passivation layer on the lithium foil adds high interface resistance to an SSB. Rough SE surfaces and high stack pressures can be used to overcome the high resistances as the SE will penetrate through the passivation layer. However, rough surfaces increase the risk of dendrite formation and stack pressures in the range of hundreds of MPa are not applicable. The concept of anode free cells may solve this problem as no passivation layer will be present on the directly plated lithium.

Reactivity tests of lithium foil with dried  $\text{N}_2$ ,  $\text{O}_2$ , and  $\text{CO}_2$ , as well as with moistened Ar show that the reaction with water residuals is probably the dominating factor for the growth of the passivation layer. For samples without covering and protecting passivation layer, ongoing conversion into  $\text{Li}_3\text{N}$  through reaction with  $\text{N}_2$  is a major problem. To overcome this and allow for the handling of fresh lithium surfaces, an

additional nitrogen filter is one successfully tested option for gloveboxes.

Overall, the results demonstrate that storage time and conditions are important factors for the surface state of a lithium foil and need to be considered for their application in batteries. The influence on the electrochemical performance in ASSBs hereby largely depends on the roughness of the used SE and the applied pressure. We like to add that the lithium metal surface and its passivation layer is probably much more critical for application in SSBs compared to LIB with liquid electrolyte. To prevent undesired surface changes, careful control of  $p(\text{H}_2\text{O})$  and—in the case of unprotected lithium surfaces—additional control of  $p(\text{N}_2)$  is most important.

## ASSOCIATED CONTENT

### Supporting Information

The Supporting Information is available free of charge at <https://pubs.acs.org/doi/10.1021/acsaem.1c02481>.

Overview of all samples; quantification of passivation layer compounds from XPS depth profiling; impact of different contamination levels in gloveboxes on lithium foil aging; impact of different storage conditions in gloveboxes on lithium foil aging; ideal lithium electrodes; representative Nyquist plots; cryo FIB-SEM for interface visualization; theory about the reactivity of lithium toward atmospheric gases; Pilling–Bedworth ratio; photo of stored lithium foil; reactivity of unprotected lithium surfaces toward atmospheric gases; and reactivity of unprotected lithium surfaces in gloveboxes with and without nitrogen filter (PDF)

## AUTHOR INFORMATION

### Corresponding Authors

**Jürgen Janek** – Institute of Physical Chemistry, Justus-Liebig-Universität Giessen, D-35392 Giessen, Germany; Center for Materials Research (ZfM), Justus-Liebig-Universität Giessen, D-35392 Giessen, Germany; [orcid.org/0000-0002-9221-4756](https://orcid.org/0000-0002-9221-4756); Email: [juergen.janek@phys.chemie.uni-giessen.de](mailto:juergen.janek@phys.chemie.uni-giessen.de)

**Anja Henss** – Institute of Physical Chemistry, Justus-Liebig-Universität Giessen, D-35392 Giessen, Germany; Center for Materials Research (ZfM), Justus-Liebig-Universität Giessen, D-35392 Giessen, Germany; [orcid.org/0000-0001-5009-6512](https://orcid.org/0000-0001-5009-6512); Email: [anja.henss@phys.chemie.uni-giessen.de](mailto:anja.henss@phys.chemie.uni-giessen.de)

### Authors

**Svenja-K. Otto** – Institute of Physical Chemistry, Justus-Liebig-Universität Giessen, D-35392 Giessen, Germany

**Till Fuchs** – Institute of Physical Chemistry, Justus-Liebig-Universität Giessen, D-35392 Giessen, Germany; Center for Materials Research (ZfM), Justus-Liebig-Universität Giessen, D-35392 Giessen, Germany

**Yannik Moryson** – Institute of Physical Chemistry, Justus-Liebig-Universität Giessen, D-35392 Giessen, Germany; Center for Materials Research (ZfM), Justus-Liebig-Universität Giessen, D-35392 Giessen, Germany

**Christian Lerch** – Institute of Physical Chemistry, Justus-Liebig-Universität Giessen, D-35392 Giessen, Germany

**Boris Mogwitz** – Institute of Physical Chemistry, Justus-Liebig-Universität Giessen, D-35392 Giessen, Germany

**Joachim Sann** – Institute of Physical Chemistry, Justus-Liebig-Universität Giessen, D-35392 Giessen, Germany

Complete contact information is available at:

<https://pubs.acs.org/10.1021/acsaem.1c02481>

### Notes

The authors declare no competing financial interest.

### ACKNOWLEDGMENTS

The authors acknowledge the financial support by the BMBF (Bundesministerium für Bildung und Forschung) within the FestBatt—Cluster of Competence for Solid-state Batteries (03XP0176D), the MaLiBa (03XP0185D) and the ProLiFest (03XP0253B) projects. S.K.O. acknowledges the financial support (Kékulé scholarship) by the Funds of the Chemical Industry (FCI). T.F. acknowledges the funding by the BMBF within the LiSI project (03XP0224E).

### REFERENCES

- (1) Janek, J.; Zeier, W. G. A solid future for battery development. *Nat. Energy* **2016**, *1*, 1167.
- (2) Meyerson, M. L.; Sheavly, J. K.; Dolocan, A.; Griffin, M. P.; Pandit, A. H.; Rodriguez, R.; Stephens, R. M.; Vanden Bout, D. A.; Heller, A.; Mullins, C. B. The effect of local lithium surface chemistry and topography on solid electrolyte interphase composition and dendrite nucleation. *J. Mater. Chem. A* **2019**, *7*, 14882.
- (3) Schmuck, R.; Wagner, R.; Hörpel, G.; Placke, T.; Winter, M. Performance and cost of materials for lithium-based rechargeable automotive batteries. *Nat. Energy* **2018**, *3*, 267–278.
- (4) Guo, R.; Gallant, B. M. Li<sub>2</sub>O Solid Electrolyte Interphase: Probing Transport Properties at the Chemical Potential of Lithium. *Chem. Mater.* **2020**, *32*, 5525–5533.
- (5) Lee, J. I.; Song, G.; Cho, S.; Han, D. Y.; Park, S. Lithium Metal Interface Modification for High-Energy Batteries: Approaches and Characterization. *Batteries Supercaps* **2020**, *3*, 828–859.
- (6) Zhou, H.; Yu, S.; Liu, H.; Liu, P. Protective coatings for lithium metal anodes: Recent progress and future perspectives. *J. Power Sources* **2020**, *450*, 227632.
- (7) Ryou, M.-H.; Lee, Y. M.; Lee, Y.; Winter, M.; Bieker, P. Mechanical Surface Modification of Lithium Metal: Towards Improved Li Metal Anode Performance by Directed Li Plating. *Adv. Funct. Mater.* **2015**, *25*, 834–841.
- (8) Becking, J.; Gröbmeyer, A.; Kolek, M.; Rodehorst, U.; Schulze, S.; Winter, M.; Bieker, P.; Stan, M. C. Lithium-Metal Foil Surface Modification: An Effective Method to Improve the Cycling Performance of Lithium-Metal Batteries. *Adv. Mater. Interfaces* **2017**, *4*, 1700166.
- (9) Kamphaus, E. P.; Angarita-Gomez, S.; Qin, X.; Shao, M.; Engelhard, M.; Mueller, K. T.; Murugesan, V.; Balbuena, P. B. Role of inorganic surface layer on solid electrolyte interphase evolution at Li-metal anodes. *ACS Appl. Mater. Interfaces* **2019**, *11*, 31467–31476.
- (10) Maslyn, J. A.; Frenck, L.; Loo, W. S.; Parkinson, D. Y.; Balsara, N. P. Extended Cycling through Rigid Block Copolymer Electrolytes Enabled by Reducing Impurities in Lithium Metal Electrodes. *ACS Appl. Mater. Interfaces* **2019**, *2*, 8197–8206.
- (11) Storelli, A.; Rousselot, S.; Alzate-Carvajal, N.; Pelé, V.; Dollé, M. On the Importance of Li Metal Morphology on the Cycling of Lithium Metal Polymer Cells. *J. Electrochem. Soc.* **2021**, *168*, 040505.
- (12) Harry, K. J.; Hallinan, D. T.; Parkinson, D. Y.; MacDowell, A. A.; Balsara, N. P. Detection of subsurface structures underneath dendrites formed on cycled lithium metal electrodes. *Nat. Mater.* **2014**, *13*, 69.
- (13) Etxebarria, A.; Koch, S. L.; Bondarchuk, O.; Passerini, S.; Teobaldi, G.; Muñoz-Márquez, M. A. Work Function Evolution in Li Anode Processing. *Adv. Energy Mater.* **2020**, *10*, 2000520.
- (14) Otto, S.-K.; Moryson, Y.; Krauskopf, T.; Pepler, K.; Sann, J.; Janek, J.; Henss, A. In-Depth Characterization of Lithium-Metal Surfaces with XPS and ToF-SIMS: Toward Better Understanding of the Passivation Layer. *Chem. Mater.* **2021**, *33*, 859–867.
- (15) Ismail, I.; Noda, A.; Nishimoto, A.; Watanabe, M. XPS study of lithium surface after contact with lithium-salt doped polymer electrolytes. *Electrochim. Acta* **2001**, *46*, 1595–1603.
- (16) Naudin, C.; Bruneel, J. L.; Chami, M.; Desbat, B.; Grondin, J.; Lassègues, J. C.; Servant, L. Characterization of the lithium surface by infrared and Raman spectroscopies. *J. Power Sources* **2003**, *124*, 518–525.
- (17) Kanamura, K.; Tamura, H.; Shiraiishi, S.; Takehara, Z. i. XPS Analysis of Lithium Surfaces Following Immersion in Various Solvents Containing LiBF<sub>4</sub>. *J. Electrochem. Soc.* **1995**, *142*, 340.
- (18) Markowitz, M. M.; Boryta, D. A. Lithium Metal-Gas Reactions: Interaction of Lithium Metal with Air and its Component Gases. *J. Chem. Eng. Data* **1962**, *7*, 586–591.
- (19) Irvine, W. R.; Lund, J. A. The Reaction of Lithium with Water Vapor. *J. Electrochem. Soc.* **1963**, *110*, 141–144.
- (20) Jeppson, D. W. *Lithium Literature Review: Lithium's Properties and Interactions*; Hanford Engineering Development Laboratory, 1978.
- (21) David, D. J.; Froning, M. H.; Wittberg, T. N.; Moddeman, W. E. Surface reactions of lithium with the environment. *Appl. Surf. Sci.* **1981**, *7*, 185–195.
- (22) Hoenigman, J. R.; Keil, R. G. An XPS study of the adsorption of oxygen and water vapor on clean lithium films. *Appl. Surf. Sci.* **1984**, *18*, 207–222.
- (23) Rhein, R. A. *Lithium Combustion: A Review*; Ordnance Systems Department: Naval Weapons Center, 1990.
- (24) Zavadil, K. R.; Armstrong, N. R. Surface chemistries of lithium: Detailed characterization of the reactions with O<sub>2</sub> and H<sub>2</sub>O using XPS, EELS, AND microgravimetry. *Surf. Sci.* **1990**, *230*, 47–60.
- (25) Wang, K.; Ross, P. N.; Kong, F.; McLarnon, F. The Reaction of Clean Li Surfaces with Small Molecules in Ultrahigh Vacuum. *J. Electrochem. Soc.* **1996**, *143*, 422.
- (26) Skinner, C. H.; Sullenberger, R.; Koel, B. E.; Jaworski, M. A.; Kugel, H. W. Plasma facing surface composition during NSTX Li experiments. *J. Nucl. Mater.* **2013**, *438*, S647–S650.
- (27) Schiemann, M.; Berghthorson, J.; Fischer, P.; Scherer, V.; Taroota, D.; Schmid, G. A review on lithium combustion. *Appl. Energy* **2016**, *162*, 948–965.
- (28) Krauskopf, T.; Hartmann, H.; Zeier, W. G.; Janek, J. Toward a Fundamental Understanding of the Lithium Metal Anode in Solid-State Batteries—An Electrochemo-Mechanical Study on the Garnet-Type Solid Electrolyte Li<sub>6</sub>2.5Al<sub>0.25</sub>La<sub>3</sub>Zr<sub>2</sub>O<sub>12</sub>. *ACS Appl. Mater. Interfaces* **2019**, *11*, 14463–14477.
- (29) Fuchs, T.; Mogwitz, B.; Otto, S. K.; Passerini, S.; Richter, F. H.; Janek, J. Working Principle of an Ionic Liquid Interlayer During Pressureless Lithium Stripping on Li<sub>6.25</sub>Al<sub>0.25</sub>La<sub>3</sub>Zr<sub>2</sub>O<sub>12</sub> (LLZO) Garnet-Type Solid Electrolyte. *Batteries Supercaps* **2021**, *4*, 1145–1155.
- (30) Han, F.; Zhu, Y.; He, X.; Mo, Y.; Wang, C. Electrochemical Stability of Li<sub>10</sub>GeP<sub>2</sub>S<sub>12</sub> and Li<sub>7</sub>La<sub>3</sub>Zr<sub>2</sub>O<sub>12</sub> Solid Electrolytes. *Adv. Energy Mater.* **2016**, *6*, 1501590.
- (31) Ma, C.; Cheng, Y.; Yin, K.; Luo, J.; Sharafi, A.; Sakamoto, J.; Li, J.; More, K. L.; Dudney, N. J.; Chi, M. Interfacial Stability of Li Metal-Solid Electrolyte Elucidated via In Situ Electron Microscopy. *Nano Lett.* **2016**, *16*, 7030–7036.
- (32) Connell, J. G.; Fuchs, T.; Hartmann, H.; Krauskopf, T.; Zhu, Y.; Sann, J.; Garcia-Mendez, R.; Sakamoto, J.; Tepavcevic, S.; Janek, J. Kinetic versus Thermodynamic Stability of LLZO in Contact with Lithium Metal. *Chem. Mater.* **2020**, *32*, 10207–10215.
- (33) Krauskopf, T.; Mogwitz, B.; Hartmann, H.; Singh, D. K.; Zeier, W. G.; Janek, J. The Fast Charge Transfer Kinetics of the Lithium Metal Anode on the Garnet-Type Solid Electrolyte Li<sub>6.25</sub>Al<sub>0.25</sub>La<sub>3</sub>Zr<sub>2</sub>O<sub>12</sub>. *Adv. Energy Mater.* **2020**, *10*, 2000945.
- (34) Wang, C.; Gong, Y.; Liu, B.; Fu, K.; Yao, Y.; Hitz, E.; Li, Y.; Dai, J.; Xu, S.; Luo, W.; Wachsmann, E. D.; Hu, L. Conformal, Nanoscale ZnO Surface Modification of Garnet-Based Solid-State Electrolyte for Lithium Metal Anodes. *Nano Lett.* **2017**, *17*, 565–571.
- (35) Xu, S.; McOwen, D. W.; Wang, C.; Zhang, L.; Luo, W.; Chen, C.; Li, Y.; Gong, Y.; Dai, J.; Kuang, Y.; Yang, C.; Hamann, T. R.;

Wachsman, E. D.; Hu, L. Three-Dimensional, Solid-State Mixed Electron-Ion Conductive Framework for Lithium Metal Anode. *Nano Lett.* **2018**, *18*, 3926–3933.

(36) Xie, H.; Yang, C.; Ren, Y.; Xu, S.; Hamann, T. R.; McOwen, D. W.; Wachsman, E. D.; Hu, L. Amorphous-Carbon-Coated 3D Solid Electrolyte for an Electro-Chemomechanically Stable Lithium Metal Anode in Solid-State Batteries. *Nano Lett.* **2021**, *21*, 6163–6170.

(37) Krauskopf, T.; Richter, F. H.; Zeier, W. G.; Janek, J. Physicochemical Concepts of the Lithium Metal Anode in Solid-State Batteries. *Chem. Rev.* **2020**, *120*, 7745–7794.

(38) Wang, M. J.; Carmona, E.; Gupta, A.; Albertus, P.; Sakamoto, J. Enabling “lithium-free” manufacturing of pure lithium metal solid-state batteries through in situ plating. *Nat. Commun.* **2020**, *11*, 1–9.

(39) Etxebarria, A.; Yun, D.-J.; Blum, M.; Ye, Y.; Sun, M.; Lee, K.-J.; Su, H.; Muñoz-Márquez, M. A.; Ross, P. N.; Crumlin, E. J. Revealing in situ Li metal anode surface evolution upon exposure to CO<sub>2</sub> using Ambient Pressure X-ray Photoelectron Spectroscopy. *ACS Appl. Mater. Interfaces* **2020**, *12*, 26607–26613.

(40) Li, Y.; Li, Y.; Sun, Y.; Butz, B.; Yan, K.; Koh, A. L.; Zhao, J.; Pei, A.; Cui, Y. Revealing Nanoscale Passivation and Corrosion Mechanisms of Reactive Battery Materials in Gas Environments. *Nano Lett.* **2017**, *17*, 5171–5178.

(41) Hart, C. A.; Skinner, C. H.; Capece, A. M.; Koel, B. E. Sorption of atmospheric gases by bulk lithium metal. *J. Nucl. Mater.* **2016**, *468*, 71–77.

(42) Rabenau, A. Lithium nitride and related materials case study of the use of modern solid state research techniques. *Solid State Ionics* **1982**, *6*, 277–293.

(43) Bertóti, I. Characterization of nitride coatings by XPS. *Surf. Coat. Technol.* **2002**, *151–152*, 194–203.

(44) Li, Y.; Sun, Y.; Pei, A.; Chen, K.; Vailionis, A.; Li, Y.; Zheng, G.; Sun, J.; Cui, Y. Robust Pinhole-free Li<sub>3</sub>N Solid Electrolyte Grown from Molten Lithium. *ACS Cent. Sci.* **2018**, *4*, 97–104.

(45) Bärman, P.; Mohrhardt, M.; Frerichs, J. E.; Helling, M.; Kolesnikov, A.; Klabunde, S.; Nowak, S.; Hansen, M. R.; Winter, M.; Placke, T. Mechanistic Insights into the Pre-Lithiation of Silicon/Graphite Negative Electrodes in “Dry State” and After Electrolyte Addition Using Passivated Lithium Metal Powder. *Adv. Energy Mater.* **2021**, *11*, 2100925.

### 3.3 Publication 3: “In situ Investigation of Lithium Metal - Solid Electrolyte Anode Interfaces with ToF-SIMS”

Publication 3 of this doctoral thesis establishes ToF-SIMS as a method to systematically study the properties and stability of Li|SE interfaces and interphases. From the previous two publications, the surface passivation layer on lithium foil is known to affect the performance of SSBs. Therefore, model systems were chosen which resemble alternative preparation concepts of LMAs, namely lithium plating for anode-free cell concepts and lithium vapor deposition on the SE pellet. The Li|SE interfaces were prepared *in situ*, either by lithium vapor deposition using a low temperature effusion cell in a side chamber of the ToF-SIMS instrument or by lithium plating using the electron flood gun of the ToF-SIMS instrument as virtual electrode. The obtained layered systems with  $\mu\text{m}$ -thick lithium layers on top of the SE pellets were analyzed by ToF-SIMS depth profiling. Three different SEs, namely LLZO, LATP and  $\text{Li}_6\text{PS}_5\text{Cl}$  (LPSCl), as well as MgO as inert reference material were characterized.

Based on the depth profiles through the vapor deposited lithium layers, the stability of the Li|SE interfaces could be classified. In order to distinguish between SEI and MCI, it proved necessary to measure multiple times, as only changes of the samples with time allow an assessment whether a thin, but growing MCI or a stable SEI with negligible growth rate is present. In addition to the evaluation of the interface stability, ToF-SIMS characterization allows the investigation of interphase microstructures, which was exemplified for the microstructure of the Li|LPSCl interphase. The interphase was found to consist of a covering  $\text{Li}_2\text{S}$ - and an additional P- and Cl-rich layer. *In situ* AFM measurements were necessary to allow comparison of the two sample types, since the sample roughness of the vapor deposited and plated lithium films was too high for depth calibration using the sputtering yield of reference compounds. For the Li|LPSCl interphase, the thickness of the  $\text{Li}_2\text{S}$  layer was found to be about 250 nm for lithium vapor deposition and plating. This is an order of magnitude more than calculated previously based on impedance spectroscopy measurements.

Overall, the publication demonstrates for the first time the full potential of ToF-SIMS analysis for the investigation of Li|SE interfaces and interphases, showing that it is a valuable method to complement established techniques like XPS. The potential was further validated in a collaborative work, where ToF-SIMS was used to show for the newly developed SE  $\text{Li}_7\text{SiPS}_8$  (LiSiPS) that a slowly, but steadily growing interphase forms in contact with lithium.<sup>120</sup>

The experiments for this publication were designed and planned by the first author under the supervision of A. Henss and J. Janek. L. Riegger performed the XPS measurements and analyzed the corresponding data. S. Kayser performed the AFM-SIMS and P. Schweitzer the AFM measurements. The first author analyzed the AFM-SIMS and AFM data. The first author performed the ToF-SIMS measurements and analyzed the data. A. Henss and S. Kayser assisted the scientific discussion of the ToF-SIMS and AFM-SIMS data, respectively. The manuscript was written by the first author and edited by seven co-authors.

Reprinted with permission from Otto, S.-K.; Riegger, L. M.; Fuchs, T.; Kayser, S.; Schweitzer, P.; Burkhardt, S.; Henss, A.; Janek, J.: In Situ Investigation of Lithium Metal-Solid Electrolyte Anode Interfaces with ToF-SIMS. *Advanced Materials Interfaces* **2022**, 9 (13), 2102387. DOI: 10.1002/admi.202102387. Copyright © 2022 Wiley-VCH GmbH.

# In Situ Investigation of Lithium Metal–Solid Electrolyte Anode Interfaces with ToF-SIMS

Svenja-K. Otto, Luise M. Riegger, Till Fuchs, Sven Kayser, Pascal Schweitzer, Simon Burkhardt, Anja Henss,\* and Jürgen Janek\*

Solid-state batteries with a lithium metal anode (LMA) are promising candidates for the next generation of energy storage systems with high energy and power density. However, successful implementation of the LMA requires deeper insight into the lithium metal–solid electrolyte (Li|SE) interface. Since lithium is highly reactive, reaction products form when it comes into contact with most solid electrolytes (SEs) and the resulting interphase can have detrimental effects on cell performance. To better understand the formation of interphases, Li|SE interfaces are studied with time-of-flight secondary-ion mass spectrometry (ToF-SIMS), which provides chemical information with high sensitivity in 2D as well as 3D and is a valuable complement to commonly used techniques. To investigate the interphase, lithium is deposited in situ on SE pellets either through lithium vapor deposition or electrochemical lithium plating. Subsequent depth profiling provides information about the stability of the Li|SE interface and about the microstructure of the formed interphase. At the Li|Li<sub>6</sub>PS<sub>5</sub>Cl interface of lithium metal with argyrodite-type Li<sub>6</sub>PS<sub>5</sub>Cl, an apparently covering Li<sub>2</sub>S-rich layer is found as major part of the interphase. Independent of the deposition method, a combination of ToF-SIMS and atomic force microscopy indicates a thickness of about 250 nm for the Li<sub>2</sub>S-rich interlayer.

## 1. Introduction

The growing demand for electric vehicles and storage of renewable energy are strong driving forces behind intensive research on next-generation batteries.<sup>[1,2]</sup> They are expected to provide advantages over state-of-the-art lithium-ion batteries (LIBs) in terms of several key performance indicators, such as energy and power density, cycle lifetime, safety, and costs. Within this context, solid-state batteries (SSBs) are intensively explored as an emerging technology. Replacing the liquid electrolyte in conventional LIBs with a nonflammable solid electrolyte (SE) is expected to improve the battery safety. Furthermore, this transition is anticipated to allow the implementation of lithium metal as anode, a concept that may enable an exceptionally high energy density.<sup>[3,4]</sup>

Several approaches exist for implementing lithium metal anodes (LMAs) in the fabrication process of SSBs.<sup>[2]</sup> They are

based either on the use of thin lithium foils, the deposition of lithium metal by physical vapor deposition or from a lithium melt, or the electrochemical deposition of lithium from a lithiated cathode active material.<sup>[4,5]</sup> While the preparation and processing of thin lithium foils is challenging, the deposition of metals has generally proven to be scalable and economically feasible. These alternatives to implement the LMA differ by depositing lithium either during the cell assembly (deposition from the gas or liquid phase) or after cell assembly (electrochemical deposition). Especially the latter, which is often referred to as “anode-free” cell technology, appears to be highly attractive due the reduced amount of electrochemically inactive lithium excess, a reduced number of production steps, and the lack of a native passivation layer on typical commercial lithium foils.<sup>[6]</sup>

For the successful implementation of the LMA in SSBs, the lithium|SE interface (Li|SE interface) is critical, as (electro)chemical side reactions occur for most SEs. The degradation products that form at the Li|SE interface can cause a large interfacial resistance and lithium loss that adversely affect the battery performance. Despite its detrimental impact on the battery performance, the chemical composition and the structure of the forming interphase, as well as its microstructure, are rarely studied in detail. The properties of these interphases are determined by the interaction of lithium and the SE, which needs to be thoroughly investigated to understand the individual challenges, develop optimization strategies and, finally, enable LMAs in SSBs.<sup>[7,8]</sup>

S.-K. Otto, L. M. Riegger, T. Fuchs, S. Burkhardt, A. Henss, J. Janek  
Institute of Physical Chemistry  
Justus-Liebig-Universität Giessen  
Heinrich-Buff-Ring 17, D 35392 Giessen, Germany  
E-mail: anja.henss@phys.Chemie.uni-giessen.de;  
Juergen.Janek@phys.Chemie.uni-giessen.de

S.-K. Otto, L. M. Riegger, T. Fuchs, P. Schweitzer, S. Burkhardt,  
A. Henss, J. Janek

Center for Materials Research (ZfM)  
Justus-Liebig-Universität Giessen  
Heinrich-Buff-Ring 16, D 35392 Giessen, Germany

S. Kayser  
IONTOF GmbH  
Heisenbergstraße 15, D 48149 Münster, Germany

P. Schweitzer  
Institute of Applied Physics  
Justus-Liebig-Universität Giessen  
Heinrich-Buff-Ring 16, D 35392 Giessen, Germany

 The ORCID identification number(s) for the author(s) of this article can be found under <https://doi.org/10.1002/admi.202102387>.

© 2022 The Authors. *Advanced Materials Interfaces* published by Wiley-VCH GmbH. This is an open access article under the terms of the Creative Commons Attribution-NonCommercial-NoDerivs License, which permits use and distribution in any medium, provided the original work is properly cited, the use is non-commercial and no modifications or adaptations are made.

DOI: 10.1002/admi.202102387

In general, three types of Li|SE interphases have originally been defined by Wenzel et al.<sup>[9]</sup> First, the SE can be thermodynamically stable against lithium and no chemical reaction takes place. Consequently, the original 2D interface remains unchanged. In the second case, the SE is thermodynamically unstable against lithium metal and the formed reaction products create an interphase with noticeable partial electronic and ionic conductivity. Thus, the forming interphase does not hinder further reaction and the resulting mixed-conducting interphase (MCI) grows steadily.<sup>[8,10]</sup> The third possibility is the formation of a solid electrolyte interphase (SEI) with negligible electronic conductivity. In this case, the SE is thermodynamically unstable against lithium, but the electronically insulating properties of the forming reaction products prevent massive interphase formation on relevant time scales. Thus, the SE is kinetically stable.<sup>[9,11–13]</sup>

For the investigation and classification of Li|SE interfaces, different characterization strategies and methods were applied so far. Mostly, X-ray photoelectron spectroscopy (XPS) was used. For example, Wenzel et al. applied an in situ XPS approach to study the reaction between lithium metal and various SEs.<sup>[9]</sup> The authors used the internal argon ion sputter gun to deposit lithium from a target on the SE surface and analyzed the forming reaction products subsequently. With this strategy, the instability of lithium lanthanum titanate (LLTO) was investigated first.<sup>[9]</sup> In further studies, Wenzel et al. studied  $\text{Li}_{10}\text{GeP}_2\text{S}_{12}$  (LGPS),  $\text{Li}_7\text{P}_3\text{S}_{11}$ , and argyrodite SEs in contact with lithium deposited through sputter deposition.<sup>[14–16]</sup> The XPS results were complemented by time-resolved electrochemical impedance spectroscopy measurements to follow the kinetics of the interphase formation, and the thickness of the SEI was estimated.<sup>[11,15]</sup> Liu et al. investigated the interaction of sulfide SE with lithium through a stepwise deposition of lithium on the SE surface and subsequent XPS characterization.<sup>[13]</sup> Also, the same authors described the effect of aging on the interphases.<sup>[15]</sup> In another XPS study, Wood et al. investigated the Li| $\text{Li}_2\text{S}-\text{P}_2\text{S}_5$  interface with an operando approach.<sup>[12]</sup> They used the bias of an electron gun to bring Li to the SE surface and ultraviolet light to reverse this effect. By applying Auger electron spectroscopy, the authors found that the forming SEI is distributed inhomogeneously at the surface and shows a layered internal structure.<sup>[12]</sup> A similar operando study on LGPS and  $\text{Li}_6\text{PS}_5\text{Cl}$  (LPSCl) in contact with lithium was published.<sup>[17]</sup>

Recently, Connell et al. highlighted that the energy input at the interface is an important factor affecting the reactivity of  $\text{Li}_7\text{La}_3\text{Zr}_2\text{O}_{12}$  with lithium metal.<sup>[18]</sup> For their study, the authors used a variety of in situ and operando XPS techniques and showed that the method for depositing lithium on the SE surface affects the reactivity with lithium metal.

Less frequently used methods for Li|SE interface characterization are transmission electron microscopy (TEM), time-of-flight secondary-ion mass spectrometry (ToF-SIMS), or others, as reviewed by Banerjee et al.<sup>[19]</sup> For example, in situ electron microscopy offers the possibility to study very thin reaction layers, as reported by Ma et al. and Hood et al., for the SEs  $\text{Li}_{7-3x}\text{Al}_x\text{La}_3\text{Zr}_2\text{O}_{12}$  and Li phosphorus oxynitride, respectively.<sup>[20,21]</sup> However, beam damage and artefacts caused by the energetic electron beam have to be taken into

account, even though the damage may be reduced by cryogenic temperatures.<sup>[22]</sup> The suitability of ToF-SIMS for studying Li|SE interfaces and interphases was demonstrated by Yang et al., who investigated LLTO after contact to lithium metal.<sup>[23]</sup> However, the method was not used to study different SEs systematically, and the important strength of ToF-SIMS to enable 3D elemental maps was not brought into play. 3D mapping with ToF-SIMS provides complementary information to that accessible with XPS and impedance characterization. In addition, ToF-SIMS bridges the length scale between XPS and TEM and is therefore a valuable complementary analytical tool.

In the present work, we focus on the characterization of Li|SE interfaces with ToF-SIMS. The interfaces are prepared either by lithium vapor deposition or electrochemical deposition. Depth profiling through micrometer-thick lithium layers on the SE substrate allows the classification of the interface type (stable, SEI, or MCI) and gives information about the 3D structure of interphases formed. In addition, we combine ToF-SIMS with complementary XPS analyses to confirm the structural information. The combination of ToF-SIMS and atomic force microscopy (AFM) is additionally used to obtain roughness and thickness information. For the argyrodite-type LPSCl, a widely used SE in SSBs, the thickness of the forming  $\text{Li}_2\text{S}$ -rich interphase layer is determined and the influence of different in situ preparation methods of the Li|SE contact is investigated.

## 2. Results and Discussion

For the ToF-SIMS investigation of Li|SE interfaces, we chose to characterize layered systems via depth profiling. With this approach, the good depth resolution of ToF-SIMS (down to 1 nm) can be used and 3D information is accessible. The samples for the study were SE pellets with a 1–3  $\mu\text{m}$  thick lithium layer on top. The lithium layer was deposited on top of the SE pellets in situ either through thermal vapor deposition with an effusion cell, as described in Section S1 (Supporting Information) or by using a flood gun as “virtual” electrode. For analysis, depth profiling was conducted through the entire lithium layer and until signals related to the SE substrate were observed. The most suitable parameters for depth profiling are discussed in Section S2 (Supporting Information).

In the following sections, we focus first on the investigation of MgO as inert reference substrate and three different SEs, namely  $\text{Li}_{6.25}\text{Al}_{0.25}\text{La}_3\text{Zr}_2\text{O}_{12}$  (LLZO), LPSCl, and  $\text{Li}_{1.5}\text{Al}_{0.5}\text{Ti}_{1.5}(\text{PO}_4)_3$  (LATP), each with an in situ deposited lithium layer on top. It is shown how the stability of the materials can be classified through interpretation of the ToF-SIMS depth profiles. Next, we concentrate on LPSCl and show that – in addition to stability information – 3D structural information can be accessed from ToF-SIMS measurements. Complementary XPS analyses confirm the results and provide quantitative information. Afterward, the concept of in situ lithium plating with a “virtual” electrode is discussed in more detail. Last, the Li|SE layered systems prepared through lithium vapor deposition and those prepared by lithium plating on LPSCl are compared with respect to the obtained ToF-SIMS depth profiles. The analyses are complemented by AFM to access roughness and thickness information.

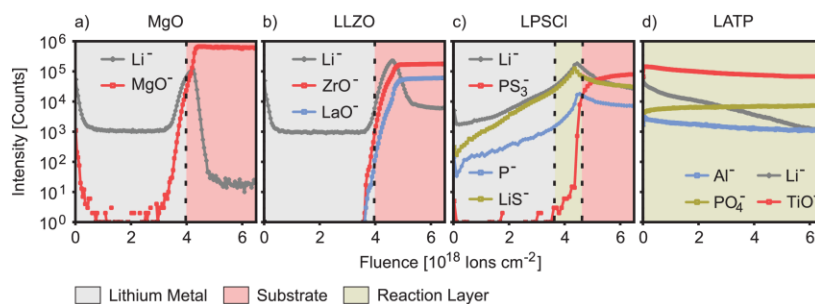


**Figure 1.** ToF-SIMS depth profiles through an originally 3  $\mu\text{m}$  thick lithium layer on top of a) MgO, b) LLZO, c) LPSCI, and d) LATP substrates. The lithium layers were prepared by vapor deposition.

### 2.1. Comparison of Different Li|SE Systems

ToF-SIMS depth profiles through a 3  $\mu\text{m}$  thick lithium layer vapor deposited on MgO, LLZO, LPSCI, and LATP are presented in **Figure 1** to provide a comprehensive overview on the results obtained from interfaces with a different stability against lithium metal. The (in)stability of all these materials is known from literature, which enables the interpretation of the profiles for the different samples.

First, MgO is shown (Figure 1a), which is stable against lithium<sup>[10,24]</sup> and can be used to document the depth profile for an inert material. The ToF-SIMS depth profile indicates that a covering layer of lithium forms on top of MgO, as no  $\text{MgO}^-$  signal is detected at the beginning of the profile. The intensity at the very beginning of the profile is attributed to surface contamination signals in the  $\text{MgO}^-$   $m/z$  region. After a sputter fluence of about  $4 \times 10^{18}$  ions  $\text{cm}^{-2}$ , the intensity of the  $\text{MgO}^-$  signal increases quickly and becomes constant at a high signal intensity. Complementary to this, the  $\text{Li}^+$  signal intensity is constant after sputtering through the uppermost surface layers, increases together with the first  $\text{MgO}^-$  signals, and drops again afterward. The increase at the interface may derive from matrix effects, meaning that the increase in signal intensity is caused by the changing chemical environment and its influence on the ionization probability. Alternatively, the increase in  $\text{Li}^+$  signal intensity may originate from reaction products formed with surface contaminations like hydrocarbons on the MgO substrate. For the interpretation of all ToF-SIMS depth profiles, it should be noted that Li signals are more intense for lithium-containing compounds than for the lithium metal itself (due to matrix effects). As a result, the  $\text{Li}^+$  signal shows lower intensity in the region of the metallic lithium than at the surface or interface.<sup>[25]</sup>

As first SE, LLZO was investigated (Figure 1b). LLZO is a garnet-type oxide SE with an ionic conductivity of up to  $1 \text{ mS cm}^{-1}$  at room temperature. There is still debate about the stability of LLZO against lithium. LLZO is reported to be thermodynamically stable in contact with lithium,<sup>[26]</sup> however, some recent reports discuss, whether a very thin passivation layer is formed. Results by Connell et al.<sup>[18]</sup> indicate that the energy input upon contact is an important factor to consider when investigating a reaction layer. In any case, a formed interphase must be very thin and, e.g., Ma et al. reported a thickness

of  $\approx 5$  unit cells.<sup>[20]</sup> Such a thin interphase would not be detectable by ToF-SIMS depth profiling. Consequently, LLZO resembles a stable SE for ToF-SIMS analyses and the ToF-SIMS depth profile shows close similarity to the one of MgO (see Figure 1a). LLZO-related signals appear only after prolonged sputtering and then increase rapidly to a constant signal intensity. The trend of the  $\text{Li}^+$  signal is the same as for a MgO substrate, except for the intensity after reaching the bulk substrate, since LLZO contains lithium ions. The maximum in  $\text{Li}^+$  signal intensity at the interface may again originate from matrix effects or contaminations on the substrate. Also, the sputter fluence required until the first LLZO-related signals appear is almost the same as for MgO. This similarity confirms that LLZO is stable against lithium. If an interlayer forms, it must be very thin and cannot be detected by ToF-SIMS depth profiling, which is consistent with the literature cited.

The next material analyzed is LPSCI, an argyrodite-type SE for which an ionic conductivity of about  $2 \text{ mS cm}^{-1}$  at room temperature has been reported.<sup>[2]</sup> Therefore, LPSCI is considered to be one of the best choices for SSB.<sup>[27]</sup> For LPSCI, the formation of a SEI in contact with lithium was found by XPS. As reaction products,  $\text{Li}_3\text{P}$ ,  $\text{Li}_2\text{S}$ , and  $\text{LiCl}$  were reported.<sup>[15]</sup> Right in the beginning of the ToF-SIMS depth profile, SE-related signals like  $\text{LiS}^-$  are detected. Also, these SE-related signals show a clear evolution and a maximum in intensity before the substrate region is reached. This indicates a layered structure of reaction products accumulated at the LPSCI interface forming the SEI. At a sputter fluence slightly higher than that required in experiments on MgO and LLZO, additional signals like the  $\text{PS}_3^-$  fragment appear and rapidly increase in intensity, probably indicating that the LPSCI substrate is reached.

Finally, LATP, which is a NASICON-type oxide SE (Na super ion conductor), was investigated. For LATP, the formation of a MCI was found as  $\text{Ti}^{4+}$  is reduced to its metallic state in contact with lithium. This leads to an increase of the partial electronic conductivity of the material. In combination with the ionic conductivity of the forming reaction products, a continuous reaction of LATP and lithium is possible.<sup>[10,28]</sup> As expected for MCI-forming SEs, the ToF-SIMS depth profile looks completely different than the profiles observed previously. SE-related signals are intense from the very beginning of the depth profile on and only a slight increase in intensity is observed until the substrate should be reached corresponding to the fluence. Also, no

additional SE signals appear through sputtering, which probably indicates that the lithium layer is completely converted into the MCI. This is in accordance with the reported ongoing reaction between LATP and lithium.

## 2.2. Classification of Li|SE Interfaces

Based on the presented results, indicators for the classification of the stability of SEs in contact with lithium from ToF-SIMS depth profiles of Li|SE layered systems can be derived. For inert materials, no SE-related signals are present at the beginning of the profile. Also, the fluence required until substrate signals are detected matches for different inert materials if the same amount of lithium is vapor deposited. For calibration, MgO can be used as a substrate.

SEs that form a stable SEI show maxima in the intensity of SE-related signals, indicating the SEI before the substrate is reached. These signals may already appear at the beginning of the profiles and their intensity depends on the amount of vapor deposited lithium and the thickness of the forming SEI. Please note that the amount of deposited lithium that is optimal to classify different materials will vary depending on the thickness of the forming SEI. In the case of potentially thick SEIs, the deposition of different amounts of lithium is recommended, starting with low amounts. For the formation of a SEI, an increasing amount of deposited lithium will add a longer period of increasing signal intensity at the beginning of the depth profile.

For the formation of a MCI, the intensity of SE-related signals is high throughout the complete depth profile. Depending on the amount of lithium deposited, the material may have reacted to such an extent that the unaltered SE region can no longer be reached by sputtering. Also, in case of MCI formation, the deposition of a higher amount of lithium will not prevent or reduce the detection of SE-related signals, at least not for amounts that can react in the given time. In case of doubt, it is recommended to measure the sample several times after some waiting time (e.g., one week). In the case of a MCI, the reaction layer will grow strongly in short time periods, whereas the growth of a SEI is negligible and the ToF-SIMS depth profiles are unchanged over time, as shown for LPSCl in Section S3 (Supporting Information).

At this point, we like to emphasize that the distinction between SEI- and MCI-type interfaces is not sharp, since the rate of negligible interphase growth is rather undefined. Cell tests with impedance spectroscopy are necessary to find out whether the interfacial resistance attributed to the interphase growth is too high for a specific application. However, the analytical approach presented herein is valuable for understanding the cell test results and for finding strategies to overcome possible limitations.

## 2.3. Microstructure of the Li|LPSCl Interphase

ToF-SIMS depth profiles of Li|SE layered systems can also provide information about the 3D structure of the forming interphase. This is shown in the following text for the example of

LPSCl, as investigation with TEM is difficult for thiophosphate SEs due to electron beam damage. Depth profiles of LPSCl with 1  $\mu\text{m}$  of vapor deposited lithium on top are shown in Figure 2.

The normalized intensity data obtained during ToF-SIMS depth profiling are depicted with a linear instead of a logarithmic intensity scale. This shows the increasing signal intensity for SE-related signals like the  $\text{LiS}^-$  signal before reaching the substrate even clearer and makes it also possible to identify the intensity maxima of different species. Interestingly, the maxima are reached after different fluences, which indicate a layered structure. It is clearly observed that the maximum of the  $\text{LiS}^-$  signal is reached first and that the maximum for the  $\text{P}^-$  signal follows later before the substrate, indicated by the  $\text{PS}_3^-$  signal, is reached. The distribution of Cl signals is similar to P signals, which can be seen in Figure 4.

The assumption of a layered SEI structure is confirmed by the 3D representation of the depth profile in Figure 2c. Apparently, a layer of S-related species is observed at the interface toward the lithium metal layer. It is followed by a P-enriched layer toward the SE interface. Laterally, the  $\text{LiS}^-$  and  $\text{P}^-$  intensities are distributed homogeneously, giving the impression of well-covering layers. Another way to assess the layered structure of the SEI is to image a wedge-shaped crater, as shown in Figure 2d. A wedge is a sputter crater prepared with increasing dose in one lateral direction. Please note that it is not possible to gain any direct depth information from the wedge image, as the sputter rates of the different layers and accordingly the slope of the regions may be different. This accounts also for the given depth profile. For the shown Li|LPSCl wedge, the depth of the crater increases from left to right. Accordingly, the 2D projection of the chemical composition within the wedge shows first an increasing  $\text{LiS}^-$  signal intensity, then the  $\text{P}^-$  signal becomes more intense before the substrate signal  $\text{PS}_3^-$  is reached. The lateral distribution of the different species perpendicular to the direction in which the sputter dose was increased can also be assessed. Only slight deviations are observed in all signals, yet the qualitative sequence is not affected and the impression of covering layers is maintained at the length scale and resolution examined.

As SIMS is a semiquantitative method, changes in signal intensity may also be attributed to a changing matrix when reaching the substrate region. Therefore, XPS depth profiles of the Li|LPSCl sample were also recorded. The results presented in Figure 2b show a maximum for the S-concentration in the form of  $\text{Li}_2\text{S}$  at lower etch time compared to the etch time at which the S-concentration in the form of  $\text{PS}_4^{3-}$ , representing the substrate, reaches its full intensity. A comparison of the atomic concentrations of the Cl-concentration in the form of  $\text{Cl}^-$  as well as the S- and P-concentrations in the form of  $\text{PS}_4^{3-}$  can be found in Section S4 (Supporting Information). No maxima were found for the complementary SEI compounds  $\text{Li}_3\text{P}$  and  $\text{LiCl}$ . This can originate either from a compound concentration below the detection limit, or from a chemical shift that is not pronounced enough to differentiate the signals of SE and reaction products by XPS. However, it seems reasonable that the enrichment of a S species in one layer comes along with an enrichment of the other elements in a different region to fit the chemical composition of the SE. The ToF-SIMS results indicate that this enrichment is present between a  $\text{Li}_2\text{S}$ -rich layer

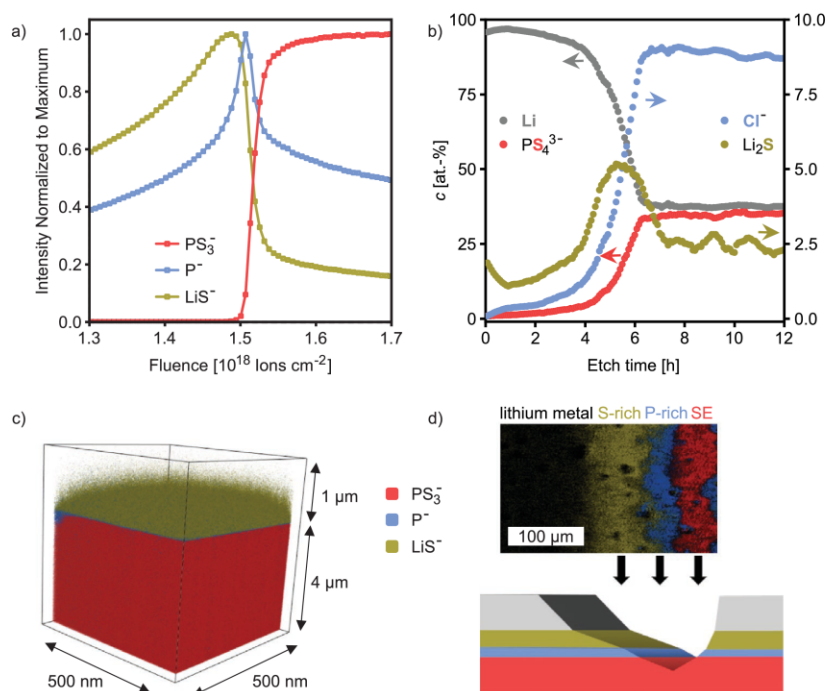


**Figure 2.** Characterization of the Li|LPSCl interface with ToF-SIMS and XPS. For the measurements, 1  $\mu\text{m}$  of lithium was vapor deposited on a LPSCl pellet. a) ToF-SIMS depth profile, b) XPS depth profile: atomic percentages are given for the elements presented in bold and color. Please mind the two different scales, the arrows point toward the scale of the corresponding data and the labels are oriented accordingly. c) 3D representation of the ToF-SIMS depth profile and d) ToF-SIMS imaging of a wedge crater.

and the SE pellet. Such a layered structure for the Li|LPSCl interphase is supported by the operando XPS data reported by Davis et al.<sup>[17]</sup> They plated lithium on the LPSCl SE and detected the resulting reaction products by XPS. Measurements after increasing lithium plating times show that  $\text{Li}_2\text{S}$  is detected much longer than P and Cl reaction products. Accordingly, the formation of  $\text{Li}_2\text{S}$  extends possibly significantly deeper into the lithium.<sup>[17]</sup>

#### 2.4. In Situ Lithium Plating

As recent studies show, the way how the Li|SE contact is created may influence the interface reactivity.<sup>[18]</sup> Also, different preparation methods may mimic the various cell concepts of SSB with LMA. Therefore, a second option to study the interfaces was tested by plating lithium electrochemically on top of the materials directly in the ToF-SIMS chamber. For this purpose, the flood gun of the SIMS instrument was used as virtual electrode to induce a lithium-ion flux through the SE. The resulting lithium film and the corresponding ToF-SIMS depth profile are shown for LLZO in Figure 3a,b, respectively.

As the picture of the sample after 1 h of plating already indicates, the plated lithium film is inhomogeneously distributed and the thickness varies across the substrate surface. Still, on the lateral scale of few hundreds of micrometers, the film is relatively homogenous and ToF-SIMS measurements can be

conducted to obtain reliable and meaningful results. The intensity data obtained by depth profiling through the lithium layer show a low intensity for LLZO-related signals at the beginning, followed by an exponential increase until the signal intensities become constant. As it is known that LLZO is stable against lithium, the observation of a slower intensity increase for substrate signals compared to the sample with vapor deposited lithium indicates a higher roughness of the plated lithium layer. For a better comparison, the  $\text{ZrO}^-$  depth profiles for plated and vapor deposited lithium are compared in Figure 3c. Due to the higher roughness of the plated lithium, the LLZO substrate is reached at various fluences for different spots of the measurement area and the profile is smeared out. Consequently, a direct comparison of ToF-SIMS depth profiles for vapor deposited and plated lithium layers is not possible. To overcome this limitation, we combined ToF-SIMS with AFM for further investigations.

#### 2.5. Comparison of Lithium Vapor Deposition with Plating for LPSCl

For the AFM-SIMS study, a vapor deposited lithium layer is compared with a plated layer for LPSCl, as shown in Figure 4. AFM does not only allow to measure the roughness of the samples but also gives access to depth information through measuring the dimensions of the ToF-SIMS crater at defined points

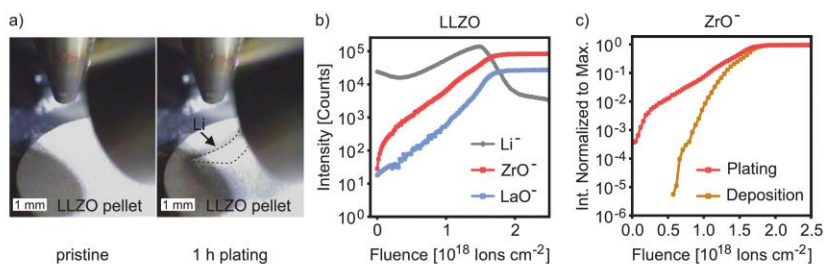


**Figure 3.** In situ lithium plating on LLZO. a) Camera images showing the LLZO sample before and after 1 h of lithium plating. b) ToF-SIMS depth profile through the plated lithium film and c) comparison of the ZrO<sup>-</sup> signals from depth profiles through plated and vapor deposited lithium on LLZO. For better comparison, the fluence scale was shifted by  $2.5 \times 10^{18}$  ions cm<sup>-2</sup> for the vapor deposited sample to match the point where the highest signal intensity is reached for both measurements.

of the depth profile. This information is used to determine the thickness of the forming Li<sub>2</sub>S-rich layers as dominant part of the observed SEI.

Only judging from the ToF-SIMS depth profile through vapor deposited and plated lithium on LPSCl shown in Figure 4a, the Li<sub>2</sub>S-rich layer defined by the LiS<sup>-</sup> signal seems to be thicker after plating, as the region of high intensity is broader. However, as shown previously, roughness effects need to be considered. Scanning electron microscope (SEM) and AFM measurements of the lithium layers in Figure 4b,c, respectively, show that the plated lithium is rougher than the vapor deposited lithium, as already indicated by the results obtained for LLZO. From the AFM measurements, a surface roughness of  $(189 \pm 14)$  and  $(297 \pm 56)$  nm was determined for vapor deposited and plated lithium layers on LPSCl, respectively. Both values are significantly higher than the roughness of pristine LPSCl pellets of  $(85 \pm 25)$  nm.

SEM and AFM investigations of the vapor deposited sample show an island-like growth with pits between the different islands. The pits may serve as a reasonable explanation for the observation of SEI-related signals like LiS<sup>-</sup> at the beginning of the ToF-SIMS depth profiles. A complete exposure of the substrate is unlikely as no substrate signals are detected before sputtering. In addition, imaging indicates covering layers as discussed previously. Consequently, the hollow parts of the surface seem to play a minor role for the overall intensity data obtained during depth profiling. For the plated sample, the lithium shows an inhomogeneous structure with facets, typically observed in crystalline materials, as well as holes. However, the ToF-SIMS depth profile indicates that the plated lithium film is covering, since no substrate signals are detected before sputtering. Still, the very inhomogeneous structure causes the observed broadening of the depth profile. Additionally, the roughness probably leads to pronounced preferential sputtering.

To determine the actual thickness of the Li<sub>2</sub>S layers, homogeneous areas were defined according to the LiS<sup>-</sup> and PS<sub>3</sub><sup>-</sup> signals in the ToF-SIMS depth profiles. The criteria for homogeneity of certain areas are that the signal intensities detected at positions within an area develop comparably at the same fluence and do not show a pronounced lateral gradient. In the defined areas, the difference profiles of AFM measurements were used to obtain depth information. The beginning and end of the

Li<sub>2</sub>S-rich layers were defined by the fluence at the inflection points of the LiS<sup>-</sup> signal intensity. The corresponding difference profiles of AFM scans before and after the Li<sub>2</sub>S reaction layer are shown in Figure 4d. The regions used for thickness evaluation are marked in brown. The determined average thicknesses are  $(269 \pm 35)$  nm for vapor deposited lithium and  $(251 \pm 26)$  nm for plated lithium. According to these values, the thickness of the Li<sub>2</sub>S layer formed between lithium and LPSCl through vapor deposition and plating is the same within the uncertainty of the experiments. The sputter yield calculated for the Li<sub>2</sub>S layers from the AFM-SIMS measurements was  $1.5 \pm 0.2$ , which fits with the one determined for a Li<sub>2</sub>S pellet ( $1.4 \pm 0.1$ ). However, the generally high roughness of the samples and the high sputter rate for the underlying LPSCl substrate (about twice the sputter rate for Li<sub>2</sub>S) complicate the analysis and cause the reported uncertainty range of about 50 nm.

In literature, the thickness of various Li|SE interphases was estimated from impedance measurements.<sup>[14,16]</sup> For LPS, which behaves quite similar to LPSCl in impedance measurements and which was also tested to show a similar ToF-SIMS depth profile after lithium deposition, a thickness of only 23 nm after one year of growth was estimated.<sup>[15]</sup> This is one order of magnitude lower than the value determined with AFM-SIMS after one week. A possible explanation for the discrepancy may be the different interface preparation. For the mentioned impedance measurements, lithium foil, which is natively covered by a thin passivation layer, was pressed to a LPSCl pellet. The lithium foil might then be less reactive than vapor deposited or plated lithium, which naturally leads to a thinner interphase. Also, for the analysis of impedance data, the SEI thickness was estimated assuming Li<sub>2</sub>S bulk properties, which may differ substantially from the actual conductivity of the interphase. Impedance measurements of differently prepared lithium films could help to improve the understanding of the experiments.

### 3. Conclusions

ToF-SIMS depth profiling is used to study Li|SE interfaces and the interphase formation taking place at such interfaces. As samples SE pellets with a micrometer-thick lithium layer on top were investigated. Stable, SEI forming, and MCI forming SEs can be differentiated from the SIMS depth profiles of thermally

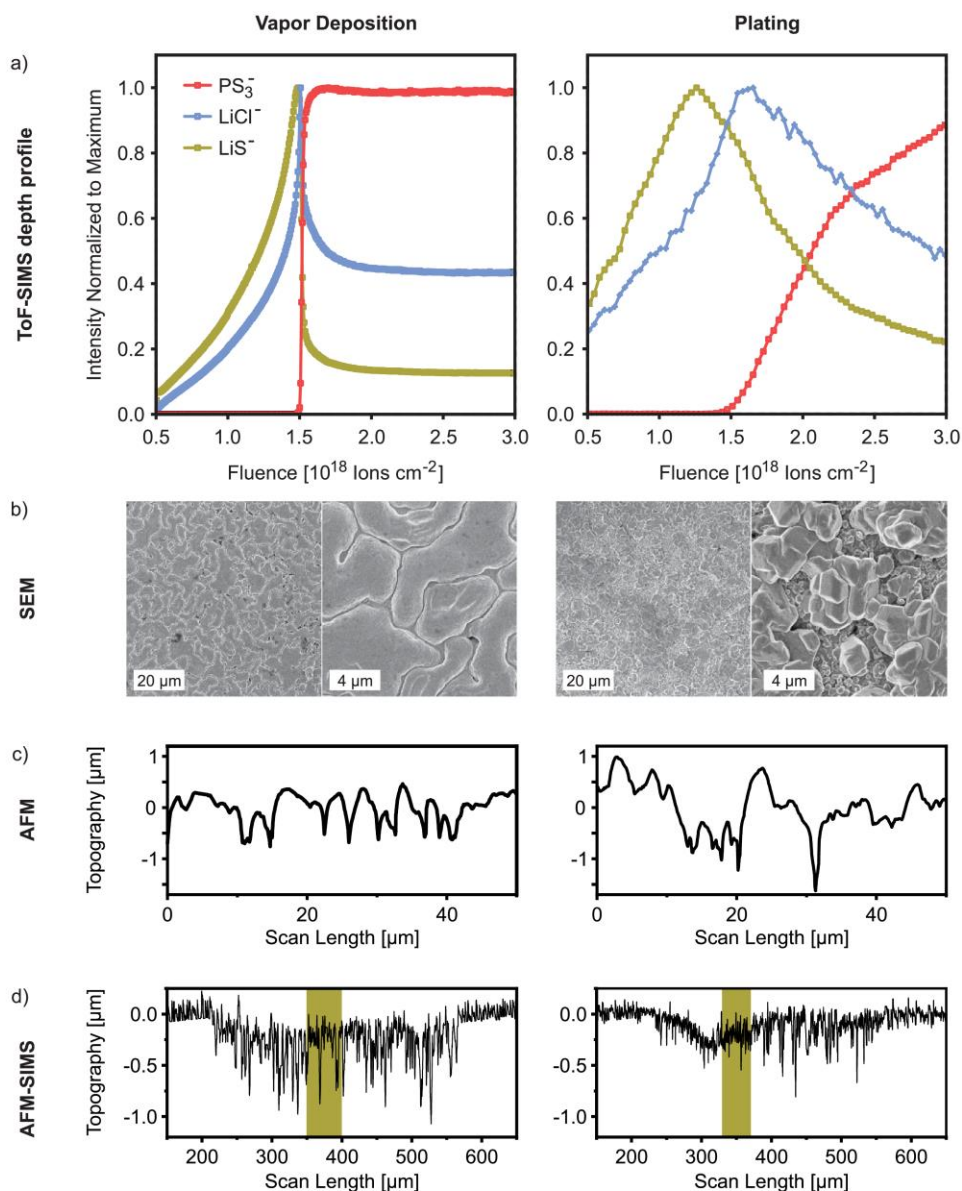


**Figure 4.** Comparison of Li|LPSCl interfaces with vapor deposited and plated lithium layers. For the measurements, 1  $\mu\text{m}$  of lithium was vapor deposited on LPSCl. Alternatively, lithium was plated for 1 h, which leads to a similar average thickness of lithium in the plating region, based on the fluence that is needed to detect the first substrate signals. a) ToF-SIMS depth profiles, b) SEM surface images, c) AFM surface scans, and d) AFM-SIMS difference profiles of scans before and after the  $\text{Li}_2\text{S}$ -rich reaction layer.

deposited lithium layers. For stable SEs, no SE-related signals are detected at sputter fluences below the fluence required to reach the substrate. For SEI- and MCI-forming SEs, SE-related signals are detected at lower fluences. In the case of a SEI, a significant increase and maxima of the signal intensities are observed during depth profiling toward the substrate. In

contrast to that, the formation of a MCI results in high signal intensities for SE-related species throughout the whole depth profile. To distinguish a thick SEI from a MCI, deposition of different thicknesses of lithium and measurements after different times for sample storage can be used. In addition to this classification, ToF-SIMS measurements give information on

the 3D structure of the forming interphases. A layered structure with  $\text{Li}_2\text{S}$  on top of potential  $\text{P}^-$  and  $\text{Cl}^-$  enrichments is found for LPSCl. Complementary XPS analyses confirmed the  $\text{Li}_2\text{S}$  layer between lithium and LPSCl substrate.

To account for the possible influence of differently deposited lithium, we compared Li|SE interfaces prepared by lithium vapor deposition and lithium plating. In this comparison, the roughness of the lithium layer plays an important role. The higher roughness of the plated lithium leads to the impression that plating results in a thicker SEI on LPSCl than vapor deposition. The combination of SIMS and AFM allows to account for this issue and to determine the thickness of the SEI layers that form. AFM–SIMS measurements demonstrate that the thickness of the  $\text{Li}_2\text{S}$ -rich layer between lithium and LPSCl has a comparable value of about 250 nm for lithium vapor deposition and lithium plating. For the reported material system and with respect to the application of lithium metal as anode active material in solid-state batteries, this information is crucial for understanding and modeling the charge transport across this interphase as well as the resulting limitations. Modifications of the Li|SE interphase, e.g., through chemical engineering or other approaches for interface design and optimization will also benefit greatly from knowledge of the internal interphase structure.

Wenzel et al. estimated a much thinner SEI of about 23 nm after one year of growth for LPS, which behaves very similar to LPSCl in impedance measurements and ToF-SIMS depth profiles.<sup>[15]</sup> We like to note that these values result from the assumption of a too low ionic conductivity of the SEI. Wenzel et al. measured the resistance of the SEI with impedance spectroscopy and assumed that the SEI shows the bulk conductivity of  $\text{Li}_2\text{S}$ .<sup>[15]</sup> In the light of our current results, this assumption was incorrect at least by one order of magnitude. In fact, we conclude that the ionic conductivity of the SEI is at least a factor of 10 higher compared to the conductivity of bulk  $\text{Li}_2\text{S}$ , which is reasonable for a nanocrystalline  $\text{Li}_2\text{S}$  layer within the SEI.

Overall, ToF-SIMS is a valuable technique to expand the knowledge on Li|SE interphases. The method described can be used to analyze a wide variety of materials, including those that may be sensitive to beam damage in TEM analyses. Through ToF-SIMS depth profiling, detailed information regarding the stability of the SE and the 3D structure of the forming interphase are accessible in comparably short time. Moreover, the information shown is complementary to that of commonly used XPS and impedance measurements. By combining ToF-SIMS with AFM, roughness and thickness information can be added to provide a complete picture of the Li|SE interphase.

#### 4. Experimental Section

All sample handling and transfer was done under argon atmosphere ( $p(\text{H}_2\text{O})/p < 0.1$  ppm,  $p(\text{O}_2)/p < 0.1$  ppm) to protect the samples from reaction with atmosphere components.

**Materials:** As reference substrate, MgO (CrysTec) was used. LPSCl was purchased from NEI Corporation (USA). LLZO was prepared as described previously.<sup>[29]</sup> LATP was prepared through the sol–gel route previously reported by Ma et al.<sup>[30]</sup> White  $\text{TiO}_2/\text{Ti}(\text{OH})_2$  nanoparticles were precipitated by slowly adding titanium(IV) isopropoxide (17 g) in deionized water (100 mL). These were filtered and washed with

deionized water before being redissolved in freshly prepared nitric acid (2 M, 150 mL). Afterward, citric acid monohydrate (25 g),  $\text{LiNO}_3$  (4.137 g),  $\text{Al}(\text{NO}_3)_3 \cdot 9 \text{H}_2\text{O}$  (7.506 g), and  $\text{NH}_4\text{H}_2\text{PO}_4$  (13.804 g) were added, gelation occurred after the addition of the latter. The gel was dried, crushed, and calcined in air heating at  $2^\circ\text{C min}^{-1}$  to  $650^\circ\text{C}$  for 3 h to give white nanopowders. To reduce particle agglomeration, the calcined powder was ball-milled using 3 mm  $\text{ZrO}_2$  milling media at 120 rpm for 6 h with mass ratios of LATP:EtOH: $\text{ZrO}_2$  equal to 1:1.5:20. After ethanol evaporation, 250 mg of powders in a 13 mm cylindrical mold were uniaxially shaped at 150 MPa and then isostatically pressed at 500 MPa for 30 min. The obtained pellets were sintered, heating at  $2^\circ\text{C min}^{-1}$  to  $950^\circ\text{C}$  for 5 h in air, achieving samples with a geometrical density >97% of the theoretical value. Each surface of the pellets was polished with SiC paper up to P4000, ultrasonicated for 10 min in acetone, and recrystallized by heating at  $2^\circ\text{C min}^{-1}$  to  $900^\circ\text{C}$  without holding the temperature.

**Lithium Vapor Deposition:** A lithium rod (99.8%, abcr GmbH) was cut into smaller pieces as vapor source. The lithium pieces were placed in a crucible of a NTEZ low-temperature effusion cell (MBE Components). Lithium was vapor deposited at a crucible temperature of  $450^\circ\text{C}$ . After a deposition time of 10 min, a lithium layer of 1  $\mu\text{m}$  thickness had formed.

**Lithium Plating:** For lithium plating, thin slices of a lithium rod (99.8%, abcr GmbH) were pressed onto the SE pellets with a Cu foil as underlay. The plating samples were attached to the sample holder with Cu tape for electrical contact. In situ plating was achieved by placing the sample under the analyzer and switching on the flood gun (21 eV, 10  $\mu\text{A}$ ) of the SIMS instrument. The current corresponded to a current density of  $\approx 0.1 \text{ mA cm}^{-2}$  assuming that one sixteenth of the pellet surface was the actual plating area. 1 h of plating resulted in a lithium layer thickness of about 1  $\mu\text{m}$  in the corresponding area. Subsequently, the samples were analyzed as described below, but without using the flood gun.

**ToF-SIMS:** ToF-SIMS measurements were carried out with a ToF-SIMS 5 instrument (IONTOF GmbH), equipped with a 25 kV Bi cluster primary-ion gun for analysis and a dual-source column for  $\text{Cs}^+$  depth profiling. Depth profiles were measured in spectrometry mode (bunched, about 40 000 cts  $\text{s}^{-1}$ , full width at half maximum (FWHM)  $m/\Delta m = 5000@m/z = 17.00$  ( $\text{OH}^-$ )) with  $\text{Cs}^+$  (300  $\times$  300  $\mu\text{m}^2$ , 2 kV, 130 nA) as sputter species and  $\text{Bi}^+$  (1.2 pA, 100  $\times$  100  $\mu\text{m}^2$ ) as primary ions. Between 25 s sputter steps with 2 s pause time, 5 frames with 2 shots  $\text{frame}^{-1}$   $\text{pxl}^{-1}$  and 128  $\times$  128  $\text{pxl}$  were analyzed in random raster mode. The wedge was prepared with a size of 400  $\times$  400  $\mu\text{m}^2$  with  $\text{Cs}^+$  (2 kV, 130 nA), 6 cycles with 25 ms of maximal dwell time were used for preparation. Images were recorded in fast-imaging mode (unbunched, about 20 000 cts  $\text{s}^{-1}$ , FWHM  $m/\Delta m = 80@m/z = 17.00$  ( $\text{OH}^-$ )). 50 scans were measured in sawtooth mode, with 1024  $\times$  1024  $\text{pxl}$ , a field of view of 500  $\times$  500  $\mu\text{m}^2$ , 1 frame  $\text{scan}^{-1}$ , and 1 shot  $\text{frame}^{-1}$   $\text{pixel}^{-1}$ . For all measurements, the cycle time was 100  $\mu\text{s}$  and negative polarity was used. Data were evaluated with SurfaceLab 7.2 (IONTOF GmbH). If not stated differently, the samples were electrically isolated from the sample holder and measured with electron neutralization of the flood gun.

**XPS:** A PHI 5000 VersaProbe II Scanning ESCA Microprobe (Physical Electronics) with monochromatized Al  $K_{\alpha}$  X-ray source (beam diameter of 200  $\mu\text{m}$ , X-ray power of 50 W) was used to measure XP spectra. To sputter through the sample, an acceleration voltage of 2 kV and an argon ion current of 4  $\mu\text{A}$  were used for 5 min per step while rotating the sample with  $360^\circ \text{min}^{-1}$  to get a homogeneous sputter crater. An analyzer pass energy of 46.95 eV, a step time of 50 ms, and a step size of 0.2 eV were used for measuring the detail spectra. Samples were measured with a floating potential and the surface was charge neutralized with slow electrons and argon ions. CasaXPS software was used for data evaluation and the charge correction was done using the  $\text{PS}_{23}^-$  signals in the S2p (161.8 eV) and P2p (131.2 eV) spectra.

**SEM:** SEM images were acquired with a Merlin high-resolution SEM (Carl Zeiss AG) at a pressure in the low  $10^{-6}$  mbar range, an electron acceleration voltage of 1 kV, and a probing current of 100 pA. An in-lens detector was used.

**AFM Roughness:** AFM was performed with a VacuScope 1000 microscope from AIST-NT, which was operated in AC mode under high vacuum below  $10^{-4}$  Pa using an inert gold coated 160AC-GG probe from Opus. A custom-built transfer module was used to prevent air contact of the samples during transport from the inert glove box atmosphere into the AFM system. Surface roughness parameters were evaluated with Gwyddion 2.55 from 50  $\mu\text{m}$  line scans at scan rates between 0.02 and 0.1 Hz. The data were leveled by subtracting the mean of the measured height. Surface roughness was determined by taking the average  $R_a$  value of 15 line scans. The standard deviation of the 15 measurements was given as uncertainty of the roughness.

**AFM-SIMS:** The combined ToF-SIMS/AFM measurements were carried out with a M6 Plus instrument (IONTOF GmbH), equipped with a 30 kV Bi cluster primary-ion gun for analysis and a dual-source column for  $\text{Cs}^+$  depth profiling. Depth profiles were measured in spectrometry mode (bunched, about 200 000 cts  $\text{s}^{-1}$ , FWHM  $m/\Delta m = 9000@m/z = 17.00$  ( $\text{OH}^-$ )) with  $\text{Cs}^+$  ( $300 \times 300 \mu\text{m}^2$ , 2 kV, 140 nA) as sputter species and  $\text{Bi}^+$  ( $2.5 \text{ pA}$ ,  $100 \times 100 \mu\text{m}^2$ ) as primary ions. Between 5 s sputter steps with 0.5 s pause time, 1 frame with 1 shot  $\text{frame}^{-1} \text{pxl}^{-1}$  and  $128 \times 128 \text{pxl}$  was analyzed in random raster mode. Negative polarity and a cycle time of 80  $\mu\text{s}$  were used. For the AFM scans, a Ni cantilever with pyramidal boron-doped diamond tip was used in contact mode. Data were analyzed with SurfaceLab 7.2 (IONTOF GmbH). Thickness information was accessed through the height difference of AFM scans over the ToF-SIMS craters at initial and final positions of the evaluated region. For determining the thickness of the  $\text{Li}_2\text{S}$ -rich region, the inflection points of the  $\text{LiS}^-$  signal intensity were used to define the initial and final positions. The uncertainty was determined from the average variation of the AFM difference profiles outside the sputter crater.

## Supporting Information

Supporting Information is available from the Wiley Online Library or from the author.

## Acknowledgements

The authors like to thank Enrico Trevisanello for the synthesis of LAMP SE and Jonas Horn for his help with AFM measurements. The authors acknowledge the financial support by the Bundesministerium für Bildung und Forschung (BMBF) within the FestBatt – Cluster of Competence for Solid-State Batteries (Grant Nos. 03XP0176D, 03XP0180). S.-K.O. acknowledges the financial support (Kékulé scholarship) by the Funds of the Chemical Industry (FCI). T.F. acknowledges the funding by the BMBF within the LISI project (Grant No. 03XP0224E).

Open access funding enabled and organized by Projekt DEAL.

## Conflict of Interest

The authors declare no conflict of interest.

## Data Availability Statement

The data that support the findings of this study are available from the corresponding author upon reasonable request.

## Keywords

interphase formation, lithium metal anodes, solid electrolytes, solid-state batteries, ToF-SIMS

Received: December 4, 2021

Revised: February 14, 2022

Published online:

- [1] a) M. J. Wang, E. Kazyak, N. P. Dasgupta, J. Sakamoto, *Joule* **2021**, 5, 1371; b) S. Randau, D. A. Weber, O. Kötz, R. Koerver, P. Braun, A. Weber, E. Ivers-Tiffée, T. Adermann, J. Kulisch, W. G. Zeier, F. H. Richter, J. Janek, *Nat. Energy* **2020**, 5, 259.
- [2] Y.-G. Lee, S. Fujiki, C. Jung, N. Suzuki, N. Yashiro, R. Omoda, D.-S. Ko, T. Shiratsuchi, T. Sugimoto, S. Ryu, J. H. Ku, T. Watanabe, Y. Park, Y. Aihara, D. Im, I. T. Han, *Nat. Energy* **2020**, 5, 299.
- [3] a) J. Janek, W. G. Zeier, *Nat. Energy* **2016**, 1, 16141; b) T. Krauskopf, F. H. Richter, W. G. Zeier, J. Janek, *Chem. Rev.* **2020**, 120, 7745; c) Y.-K. Sun, *ACS Energy Lett.* **2020**, 5, 3221.
- [4] Y. Guo, H. Li, T. Zhai, *Adv. Mater.* **2017**, 29, 1700007.
- [5] J. Liu, Z. Bao, Y. Cui, E. J. Dufek, J. B. Goodenough, P. Khalifah, Q. Li, B. Y. Liaw, P. Liu, A. Manthiram, Y. S. Meng, V. R. Subramanian, M. F. Toney, V. V. Viswanathan, M. S. Whittingham, J. Xiao, W. Xu, J. Yang, X.-Q. Yang, J.-G. Zhang, *Nat. Energy* **2019**, 4, 180.
- [6] a) M. J. Wang, E. Carmona, A. Gupta, P. Albertus, J. Sakamoto, *Nat. Commun.* **2020**, 11, 1; b) S.-K. Otto, T. Fuchs, Y. Moryson, C. Lerch, B. Mogwitz, J. Sann, J. Janek, A. Henss, *ACS Appl. Energy Mater.* **2021**, 4, 12798.
- [7] a) R. Chen, Q. Li, X. Yu, L. Chen, H. Li, *Chem. Rev.* **2020**, 120, 6820; b) A. Gurung, J. Pokharel, A. Baniya, R. Pathak, K. Chen, B. S. Lamsal, N. Ghimire, W.-H. Zhang, Y. Zhou, Q. Qiao, *Sustainable Energy Fuels* **2019**, 3, 3279; c) K. J. Kim, M. Balaish, M. Wadaguchi, L. Kong, J. L. M. Rupp, *Adv. Energy Mater.* **2020**, 11, 2002689; d) Y. Xiao, Y. Wang, S.-H. Bo, J. C. Kim, L. J. Miara, G. Ceder, *Nat. Rev. Mater.* **2020**, 5, 105; e) X. Chen, J. Xie, X. Zhao, T. Zhu, *Adv. Energy Sustainability Res.* **2021**, 2, 2000101; f) C.-Z. Zhao, H. Duan, J.-Q. Huang, J. Zhang, Q. Zhang, Y.-G. Guo, L.-J. Wan, *Sci. China: Chem.* **2019**, 62, 1286.
- [8] L. M. Riegger, R. Schlem, J. Sann, W. G. Zeier, J. Janek, *Angew. Chem., Int. Ed. Engl.* **2021**, 60, 6718.
- [9] S. Wenzel, T. Leichtweiss, D. Krüger, J. Sann, J. Janek, *Solid State Ionics* **2015**, 278, 98.
- [10] P. Hartmann, T. Leichtweiss, M. R. Busche, M. Schneider, M. Reich, J. Sann, P. Adelhelm, J. Janek, *J. Phys. Chem. C* **2013**, 117, 21064.
- [11] F. J. Simon, M. Hanauer, F. H. Richter, J. Janek, *ACS Appl. Mater. Interfaces* **2020**, 12, 11713.
- [12] K. N. Wood, K. X. Steirer, S. E. Hafner, C. Ban, S. Santhanagopalan, S.-H. Lee, G. Teeter, *Nat. Commun.* **2018**, 9, 1.
- [13] Z. Liu, A. Borodin, G. Li, X. Liu, Y. Li, F. Endres, *J. Phys. Chem. C* **2020**, 124, 300.
- [14] S. Wenzel, S. Randau, T. Leichtweiß, D. A. Weber, J. Sann, W. G. Zeier, J. Janek, *Chem. Mater.* **2016**, 28, 2400.
- [15] S. Wenzel, S. J. Sedlmaier, C. Dietrich, W. G. Zeier, J. Janek, *Solid State Ionics* **2018**, 318, 102.
- [16] S. Wenzel, D. A. Weber, T. Leichtweiss, M. R. Busche, J. Sann, J. Janek, *Solid State Ionics* **2016**, 286, 24.
- [17] A. L. Davis, E. Kazyak, D. W. Liao, K. N. Wood, N. P. Dasgupta, *J. Electrochem. Soc.* **2021**, 168, 070557.
- [18] J. G. Connell, T. Fuchs, H. Hartmann, T. Krauskopf, Y. Zhu, J. Sann, R. Garcia-Mendez, J. Sakamoto, S. Tepavcevic, J. Janek, *Chem. Mater.* **2020**, 32, 10207.
- [19] A. Banerjee, X. Wang, C. Fang, E. A. Wu, Y. S. Meng, *Chem. Rev.* **2020**, 120, 6878.
- [20] C. Ma, Y. Cheng, K. Yin, J. Luo, A. Sharafi, J. Sakamoto, J. Li, K. L. More, N. J. Dudney, M. Chi, *Nano Lett.* **2016**, 16, 7030.
- [21] Z. D. Hood, X. Chen, R. L. Sacchi, X. Liu, G. M. Veith, Y. Mo, J. Niu, N. J. Dudney, M. Chi, *Nano Lett.* **2021**, 21, 151.
- [22] Y. Li, Y. Li, A. Pei, K. Yan, Y. Sun, C.-L. Wu, L.-M. Joubert, R. Chin, A. L. Koh, Y. Yu, J. Perrino, B. Butz, S. Chu, Y. Cui, *Science* **2017**, 358, 506.
- [23] K.-Y. Yang, I.-C. Leu, K.-Z. Fung, M.-H. Hon, M.-C. Hsu, Y.-J. Hsiao, M.-C. Wang, *J. Mater. Res.* **2008**, 23, 1813.
- [24] R. J. Lauf, J. H. DeVan, *J. Electrochem. Soc.* **1992**, 139, 2087.

- [25] S.-K. Otto, Y. Moryson, T. Krauskopf, K. Pepler, J. Sann, J. Janek, A. Henss, *Chem. Mater.* **2021**, *33*, 859.
- [26] a) F. Han, Y. Zhu, X. He, Y. Mo, C. Wang, *Adv. Energy Mater.* **2016**, *6*, 1501590; b) K. Fu, Y. Gong, B. Liu, Y. Zhu, S. Xu, Y. Yao, W. Luo, C. Wang, S. D. Lacey, J. Dai, Y. Chen, Y. Mo, E. Wachsman, L. Hu, *Sci. Adv.* **2017**, *3*, e1601659.
- [27] a) T. Chen, L. Zhang, Z. Zhang, P. Li, H. Wang, C. Yu, X. Yan, L. Wang, B. Xu, *ACS Appl. Mater. Interfaces* **2019**, *11*, 40808; b) F. Zhao, Q. Sun, C. Yu, S. Zhang, K. Adair, S. Wang, Y. Liu, Y. Zhao, J. Liang, C. Wang, X. Li, X. Li, W. Xia, R. Li, H. Huang, L. Zhang, S. Zhao, S. Lu, X. Sun, *ACS Energy Lett.* **2020**, *5*, 1035; c) S. Wang, X. Zhang, S. Liu, C. Xin, C. Xue, F. Richter, L. Li, L. Fan, Y. Lin, Y. Shen, J. Janek, C.-W. Nan, *J. Materiomics* **2020**, *6*, 70.
- [28] Z. Tong, S.-B. Wang, Y.-K. Liao, S.-F. Hu, R.-S. Liu, *ACS Appl. Mater. Interfaces* **2020**, *12*, 47181.
- [29] T. Krauskopf, H. Hartmann, W. G. Zeier, J. Janek, *ACS Appl. Mater. Interfaces* **2019**, *11*, 14463.
- [30] Q. Ma, Q. Xu, C.-L. Tsai, F. Tietz, O. Guillon, *J. Am. Ceram. Soc.* **2016**, *99*, 410.



## 4 Conclusions

An important and central conclusion that can be drawn from this thesis and the three publications is rather general and should actually be known: Careful reading of older literature and reports from other scientific fields on one's own topic is essential. Only against this background it is possible to obtain the complete state of knowledge on which the own research can be based. The knowledge about the existence of lithium surface passivation layers, as well as their effect on batteries with liquid electrolytes was already well known and accessible in literature at the beginning of this doctoral thesis. However, it is mostly neglected in current research. The same applies for the reactivity of lithium towards atmospheric gases. Current literature usually does not mention sample changes due to reactive lithium under glovebox atmosphere. Instead, lithium foil or samples prepared by polishing are considered and interpreted as pure lithium. The detailed literature review in the introduction clearly shows that this cannot be the case and lithium surfaces are always covered by some kind of reaction layer, which is the next important conclusion from this work.

Accordingly, characterization of lithium surface properties is vital to understand and modify anode interfaces in batteries. By exploring the characterization of lithium surfaces for this thesis, pitfalls were identified that are generally important for the investigation of LMAs and other battery samples. As first obstacle, electron irradiation may lead to lithium plating on top of the passivation layer if the lithium sample is electronically grounded. In literature, this effect was described before, but never identified as plating.<sup>71</sup> Importantly, the effect can occur with every sample covered by an ionically conductive, but electronically insulating film, which is an important finding for characterization in general. Next, the reactivity of lithium metal under UHV conditions was identified as important pitfall for lithium surface characterization. Even though a few authors previously mentioned reactions of lithium with residual gases in UHV<sup>47,71,121,122</sup>, none of them concluded that varying background pressures and conditions, for example at different analysis days, make the comparability of measurements impossible. This conclusion should be considered for any characterization of LMAs. The next pitfall is sputter damage. Sputtering is needed for lithium surface characterization to reach the lower parts of the passivation film and get a full picture of the lithium surface layers. However, it is mentioned in early literature that argon sputtering leads to decomposition of LiOH and Li<sub>2</sub>CO<sub>3</sub> to Li<sub>2</sub>O.<sup>20,123</sup> Accordingly, the quantitative composition of the lithium passivation layer or other samples containing these compounds, determined with XPS after argon sputtering, is not reliable. Still, if the same measurement routine is used, a semi-quantitative comparison of the samples is possible. The same accounts for potential decomposition by irradiation during measurements.<sup>47</sup> This concept can be applied for all kinds of samples. Generally, potential sputter damage should be evaluated for all analyzed compounds using reference samples. The last important pitfall is the calibration of XP spectra. It is generally known that charging needs to be considered for XPS data interpretation<sup>47</sup>, still the calibration of some features may be misleading<sup>124</sup> and depth profiling can be crucial for consistent data interpretation.<sup>125</sup> Concluding from the presented work, the analysis of reference compounds is a useful concept to get reliable results for LMA characterization. Other authors suggest that the separation in binding energy between core levels present in a particular phase should be used to improve the reliability of phase identification<sup>126</sup>, what is another reasonable approach.

The lithium surface characterization with XPS and ToF-SIMS as presented in this work showed that commercial lithium foil, as well as freshly sliced lithium surfaces, which are exposed to glovebox atmosphere, are covered with nanometer-thick passivation layers consisting of an upper lithium hydroxide and carbonate rich region on top of an more oxide rich region, which is in contact with the lithium metal. The upper surface region is more carbonate rich for the lithium foil what

indicates a reaction layer formed upon CO<sub>2</sub> exposure. Reaction with CO<sub>2</sub> is described as surface modification for commercial lithium surfaces in literature and is according to the mentioned similarities of fresh lithium surfaces after CO<sub>2</sub>-exposure and commercial lithium foil probably a common strategy in industry.

Generally, the literature review presented in the introduction on the reactivity of lithium towards atmospheric gases showed that the reports are quite inconsistent. Consequently, it is not possible to draw general, reliable conclusions about the reactivity of pure gases and defined mixtures. Still, most reports agree that traces of water contaminations influence the reactivity of lithium importantly. Therefore, it is more interesting for battery research to investigate the reactivity under actual handling conditions. For a typical glovebox environment, the presented work has shown that water is the main cause for degradation of lithium. However, the on-going reaction with nitrogen can become a problem for freshly sliced lithium samples or samples without covering passivation layer. Accordingly, tracking and minimizing the water and nitrogen contamination in the glovebox is most important for research with LMAs.

Protection layers as the carbonate rich layer on commercial lithium foil, can prevent the reaction with nitrogen and reduce the reaction rate with water. Additionally, gloveboxes with very low degree of contamination and storage in pouch bags can minimize sample changes. However, already nanometer-thick lithium surface passivation layers were shown to have a detrimental influence on the anode interface resistance of the LMA in SSBs. Since the options which were identified to overcome the high interfacial resistances caused by the passivation film, namely rough SE pellets and high preparation pressures, cannot practically be implemented, the results of this work led to the conclusion that alternative concepts for LMA preparation in SSBs are more promising. In particular, anode-free cells and lithium vapor deposition could be a solution.

Still, also for these anode-types, the Li|SE interface reactivity remains a challenge. Interphases, which form due to the high reactivity of lithium, may add high resistance and therefore reduce the SSB performance. Detailed characterization of the interphases is essential to understand their formation and to design suitable interfaces for battery applications. In this doctoral thesis, the potential of ToF-SIMS for the investigation of Li|SE interfaces was explored, concluding that ToF-SIMS is a valuable method to provide additional information on the interface stability and interphase microstructure. Furthermore, the results are another example for the importance of combining analytical techniques that provide complementary scales and information type to obtain a complete picture of the samples.

Overall, this doctoral thesis expands the understanding for LMA surfaces and interfaces in SSBs. The work shows how the surface properties of LMAs can be reliably determined and how typical handling can affect these properties. The results are set into the context of all available literature on lithium reactivity. Furthermore, the thesis demonstrates that the surface passivation layer on LMAs is important for the performance of SSBs. Finally, the full potential of ToF-SIMS for the characterization of Li|SE interfaces is described.

## 5 Outlook

To complement the results of the present thesis, several investigations are suitable and should be considered in future work. Especially, three different subject areas may be targeted.

### i. Theoretical studies about the reactivity of lithium toward atmospheric gases

First, theoretical methods should be used to explore the reactivity of lithium towards the atmospheric gases in detail to get a better basic understanding of the on-going reactions. In particular, the reactivity of the pure gases towards clean lithium surfaces can probably only be studied theoretically since trace contaminations are always present in experimental studies. So far, only few theoretical studies are available and the results are mainly contradicting. Investigation of the impact of trace gases acting as catalysts would also be highly interesting as these may explain experimental observations and are expected to be highly important. Based on the theoretical results, new experiments could be designed to study and deeply understand the degradation phenomena which are interesting for battery research. For instance, the mechanism of the interaction of water with the lithium surface should be further explored, as water is regarded as main driving force for lithium degradation. Understanding the process may help to avoid degradation by tailored protection layers. In addition, investigating the changes of lithium samples under dry-room conditions should be targeted, as dry-rooms are an important handling option for LMA and are an alternative to gloveboxes.

### ii. Further exploration of the impact of lithium surface passivation layers on SSBs

Next, the lithium surface status needs to be considered for future research on LMAs applying the developed reliable characterization strategies. Linking the surface status with the results in electrochemical testing will give more and highly important insights on the role of the lithium surface passivation layer on the battery performance. Specifically, the impact of the lithium surface passivation layer thickness should be tested for other SEs than LLZO to find out, how the different mechanical properties and the Li|SE reactivity influence the observed effects. SEs which are softer than the investigated LLZO are probably not able to penetrate through the passivation layer what will influence the effect of cell preparation pressure. Additionally, the cells should be cycled to investigate the long-term effect of the passivation layer thickness and its potential role for dendrite formation. Next, the composition of the lithium surface film may be changed to potentially overcome detrimental effects. Lithium surface modification is already a widely explored topic in literature, however, reliable studies which compare their results with reference systems and apply reliable characterization are rare. So far, untreated lithium foil is usually regarded as reference system to show the impact of surface modifications. However, without characterization of the lithium foil, a real comparison between the studies is impossible and the impact of modifications cannot be judged. Ideally, the lithium surface passivation layer may become a protective layer, reducing interface reactivity while adding no interphase resistance.

### iii. ToF-SIMS characterization of Li|SE interfaces

The interface properties of many other Li|SE systems could be analyzed with ToF-SIMS to get additional insights on the forming interphases and their microstructure. So far, no polymer electrolytes were investigated, thus the method should be expanded to this class of SEs. Furthermore, the investigation of tailored interphases such as protective layers which are applied on the SE could be implemented easily. Also, combination with *in situ* electrochemical testing could

be targeted to link the ToF-SIMS characterization results with electrochemical data. At this point the experiments also nicely fit the previous section about lithium surface passivation layers as a comparison with resistances of direct Li|SE interfaces without any passivation layer becomes accessible. Comparison of the results would be highly interesting and help the understanding of both issues.

## 6 References

- (1) Lin, D.; Liu, Y.; Cui, Y. Reviving the lithium metal anode for high-energy batteries. *Nature nanotechnology* **2017**, *12* (3), 194–206. DOI: 10.1038/nnano.2017.16.
- (2) Cheng, X.-B.; Zhang, R.; Zhao, C.-Z.; Zhang, Q. Toward Safe Lithium Metal Anode in Rechargeable Batteries: A Review. *Chemical reviews* **2017**, *117* (15), 10403–10473. DOI: 10.1021/acs.chemrev.7b00115.
- (3) Service, R. F. Lithium-ion battery development takes Nobel. *Science* **2019**, *366* (6463), 292. DOI: 10.1126/science.366.6463.292.
- (4) Shen, X.; Liu, H.; Cheng, X.-B.; Yan, C.; Huang, J.-Q. Beyond lithium ion batteries: Higher energy density battery systems based on lithium metal anodes. *Energy Storage Materials* **2018**, *12*, 161–175. DOI: 10.1016/j.ensm.2017.12.002.
- (5) Janek, J.; Zeier, W. G. A solid future for battery development. *Nature Energy* **2016**, *1* (9), 1167. DOI: 10.1038/nenergy.2016.141.
- (6) Zhang, K.; Lee, G.-H.; Park, M.; Li, W.; Kang, Y.-M. Recent Developments of the Lithium Metal Anode for Rechargeable Non-Aqueous Batteries. *Advanced Energy Materials* **2016**, *6* (20), 1600811. DOI: 10.1002/aenm.201600811.
- (7) Li, N.-W.; Yin, Y.-X.; Yang, C.-P.; Guo, Y.-G. An Artificial Solid Electrolyte Interphase Layer for Stable Lithium Metal Anodes. *Advanced Materials* **2016**, *28* (9), 1853–1858. DOI: 10.1002/adma.201504526.
- (8) Li, S.; Jiang, M.; Xie, Y.; Xu, H.; Jia, J.; Li, J. Developing High-Performance Lithium Metal Anode in Liquid Electrolytes: Challenges and Progress. *Advanced Materials* **2018**, *30* (17), e1706375. DOI: 10.1002/adma.201706375.
- (9) Xu, R.; Cheng, X.-B.; Yan, C.; Zhang, X.-Q.; Xiao, Y.; Zhao, C.-Z.; Huang, J.-Q.; Zhang, Q. Artificial Interphases for Highly Stable Lithium Metal Anode. *Matter* **2019**, *1* (2), 317–344. DOI: 10.1016/j.matt.2019.05.016.
- (10) Lang, J.; Qi, L.; Luo, Y.; Wu, H. High performance lithium metal anode: Progress and prospects. *Energy Storage Materials* **2017**, *7*, 115–129. DOI: 10.1016/j.ensm.2017.01.006.
- (11) Schmuch, R.; Wagner, R.; Hörpel, G.; Placke, T.; Winter, M. Performance and cost of materials for lithium-based rechargeable automotive batteries. *Nature Energy* **2018**, *3* (4), 267–278. DOI: 10.1038/s41560-018-0107-2.
- (12) Krauskopf, T.; Richter, F. H.; Zeier, W. G.; Janek, J. Physicochemical Concepts of the Lithium Metal Anode in Solid-State Batteries. *Chemical reviews* **2020**, *120* (15), 7745–7794. DOI: 10.1021/acs.chemrev.0c00431.
- (13) Kim, K. J.; Balaish, M.; Wadaguchi, M.; Kong, L.; Rupp, J. L. M. Solid-State Li–Metal Batteries: Challenges and Horizons of Oxide and Sulfide Solid Electrolytes and Their Interfaces. *Advanced Energy Materials* **2020**, *11* (1), 2002689. DOI: 10.1002/aenm.202002689.
- (14) López, I.; Morey, J.; Ledeuil, J. B.; Madec, L.; Martinez, H. A critical discussion on the analysis of buried interfaces in Li solid-state batteries. Ex situ and in situ/operando studies. *Journal of Materials Chemistry A* **2021**, *9* (45), 25341–25368. DOI: 10.1039/D1TA04532F.
- (15) Zhang, X.-Q.; Cheng, X.-B.; Zhang, Q. Advances in Interfaces between Li Metal Anode and Electrolyte. *Advanced Materials Interfaces* **2018**, *5* (2), 1701097. DOI: 10.1002/admi.201701097.

- (16) Zhao, Y.; Zheng, K.; Sun, X. Addressing Interfacial Issues in Liquid-Based and Solid-State Batteries by Atomic and Molecular Layer Deposition. *Joule* **2018**, *2* (12), 2583–2604. DOI: 10.1016/j.joule.2018.11.012.
- (17) Chen, Y.; Luo, Y.; Zhang, H.; Qu, C.; Zhang, H.; Li, X. The Challenge of Lithium Metal Anodes for Practical Applications. *Small Methods* **2019**, *3* (7), 1800551. DOI: 10.1002/smt.201800551.
- (18) Chen, H.; Pei, A.; Lin, D.; Xie, J.; Yang, A.; Xu, J.; Lin, K.; Wang, J.; Wang, H.; Shi, F.; Boyle, D.; Cui, Y. Uniform High Ionic Conducting Lithium Sulfide Protection Layer for Stable Lithium Metal Anode. *Advanced Energy Materials* **2019**, *9* (22), 1900858. DOI: 10.1002/aenm.201900858.
- (19) Park, S.; Lee, J.-I.; Song, G.; Cho, S.; Han, D.-Y. Lithium Metal Interface Modification for High-Energy Batteries: Approaches and Characterization. *Batteries & Supercaps* **2020**, *3* (9), 828–859. DOI: 10.1002/batt.202000016.
- (20) Kanamura, K.; Tamura, H.; Takehara, Z.-i. XPS analysis of a lithium surface immersed in propylene carbonate solution containing various salts. *Journal of Electroanalytical Chemistry* **1992**, *333* (1-2), 127–142. DOI: 10.1016/0022-0728(92)80386-I.
- (21) Becking, J.; Gröbmeyer, A.; Kolek, M.; Rodehorst, U.; Schulze, S.; Winter, M.; Bieker, P.; Stan, M. C. Lithium-Metal Foil Surface Modification: An Effective Method to Improve the Cycling Performance of Lithium-Metal Batteries. *Advanced Materials Interfaces* **2017**, *4* (16), 1700166. DOI: 10.1002/admi.201700166.
- (22) Otto, S.-K.; Moryson, Y.; Krauskopf, T.; Peppler, K.; Sann, J.; Janek, J.; Henss, A. In-Depth Characterization of Lithium-Metal Surfaces with XPS and ToF-SIMS: Toward Better Understanding of the Passivation Layer. *Chemistry of Materials* **2021**, *33* (3), 859–867. DOI: 10.1021/acs.chemmater.0c03518.
- (23) Otto, S.-K.; Fuchs, T.; Moryson, Y.; Lerch, C.; Mogwitz, B.; Sann, J.; Janek, J.; Henss, A. Storage of Lithium Metal: The Role of the Native Passivation Layer for the Anode Interface Resistance in Solid State Batteries. *ACS Applied Energy Materials* **2021**, *4* (11), 12798–12807. DOI: 10.1021/acsaem.1c02481.
- (24) Otto, S.-K.; Riegger, L. M.; Fuchs, T.; Kayser, S.; Schweitzer, P.; Burkhardt, S.; Henss, A.; Janek, J. In Situ Investigation of Lithium Metal–Solid Electrolyte Anode Interfaces with ToF-SIMS. *Advanced Materials Interfaces* **2022**, *9* (13), 2102387. DOI: 10.1002/admi.202102387.
- (25) Deal, B. E.; Svec, H. J. Kinetics of the reaction between lithium and water vapor. *Ames laboratory ISC Technical Reports* **1953**.
- (26) Swonger, L. R.; Bodoïn, E. High purity lithium and associated products and processes. Patent US 2016/0351889 A1.
- (27) Jeppson, D. W.; Ballif, J. L.; Yuan, W. W.; Chou, B. E. Lithium Literature Review: Lithium's Properties and Interactions. *Office of Scientific and Technical Information* **1978**. DOI: 10.2172/6885395.
- (28) Lott, L. A. Literature Survey: Physical Properties of Lithium and Beryllium at Low Temperatures. *Office of Scientific and Technical Information* **1967**. DOI: 10.2172/4574618.
- (29) Hryn, J. N.; Ignacio-deleon, P. A.; Tang, L.; Arenas, D. Y. Lithium metal synthesis. Patent US11111590B2.

- (30) Zhang, X.; Lv, R.; Tang, W.; Li, G.; Wang, A.; Dong, A.; Liu, X.; Luo, J. Challenges and Opportunities for Multivalent Metal Anodes in Rechargeable Batteries. *Advanced Functional Materials* **2020**, *30* (45), 2004187. DOI: 10.1002/adfm.202004187.
- (31) Addison, C. C. *The chemistry of the liquid alkali metals*; Wiley, 1984.
- (32) Etxebarria, A.; Koch, S. L.; Bondarchuk, O.; Passerini, S.; Teobaldi, G.; Muñoz-Márquez, M. Á. Work Function Evolution in Li Anode Processing. *Advanced Energy Materials* **2020**, *10* (24), 2000520. DOI: 10.1002/aenm.202000520.
- (33) Markowitz, M. M.; Boryta, D. A. Lithium Metal-Gas Reactions: Interaction of Lithium Metal with Air and its Component Gases. *Journal of Chemical and Engineering Data* **1962**, *7* (4), 586–591. DOI: 10.1021/je60015a047.
- (34) Fischer, P.; Schiemann, M.; Scherer, V.; Maas, P.; Schmid, G.; Taroata, D. Experimental characterization of the combustion of single lithium particles with CO<sub>2</sub>. *Fuel* **2015**, *153*, 90–101. DOI: 10.1016/j.fuel.2015.02.098.
- (35) Pilling, N. B.; Bedworth, R. J. The Oxidation of Metals at High Temperature. *Journal of the Institute of Metals* **1923**, *29*, 529–582.
- (36) Hart, C. A.; Skinner, C. H.; Capece, A. M.; Koel, B. E. Sorption of atmospheric gases by bulk lithium metal. *Journal of Nuclear Materials* **2016**, *468*, 71–77. DOI: 10.1016/j.jnucmat.2015.11.006.
- (37) Deal, B. E.; Svec, H. J. Metal-Water Reactions. II. Kinetics of the Reaction between Lithium and Water Vapor. *Journal of the American Chemical Society* **1953**, *75* (24), 6173–6175. DOI: 10.1021/ja01120a019.
- (38) Irvine, W. R.; Lund, J. A. The Reaction of Lithium with Water Vapor. *Journal of the Electrochemical Society* **1963**, *110* (2), 141–144. DOI: 10.1149/1.2425691.
- (39) Hoenigman, J. R.; Keil, R. G. An XPS study of the adsorption of oxygen and water vapor on clean lithium films. *Applications of Surface Science* **1984**, *18* (1-2), 207–222. DOI: 10.1016/0378-5963(84)90045-X.
- (40) Hoenigman, J. R.; Keil, R. G. *Lithium: current applications in science, medicine, and technology*; Wiley, 1985.
- (41) Zavadil, K. R.; Armstrong, N. R. Surface chemistries of lithium: Detailed characterization of the reactions with O<sub>2</sub> and H<sub>2</sub>O using XPS, EELS, and microgravimetry. *Surface Science* **1990**, *230* (1-3), 47–60. DOI: 10.1016/0039-6028(90)90015-Z.
- (42) Rhein, R. A. Lithium Combustion: A Review. *Defense Technical Information Center* **1990**. DOI: 10.21236/ada238154.
- (43) Phillips, J.; Tanski, J. Structure and kinetics of formation and decomposition of corrosion layers formed on lithium compounds exposed to atmospheric gases. *International Materials Reviews* **2005**, *50* (5), 265–286. DOI: 10.1179/174328005X41122.
- (44) Skinner, C. H.; Sullenberger, R.; Koel, B. E.; Jaworski, M. A.; Kugel, H. W. Plasma facing surface composition during NSTX Li experiments. *Journal of Nuclear Materials* **2013**, *438*, 647–650. DOI: 10.1016/j.jnucmat.2013.01.136.
- (45) Wulfsberg, S. M.; Koel, B. E.; Bernasek, S. L. The low temperature oxidation of lithium thin films on HOPG by O<sub>2</sub> and H<sub>2</sub>O. *Surface Science* **2016**, *651*, 120–127. DOI: 10.1016/j.susc.2016.04.003.

- (46) David, D. J.; Froning, M. H.; Wittberg, T. N.; Moddeman, W. E. Surface reactions of lithium with the environment. *Applications of Surface Science* **1981**, 7 (3), 185–195. DOI: 10.1016/0378-5963(81)90108-2.
- (47) Fujieda, T.; Yamamoto, N.; Saito, K.; Ishibashi, T.; Honjo, M.; Koike, S.; Wakabayashi, N.; Higuchi, S. Surface of lithium electrodes prepared in Ar + CO<sub>2</sub> gas. *Journal of Power Sources* **1994**, 52 (2), 197–200. DOI: 10.1016/0378-7753(94)01961-4.
- (48) Li, W.-j.; Li, Q.; Huang, J.; Peng, J.-y.; Chu, G.; Lu, Y.-x.; Zheng, J.-y.; Li, H. Gas treatment protection of metallic lithium anode. *Chinese Physics B* **2017**, 26 (8), 88202. DOI: 10.1088/1674-1056/26/8/088202.
- (49) Yang, T.; Jia, P.; Liu, Q.; Zhang, L.; Du, C.; Chen, J.; Ye, H.; Li, X.; Li, Y.; Shen, T.; Tang, Y.; Huang, J. Air-Stable Lithium Spheres Produced by Electrochemical Plating. *Angewandte Chemie (International ed. in English)* **2018**, 57 (39), 12750–12753. DOI: 10.1002/anie.201807355.
- (50) Mizusaki, J.; Tagawa, H.; Saito, K.; Uchida, K.; Tezuka, M. Lithium carbonate as a solid electrolyte. *Solid State Ionics* **1992**, 53, 791–797. DOI: 10.1016/0167-2738(92)90256-O.
- (51) Gan, H.; Takeuchi, E. S. Lithium electrodes with and without CO<sub>2</sub> treatment: electrochemical behavior and effect on high rate lithium battery performance. *Journal of Power Sources* **1996**, 62 (1), 45–50. DOI: 10.1016/S0378-7753(96)02405-6.
- (52) Zhuang, G.; Chen, Y.; Ross, P. N. The reaction of lithium with carbon dioxide studied by photoelectron spectroscopy. *Surface Science* **1998**, 418 (1), 139–149. DOI: 10.1016/S0039-6028(98)00710-9.
- (53) Etxebarria, A.; Yun, D.-J.; Blum, M.; Ye, Y.; Sun, M.; Lee, K.-J.; Su, H.; Muñoz-Márquez, M. A.; Ross, P. N.; Crumlin, E. J. Revealing In Situ Li metal anode surface evolution upon exposure to CO<sub>2</sub> using Ambient Pressure X-ray Photoelectron Spectroscopy. *ACS applied materials & interfaces* **2020**, 12 (23), 26607–26613. DOI: 10.1021/acsami.0c04282.
- (54) Axelsson, O.; Shao, Y.; Paul, J.; Hoffmann, F. M. A Theoretical and Experimental Study of Reaction Pathways for the Interaction of CO<sub>2</sub> with Alkali-Modified Surfaces. *The Journal of Physical Chemistry* **1995**, 99 (18), 7028–7035. DOI: 10.1021/j100018a040.
- (55) Schily, U.; Heitbaum, J. Surface analysis of freshly cut Li samples: Na-segregation and film forming reaction by O<sub>2</sub>, SO<sub>2</sub>, and liquid LiAlCl<sub>4</sub> · 3(SO<sub>2</sub>). *Electrochimica Acta* **1992**, 37 (4), 731–738. DOI: 10.1016/0013-4686(92)80077-Y.
- (56) Koch, S. L.; Morgan, B. J.; Passerini, S.; Teobaldi, G. Density functional theory screening of gas-treatment strategies for stabilization of high energy-density lithium metal anodes. *Journal of Power Sources* **2015**, 296, 150–161. DOI: 10.1016/j.jpowsour.2015.07.027.
- (57) Shang, J.; Shirazian, S. Facilitated Dissociation of Water in the Presence of Lithium Metal at Ambient Temperature as a Requisite for Lithium–Gas Reactions. *The Journal of Physical Chemistry C* **2018**, 122 (28), 16016–16022. DOI: 10.1021/acs.jpcc.8b01817.
- (58) Guo, R.; Gallant, B. M. Li<sub>2</sub>O Solid Electrolyte Interphase: Probing Transport Properties at the Chemical Potential of Lithium. *Chemistry of Materials* **2020**, 32 (13), 5525–5533. DOI: 10.1021/acs.chemmater.0c00333.
- (59) Aurbach, D. Identification of Surface Films Formed on Lithium Surfaces in  $\gamma$ -Butyrolactone Solutions. *Journal of the Electrochemical Society* **1989**, 136 (6), 1611. DOI: 10.1149/1.2096978.

- (60) Schiemann, M.; Bergthorson, J.; Fischer, P.; Scherer, V.; Taroata, D.; Schmid, G. A review on lithium combustion. *Applied Energy* **2016**, *162*, 948–965. DOI: 10.1016/j.apenergy.2015.10.172.
- (61) Wang, K.; Ross, P. N.; Kong, F.; McLarnon, F. The Reaction of Clean Li Surfaces with Small Molecules in Ultrahigh Vacuum. *Journal of the Electrochemical Society* **1996**, *143* (2), 422. DOI: 10.1149/1.1836460.
- (62) Li, Y.; Li, Y.; Sun, Y.; Butz, B.; Yan, K.; Koh, A. L.; Zhao, J.; Pei, A.; Cui, Y. Revealing Nanoscale Passivation and Corrosion Mechanisms of Reactive Battery Materials in Gas Environments. *Nano letters* **2017**, *17* (8), 5171–5178. DOI: 10.1021/acs.nanolett.7b02630.
- (63) Jain, A.; Miyaoka, H.; Kumar, S.; Ichikawa, T.; Kojima, Y. A new synthesis route of ammonia production through hydrolysis of metal – Nitrides. *International Journal of Hydrogen Energy* **2017**, *42* (39), 24897–24903. DOI: 10.1016/j.ijhydene.2017.08.027.
- (64) Li, Y.; Sun, Y.; Pei, A.; Chen, K.; Vailionis, A.; Li, Y.; Zheng, G.; Sun, J.; Cui, Y. Robust Pinhole-free Li<sub>3</sub>N Solid Electrolyte Grown from Molten Lithium. *ACS central science* **2018**, *4* (1), 97–104. DOI: 10.1021/acscentsci.7b00480.
- (65) Zhang, Z.; Wu, S.; Yang, C.; Zheng, L.; Xu, D.; Zha, R.; Tang, L.; Cao, K.; Wang, X.-g.; Zhou, Z. Li-N<sub>2</sub> Batteries: A Reversible Energy Storage System? *Angewandte Chemie (International ed. in English)* **2019**, *131* (49), 17946–17951. DOI: 10.1002/ange.201911338.
- (66) Wu, M.; Wen, Z.; Liu, Y.; Wang, X.; Huang, L. Electrochemical behaviors of a Li<sub>3</sub>N modified Li metal electrode in secondary lithium batteries. *Journal of Power Sources* **2011**, *196* (19), 8091–8097. DOI: 10.1016/j.jpowsour.2011.05.035.
- (67) Momma, T.; Nara, H.; Yamagami, S.; Tatsumi, C.; Osaka, T. Effect of the atmosphere on chemical composition and electrochemical properties of solid electrolyte interface on electrodeposited Li metal. *Journal of Power Sources* **2011**, *196* (15), 6483–6487. DOI: 10.1016/j.jpowsour.2011.03.095.
- (68) Otero, M.; Lener, G.; Trincavelli, J.; Barraco, D.; Nazzarro, M. S.; Furlong, O.; Leiva, E. P. M. New kinetic insight into the spontaneous oxidation process of lithium in air by EPMA. *Applied Surface Science* **2016**, *383*, 64–70. DOI: 10.1016/j.apsusc.2016.04.060.
- (69) Herle, S. P.; Frey, B.; Haas, D. Low melting temperature metal purification and deposition. Patent US10916761B2.
- (70) Huang, C.; Kresin, V. V. Note: Contamination-free loading of lithium metal into a nozzle source. *The Review of scientific instruments* **2016**, *87* (6), 66105. DOI: 10.1063/1.4953918.
- (71) Kamphaus, E. P.; Angarita-Gomez, S.; Qin, X.; Shao, M.; Engelhard, M. H.; Mueller, K. T.; Murugesan, V.; Balbuena, P. B. Role of inorganic surface layer on solid electrolyte interphase evolution at Li-metal anodes. *ACS applied materials & interfaces* **2019**, *11* (34), 31467–31476. DOI: 10.1021/acsami.9b07587.
- (72) Hovsepiyan, B. Rolling of lithium. Patent US3721113A.
- (73) Gauthier, M.; Bouchard, P.; Guerin, P.; Armand, M. Additives for lubricating agents used in the lamination of lithium sheets into thin films. Patent US5837401A.
- (74) Wietelmann, U. Surface-passivated lithium metal and method for the production thereof. Patent US20130122318A1.

- (75) Myers, S. E.; Cook, J. A.; Park, G. B.; McLoughlin, R. H. Protection of sensitive material. Patent WO/1985/002063.
- (76) Krystian, M.; Pichl, W. Metallography of alkali metal single crystals. *Materials Characterization* **2001**, *46* (1), 1–9. DOI: 10.1016/S1044-5803(00)00079-6.
- (77) Harry, K. J.; Hallinan, D. T.; Parkinson, D. Y.; MacDowell, A. A.; Balsara, N. P. Detection of subsurface structures underneath dendrites formed on cycled lithium metal electrodes. *Nature Materials* **2014**, *13* (1), 69. DOI: 10.1038/nmat3793.
- (78) Maslyn, J. A.; Frenck, L.; Loo, W. S.; Parkinson, D. Y.; Balsara, N. P. Extended Cycling through Rigid Block Copolymer Electrolytes Enabled by Reducing Impurities in Lithium Metal Electrodes. *ACS Applied Energy Materials* **2019**, *2* (11), 8197–8206. DOI: 10.1021/acsaem.9b01685.
- (79) Meyerson, M. L.; Sheavly, J. K.; Dolocan, A.; Griffin, M. P.; Pandit, A. H.; Rodriguez, R.; Stephens, R. M.; Vanden Bout, D. A.; Heller, A.; Mullins, C. B. The effect of local lithium surface chemistry and topography on solid electrolyte interphase composition and dendrite nucleation. *Journal of Materials Chemistry A* **2019**, *7* (24), 513. DOI: 10.1039/C9TA03371H.
- (80) Westmore, T. H.; Eitouni, H. B.; Nuval, A.; Pratt, R. C. Lithium metal foils with low defect density. Patent US 20190280292A1.
- (81) Ahn, J.; Park, J.; Kim, J. Y.; Yoon, S.; Lee, Y. M.; Hong, S.; Lee, Y.-G.; Phatak, C.; Cho, K. Y. Insights into Lithium surface: Stable Cycling by Controlled 10- $\mu$ m-deep Surface Relief, Reinterpreting the Natural Surface Defect on Lithium Metal Anode. *ACS Applied Energy Materials* **2019**, *2* (8), 5656–5664. DOI: 10.1021/acsaem.9b00805.
- (82) Storelli, A.; Rousselot, S.; Alzate-Carvajal, N.; Pelé, V.; Dollé, M. On the Importance of Li Metal Morphology on the Cycling of Lithium Metal Polymer Cells. *Journal of the Electrochemical Society* **2021**, *168* (4), 40505. DOI: 10.1149/1945-7111/abf017.
- (83) Wang, H.; Yi, Z.-L.; Su, F.-Y.; Song, G.; Xie, L.-J.; Wang, Z.-B.; Chen, C.-M. The effect of removing the native passivation film on the electrochemical performance of lithium metal electrodes. *Journal of Power Sources* **2022**, *520*, 230817. DOI: 10.1016/j.jpowsour.2021.230817.
- (84) Krauskopf, T.; Hartmann, H.; Zeier, W. G.; Janek, J. Toward a Fundamental Understanding of the Lithium Metal Anode in Solid-State Batteries-An Electrochemo-Mechanical Study on the Garnet-Type Solid Electrolyte  $\text{Li}_{6.25}\text{Al}_{0.25}\text{La}_3\text{Zr}_2\text{O}_{12}$ . *ACS applied materials & interfaces* **2019**, *11* (15), 14463–14477. DOI: 10.1021/acsaem.9b02537.
- (85) Krauskopf, T.; Mogwitz, B.; Hartmann, H.; Singh, D. K.; Zeier, W. G.; Janek, J. The Fast Charge Transfer Kinetics of the Lithium Metal Anode on the Garnet-Type Solid Electrolyte  $\text{Li}_{6.25}\text{Al}_{0.25}\text{La}_3\text{Zr}_2\text{O}_{12}$ . *Advanced Energy Materials* **2020**, *10* (27), 2000945. DOI: 10.1002/aenm.202000945.
- (86) Moulder, J. F.; Stickle, W. F.; Sobol, P. E.; Bomben, K. D. *Handbook of X-ray Photoelectron Spectroscopy*; Physical Electronics, 1992.
- (87) Vickermann, J. C.; Gilmore, I. S. *Surface Analysis: The Principle Techniques*, 2nd ed.; Wiley, 2009.
- (88) Kanamura, K.; Tamura, H.; Shiraishi, S.; Takehara, Z.-i. XPS Analysis of Lithium Surfaces Following Immersion in Various Solvents Containing  $\text{LiBF}_4$ . *Journal of the Electrochemical Society* **1995**, *142* (2), 340. DOI: 10.1149/1.2044000.

- (89) Kanamura, K.; Tamura, H.; Shiraishi, S.; Takehara, Z.-i. XPS Analysis for Lithium Surface Immersed in Tetrahydrofuran Containing Various Salts. *Journal of the Electrochemical Society of Japan* **1993**, *61* (12), 1377–1382. DOI: 10.5796/electrochemistry.61.1377.
- (90) Kanamura, K.; Tamura, H.; Shiraishi, S.; Takehara, Z.-i. Morphology and chemical compositions of surface films of lithium deposited on a Ni substrate in nonaqueous electrolytes. *Journal of Electroanalytical Chemistry* **1995**, *394* (1-2), 49–62. DOI: 10.1016/0022-0728(95)03972-J.
- (91) Ismail, I.; Noda, A.; Nishimoto, A.; Watanabe, M. XPS study of lithium surface after contact with lithium-salt doped polymer electrolytes. *Electrochimica Acta* **2001**, *46* (10-11), 1595–1603. DOI: 10.1016/S0013-4686(00)00758-1.
- (92) Yen, S. P. S.; Shen, D.; Vasquez, R. P.; Grunthaner, F. J.; Somonao, R. B. Chemical and Morphological Characteristics of Lithium Electrode Surfaces. *Journal of the Electrochemical Society* **1981**, *128* (7), 1434. DOI: 10.1149/1.2127657.
- (93) Morigaki, K.-i.; Ohta, A. Analysis of the surface of lithium in organic electrolyte by atomic force microscopy, Fourier transform infrared spectroscopy and scanning auger electron microscopy. *Journal of Power Sources* **1998**, *76* (2), 159–166. DOI: 10.1016/S0378-7753(98)00151-7.
- (94) Naudin, C.; Bruneel, J. L.; Chami, M.; Desbat, B.; Grondin, J.; Lassègues, J. C.; Servant, L. Characterization of the lithium surface by infrared and Raman spectroscopies. *Journal of Power Sources* **2003**, *124* (2), 518–525. DOI: 10.1016/S0378-7753(03)00798-5.
- (95) Schmitz, R.; Müller, R.; Krüger, S.; Schmitz, R. W.; Nowak, S.; Passerini, S.; Winter, M.; Schreiner, C. Investigation of lithium carbide contamination in battery grade lithium metal. *Journal of Power Sources* **2012**, *217*, 98–101. DOI: 10.1016/j.jpowsour.2012.05.038.
- (96) Gireaud, L.; Grugeon, S.; Laruelle, S.; Yrieix, B.; Tarascon, J.-M. Lithium metal stripping/plating mechanisms studies: A metallurgical approach. *Electrochemistry Communications* **2006**, *8* (10), 1639–1649. DOI: 10.1016/j.elecom.2006.07.037.
- (97) Wang, M. J.; Carmona, E.; Gupta, A.; Albertus, P.; Sakamoto, J. Enabling “lithium-free” manufacturing of pure lithium metal solid-state batteries through in situ plating. *Nature communications* **2020**, *11* (1), 1–9. DOI: 10.1038/s41467-020-19004-4.
- (98) Albertus, P.; Babinec, S.; Litzelman, S.; Newman, A. Status and challenges in enabling the lithium metal electrode for high-energy and low-cost rechargeable batteries. *Nature Energy* **2018**, *3* (1), 16–21. DOI: 10.1038/s41560-017-0047-2.
- (99) Tong, Z.; Wang, S.-B.; Liao, Y.-K.; Hu, S.-F.; Liu, R.-S. Interface Between Solid-State Electrolytes and Li-Metal Anodes: Issues, Materials, and Processing Routes. *ACS Applied Materials Interfaces* **2020**, *12* (42), 47181–47196. DOI: 10.1021/acsami.0c13591.
- (100) Wenzel, S.; Leichtweiss, T.; Krüger, D.; Sann, J.; Janek, J. Interphase formation on lithium solid electrolytes - An in situ approach to study interfacial reactions by photoelectron spectroscopy. *Solid State Ionics* **2015**, *278*, 98–105. DOI: 10.1016/j.ssi.2015.06.001.
- (101) Wenzel, S.; Randau, S.; Leichtweiß, T.; Weber, D. A.; Sann, J.; Zeier, W. G.; Janek, J. Direct Observation of the Interfacial Instability of the Fast Ionic Conductor  $\text{Li}_{10}\text{GeP}_2\text{S}_{12}$  at the Lithium Metal Anode. *Chemistry of Materials* **2016**, *28* (7), 2400–2407. DOI: 10.1021/acs.chemmater.6b00610.

(102) Lou, S.; Yu, Z.; Liu, Q.; Wang, H.; Chen, M.; Wang, J. Multi-scale Imaging of Solid-State Battery Interfaces: From Atomic Scale to Macroscopic Scale. *Chem* **2020**, *6* (9), 2199–2218. DOI: 10.1016/j.chempr.2020.06.030.

(103) Connell, J. G.; Fuchs, T.; Hartmann, H.; Krauskopf, T.; Zhu, Y.; Sann, J.; Garcia-Mendez, R.; Sakamoto, J.; Tepavcevic, S.; Janek, J. Kinetic versus Thermodynamic Stability of LLZO in Contact with Lithium Metal. *Chemistry of Materials* **2020**, *32* (23), 10207–10215. DOI: 10.1021/acs.chemmater.0c03869.

(104) Gibson, J. S.; Narayanan, S.; Swallow, J. E. N.; Kumar-Thakur, P.; Pasta, M.; Lee, T.-L.; Weatherup, R. S. Gently does it!: in situ preparation of alkali metal-solid electrolyte interfaces for photoelectron spectroscopy. *Faraday discussions* **2022**. DOI: 10.1039/d1fd00118c.

(105) Zhao, F.; Zhang, S.; Li, Y.; Sun, X. Emerging characterization techniques for electrode interfaces in sulfide-based all-solid-state lithium batteries. *Small Structures* **2021**, *3* (1), 2100146. DOI: 10.1002/ssr.202100146.

(106) Li, Y.; Li, Y.; Pei, A.; Yan, K.; Sun, Y.; Wu, C.-L.; Joubert, L.-M.; Chin, R.; Koh, A. L.; Yu, Y.; Perrino, J.; Butz, B.; Chu, S.; Cui, Y. Atomic structure of sensitive battery materials and interfaces revealed by cryo-electron microscopy. *Science* **2017**, *358* (6362), 506–510. DOI: 10.1126/science.aam6014.

(107) A. L. Davis; E. Kazyak; D. W. Liao; K. N. Wood; N. P. Dasgupta. Operando Analysis of Interphase Dynamics in Anode-Free Solid-State Batteries with Sulfide Electrolytes. *Journal of the Electrochemical Society* **2021**, *168* (7), 70557. DOI: 10.1149/1945-7111/ac163d.

(108) Wenzel, S.; Weber, D. A.; Leichtweiss, T.; Busche, M. R.; Sann, J.; Janek, J. Interphase formation and degradation of charge transfer kinetics between a lithium metal anode and highly crystalline  $\text{Li}_7\text{P}_3\text{S}_{11}$  solid electrolyte. *Solid State Ionics* **2016**, *286*, 24–33. DOI: 10.1016/j.ssi.2015.11.034.

(109) Liu, Z.; Borodin, A.; Li, G.; Liu, X.; Li, Y.; Endres, F. X-ray Photoelectron Spectroscopy Probing of the Interphase between Solid-State Sulfide Electrolytes and a Lithium Anode. *The Journal of Physical Chemistry C* **2020**, *124* (1), 300–308. DOI: 10.1021/acs.jpcc.9b06384.

(110) Wenzel, S.; Sedlmaier, S. J.; Dietrich, C.; Zeier, W. G.; Janek, J. Interfacial reactivity and interphase growth of argyrodite solid electrolytes at lithium metal electrodes. *Solid State Ionics* **2018**, *318*, 102–112. DOI: 10.1016/j.ssi.2017.07.005.

(111) Liu, Y.; Sun, Q.; Zhao, Y.; Wang, B.; Kaghazchi, P.; Adair, K. R.; Li, R.; Zhang, C.; Liu, J.; Kuo, L.-Y.; Hu, Y.; Sham, T.-K.; Zhang, L.; Yang, R.; Lu, S.; Song, X.; Sun, X. Stabilizing the Interface of NASICON Solid Electrolyte against Li Metal with Atomic Layer Deposition. *ACS applied materials & interfaces* **2018**, *10* (37), 31240–31248. DOI: 10.1021/acsami.8b06366.

(112) Wood, K. N.; Steirer, K. X.; Hafner, S. E.; Ban, C.; Santhanagopalan, S.; Lee, S.-H.; Teeter, G. Operando X-ray photoelectron spectroscopy of solid electrolyte interphase formation and evolution in  $\text{Li}_2\text{S-P}_2\text{S}_5$  solid-state electrolytes. *Nature communications* **2018**, *9* (1), 1–10. DOI: 10.1038/s41467-018-04762-z.

(113) Davis, A. L.; Garcia-Mendez, R.; Wood, K. N.; Kazyak, E.; Chen, K.-H.; Teeter, G.; Sakamoto, J.; Dasgupta, N. P. Electro-chemo-mechanical evolution of sulfide solid electrolyte/Li metal interfaces: operando analysis and ALD interlayer effects. *Journal of Materials Chemistry A* **2020**, *8* (13), 6291–6302. DOI: 10.1039/C9TA11508K.

- (114) Ma, C.; Cheng, Y.; Yin, K.; Luo, J.; Sharafi, A.; Sakamoto, J.; Li, J.; More, K. L.; Dudney, N. J.; Chi, M. Interfacial Stability of Li Metal-Solid Electrolyte Elucidated via in Situ Electron Microscopy. *Nano letters* **2016**, *16* (11), 7030–7036. DOI: 10.1021/acs.nanolett.6b03223.
- (115) Hood, Z. D.; Chen, X.; Sacci, R. L.; Liu, X.; Veith, G. M.; Mo, Y.; Niu, J.; Dudney, N. J.; Chi, M. Elucidating Interfacial Stability between Lithium Metal Anode and Li Phosphorus Oxynitride via In Situ Electron Microscopy. *Nano letters* **2021**, *21* (1), 151–157. DOI: 10.1021/acs.nanolett.0c03438.
- (116) Xiang, Y.; Li, X.; Cheng, Y.; Sun, X.; Yang, Y. Advanced characterization techniques for solid state lithium battery research. *Materials Today* **2020**, *36*, 139–157. DOI: 10.1016/j.mattod.2020.01.018.
- (117) Xiao, Y.; Wang, Y.; Bo, S.-H.; Kim, J. C.; Miara, L. J.; Ceder, G. Understanding interface stability in solid-state batteries. *Nature Reviews Materials* **2020**, *5* (2), 105–126. DOI: 10.1038/s41578-019-0157-5.
- (118) Strauss, F.; Kitsche, D.; Ma, Y.; Teo, J. H.; Goonetilleke, D.; Janek, J.; Bianchini, M.; Brezesinski, T. Operando Characterization Techniques for All-Solid-State Lithium-Ion Batteries. *Advanced Energy and Sustainability Research* **2021**, *2* (6), 2100004. DOI: 10.1002/aesr.202100004.
- (119) Chen, X.; Xie, J.; Zhao, X.; Zhu, T. Electrochemical Compatibility of Solid-State Electrolytes with Cathodes and Anodes for All-Solid-State Lithium Batteries: A Review. *Advanced Energy and Sustainability Research* **2021**, *2* (5), 2000101. DOI: 10.1002/aesr.202000101.
- (120) Riegger, L. M.; Otto, S.-K.; Sadowski, M.; Jovanovic, S.; Kötz, O.; Harm, S.; Balzat, L. G.; Merz, S.; Burkhardt, S.; Richter, F. H.; Sann, J.; Eichel, R.-A.; Lotsch, B. V.; Granwehr, J.; Albe, K.; Janek, J. Instability of the  $\text{Li}_7\text{SiPS}_8$  Solid Electrolyte at the Lithium Metal Anode and Interphase Formation. *Chemistry of Materials* **2022**, *34* (8), 3659–3669. DOI: 10.1021/acs.chemmater.1c04302.
- (121) Kanamura, K.; Shiraishi, S.; Tamura, H.; Takehara, Z.-i. X-Ray Photoelectron Spectroscopic Analysis and Scanning Electron Microscopic Observation of the Lithium Surface Immersed in Nonaqueous Solvents. *Journal of the Electrochemical Society* **1994**, *141* (9), 2379–2385. DOI: 10.1149/1.2055129.
- (122) Harilal, S. S.; Allain, J. P.; Hassanein, A.; Hendricks, M. R.; Nieto-Perez, M. Reactivity of lithium exposed graphite surface. *Applied Surface Science* **2009**, *255* (20), 8539–8543. DOI: 10.1016/j.apsusc.2009.06.009.
- (123) Edström, K.; Herstedt, M.; Abraham, D. P. A new look at the solid electrolyte interphase on graphite anodes in Li-ion batteries. *Journal of Power Sources* **2006**, *153* (2), 380–384. DOI: 10.1016/j.jpowsour.2005.05.062.
- (124) Ciosek Högrström, K.; Malmgren, S.; Hahlin, M.; Gorgoi, M.; Nyholm, L.; Rensmo, H.; Edström, K. The Buried Carbon/Solid Electrolyte Interphase in Li-ion Batteries Studied by Hard X-ray Photoelectron Spectroscopy. *Electrochimica Acta* **2014**, *138*, 430–436. DOI: 10.1016/j.electacta.2014.06.129.
- (125) Maibach, J.; Lindgren, F.; Eriksson, H.; Edström, K.; Hahlin, M. Electric Potential Gradient at the Buried Interface between Lithium-Ion Battery Electrodes and the SEI Observed Using Photoelectron Spectroscopy. *The journal of physical chemistry letters* **2016**, *7* (10), 1775–1780. DOI: 10.1021/acs.jpcclett.6b00391.

(126) Wood, K. N.; Teeter, G. XPS on Li-Battery-Related Compounds: Analysis of Inorganic SEI Phases and a Methodology for Charge Correction. *ACS Applied Energy Materials* **2018**, *1* (9), 4493–4504. DOI: 10.1021/acsaem.8b00406.

## 7 Appendix

### 7.1 Supporting Information

#### 7.1.1 Publication 1

#### Supporting Information

#### **In-Depth Characterization of Lithium Metal Surfaces with XPS and ToF-SIMS: Toward better Understanding of the Passivation Layer**

Svenja-K. Otto <sup>a</sup>, Yannik Moryson <sup>a</sup>, Thorben Krauskopf <sup>a</sup>, Klaus Peppler <sup>a</sup>, Joachim Sann <sup>a</sup>,  
Jürgen Janek <sup>a,b</sup> and Anja Henss <sup>a,b</sup> \*

*<sup>a</sup>Institute of Physical Chemistry, Justus-Liebig-Universität Giessen,  
Heinrich-Buff-Ring 17, D-35392 Giessen, Germany*

*<sup>b</sup>Center for Materials Research (LaMa), Justus-Liebig-Universität Giessen,  
Heinrich-Buff-Ring 16, D-35392 Giessen, Germany*

\* E-Mail: [anja.henss@phys.chemie.uni-giessen.de](mailto:anja.henss@phys.chemie.uni-giessen.de)

#### **This PDF file includes:**

- S1: Characterization of reference samples with XPS
- S2: XPS depth profiling
- S3: Decomposition by argon sputtering
- S4: Characterization of reference samples with ToF-SIMS
- S5: ToF-SIMS depth profiling
- S6: Determination of sputter rates with ToF-SIMS
- S7: ToF-SIMS imaging
- S8: Variation in ToF-SIMS depth profiles
- S9: EDX analysis of lithium samples with thicker passivation layers
- S10: Lithium plating through ToF-SIMS measurements
- S11: Lithium plating through EDX measurements

### S1: Characterization of reference samples with XPS

To enable the identification of the different compounds on the lithium samples, we analyzed reference samples of several lithium compounds. Since XPS is one of the most common characterization methods for the investigation of lithium metal anodes, the binding energies for common lithium compounds have been reported by many authors and were for example reviewed by Wood *et al.* in 2018.<sup>1</sup> In their publication, the authors discuss that charging during the XPS measurements is the main reason for the wide spread of the reported absolute XPS core level binding energies. They used the separations between different core levels and the valence band of the different compounds to define a set of binding energies for lithium compounds. In addition to this report, we analyzed the lithium compounds LiOH, Li<sub>2</sub>O<sub>2</sub>, Li<sub>2</sub>CO<sub>3</sub>, Li<sub>2</sub>O and LiH as reference samples, to determine the absolute binding energies for our study, *i.e.* for our XPS instrument. Besides, to clean the compounds and to evaluate their stability against Ar<sup>+</sup>-sputtering, depth profiles were measured. The carbon contaminations were removed through sputtering. Also, LiOH, Li<sub>2</sub>O<sub>2</sub> and Li<sub>2</sub>CO<sub>3</sub> partly decomposed to Li<sub>2</sub>O, as reported previously.<sup>2,3</sup> The influence of this decomposition on the investigation of lithium samples is discussed in S3. The decomposition was more pronounced for Li<sub>2</sub>O<sub>2</sub> and LiOH than for Li<sub>2</sub>CO<sub>3</sub>. Furthermore, a little amount of carbide formed on the Li<sub>2</sub>CO<sub>3</sub> sample through sputtering. The Li<sub>2</sub>O sample was sputter cleaned without any signs of decomposition. For LiH, the carbonate and hydroxide peaks in the O 1s region vanished completely through sputtering and only the oxide peak remained. In the Li 1s region a peak evolved at 52.6 eV and plasmon-loss features appeared. These observations indicate the formation of lithium metal. Possibly LiH decomposes to Li and H<sub>2</sub> through sputtering. Therefore, no Li 1s binding energy for LiH was determined. The O 1s and Li 1s binding energies for the other measured lithium compounds are summarized in Figure S1. We like to emphasize that the absolute values can vary due to charging, as discussed above.<sup>1</sup> Nevertheless, the relative positions of the different compounds do not change and were used by us for the interpretation of XPS spectra. The Li 1s binding energy for lithium metal is also shown in Figure S1. The value was determined from depth profiles of lithium foils.

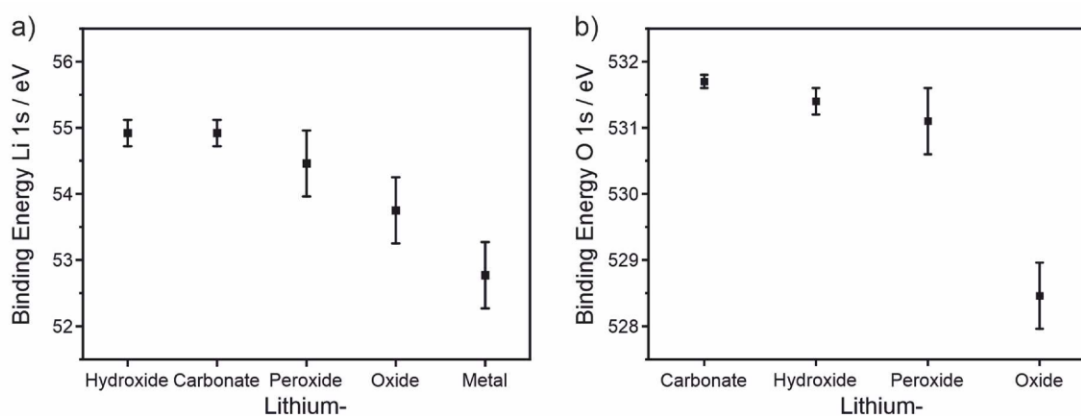


Figure S1. a) Li 1s and b) O 1s binding energies of lithium compounds and lithium metal. The sigma values are displayed as error bars. The error of the values for lithium oxide was applied to the values for lithium metal and peroxide, as the oxide signal was used for calibration of the corresponding spectra.

### S2: XPS depth profiling

On the surface of all lithium samples (before sputtering), peaks were observed at 531.7 eV for O 1s and at 54.6 eV for Li 1s. These values fit in general with the ones determined for LiOH, Li<sub>2</sub>CO<sub>3</sub> and Li<sub>2</sub>O<sub>2</sub>, as well as with common surface adsorbates. However, the existence of Li<sub>2</sub>O<sub>2</sub> is unlikely, as the peroxide is thermodynamically unstable against lithium metal. Therefore, Li<sub>2</sub>O<sub>2</sub> is not taken into further account. Apart from this assumption, LiOH and Li<sub>2</sub>O<sub>2</sub> are hard to distinguish in the XPS by just evaluating the O 1s and Li 1s spectra. Even though the binding energies for Li<sub>2</sub>CO<sub>3</sub> and LiOH are also very similar, the

compounds can be fitted with separate peaks using an area constraint from the C 1s carbonate peak for the corresponding O 1s and Li 1s peaks. Surface adsorbates were minimized by always keeping the samples under inert gas or vacuum and were neglected as the fit quality was satisfying without considering them. Adventitious carbon was detected on the surface and removed through sputtering. After longer sputtering, the formation of minor amounts of carbide was observed. Schmitz *et al.* highlighted  $\text{Li}_2\text{C}_2$  as important surface and bulk contamination of battery grade lithium metal based on Raman, MS, ICP-OES and EDX analyses.<sup>4</sup> Nevertheless,  $\text{Ar}^+$ -sputtering of metal carbonates or oxides with carbon contaminations is known to induce the formation of carbides. Therefore, carbide is not regarded as a component of the passivation layer but as a decomposition product of carbon from different sources. This interpretation is in accordance with previous XPS studies.<sup>4,5</sup> After the first sputter cycle, additional peaks at lower binding energy appeared for the O 1s and Li 1s regions. These peaks were attributed to  $\text{Li}_2\text{O}$  (528.5 eV for O 1s and 53.8 eV for Li 1s). With longer sputter time, the carbonate vanished completely, the intensity of the hydroxide peak dropped significantly and the oxide peak intensity became virtually stable. At the same time, another peak at even lower binding energy evolved in the Li 1s region (52.6 eV). The peak came with plasmon-loss features at around 60 eV, which is a clear indication for lithium metal.

The residual standard deviations (STDs) of all fits were between 1 and 2 for the Li 1s and O 1s regions. These values are sufficiently low to guarantee that no major fraction of other compounds, such as LiH, was probed, but minor amounts in the range of the quantification error cannot be ruled out. The quantification error was estimated to be  $\pm 5\%$  and is dominated by the low sensitivity of XPS towards Li. It is worth mentioning that the STD is a measure for the mathematical fit quality and a low value does not ensure that the sample composition is determined correctly, as the physicochemical model underlying the fit is more important. Also, it should be emphasized that oxidation of lithium metal during measurement and decomposition of lithium compounds through sputtering influence the quantitative results and the accuracy of the fit. Still, since the carbonate vanished completely, the compound can only be present on the sample surface. The LiOH fraction was most likely reduced through decomposition (see S3) and the fraction of lithium metal decreased through reactions. It is also important to note that the spectra were measured after each other and therefore represent different reaction states, what influences the accuracy of the fit which is based on area constraints, too.

### **S3: Decomposition by argon sputtering**

In order to evaluate the influence of argon sputtering and the extent of sputter-induced decomposition during depth profiling of the lithium foils, the decomposition by argon sputtering was evaluated on reference compounds and compared to the lithium samples. As mentioned before, LiOH and  $\text{Li}_2\text{CO}_3$  were identified on the lithium foil (S2) and were found to decompose partly to  $\text{Li}_2\text{O}$  by argon sputtering (S1). Pure carbonate was observed on the surface of the  $\text{Li}_2\text{CO}_3$  reference sample (Figure S2a). After two sputter intervals of 3 min at 1 kV and 8 min at 2 kV, the composition changed to about 79% carbonate and 21% oxide. For the LiOH reference sample (Figure S2b), some carbonate contamination was observed on the surface. Neglecting the carbonate and its decomposition to obtain the highest possible degree of hydroxide decomposition, the same sputtering steps yield 59% hydroxide and 41% oxide. However, for a lithium sample 17% hydroxide and 83% oxide were observed after the same sputter steps under the same conditions. Even the calculated maximum degree of decomposition of hydroxide cannot explain this ratio, what leaves an oxide-rich region under the carbonate and hydroxide passivation layer as most likely explanation. Please note that sputter steps were chosen which do not lead to lithium metal for the lithium sample, so that the reactivity of lithium metal does not need to be considered for this comparison. Also, the ratio of hydroxide to oxide always shifted towards a higher hydroxide fraction during these XPS measurements. Accordingly, detrimental reactions cannot explain the observed excess oxide fraction. However, the decomposition by sputtering is an important factor which underlines that conclusions based on absolute quantification are not valid for the discussed measurements. Although other groups published nondestructive methods to probe lithium-containing

samples, for example by using high-energy photons to increase the XPS probing depth<sup>6</sup>, our approach has the advantage that most XPS machines are capable of such measurements.

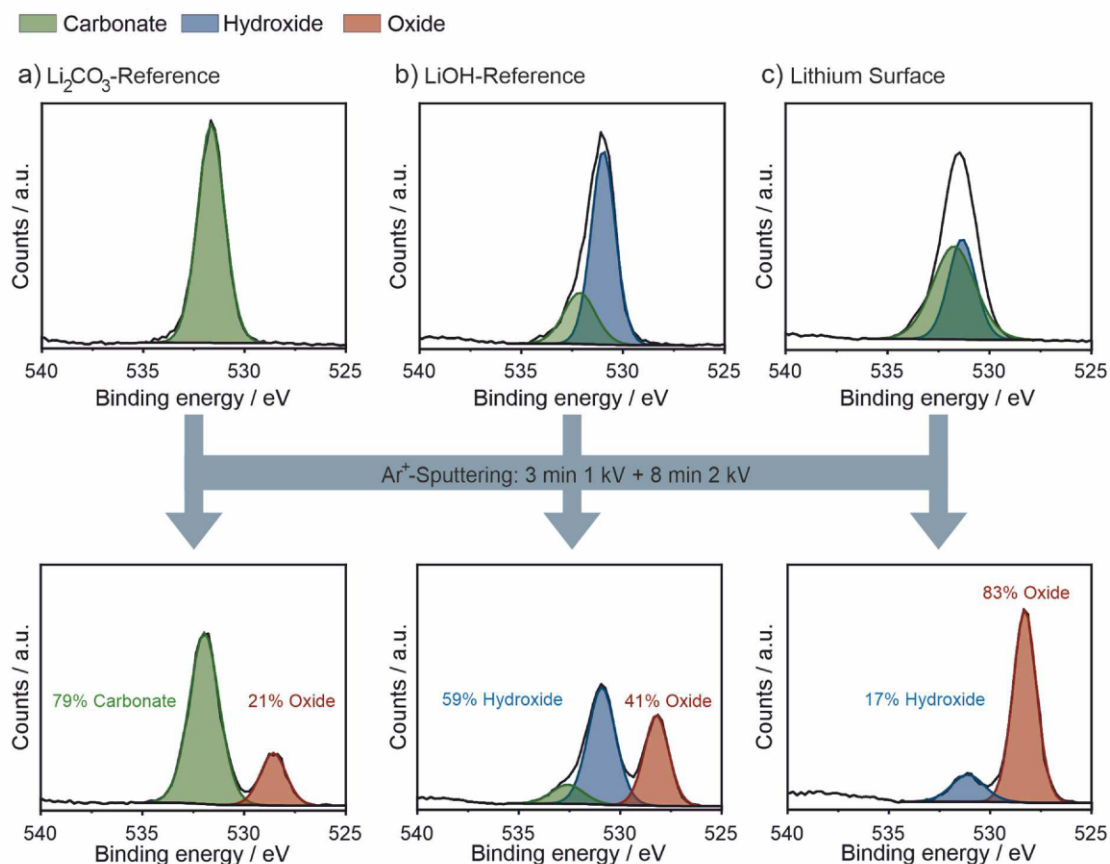


Figure S2: Comparison of the decomposition induced by argon sputtering (3 min at 1 kV and 8 min at 2 kV) for a) a  $\text{Li}_2\text{CO}_3$ -reference, b) a  $\text{LiOH}$ -reference and c) a lithium surface. The oxide fraction on the lithium sample after sputtering cannot be explained only by the degree of decomposition which was observed on the reference samples. The given numbers are atom fractions of the examined lithium compounds.

#### S4: Characterization of reference samples with ToF-SIMS

To identify secondary ions that are specific for the different lithium compounds, the reference samples  $\text{LiOH}$ ,  $\text{Li}_2\text{O}_2$ ,  $\text{Li}_2\text{CO}_3$ ,  $\text{Li}_2\text{O}$  and  $\text{LiH}$  were investigated with ToF-SIMS, similarly as reported for other lithium containing samples.<sup>7</sup> In a first step, depth profiles of pressed pellets were analyzed to distinguish between signals originating from contaminations and from the reference compound. Signals with rising or constant intensity in the depth profile were regarded as potentially specific; signals with decreasing intensity were defined as contaminants. Depth profiles for characterization of the reference samples were performed on pressed pellets in spectrometry mode.  $\text{Bi}^+$  primary ions (25 kV, 1.2 pA,  $100 \times 100 \mu\text{m}^2$ ) and  $\text{Ar}_{1500}^+$  sputter ions (10 kV, 10 nA,  $300 \times 300 \mu\text{m}^2$ ) were used. For charge compensation a flood gun with an energy of 21 eV and a current of  $10 \mu\text{A}$  was used. Between two sputter frames, analysis was done after 2 s of waiting time, in random raster mode, measuring 2 frames with  $128 \times 128$  pixels and 1 shot/pixel. In a second step, ToF-SIMS spectra of the sputter-cleaned samples were measured with a defined ion dose density. The potentially specific signals, which showed highest intensity in comparison to all other investigated compounds, were defined as specific for the

corresponding lithium compound. Spectra of the reference samples were measured after sputter cleaning with  $\text{Ar}_{1500}^+$  using a dose density of  $4 \cdot 10^{15}$  ions/cm<sup>2</sup>. For each sample, 12 areas of  $100 \times 100 \mu\text{m}^2$  were measured with a primary ion dose of  $10^{12}$  ions/cm<sup>2</sup>. To compare the secondary ion signal intensities of different compounds, the average intensity of all areas from one compound was taken. As error, the standard deviation was calculated. The procedure is shown for the secondary ion  $\text{Li}_2\text{H}^-$  as a specific signal for LiH in Figure S3. The specific signals, which were used for the interpretation of the depth profiles, are summarized in Table S1. They were chosen because they do not overlap with other peaks. Other related secondary ions which showed similar profiles and were used as group of specific signals are also given. It is important to note that signals, which are discussed as specific for one compound, may also be quite intense for another one. Consequently, the intensity of the signal can be high even though the corresponding compound is only present in minor amounts.

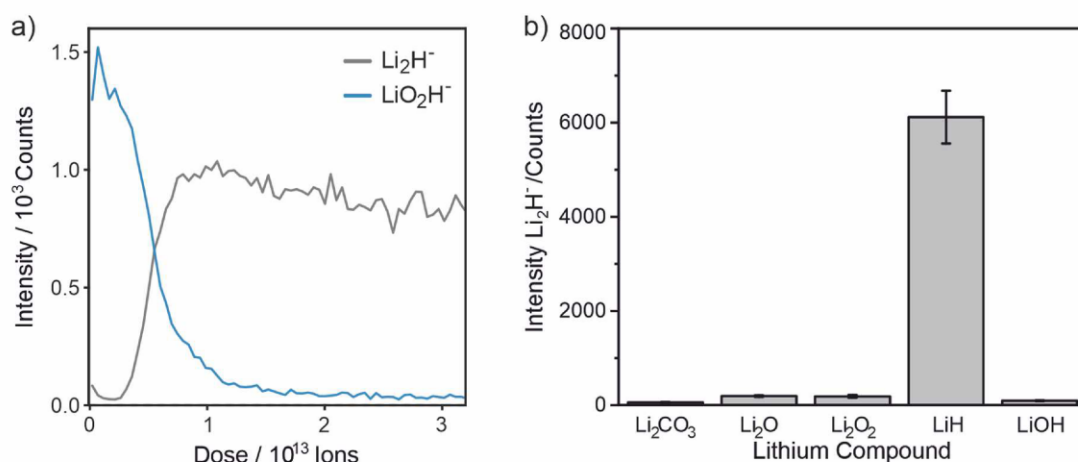


Figure S3. Example for the classification of a specific secondary ion for a lithium compound: a) Depth profile of the LiH pellet. The signal intensity of  $\text{LiO}_2\text{H}^-$  dropped, while the intensity of  $\text{Li}_2\text{H}^-$  increased with sputtering. Therefore,  $\text{Li}_2\text{H}^-$  was identified as a potentially specific secondary ion for LiH, whereas  $\text{LiO}_2\text{H}^-$  was regarded as originating from a surface contamination of the sample. b) Comparison of the signal intensity of  $\text{Li}_2\text{H}^-$  for all spectra measured on sputter-cleaned pellets of the reference compounds with the same ion dose density: The intensity is highest for the LiH sample. Consequently, the  $\text{Li}_2\text{H}^-$  signal was classified as specific for LiH.

Table S1. Representative specific secondary ions which were used for the interpretation of the ToF-SIMS depth profiles and other specific signals with similar profiles.

Compound	Specific signal(s) negative polarity	Related signal(s)	Specific signal(s) positive polarity	Related signal(s)
Hydrocarbons	$\text{C}_2\text{H}^-$	$\text{CH}_2^-$ , $\text{CH}^-$ , $\text{C}_2\text{H}_3^-$ , $\text{CH}_3^-$ , $\text{C}_3\text{H}^-$ , $\text{C}_3\text{H}_2^-$	$\text{C}_3\text{H}_3^+$	$\text{CH}^+$ , $\text{CH}_2^+$ , $\text{CH}_3^+$ , $\text{C}_2\text{H}_3^+$
Carbonate	$\text{CO}_3^-$	$\text{LiCO}_3^-$		
Hydroxide	$\text{OH}^-$ and $\text{LiO}_2\text{H}^-$	$\text{HO}_2^-$ , $\text{LiO}_2\text{H}_2^-$	$\text{Li}_2\text{OH}^+$ and $\text{LiOH}^+$	$\text{LiOH}_2^+$
Oxide	$\text{O}^-$ and $\text{LiO}^-$	$\text{LiO}_2^-$	$\text{Li}_2\text{O}^+$	$\text{LiO}^+$
Hydride	$\text{LiH}_2^-$	${}^6\text{LiH}^-$ , $\text{LiH}^-$ , $\text{Li}_2\text{H}^-$	$\text{Li}_2\text{H}^+$	${}^6\text{LiLiH}^+$

### S5: ToF-SIMS depth profiling

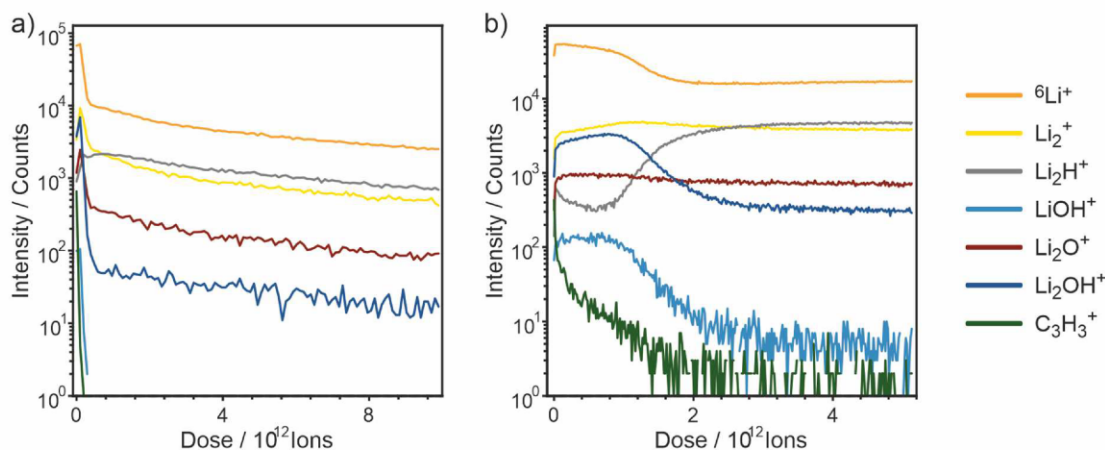


Figure S4. ToF-SIMS depth profiles of lithium foil 1 as-received measured in (spectrometry) positive ion mode. The unspecific secondary ions  ${}^6\text{Li}^+$  and  $\text{Li}_2^+$  are shown to visualize that all signal intensities drop for higher sputter dose.

Other elements than Li, C, O and H, which could be identified in the negative mode ToF-SIMS spectra of lithium foils, are P, F, S, Cl, Br and N. In the positive ion mode Mg, K, Si, Na, Ca and Fe were identified as additional trace elements.

### S6: Determination of sputter rates with ToF-SIMS

In order to access sputter rates of lithium and lithium compounds, sputter craters were prepared with defined sputter doses. Sputter rates and yields were calculated from the sputter time and current that were necessary to prepare the craters. The depth of the sputter craters ranged from 5 to 15  $\mu\text{m}$ . 3 to 5 craters were prepared on as received lithium foil for each sputter species, namely for  $\text{Cs}^+$  (2 keV – 190 nA),  $\text{Ar}^+$  (1 keV – 210 nA),  $\text{Ar}_{750}^+$  (10 keV – 9 nA), and  $\text{Ar}_{1500}^+$  (10 keV – 10 nA). The rates for sputtering lithium compounds were determined with  $\text{Ar}_{1500}^+$  (10 keV – 10 nA) by preparing 2 craters on pressed pellets. The crater size was  $300 \times 300 \mu\text{m}^2$  in all cases. The depth of the craters was measured with a profilometer (Alpha-Step IQ Surface Profiler, KLA Tencor) under argon atmosphere. The obtained sputter rates and yields for the different sputter species are given in Figure S5. In literature some estimates for the sputter rates of lithium and its compounds are given<sup>8–10</sup>, but no experimental values for lithium foils and different sputter species are reported.

For bigger argon cluster ions ( $\text{Ar}_{1500}^+$ , 10 kV, 10 nA,  $300 \times 300 \mu\text{m}^2$ ) a sputter rate of about 0.15 nm/s was obtained for lithium foils, when using 100 s sputter steps. The rate was also determined for 2 s sputter steps (0.17 nm/s). Considering the error range, the sputter rates for sputter steps between 2 and 100 s can be regarded as approximately constant. For continuous sputtering a significantly higher value of 0.33 nm/s was determined, showing that the estimation cannot be applied for very long sputter steps. The given values are averages over the passivation layer and the bulk of the lithium foils. As the thickness of the passivation layer was at least two orders of magnitude smaller than the crater depth, the given sputter rates represent approximate values for the bulk lithium. The sputter rates for lithium compounds were determined for pressed pellets of the materials (Figure S5b). For  $\text{Li}_2\text{CO}_3$  and  $\text{Li}_2\text{O}$  the sputter rate with  $\text{Ar}_{1500}^+$  (10 kV, 10 nA,  $300 \times 300 \mu\text{m}^2$ ) was about 0.25 nm/s. For  $\text{LiOH}$  a value of about 1.20 nm/s was determined. As the XPS results showed that these three compounds are the main components of the lithium foil passivation layer, an intermediate rate of 0.5 nm/s was used to estimate the thickness of the passivation layer. It is important to note that varying rates within the passivation

layer were neglected. Also, sputter rates depend on many factors, such as crystallographic orientation.<sup>8</sup> Consequently, the given value remains an estimate, especially as the determined thicknesses on the lithium samples are close to the depth resolution limit of the GCIB. The actual value for the sputter rate and thickness of the passivation layer could be accessed by applying AFM in combination with SIMS depth profiling. Alternatively, synchrotron-XPS measurements with varying high photon energies may be used to access detailed information about the passivation layer structure and thickness.

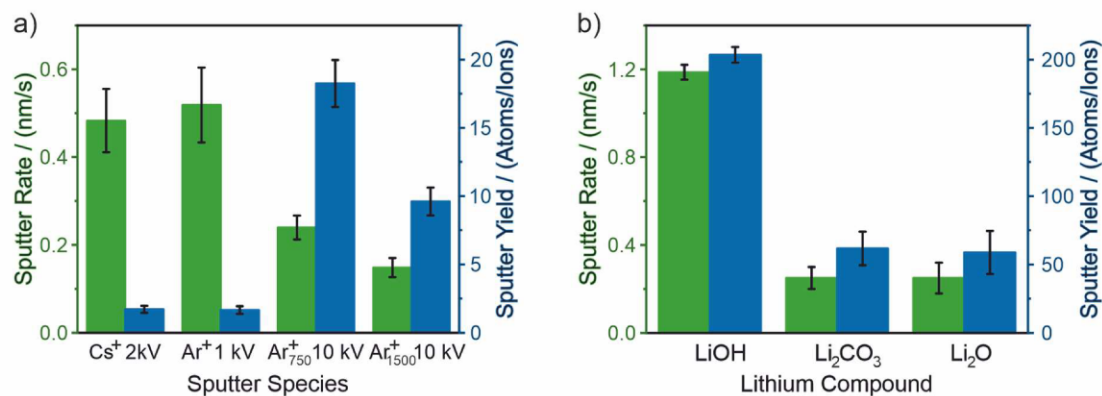


Figure S5. Sputter rates and yields for a) lithium foils with different sputter species and for b) lithium compounds with Ar<sub>1500</sub><sup>+</sup>, 10 keV. All shown values were determined in 100 s sputter steps.

### S7: ToF-SIMS imaging

While the lateral resolution is better in imaging mode, mass resolution and count rates are worse than in spectrometry mode. Consequently, it is necessary to invest longer measurement time, and signal interpretation becomes more complex. In general, mass spectra obtained in the imaging mode need to be compared with mass spectra taken in spectrometry mode and only  $m/z$ -regions without overlapping peaks can be used. Alternatively, single-pixel normalization of multiple  $m/z$ -regions, which include peaks giving the same information but overlap with other peaks, can be applied.<sup>11</sup>

In Figure S6 high resolution images from depth profiles of the lithium foils are shown. In most regions the passivation film was layered as described in most XPS-based literature.<sup>12</sup> On the very surface, a homogeneous coverage with hydrocarbon species that were quickly removed by sputtering, was detected. Below, hydroxide and oxide signals, also indicating homogeneous distribution, were more prominent. The hydroxide signal intensity decreased after a lower sputter dose than the oxide signal intensity. Beside the regions, which were homogeneously covered with the layered passivation, organic and inorganic contaminations were detected. As already found in the spectrometry mode, chemical information about the samples was easier to access in negative ion mode. For example, hydroxide contaminations were hard to visualize in the positive ion mode.

Contaminations on lithium foils are also reported in literature. For instance, Harry *et al.* used synchrotron hard X-ray micro tomography to study battery failure caused by dendrite growth and found crystalline impurities in the lithium anode that lead the nucleation of dendritic structures.<sup>13</sup> Similarly, Maslyn *et al.* reported, based on X-ray tomography analyses, the presence of impurity particles with diameters between 2 and 30  $\mu\text{m}$  in commercial lithium metal foils.<sup>14</sup> With ToF-SIMS depth profiles in imaging mode, the contaminations can be visualized and chemically characterized, what allowed Meyerson *et al.* to identify inhomogeneously distributed organic material on a lithium anode as dominating factor for dendrite nucleation.<sup>15</sup>

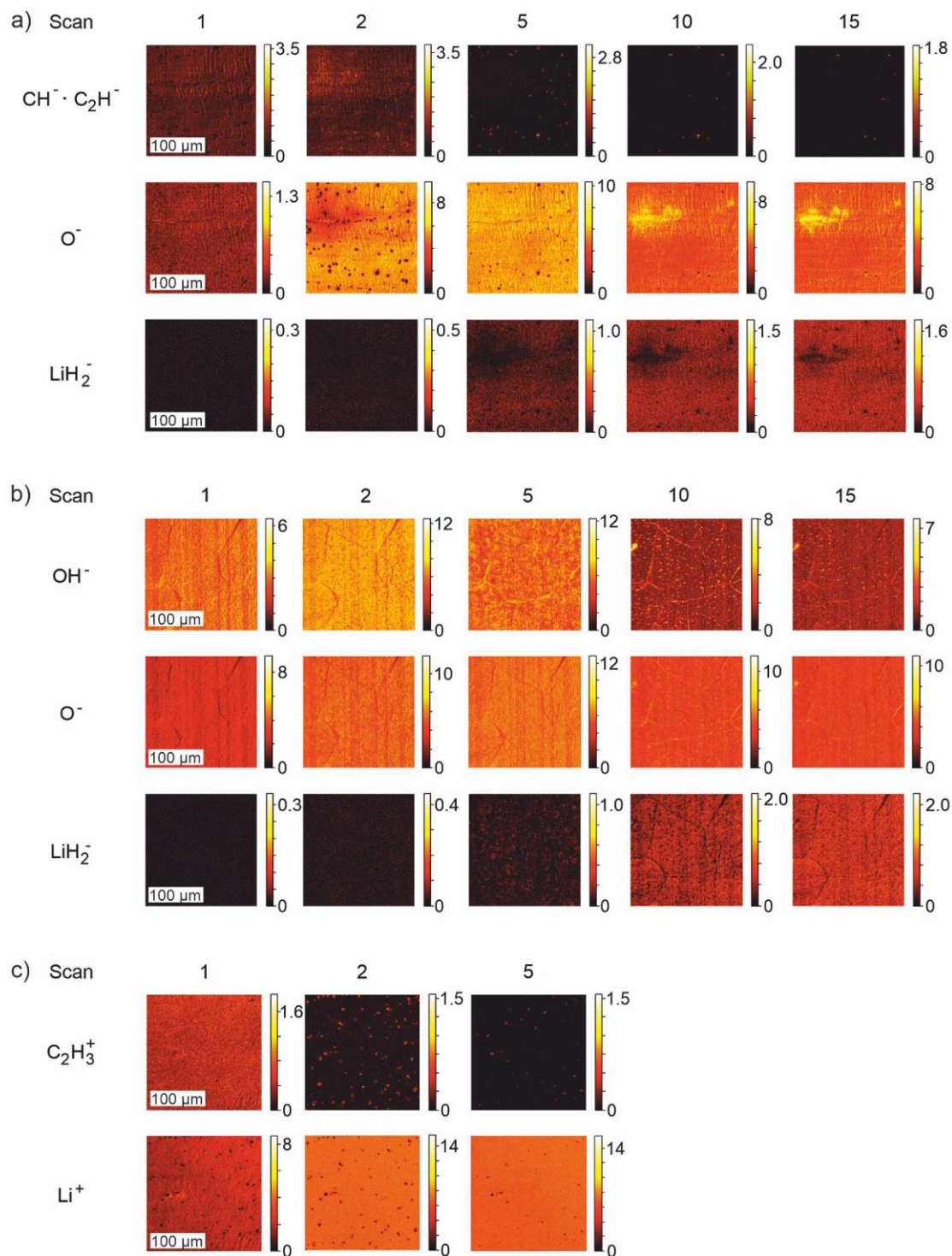


Figure S6. Single scan ToF-SIMS images of the depth profiles in imaging positive and negative ion mode. The evolution of organic contamination is shown in a) negative and c) positive ion mode. A region with hydroxide contamination is presented only in b) negative ion mode, as the information cannot be accessed properly in positive ion mode. Scan 1 shows the surface of the lithium foil before sputtering.

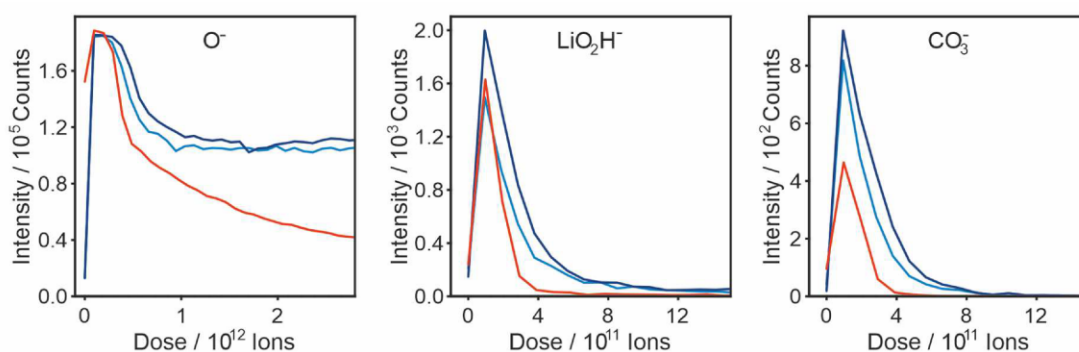
**S8: Variation in ToF-SIMS depth profiles**

Figure S7. Homogeneity of the ToF-SIMS depth profiles measured for lithium foil 2. Two different measurements of lithium foil 2 are shown in blue. The one presented in dark blue is a representative measurement, the one in light blue an example for the possible spread of the results. For comparison, a representative measurement for lithium foil 1 is shown in red. The spread for the thinner passivated foil is not significant.

**S9: EDX analysis of lithium samples with thicker passivation layers**

For an electron acceleration voltage of 1 kV, the average generation depth of Li  $K_{\alpha}$  emission in lithium is 47 nm, which is an order of magnitude more than the thickness of the upper surface passivation layer. Using an even lower beam energy is not reasonable as the count rates become very low, and a minimum energy is needed for excitation. Consequently, the information that is accessible by EDX analysis comes mainly from deeper regions of the lithium foils than the upper passivation layer probed by XPS and ToF-SIMS. This offers the chance to get additional information on the samples and to probe thicker passivation layers, that require very long sputter time. For EDX no sputtering is necessary to probe deeper regions of the sample (static depth profile). Therefore, deeper regions are analysed in their pristine state and no unwanted reactions with the chamber atmosphere disturb the analysis like in the case of XPS after sputtering. However, it is important to note that the typical SEM chambers operate under HV conditions. Consequently, the risk of surface contamination is even higher than during XPS or SIMS analyses (UHV conditions). Furthermore, the lack of sputtering is also a drawback, since many factors influence the analysis result at once. For example, the lateral spread of the X-ray generation also changes with the beam energy, material out of different depths is probed and all factors vary for the different elements due to their distribution and characteristic X-ray energy. Also, the sensitivity and the quantification error for lithium are unknown for the used software so far. Probably the error is quite high, as there is an intense background in the corresponding low-energy region. Defined model systems and careful data evaluation are needed to extract useful information. To show that differences between lithium samples can be investigated with EDX, a stored lithium foil 1 is compared to an as received lithium foil 2. The results are shown in Figure S8. For every beam energy, we determined a higher lithium fraction and a lower oxygen fraction for the as received foil than for the stored one. As error the standard deviation of three measurements is given. Please note that small changes of few at% occur between successive measurements at the same spot, what is attributed to damage induced by the electron beam. We took this into account by using a new spot for each measurement and by starting the measurement immediately after reaching the spot to make the damage comparable for different samples.

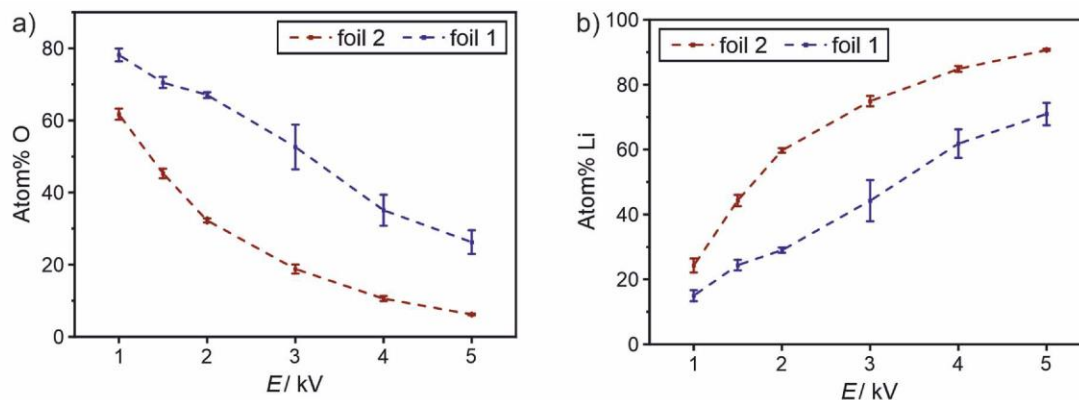


Figure S8. a) O and b) Li atomic fractions as a function of the electron beam energy determined from EDX analyses for an as received lithium foil 2 in comparison to a stored lithium foil 1.

### S10: Lithium plating through ToF-SIMS measurements

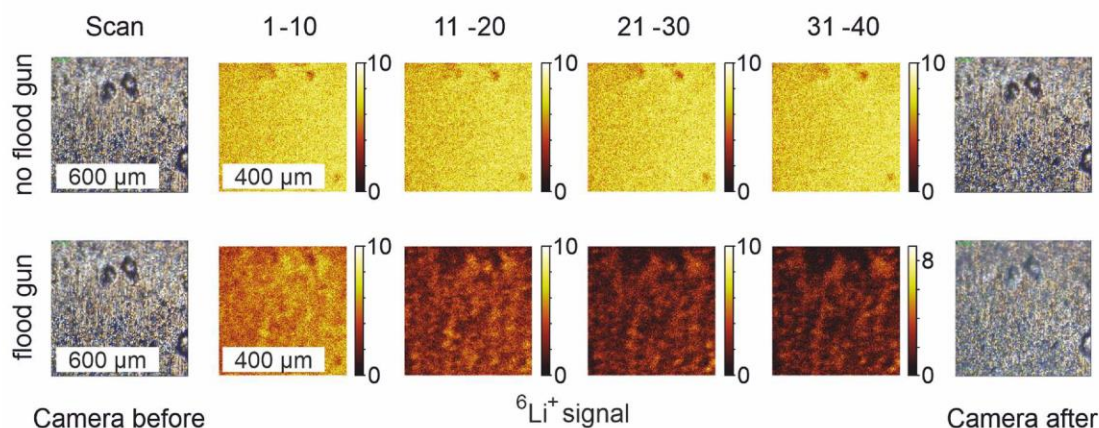


Figure S9. Lithium plating on a grounded lithium foil through electron beam exposure: comparison between spectrometry mode surface scans without (upper row) and with (bottom row) electron beam exposure using the flood gun. While the surface did not change without electron beam exposure, lithium was plated on the surface with the electron flood gun. The lithium was inhomogeneously distributed which explains the dark color of the plated lithium in the XPS camera images. Interestingly, all secondary ion intensities, such as the shown  ${}^6\text{Li}^+$  signal intensity, decreased through the lithium plating. Only some very weak signals of trace metals, like Ni and Cu, increased. The observation indicates that the ionization probability of all lithium related secondary ions is lower for metal than for lithium compounds. Consequently, there are no specific secondary ions for lithium metal.

### S11: Lithium plating through EDX measurements

EDX is used in literature to characterize for example reactions of lithium samples.<sup>16,17</sup> Typical EDX detectors cannot detect Li  $K_{\alpha}$  emission because of its low energy. Improved EDX detectors without a vacuum window can detect elemental lithium in high concentration, as in lithium metal.<sup>18</sup> Lithium ions have no 2s electrons, therefore no X-ray emission takes place and lithium ions cannot be detected. As for XPS and ToF-SIMS analyses, the sample preparation can influence the results quite strongly. In Figure S10 the effect of electron neutralization on a stored lithium foil 1 prepared in electrical contact (grounded) or isolated (floating) is shown. A higher lithium metal fraction and a lower oxygen fraction

were determined for the contacted sample, what indicates that the sample changed due to lithium plating. The changes observed through this effect varied for the different samples. For example, no significant changes were observed for as received lithium foils. For the EDX measurements electron beam impact is unavoidable since the SEM electron beam causes the X-ray emission. Consequently, measuring isolated samples is the only valid option. It is important to note that isolated preparation leads to charging, especially at higher acceleration voltages.

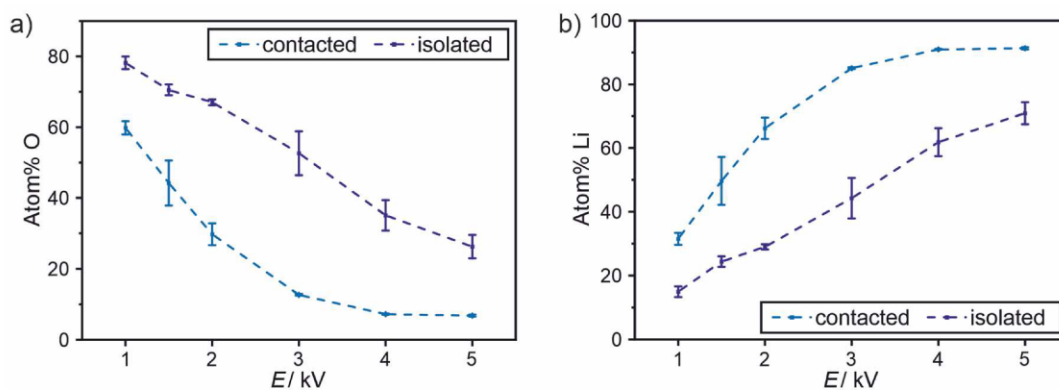


Figure S10. a) O and b) Li atomic fractions as a function of the electron acceleration voltage determined from EDX analyses for a stored lithium foil 1 prepared in electrical contact with the sample holder (grounded, light blue) or isolated from the holder (isolated, dark blue).

## References

- (1) Wood, K. N.; Teeter, G. XPS on Li-Battery-Related Compounds: Analysis of Inorganic SEI Phases and a Methodology for Charge Correction. *ACS Appl. Energy Mater.* **2018**, *1* (9), 4493–4504. DOI: 10.1021/acsaem.8b00406.
- (2) Dedryvère, R.; Laruelle, S.; Grugeon, S.; Poizot, P.; Gonbeau, D.; Tarascon, J.-M. Contribution of X-ray Photoelectron Spectroscopy to the Study of the Electrochemical Reactivity of CoO toward Lithium. *Chemistry of Materials* **2004**, *16* (6), 1056–1061. DOI: 10.1021/cm0311269.
- (3) Edström, K.; Herstedt, M.; Abraham, D. P. A new look at the solid electrolyte interphase on graphite anodes in Li-ion batteries. *Journal of Power Sources* **2006**, *153* (2), 380–384. DOI: 10.1016/j.jpowsour.2005.05.062.
- (4) Schmitz, R.; Müller, R.; Krüger, S.; Schmitz, R. W.; Nowak, S.; Passerini, S.; Winter, M.; Schreiner, C. Investigation of lithium carbide contamination in battery grade lithium metal. *J. Power Sources* **2012**, *217*, 98–101. DOI: 10.1016/j.jpowsour.2012.05.038.
- (5) Kanamura, K. X-Ray Photoelectron Spectroscopic Analysis and Scanning Electron Microscopic Observation of the Lithium Surface Immersed in Nonaqueous Solvents. *J. Electrochem. Soc.* **1994**, *141* (9), 2379. DOI: 10.1149/1.2055129.
- (6) Ciosek Högstöm, K.; Malmgren, S.; Hahlin, M.; Gorgoi, M.; Nyholm, L.; Rensmo, H.; Edström, K. The Buried Carbon/Solid Electrolyte Interphase in Li-ion Batteries Studied by Hard X-ray Photoelectron Spectroscopy. *Electrochimica Acta* **2014**, *138*, 430–436. DOI: 10.1016/j.electacta.2014.06.129.
- (7) Karen, A.; Ito, K.; Kubo, Y. TOF-SIMS analysis of lithium air battery discharge products utilizing gas cluster ion beam sputtering for surface stabilization. *Surf. Interface Anal.* **2014**, *46* (S1), 344–347. DOI: 10.1002/sia.5508.
- (8) Bessette, S.; Paoletta, A.; Kim, C.; Zhu, W.; Hovington, P.; Gauvin, R.; Zaghbi, K. Nanoscale Lithium Quantification in LiXNi<sub>y</sub>CowMnZO<sub>2</sub> as Cathode for Rechargeable Batteries. *Sci. Rep* **2018**, *8* (1), 17575. DOI: 10.1038/s41598-018-33608-3.
- (9) Stark, J. K.; Ding, Y.; Kohl, P. A. Role of Dissolved Gas in Ionic Liquid Electrolytes for Secondary Lithium Metal Batteries. *J. Phys. Chem. C* **2013**, *117* (10), 4980–4985. DOI: 10.1021/jp4001303.
- (10) Zu, C.; Dolocan, A.; Xiao, P.; Stauffer, S.; Henkelman, G.; Manthiram, A. Breaking Down the Crystallinity: The Path for Advanced Lithium Batteries. *Adv. Energy Mater.* **2016**, *6* (5), 1501933. DOI: 10.1002/aenm.201501933.
- (11) Walther, F.; Koerver, R.; Fuchs, T.; Ohno, S.; Sann, J.; Rohnke, M.; Zeier, W. G.; Janek, J. Visualization of the Interfacial Decomposition of Composite Cathodes in Argyrodite-Based All-Solid-State Batteries Using Time-of-Flight Secondary-Ion Mass Spectrometry. *Chem. Mater.* **2019**, *31*, 10, 3745–3755. DOI: 10.1021/acs.chemmater.9b00770.
- (12) Naudin, C.; Bruneel, J. L.; Chami, M.; Desbat, B.; Grondin, J.; Lassègues, J. C.; Servant, L. Characterization of the lithium surface by infrared and Raman spectroscopies. *J. Power Sources* **2003**, *124* (2), 518–525. DOI: 10.1016/S0378-7753(03)00798-5.
- (13) Harry, K. J.; Hallinan, D. T.; Parkinson, D. Y.; MacDowell, A. A.; Balsara, N. P. Detection of subsurface structures underneath dendrites formed on cycled lithium metal electrodes. *Nat. Mater.* **2014**, *13* (1), 69. DOI: 10.1038/nmat3793.
- (14) Maslyn, J. A.; Frenck, L.; Loo, W. S.; Parkinson, D. Y.; Balsara, N. P. Extended Cycling through Rigid Block Copolymer Electrolytes Enabled by Reducing Impurities in Lithium Metal Electrodes. *ACS Appl. Energy Mater.* **2019**, *2*, 11, 8197–8206. DOI: 10.1021/acsaem.9b01685.
- (15) Meyerson, M. L.; Sheavly, J. K.; Dolocan, A.; Griffin, M. P.; Pandit, A. H.; Rodriguez, R.; Stephens, R. M.; Vanden Bout, D. A.; Heller, A.; Mullins, C. B. The effect of local lithium surface chemistry and topography on solid electrolyte interphase composition and dendrite nucleation. *J. Mater. Chem. A* **2019**, *7*, 513. DOI: 10.1039/C9TA03371H.
- (16) Li, N.-W.; Yin, Y.-X.; Yang, C.-P.; Guo, Y.-G. An Artificial Solid Electrolyte Interphase Layer for Stable Lithium Metal Anodes. *Adv. Mater.* **2016**, *28* (9), 1853–1858. DOI: 10.1002/adma.201504526.

(17) Otero, M.; Lener, G.; Trincavelli, J.; Barraco, D.; Nazzarro, M. S.; Furlong, O.; Leiva, E. P. M. New kinetic insight into the spontaneous oxidation process of lithium in air by EPMA. *Appl. Surf. Sci.* **2016**, *383*, 64–70. DOI: 10.1016/j.apsusc.2016.04.060.

(18) Zachman, M.; Tu, Z.; Archer, L. A.; Kourkoutis, L. F. Nanoscale Elemental Mapping of Intact Solid-Liquid Interfaces and Reactive Materials in Energy Devices Enabled by Cryo-FIB/SEM. *ACS Energy Lett.* **2020**, *5*, 4, 1224–1232. DOI: 10.1021/acseenergylett.0c00202.

## 7.1.2 Publication 2

Supporting Information

**Storage of Lithium Metal: The Role of the Native Passivation Layer  
for the Anode Interface Resistance in Solid State Batteries**

Svenja-K. Otto <sup>a</sup>, Till Fuchs <sup>a,b</sup>, Yannik Moryson <sup>a,b</sup>, Christian Lerch <sup>a</sup>, Boris Mogwitz <sup>a</sup>,  
Joachim Sann <sup>a</sup>, Jürgen Janek <sup>a,b</sup> \* and Anja Henss <sup>a,b</sup> \*\*

<sup>a</sup> *Institute of Physical Chemistry, Justus-Liebig-Universität Giessen,  
Heinrich-Buff-Ring 17, D-35392 Giessen, Germany*

<sup>b</sup> *Center for Materials Research (ZfM), Justus-Liebig-Universität Giessen,  
Heinrich-Buff-Ring 16, D-35392 Giessen, Germany*

\*E-Mail: [juergen.janek@phys.chemie.uni-giessen.de](mailto:juergen.janek@phys.chemie.uni-giessen.de)

\*\*E-Mail: [anja.henss@phys.chemie.uni-giessen.de](mailto:anja.henss@phys.chemie.uni-giessen.de)

**This PDF file includes:**

SI 1: Overview of all samples

SI 2: Quantification of passivation layer compounds from XPS depth profiling

SI 3: Impact of different contamination levels in gloveboxes on lithium foil aging

SI 4: Impact of different storage conditions in gloveboxes on lithium foil aging

SI 5: Ideal lithium electrodes

SI 6: Representative Nyquist Plots

SI 7: Cryo FIB-SEM for interface visualization

SI 8: Theory about the reactivity of lithium toward atmospheric gases

SI 9: Pilling-Bedworth ratio

SI 10: Photo of stored lithium foil

SI 11: Reactivity of unprotected lithium surfaces toward atmospheric gases

SI 12: Reactivity of unprotected lithium surfaces in gloveboxes with and without nitrogen filter

### SI 1: Overview of all samples

Table S1: Overview of all samples which were stored in gloveboxes: glovebox 1 -  $p(\text{H}_2\text{O}$  and  $\text{O}_2)/p$  of about 1 ppm and variations up to 10 ppm), glovebox 2 -  $p(\text{H}_2\text{O}$  and  $\text{O}_2)/p < 0.1$  ppm and variations of up to 1 ppm and glovebox 3 -  $p(\text{H}_2\text{O}$  and  $\text{O}_2)/p < 0.1$  ppm and variations of up to 3 ppm,  $p(\text{N}_2)/p$  about 1 ppm.

Sample type	Glovebox	Storage condition	Storage time / weeks	Data in Figure(s)
Lithium foil	1	Closed plastic boxes	2, 5, 10	1, 2, 5, S2, S3, S4, S8
Lithium foil	1	Original transport package	Reference (0)	1, 2, S2, S4, S8
Lithium foil	2	Closed plastic boxes	2, 5, 10	2, S3
Lithium foil	2	Original transport package	Reference (0)	2
Lithium foil	1	Closed plastic boxes	5, 20	3
Lithium foil	1	Closed plastic boxes + pouch	5	S4
Lithium foil	1	Open boxes	5	S4
Sliced lithium rod	1	Closed plastic boxes	5	S10
Sliced lithium rod	3	Closed plastic boxes	5	S10

Table S2: Overview of all samples which were exposed to pure gases.

Sample type	Treatment	Conditions	Time	Data in Figure(s)
Lithium foil	Gas exposure	100 sccm of dried $\text{N}_2$ , $\text{O}_2$ and $\text{CO}_2$ , $\text{H}_2\text{O}$ with Ar as carrier gas	22 h	4
Sliced lithium rod	Gas exposure	100 sccm of dried $\text{N}_2$ , $\text{O}_2$ and $\text{CO}_2$ , $\text{H}_2\text{O}$ with Ar as carrier gas	22 h	S9

### SI 2: Quantification of passivation layer compounds from XPS depth profiling

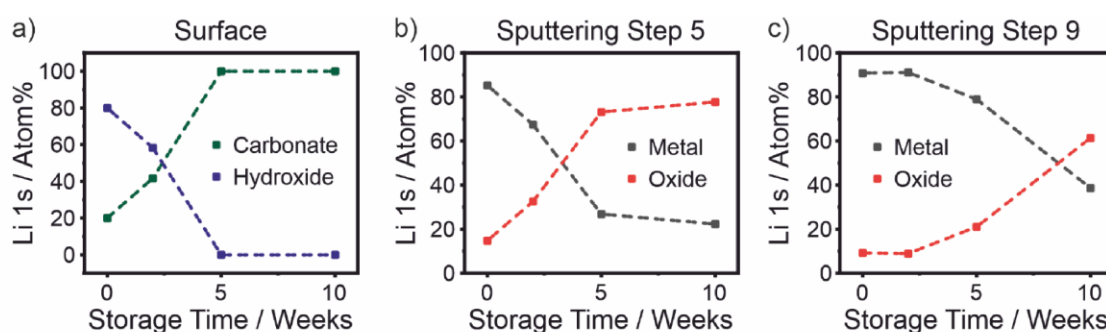


Figure S1: XPS depth profiling. Quantification of the compounds on lithium metal foil stored in glovebox 1 as a function of storage time. a) Carbonate and hydroxide fractions on the sample surfaces (without sputtering) b) + c) Metal and oxide fractions after sputter steps 5 (sputtering with 1 kV for 3 min, 2 kV for 8 min and 4 kV for 15 min) and 9 (sputtering with 1 kV for 3 min, 2 kV for 8 min and 4 kV for 105 min), respectively. The variances between the samples are differently pronounced for the sputter steps. Sputter step 5 shows the differences most pronounced for 0, 2 and 5 weeks, whereas sputter step 9 shows the difference between the foils stored for 5 and 10 weeks.

### SI 3: Impact of different contamination levels in gloveboxes on lithium foil aging

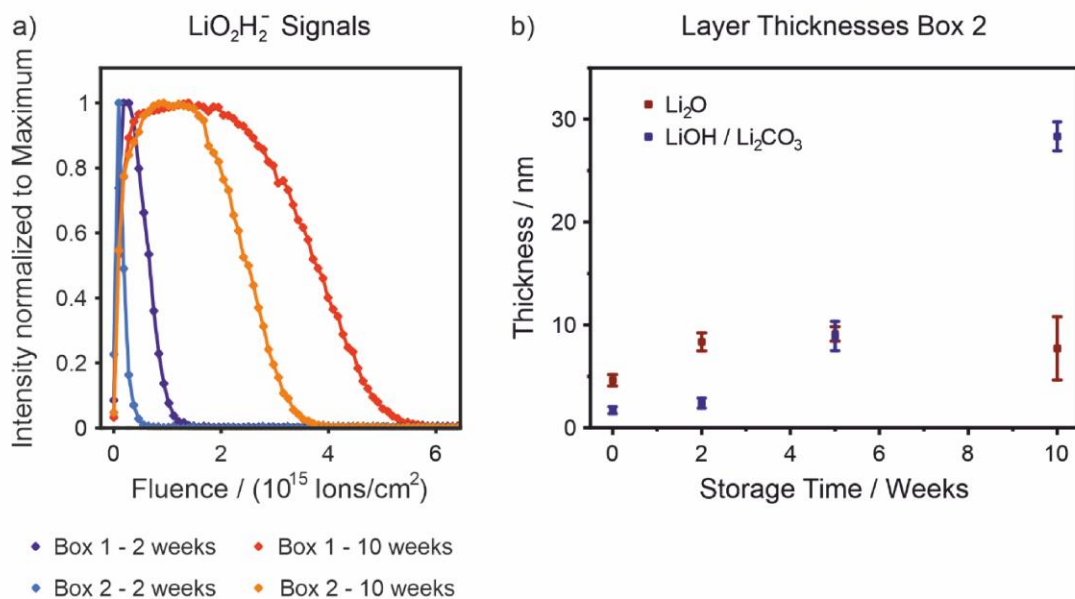


Figure S2: Results from ToF-SIMS depth profiling. a) Comparison of the surface passivation layer of lithium foil stored in glovebox 1 ( $p(\text{H}_2\text{O}$  and  $\text{O}_2)/p$  of about 1 ppm and variations up to 10 ppm) and glovebox 2 ( $p(\text{H}_2\text{O}$  and  $\text{O}_2)/p < 0.1$  ppm and variations of only up to 1 ppm). Samples were stored in closed plastic boxes. The  $\text{LiO}_2\text{H}_2^-$  signal of the ToF-SIMS depth profiles is shown as representative for LiOH to visualize the growth of the passivation layer. b) Quantification of the passivation layer thicknesses on lithium metal foil after storage in closed plastic boxes in glovebox 2 from the ToF-SIMS depth profiles. The trends are similar as in box 1, but less pronounced.

### SI 4: Impact of different storage conditions in gloveboxes on lithium foil aging

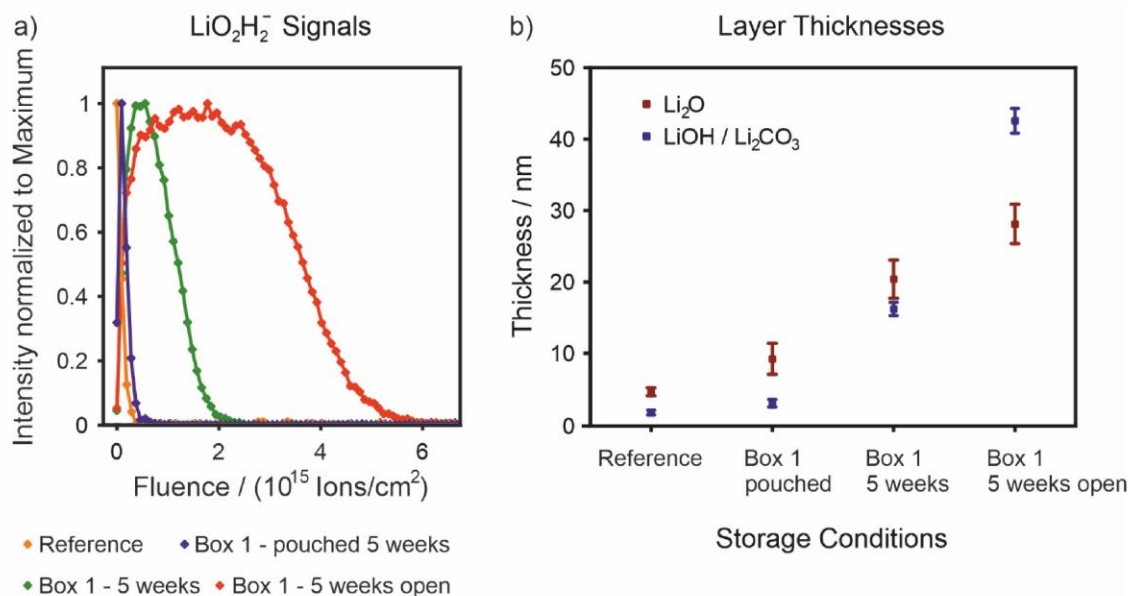


Figure S3: a) Comparison of the surface passivation layer of lithium foil stored in glovebox 1 ( $p(\text{H}_2\text{O}$  and  $\text{O}_2)/p$  of about 1 ppm and variations up to 10 ppm) under different conditions. The  $\text{LiO}_2\text{H}_2^-$  signal

is shown as representative for LiOH. The reference was taken from an unopened transport package, the Box 1 - pouched sample was stored in a closed plastic box which was additionally sealed in a pouch bag. Sample Box 1 – 5 weeks was stored as described before only in a closed plastic box and sample Box 1 – 5 weeks open was put in a box without lid. Samples taken from other unopened transport packages after up to 6 months of storage in gloveboxes showed no significant differences compared to the reference. b) Quantification of the passivation layer thicknesses on lithium metal foil after storage under different conditions in glovebox 1 from the ToF-SIMS depth profiles. The sample which was protected by an additional pouch bag shows only minor passivation layer growth. Open storage increases the growth of the passivation layer importantly.

### SI 5: Ideal lithium electrodes

The concept of “ideal” lithium electrodes ( $\text{Li}_{\text{id}}$ ) for LLZO solid electrolyte was introduced by Krauskopf et al. in 2019.<sup>1</sup> They showed that the interfacial resistance between LLZO and lithium becomes practically  $0 \Omega \cdot \text{cm}^2$  after isostatic pressing at high external pressure of several 100 MPa and remains low. Consequently, only LLZO bulk and grain boundary (GB) contributions are measured for an ideal lithium electrode, as shown by the Nyquist plot in Figure S4. The authors showed that the contact geometry and the ionic transport in the LLZO control the interfacial contributions for a clean interface in equilibrium and they validated their findings with microelectrode studies.<sup>2</sup> Observed interface contributions can therefore be attributed to constriction resistances, which originate from insufficient contact through pores or passivation layers.

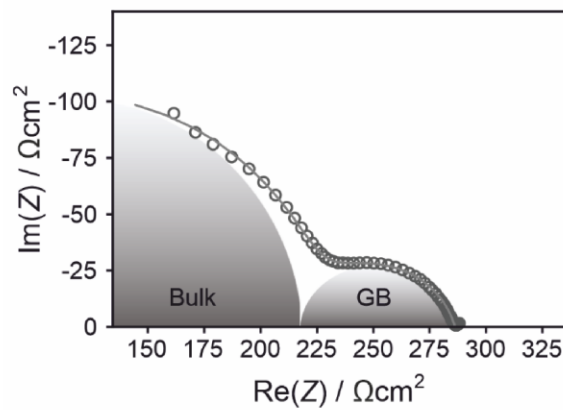


Figure S4: Nyquist plot for  $\text{Li}_{\text{id}}|\text{LLZO}|\text{Li}_{\text{id}}$ . Only bulk and grain boundary, but no interface contributions, are present.

### SI 6: Representative Nyquist plots

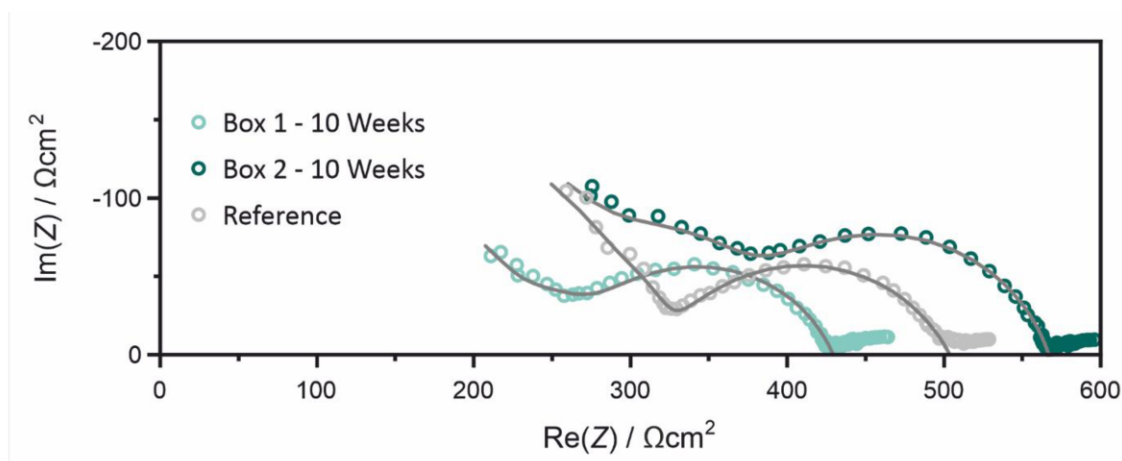


Figure S5: Exemplary Nyquist plots which were used to determine the interface resistances of Li|LLZO for the stored lithium foil samples. The measurements for lithium foil stored for 10 weeks in glovebox 1 ( $p(\text{H}_2\text{O}$  and  $\text{O}_2)/p$  of about 1 ppm and variations up to 10 ppm) or glovebox 2 ( $p(\text{H}_2\text{O}$  and  $\text{O}_2)/p < 0.1$  ppm and variations of only up to 1 ppm) are shown in comparison to the measurement for a reference lithium foil which was taken from an unopened transport package. The interface contributions are similar for all samples.

### SI 7: Cryo FIB-SEM for interface visualization

Cryo focussed ion beam scanning electron microscopy (FIB-SEM) measurements were performed with a XEIA3 GMU SEM/Plasma-FIB (Tescan) instrument in combination with a Leica VCT500 transfer module and a liquid nitrogen cooling stage ( $-130$  °C). As samples, lithium foil with an overall passivation layer thickness of about 100 nm was pressed with a preparation pressure of 40 or 400 MPa to LLZO polished with P1000. On the FIB crater walls, the interface between lithium and LLZO was investigated with SEM (measured at 3 kV, SE in beam detector). For a preparation pressure of 40 MPa (Figure S6a), pores are present at the interface. In contrast, the lithium fills every void of the solid electrolyte for a preparation pressure of 400 MPa (Figure S6b). The passivation layer of the lithium foil could not be identified definitely due to edge effects at the interfaces as well as limited morphological and topological contrast.

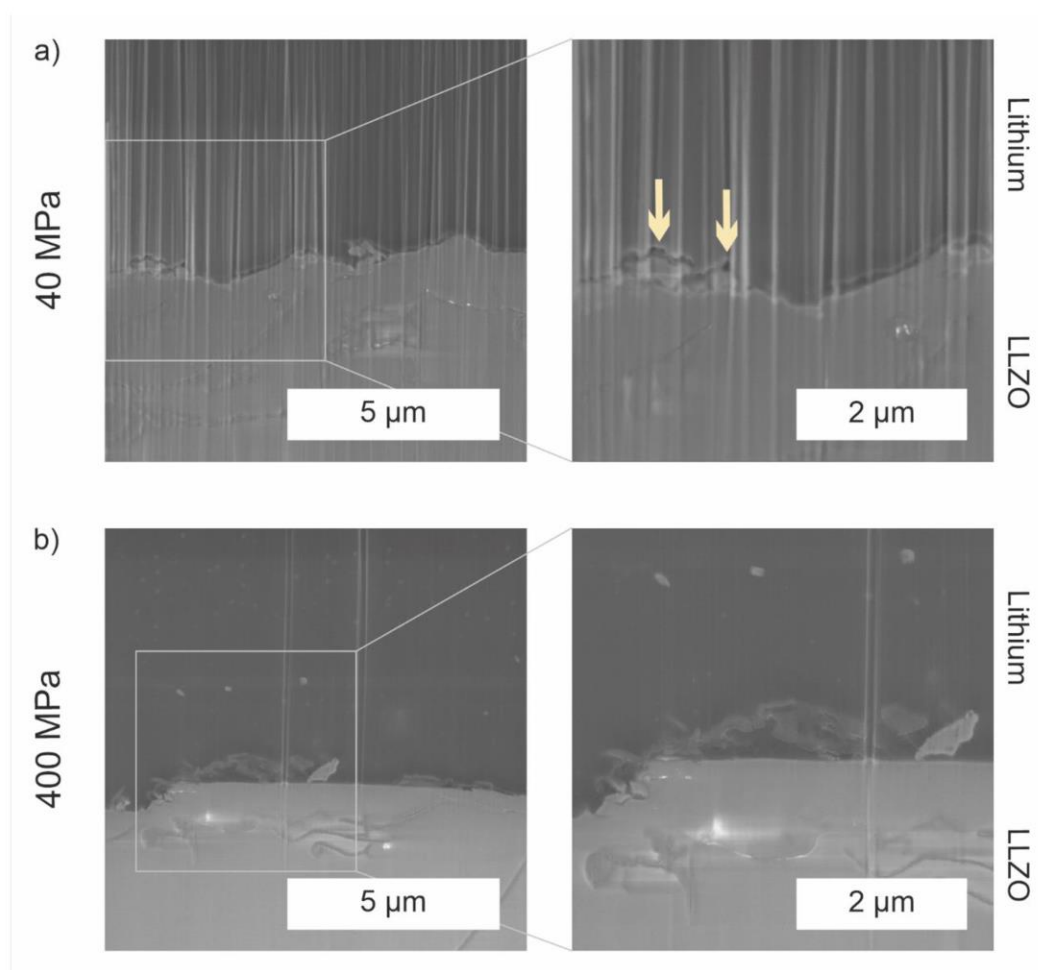


Figure S6: Cryo FIB-SEM SE images of Li|LLZO interfaces. LLZO pellets were polished with P1000 to an average roughness of about 160 nm including a maximal variation of 1.9  $\mu\text{m}$  in height. The overall thickness of the lithium passivation layer was about 100 nm. For a preparation pressure of 40 MPa (a), pores are visible at the interface (arrows) whereas a preparation pressure of 400 MPa (b) led to a close contact between lithium and solid electrolyte.

### SI 8: Theory about the reactivity of lithium toward atmospheric gases

In 2016, Schiemann et al. published a review on lithium combustion, in which the authors also discuss the main findings about the reaction of the atmospheric gases with lithium.<sup>3</sup> They conclude that the reaction of lithium with dry oxygen, nitrogen and carbon dioxide is negligible at room temperature. This is in accordance with a theoretical study by Shang et al. who claim that the reaction between lithium and the three named pure gases cannot occur at ambient temperature.<sup>4</sup> Also, the fact that lithium metal can be handled in dry-rooms where only  $p(\text{H}_2\text{O})$  is reduced to a minimum, supports a limited reactivity toward the other air components. However, both authors highlight that the reactivity largely depends on the surface state of lithium. According to Shang et al., the reaction between lithium and water can enable the reaction with other gases via the reaction products LiH and LiOH.<sup>4</sup> Schiemann et al. emphasize that the reaction of lithium is very sensitive to the presence of impurities like water in the reaction gas or already existing LiOH or  $\text{Li}_3\text{N}$  on the lithium surface.<sup>3</sup> Still, there are also recent reports about the interaction of pure lithium metal and dry atmospheric gases which claim an intrinsic interaction. Etxebarria et al. combined XPS, UPS and DFT to characterize the interaction of  $\text{O}_2$ ,  $\text{CO}_2$  and  $\text{N}_2$  with clean lithium surfaces and found oxidation of lithium metal by  $\text{O}_2$  and  $\text{CO}_2$ .  $\text{N}_2$  showed no reactivity

with clean lithium metal. However, also these authors stress that traces of impurities have a major impact on the reactivity of lithium surfaces and strongly influence the obtained results.<sup>5</sup>

### SI 9: Pilling-Bedworth ratio

Pilling and Bedworth found that it depends on the relative molar volume of a metal and the corresponding metal oxide if the metal oxide can form a covering and protective layer on the metal.<sup>6,7</sup> To classify different metal oxides, the Pilling-Bedworth ratio is calculated as follows:

$$\text{PBR} = \frac{V_{\text{Oxide}}}{n \cdot V_{\text{Metal}}} = \frac{M_{\text{Oxide}} \cdot \rho_{\text{Metal}}}{n \cdot M_{\text{Metal}} \cdot \rho_{\text{Oxide}}}$$

$V_x$  : molar volume of x

$n$  : number of metal atoms in the formula of the oxide

$M_x$  : molar mass of x

$\rho_x$  : density of x

For a ratio smaller than one, the oxide film is unprotective, as it will be porous and/or cracked. Consequently, the oxidation reaction is not self-limiting and the thickness of the oxide film will increase steadily. For ratios between one and two, a covering and protective film forms, whereas a ratio larger than two will again lead to cracking and therefore to an unprotective film.

The PBR can also be used to estimate, if products other than oxides may form covering films on a metal. In this context, the ratios are no irrevocable proof or fixed limit. However, values which are much smaller than 1 or importantly larger than 2, give a valid basis to explain an on-going reaction. Also, values which lie between 1 and 2 indicate the formation of a covering and protective reaction layer.

In Table S3 the PBRs for selected lithium compounds on lithium metal are given. The ratios for  $\text{Li}_2\text{CO}_3$  and  $\text{LiOH}$  are between 1 and 2, what indicated the formation of a covering film on lithium metal. For  $\text{Li}_3\text{N}$ , the ratio is importantly smaller than one what may explain the on-going reaction of lithium metal with  $\text{N}_2$ .

*Table S3: Pilling-Bedworth ratio for lithium compounds on lithium metal. Ratios smaller than one indicate the formation of a porous and/or cracked film. Ratios between one and two direct the formation of a covering and protective film.*

Compound	$\text{Li}_2\text{CO}_3$	$\text{Li}_2\text{O}$	$\text{LiOH}$	$\text{LiH}$	$\text{Li}_2\text{O}_2$	$\text{Li}_3\text{N}$
<b>PBR</b>	1.35	0.57	1.26	0.78	0.75	0.69

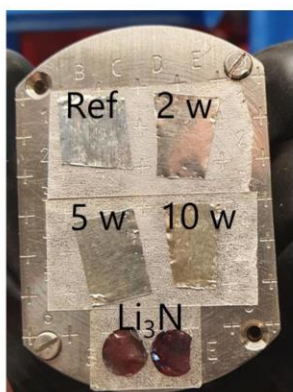
**SI 10: Photo of stored lithium foil**

Figure S7: Photograph of lithium foil samples after storage in glovebox 1. The larger lithium foil pieces showed a color change from metallic towards yellowish-brown for storage of up to 10 weeks. Some samples, here the two punched out samples at the bottom of the picture, tarnished and became brittle during storage due to  $\text{Li}_3\text{N}$  formation.

**SI 11: Reactivity of unprotected lithium surfaces toward atmospheric gases**

To investigate the reactivity of lithium without protective passivation layer, fresh lithium surfaces were exposed to pure atmospheric gases. The samples were cut directly in the gas stream to prevent undefined sample changes before the actual reaction. Results from XPS and ToF-SIMS characterization of the samples are shown in Figure S6. For exposure to  $\text{CO}_2$  and  $\text{O}_2$  only thin reaction layers formed and after sputtering lithium metal was detected by XPS. This was not possible for the samples exposed to  $\text{N}_2$  or  $\text{H}_2\text{O}$ . For these two samples, only reaction products were accessible, what indicates the formation of thick reaction layers.

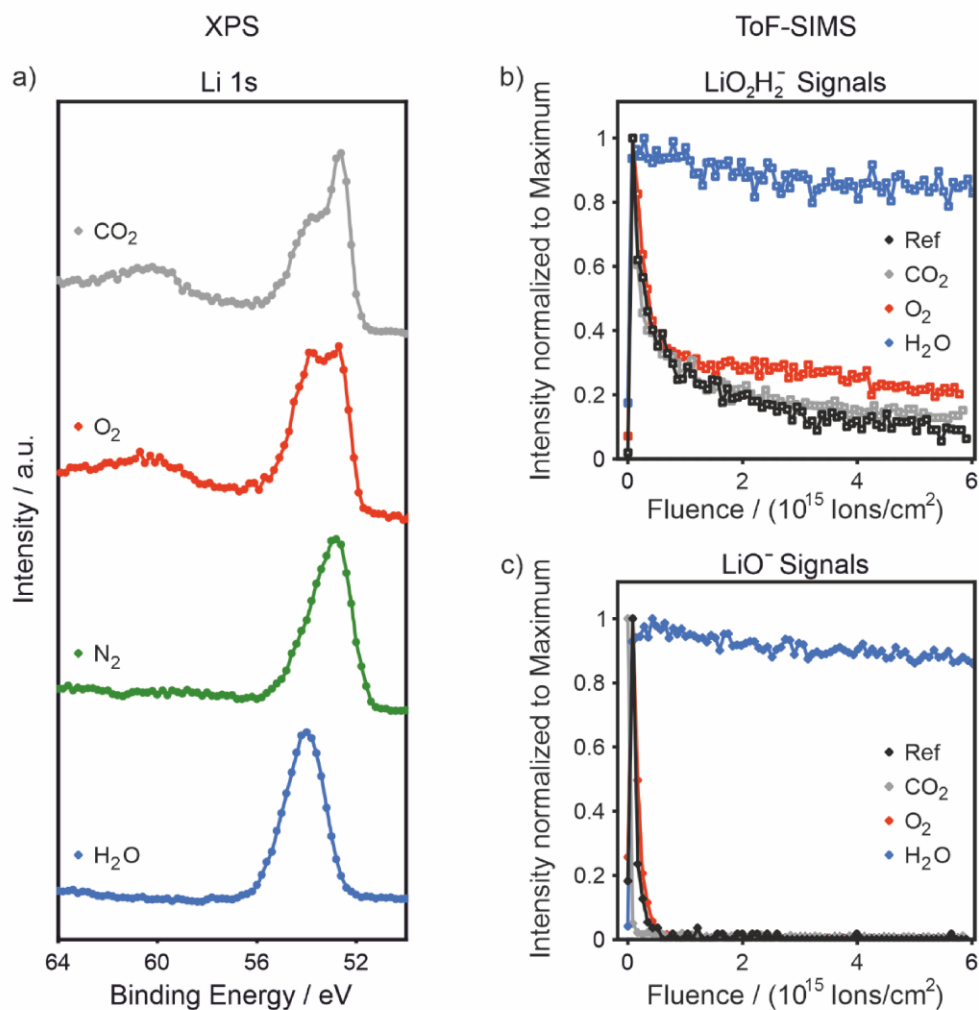


Figure S8: Reaction of fresh lithium surfaces with the atmosphere gases O<sub>2</sub>, CO<sub>2</sub>, N<sub>2</sub> and H<sub>2</sub>O (Ar as carrier gas). a) XP spectra of the Li 1s region after sputter step 6 (sputtering with 1 kV for 3 min, 2 kV for 8 min and 4 kV for 30 min). For exposure to CO<sub>2</sub> and O<sub>2</sub>, the plasmon-loss features show the presence of lithium metal. For exposure to N<sub>2</sub>, no plasmon-loss features are observed and the shift of the signal to low binding energies indicates the presence of Li<sub>3</sub>N. Accordingly, signals are observed in the N 1s region. After reaction with water the signal only shows the presence of LiOH and Li<sub>2</sub>O. b) + c) ToF-SIMS depth profiles after reaction showing the LiOH and Li<sub>2</sub>O rich regions respectively. Only for exposure to water pronounced differences compared to the reference sample were observed.

### SI 12: Reactivity of unprotected lithium surfaces in gloveboxes with and without nitrogen filter

A sliced sample of lithium was prepared and stored in a closed plastic box in glovebox 1. Within only 5 weeks, the about 3 mm thick slice of lithium became completely brownish-red and brittle. With XPS, the formation of Li<sub>3</sub>N could be confirmed as shown in Figure S7. For comparison, a slice of lithium was stored in a glovebox with additional N<sub>2</sub> filter (glovebox 3), where the N<sub>2</sub> partial pressure fraction was within the 5 weeks of storage always around 1 ppm. For this sample, no Li<sub>3</sub>N was detected by XPS and lithium metal was identified after sputtering by the plasmon-loss features at around 60 eV.

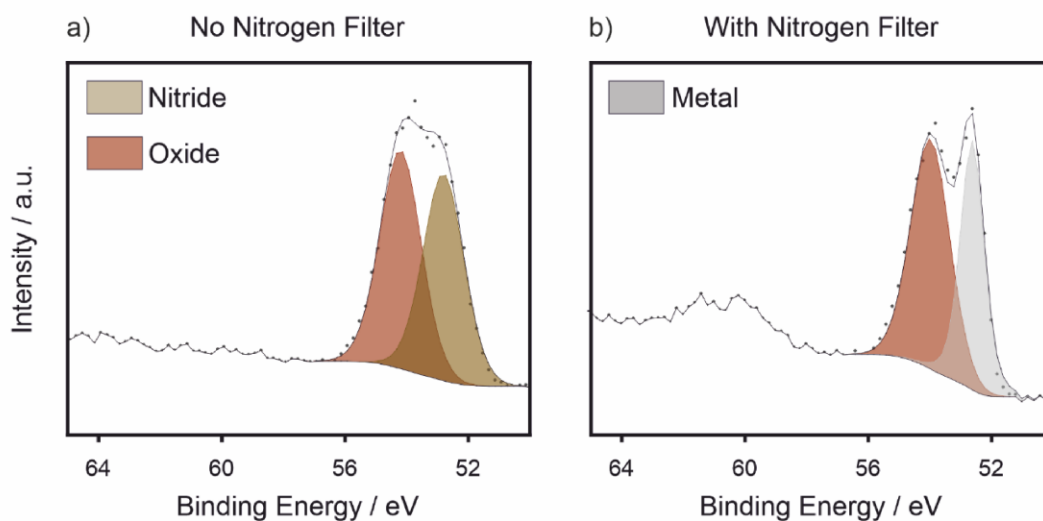


Figure S9: XP spectra of fresh lithium surfaces stored in gloveboxes without and with nitrogen filter. XP spectra of the Li 1s region for sputter step 6 (sputtering with 1 kV for 3 min, 2 kV for 8 min and 4 kV for 30 min) are shown. a) Without nitrogen filter, no plasmon-loss features are observed and the shift of the signal to low binding energies indicates the presence of  $\text{Li}_3\text{N}$ . Accordingly, signals are observed in the N 1s region. b) With nitrogen filter, the plasmons-loss features show the presence of lithium metal, what indicates that only a comparably thin reaction layer formed.

## References

- (1) Krauskopf, T.; Hartmann, H.; Zeier, W. G.; Janek, J. Toward a Fundamental Understanding of the Lithium Metal Anode in Solid-State Batteries-An Electrochemo-Mechanical Study on the Garnet-Type Solid Electrolyte  $\text{Li}_{6.25}\text{Al}_{0.25}\text{La}_3\text{Zr}_2\text{O}_{12}$ . *ACS applied materials & interfaces* **2019**, *11* (15), 14463–14477. DOI: 10.1021/acsami.9b02537.
- (2) Krauskopf, T.; Mogwitz, B.; Hartmann, H.; Singh, D. K.; Zeier, W. G.; Janek, J. The Fast Charge Transfer Kinetics of the Lithium Metal Anode on the Garnet-Type Solid Electrolyte  $\text{Li}_{6.25}\text{Al}_{0.25}\text{La}_3\text{Zr}_2\text{O}_{12}$ . *Adv. Energy Mater.* **2020**, *10* (27), 2000945. DOI: 10.1002/aenm.202000945.
- (3) Schiemann, M.; Bergthorson, J.; Fischer, P.; Scherer, V.; Taroata, D.; Schmid, G. A review on lithium combustion. *Applied Energy* **2016**, *162*, 948–965. DOI: 10.1016/j.apenergy.2015.10.172.
- (4) Shang, J.; Shirazian, S. Facilitated Dissociation of Water in the Presence of Lithium Metal at Ambient Temperature as a Requisite for Lithium–Gas Reactions. *J. Phys. Chem. C* **2018**, *122* (28), 16016–16022. DOI: 10.1021/acs.jpcc.8b01817.
- (5) Etxebarria, A.; Koch, S. L.; Bondarchuk, O.; Passerini, S.; Teobaldi, G.; Muñoz-Márquez, M. Á. Work Function Evolution in Li Anode Processing. *Adv. Energy Mater.* **2020**, *10* (24), 2000520. DOI: 10.1002/aenm.202000520.
- (6) Hart, C. A.; Skinner, C. H.; Capece, A. M.; Koel, B. E. Sorption of atmospheric gases by bulk lithium metal. *Journal of Nuclear Materials* **2016**, *468*, 71–77. DOI: 10.1016/j.jnucmat.2015.11.006.
- (7) Pilling, N. B. The Oxidation of Metals at High Temperature. *J. Inst. Met.* **1923**, *29*, 529–582.

**ADVANCED  
MATERIALS**  
INTERFACES**Supporting Information**

for *Adv. Mater. Interfaces*, DOI: 10.1002/admi.202102387

**In Situ Investigation of Lithium Metal–Solid Electrolyte  
Anode Interfaces with ToF-SIMS**

*Svenja-K. Otto, Luise M. Riegger, Till Fuchs, Sven  
Kayser, Pascal Schweitzer, Simon Burkhardt, Anja  
Henss,\* and Jürgen Janek\**

## Supporting Information

### In situ Investigation of Lithium Metal - Solid Electrolyte Anode Interfaces with ToF-SIMS

*Svenja-K. Otto, Luise M. Riegger, Till Fuchs, Sven Kayser, Pascal Schweitzer, Simon Burkhardt, Anja Henss\* and Jürgen Janek \**

#### **S1: Thermal deposition of lithium with a low-temperature effusion cell**

Lithium is deposited on the surface of a solid electrolyte pellet with a low-temperature effusion cell, which is attached to a side chamber of the ToF-SIMS instrument. After the deposition, the sample is directly transferred into the SIMS instrument for depth profiling.

To find suitable parameters for lithium deposition, the deposition was tested on MgO, which is inert to lithium. Lithium was deposited on a MgO substrate at different crucible temperatures of the effusion cell. The temperatures and corresponding results are shown in **Table S1**. The layer thickness of lithium was determined through ToF-SIMS depth-profiling with Cs<sup>+</sup> (2 kV, 115 nA) and subsequent measurement of the crater depth with a profilometer (Alpha-Step IQ Surface Profiler, KLA Tencor) under argon atmosphere. The inflection point of the appearing MgO<sup>-</sup> signal intensity was used to define the thickness of the deposited lithium. The profiler was also used to specify the roughness of the deposited lithium layers, but no significant differences were observed within the tested temperature range. The determined  $R_a$  value was in all cases approx. 200 nm.

**Table S1.** Parameters of lithium deposited on MgO substrates with a low-temperature effusion cell. The given temperature corresponds to the crucible temperature during deposition. The thickness of the resulting lithium layer was determined from sputter craters, which were prepared with the given fluence of Cs<sup>+</sup>, 2 kV.

Temperature [°C]	Deposition time [min]	Thickness Li layer [μm]	Fluence [Ions cm <sup>-2</sup> ]
425	60	2.6	$3.85 \cdot 10^{18}$
450	10	1.0	$1.47 \cdot 10^{18}$
465	10	1.6	$2.36 \cdot 10^{18}$

As the roughness of the deposited lithium layer does not correlate with the deposition temperature, a temperature that is easy to handle was chosen. At a crucible temperature of 450 °C, 10-minute deposition results in a lithium layer thickness of 1  $\mu\text{m}$ , which is suitable for the thickness range accessible with ToF-SIMS (up to 10  $\mu\text{m}$ ) and easy to control.

### S2: Parameters for ToF-SIMS depth profiling

The appropriate measuring parameters for ToF-SIMS depth profiling were also tested for a lithium layer on a MgO substrate. In **Figure S1** the ToF-SIMS depth profiles with  $\text{Ar}_{1500}^+$  (10 kV, GCIB) and  $\text{Cs}^+$  (2 kV, DSC) as sputter species are shown. For sufficient interface resolution, the dual-source column is needed as a sputter source. The use of  $\text{O}_2^+$  is not an option due to the reactivity of oxygen towards lithium. Consequently,  $\text{Cs}^+$  was used for all following depth profiles. Additionally, using negative polarity was useful as Cs increases the ionization probability in the negative mode and Li-ions tend to be oversaturated in the positive mode.

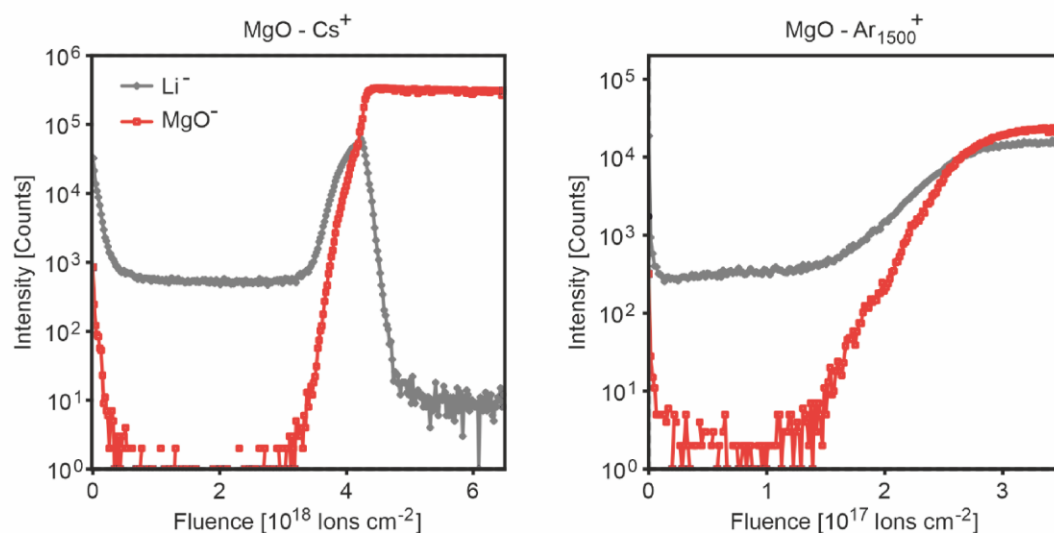


**Figure S1:** ToF-SIMS depth profiles of 3  $\mu\text{m}$  lithium on a MgO substrate with  $\text{Cs}^+$  (2 kV, left) or  $\text{Ar}_{1500}^+$  (10 kV, right) as sputter species. For  $\text{Cs}^+$ , the interface resolution is better as the intensity increase of the  $\text{MgO}^-$  signal is steeper.

### S3: Temporal evolution of depth profiles obtained from SEI-forming Li-SE-interfaces

For one Li|LPSCl sample ToF-SIMS depth profiling was repeated after different storage times of up to one week. Storage was done in a side chamber of the ToF-SIMS instrument at a pressure of below  $5 \cdot 10^{-9}$  mbar. The resulting depth profiles are the same within the accuracy of the measurements as shown in **Figure S2** for the  $\text{LiS}^-$  signal. This confirms the formation of a SEI

that grows very slowly due to the negligible electronic conductivity of the reaction products that form.

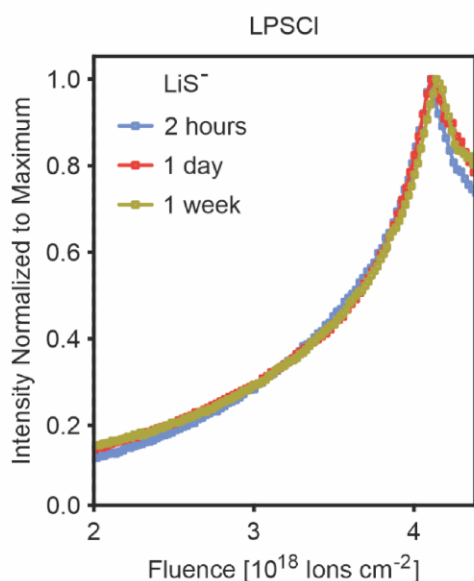


**Figure S2:** ToF-SIMS depth profiles of a LPSCI pellet with 3  $\mu\text{m}$  lithium on top. The profile of the  $\text{LiS}^-$  signal shown does not change measurably with time, confirming the formation of a SEI for LPSCI in contact with lithium.

#### S4: Evolution of the atomic concentrations of the LPSCI signals in the XPS depth profile

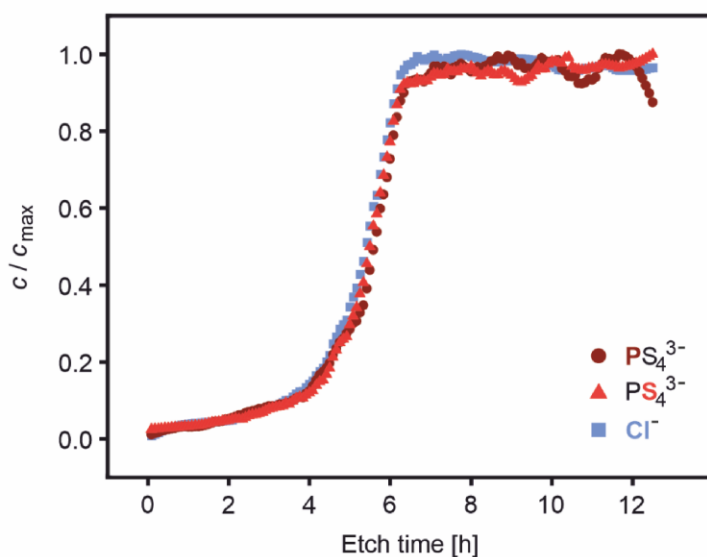


**Figure S3:** Normalized XP signals of the  $\text{Cl}^-$  and  $\text{PS}_4^{3-}$  signals of the Cl-1s, S-2p and P-2p spectra. The corresponding atom is written in bold and color. The parallel evolution of the three signals shows clearly that the bulk is reached after 6 h of sputtering.

## 7.2 Scientific Contributions

### 7.2.1 List of Publications

- 2022 **S.K. Otto**, L. M. Riegger, T. Fuchs, S. Kayser, P. Schweitzer, S. Burkhardt, A. Henss, J. Janek (2022). *In Situ Investigation of Lithium Metal-Solid Electrolyte Anode Interfaces with ToF-SIMS*. *Adv. Mater. Interfaces* 9(13).
- L. M. Riegger, **S.K. Otto**, M. Sadowski, S. Jovanovic, O. Kötz, S. Harm, L. G. Balzat, S. Merz, S. Burkhardt, F. H. Richter, J. Sann, R.-A. Eichel, B. V. Lotsch, J. Granwehr, K. Albe, J. Janek (2022). *Instability of the  $\text{Li}_7\text{SiPS}_8$  Solid Electrolyte at the Lithium Metal Anode and Interphase Formation*. *Chem. Mater.* 34(8).
- M. Malaki, A. Pokle, **S.K. Otto**, A. Henss, J. P. Beaupain, A. Beyer, J. Müller, B. Butz, K. Wätzig, M. Kusnezoff, J. Janek, K. Volz (2022). *Advanced Analytical Characterization of Interface Degradation in Ni-Rich NCM Cathode Co-Sintered with LATP Solid Electrolyte*. *ACS Appl. Energy Mater.* 5(4).
- 2021 **S.K. Otto**, T. Fuchs, Y. Moryson, C. Lerch, B. Mogwitz, J. Sann, J. Janek, A. Henss (2021). *Storage of Lithium Metal: The Role of the Native Passivation Layer for the Anode Interface Resistance in Solid State Batteries*. *ACS Appl. Energy Mater.* 4(11).
- J. P. Beaupain, K. Wätzig, **S.K. Otto**, A. Henss, J. Janek, M. Malaki, A. Pokle, J. Müller, B. Butz, K. Volz, M. Kusnezoff, A. Michaelis (2021). *Reaction of  $\text{Li}_{1.3}\text{Al}_{0.3}\text{Ti}_{1.7}(\text{PO}_4)_3$  and  $\text{LiNi}_{0.6}\text{Co}_{0.2}\text{Mn}_{0.2}\text{O}_2$  in Co-Sintered Composite Cathodes for Solid-State Batteries*. *ACS Appl Mater Interfaces* 13(40).
- T. Fuchs, B. Mogwitz, **S.K. Otto**, S. Passerini, F. H. Richter, J. Janek (2021). *Working Principle of an Ionic Liquid Interlayer During Pressureless Lithium Stripping on  $\text{Li}_{6.25}\text{Al}_{0.25}\text{La}_3\text{Zr}_2\text{O}_{12}$  (LLZO) Garnet-Type Solid Electrolyte*. *Batteries & Supercaps* 4(7).
- S.K. Otto**, Y. Moryson, T. Krauskopf, K. Pepler, J. Sann, J. Janek, A. Henss (2021). *In-Depth Characterization of Lithium Metal Surfaces with XPS and ToF-SIMS: Toward better Understanding of the Passivation Layer*. *Chem. Mater.* 33(3).
- 2020 Y. Zhao, **S.K. Otto**, N. Brandt, M. Selzer, B. Nestler (2020). *Application of Random Forest in ToF-SIMS Data*. *Procedia Computer Science* 176(410).
- 2019 **S.K. Otto**, K. Kousi, D. Neagu, L. Bekris, J. Janek, I.S. Metcalfe (2019). *Exsolved Ni nanoparticles acting as oxygen storage reservoirs and active sites for redox  $\text{CH}_4$  conversion*. *ACS appl. Energy Mater* 2(10).
- 2018 A. Henss, **S.K. Otto**, K. Schaepe, L. Pauusch, K.S. Lips, M. Rohnke (2018). *High resolution analysis of AgNP in hMSCs with ToF-SIMS and delayed extraction*. *Biointerphases* 13(3).
- 2017 M. Rohnke, S. Pfitzenreuter, B. Mogwitz, A. Henß, J. Thomas, D. Bieberstein, T. Gemming, **S.K. Otto**, S. Ray, M. Schumacher, M. Gelinsky, V. Alt (2017). *Strontium release from  $\text{Sr}^{2+}$  loaded bone cements and dispersion in healthy and osteoporotic rat bone*. *J Control Release* (262).

## 7.2.2 List of Conference Contributions

- 2022 Oral Presentation: **ECASIA 2022**, Limerick, Ireland (05/2022): *The Role of the Native Passivation Layer on Lithium Metal Anodes for Battery Research*.
- Online Oral Presentation: **Online Symposium “Lithium Metal Anodes and their Application in Batteries”** (02/2022): *Lithium Metal Reactivity - The Impact of the Surface Reaction Layer on the Lithium Anode*
- 2021 Online Poster Presentation: **BASF Summer School 2021**, online Conference (08/2021): *ToF-SIMS and XPS Characterization of Lithium Metal Surfaces*.
- Online Poster Presentation: **Bunsen-Tagung 2021**, online Conference (05/2021): *ToF-SIMS and XPS Characterization of Lithium Metal Surfaces*.
- 2019 Oral Presentation: **XXII. International Conference on Secondary Ion Mass Spectrometry**, Kyoto, Japan (10/2019): *Drug detection at the limit – Localization of bortezomib in myeloma cells*.
- 2018 Poster Presentation: **SIMS Europe 2018**, Münster, Deutschland (09/2018): *ToF-SIMS Study on Lithium Metal Electrodes*.
- 2017 Poster Presentation: **XXI. International Conference on Secondary Ion Mass Spectrometry**, Krakau, Polen (09/2017): *3D analysis using delayed extraction for the detection of Ag Nanoparticles in cells*.



## 8 Acknowledgement

First of all, I would like to thank my doctoral supervisor Prof. Dr. Jürgen Janek for setting the overall topic of my PhD thesis and giving me the opportunity to work and study in his group. Furthermore, I gratefully thank him for his support, his interest in my work and the various opportunities to develop myself, which he kindly made possible.

I especially thank Dr. Anja Henß for further supervising me, always supporting me in terms of technical and personal questions, as well as giving me the opportunity to be part of her junior research group during my time as a PhD student.

Special thanks also go to PD Dr. Marcus Rohnke for his continued support all throughout my time at the university of Giessen, starting already in the 3<sup>rd</sup> Bachelor semester when giving me the opportunity to work with him as a student assistant and introducing me to the topic of surface analytics.

Furthermore, I like to thank Prof. Dr. Herbert Over for being the 2<sup>nd</sup> reviewer of this thesis.

I acknowledge the financial support of my work as a PhD student (Kekulé scholarship) by the Funds of the Chemical Industry (FCI).

Special thanks go to Dr. Julie Michaud-Bernlochner who supported me during the last year as a mentor and helped me very much to grow as a person.

I would like to thank the project- and cooperation partners I had the pleasure to work with, for many valuable exchanges and fruitful research. Particularly, I thank my current and former colleagues and friends in the Janek group, especially Dr. Kaija Schäpe, Dr. Felix Walther, Dr. Adrian Schürmann, Christine Kern, Luise Riegger, Yannik Moryson, Bastian Krauskopf, Bianca Helm and Dennis S. Pietruschka. On the one hand I thank them for supporting my scientific research, but even more I thank them for supporting me personally and as a friend.

Last but not least, I thank my family and friends who supported me during my time as a PhD student.